STUDIA UNIVERSITATIS
BABEŞ-BOLYAI

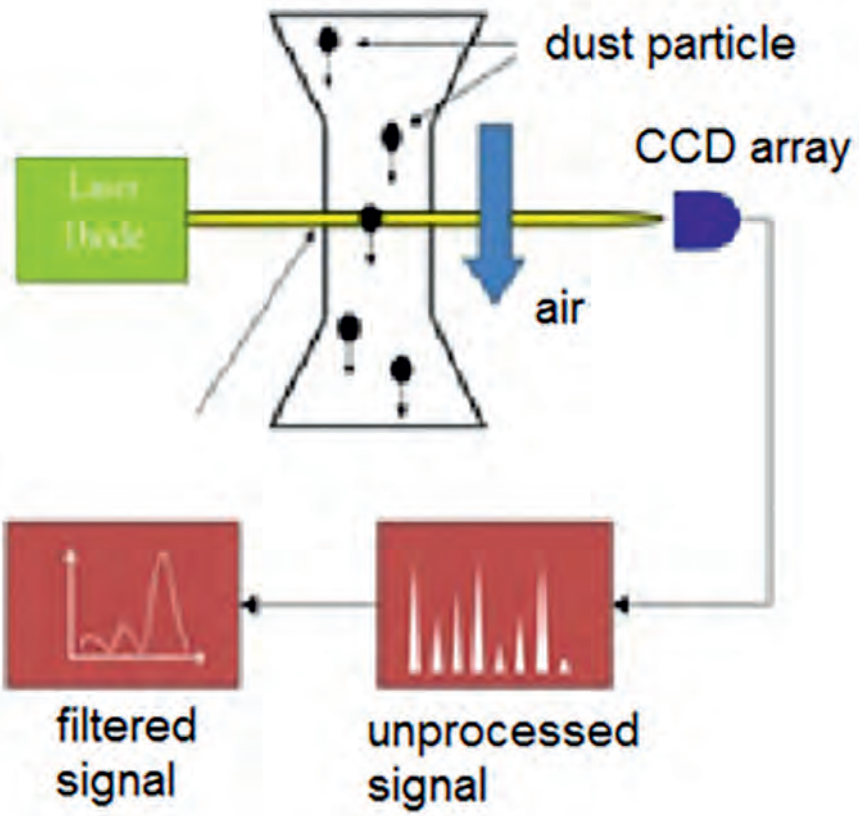

CHEMIA

2/2021

STUDIA UNIVERSITATIS BABEȘ-BOLYAI CHEMIA

2/2021

http://chem.ubbcluj.ro/~studiachemia/;
studiachemia@chem.ubbcluj.ro
http://www.studia.ubbcluj.ro/serii/chemia/index_en.html

YEAR **Volume 66 (LXVI) 2021**
MONTH **JUNE**
ISSUE **2**

S T U D I A
UNIVERSITATIS BABEŞ–BOLYAI
CHEMIA

2

ISSUE DOI:10.24193/subbchem.2021.2

STUDIA UBB EDITORIAL OFFICE: B.P. Hasdeu no. 51, 400371 Cluj-Napoca, Romania, Phone + 40 264 405300 *6452

CUPRINS – CONTENT – SOMMAIRE – INHALT

Studia Universitatis Babes-Bolyai Chemia has been selected for coverage in Thomson Reuters products and custom information services. Beginning with V. 53 (1) 2008, this publication is indexed and abstracted in the following:

- Science Citation Index Expanded (also known as SciSearch®)
- Chemistry Citation Index®
- Journal Citation Reports/Science Edition

STUDIA UBB CHEMIA, LXVI, 2, 2021 (p. 7-8)
(RECOMMENDED CITATION)

In Memoriam Prof. Emil Cordoș Ph.D.
1936 - 2021

Prof. Emil Cordoş Ph.D was part of a student generation that made the most representative connection between the group of professors that founded the chemistry department in early 1920 and the generation that graduated in early 1960 and developed the chemistry department in both fundamental and engineering chemistry. Professor Cordoș became a student of the Faculty of Chemistry in 1954 and graduated in 1959 with a degree of merit (red diploma), specialty Inorganic Chemistry. He obtained, by competition, a preparatory position in 1960, followed in 1961 by a promotion to assistant, lecturer in 1968, associate professor in 1976, professor in 1990 and consulting professor in 2005. Professor Cordoş occupied leadership positions at the Babes-Bolyai University, Faculty of Chemistry: Vice Dean, 1977-1981, Dean, 1990-1992 and Head of Analytical Chemistry Chair, 1996-2002. Specialization of Professor Cordoş in Analytical Chemistry was the Instrumental Analysis, mainly in spectrometric methods. He made the first steps in this field at the University of

Illinois, USA, where he worked for three years as Fulbright fellow and postdoctoral research associate. As a matter of fact he defended his Ph.D in 1969 with a thesis entitled "Contributions to the automation of kinetic methods of analysis". He understood that valuable research in the analytical instrumentation implies an interdisciplinary approach. Therefore, besides the remodeling of the Instrumental Analysis course he set up and organized research teams and groups within specific projects. In 1990 these collectives merged and, finally, in 1996 they became the Research Institute for Analytical Instrumentation, Cluj-Napoca, a subsidiary of the National Institute of Research and Development in Optoelectronics. Professor Cordoş achievements in the fields of instrumental analysis, are described in 207 papers, 130 of these being published in ISI indexed journals. He published five books: Electronics for Chemists, Ed. Stiintifica (1978), Atomic Absorption and Fluorescence Spectrometry, Ed. Academiei (1984), Analysis by Atomic Spectrometry, Ed. INOE (1998). Analysis by UV- Vis Molecular Absorption Spectrometry, Ed. INOE (2001), Analytical Atomic Spectrometry with Plasma Sources, Ed. INOE (2007); three chapters in books and a chapter in a megaencyclopedia devoted to analytical chemistry into the third millennium. The encyclopedia had 14 volumes and 700 contributors as experts in their fields. Only two of them were Romanians. To these should be added 12 patents, studies, methods and instrumentation resulted from more than 100 projects and research contracts or grants covered as project leader. A special note for the spectrometric systems based on radio frequency generated plasma sources, made before 1990 and continued through a series of projects to date and for the environmental projects in European programs. Under his leadership were presented 23 doctoral thesis. Regarding the connection with Studia, Prof. Cordos, as Dean, was Studia's responsible editor in 1990-92. He published his first paper in Studia in 1962, volume VII. Professor Cordos was member of many professional societies among them stands: American Chemical Society, Romanian Society of Chemistry, Society for Applied Spectroscopy, International Society of Environmental Epidemiology, EURACHEM Romania (founding member). He was president of the first subsidiary in Cluj-Napoca of the Romanian Society of Chemistry and was president and founder of PROANALITICA XXI.

Cluj-Napoca, June 2021

Prof. dr. Tiberiu Frentiu

STUDIA UBB CHEMIA, LXVI, 2, 2021 (p. 9-22)
(RECOMMENDED CITATION)
DOI:10.24193/subbchem.2021.2.01

REGIONAL PATTERN AND CHARACTERISTICS OF ESSENTIAL ELEMENTS IN SEVERAL MEDICINAL PLANTS USING SPECTROMETRIC METHODS COMBINED WITH MULTIVARIATE STATISTICAL APPROACHES

SIMONA CODRUȚA AURORA COBZAC[a,b], TIBERIU FRENȚIU[a,b], BILIJANA BALABANOVA[c], NATALJA MARKOVA RUZDIK[d], DORINA CASONI[a,b*]

ABSTRACT. The aim of this study was to provide a regional pattern and characteristics of essential elements in several medicinal plants from North Macedonia and Romania. The content of Ca, Mg, Al, Fe, Cu, Ba and Zn was determined by ICP-OES while Na and K by FAES in some medicinal plants belonging to sixteen families. Similar profiles of elements with a high content of Ca, Mg and K were observed. Peppermint and blackberry from both countries showed extreme content in Al and Fe. A symmetric distribution for K, Ca and Zn and an asymmetric one for Na, Al, Fe and Ba were found in medicinal plants from both countries. Potassium, Ca, Mg, Al and Fe could be considered as markers for growing area. Principal Component Analysis highlighted that the variability of elements content was described by four factors (83.4%) in North Macedonia and three factors (70.0%) in Romania. The first factor could explain the influence of soil nature upon variability of elemental composition, calcareous in North Macedonia (Mg and Ca – 29.4% variance) and a rich one in hydroxides in Romania (Al and Fe – 33.1% variance).

Keywords: *essential element, medicinal plant, inductively coupled plasma optical emission spectrometry, flame atomic emission spectrometry, Principal Component Analysis, two-way joining Cluster Analysis*

[a] *Babeş-Bolyai University, Faculty of Chemistry and Chemical Engineering, 11 Arany Janos str., RO-400028, Cluj-Napoca, Romania*
[b] *Research Center for Advanced Chemical Analysis, Instrumentation and Chemometrics, Arany Janos 11, 400028 Cluj-Napoca, Romania*
[c] *Department of Soil Chemistry and Hydrology, Faculty of Agriculture, Goce Delcev University, Krste Misirkov 10-A, 2000, Stip, Republic of North Macedonia*
[d] *Department of Plant Production, Faculty of Agriculture, Goce Delcev University, Krste Misirkov 10-A, 2000, Stip, Republic of North Macedonia*
** Corresponding author: dorina.casoni@ubbcluj.ro*

INTRODUCTION

The medicinal plants consumed preferable as teas or tinctures, have a long and rich history regarding their usage as therapeutics. The World Health Organization (WHO) estimated that 80% of the current population use medicinal plants for some aspect of primary healthcare [1]. It is thought that some medicinal plants contain elements of vital importance for human metabolism, disease prevention and healing [2]. Besides their use for treatment of diseases, the medicinal plants are also used as dietary supplements once they are found to be rich in one or more elements. So, their chemical composition in terms of nutrients, minerals, vitamins, and essential antioxidants need to be permanently monitored. Elemental content can vary in a wide range, depending on factors such as soil geochemical characteristics, the climate conditions, irrigation water, use of fertilizers and the ability of each plant species to selectively accumulate some of them [3, 4]. Metals, categorized as macro (primary) or micro (trace) elements play an essential role in the body some of them being crucial for many body functions. Essential elements such as sodium, potassium, calcium, magnesium, phosphorus, iron, zinc, copper, manganese and non-essential elements such as aluminium, barium, cadmium and lead were found in various medicinal plants [5]. Macroelements such as potassium, calcium, magnesium, phosphorus, and sodium are contained in concentration greater than 100 mg kg^{-1} while trace elements including iron, zinc, manganese, molybdenum, selenium, chromium, copper, cobalt and sulphur are usually contained in concentration less than 100 mg kg^{-1} [6].

The determination of elements in medicinal plants and their impact on human health is of great importance. Besides, their essential importance in the living system, several elements can be toxic when the concentrations exceed those necessary for metabolic functions [7, 8]. The level of elements permitted by the WHO should not endanger the health of consumers [9, 10]. Inductively coupled plasma-optical emission spectrometry (ICP-OES), atomic absorption spectrometry (AAS) and neutron activation analysis (NAA) methods have been used for the determination of elements concentration in medicinal plants and plant based multivitamin preparations [11, 12].

The aim of this paper was to provide a regional pattern and characteristics of essential elements in several medicinal plants from Romania and North Macedonia using spectrometric methods combined with multivariate statistical approaches. Romania and North Macedonia possesses a great vegetal genetic diversity, as for example Romania cover 30% of the European flora with a number of 3700 plant taxa, from which 283 were identified as medicinal plants [13, 14]. However, according to our best knowledge there are

few studies related to determination of essential elements in medicinal plants from two countries. From this point of view, the study has relevance and is of general interest for both producers and consumers. The content of Ca, Mg, Cu, Fe, Zn, Al and Ba were determined by ICP-OES, while Na and K content was determined by flame atomic emission spectrometry (FAES) in different parts (root, leaves, flowers, fruits) of different variety of medicinal plants originating from two countries. Principal Component Analysis (PCA) and two-way joining Cluster Analysis were used to describe variability of chemical composition of the medicinal plants under study and recognize the parameters significantly different. It is expected that the elemental composition to be different depending of variety and region of provenience due to soil and climatic conditions influence. So far a similar complex approach has not been performed on medicinal plants from Romania and North Macedonia.

RESULTS AND DISCUSSION

Patterns of essential elements in medicinal plants

Results obtained in the determination of elements concentration in medicinal plants originated from North Macedonia and Romania are given in Supplementary material (Table S1). The sample code of medicinal plants is presented in the experimental part, Table 5.

The content of Co, Cr, Cd, Ag, Mn, Ni, Sr, Pb were below LOD in ICP-OES. The elemental profiles of the selected medicinal plants are presented in Figure 1, while summary statistics is provided in Table 1.

Figure 1 reveal that the selected medicinal plants from both countries show similar profiles but different content of macroelements and microelements depending of variety and the nature of the plant sample. Therefore, the analysed plants are mainly characterized by high content of Ca, K and Mg. Interestingly is the high content of Al and Fe for *Peppermint* (Pe) and *Blackberry* (Bl) from both countries.

Data in Table 1 shows either asymetric or symetric distribution of elements content around the mean.

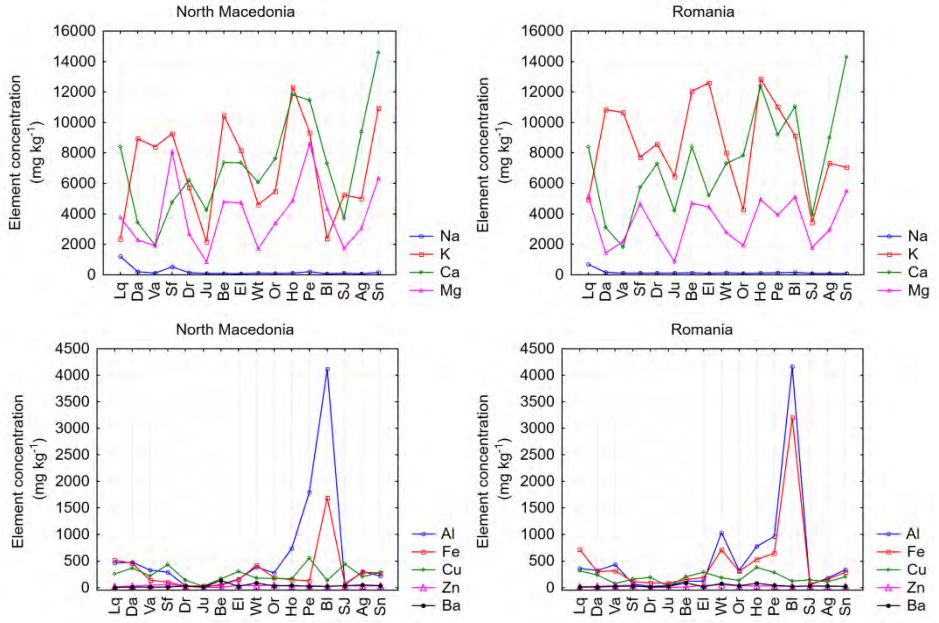

Figure 1. Profiles of the elemental content in the analysed medicinal plants from North Macedonia and Romania. The sample code of medicinal plants is presented in the experimental part, Table 5.

A positive Skewness and leptokurtic distribution was observed for Na, Al, Fe and Ba in the samples from both countries. These distributions are consistent with extreme values observed for Na in *Liquorice (*Lq), Al and Fe in *Blackberry (*Bl) and Ba in *Wild thyme* (Wt) and *Bean* (Be) samples (Figure 2). An symetric repartition with platikurtic distribution could be observed for K, Ca and Zn in samples from both countries while Mg and Cu show a symetric distribution only for plants of Romanian provenience.

Therefore, the median and the mean values for asymetric and symetric distribution, respectively, were considered for an overall comparison of metals content in analysed plants. In case of plants from North Macedonia, the following decreasing order for macroelements Ca> K> Mg> Na, for microelements Al> Cu> Fe> Zn≈Ba respectively, was observed. In case on Romanian samples the following order was observed K>Ca>Mg>Na and Al≈Fe>Cu>Zn≈Ba. These differences could be explained by influence of the soil composition on metals bioavailability in medicinal plants.

Table 1. Summary statistics for elements content (mg kg $^{-1}$) in medicinal plants samples from North Macedonia ([1]) and Romania ([2]), described in the experimental part, Table 5.

Element	Min	Max	Mean	Median	STDEV	SKEW	KURT
Na[1]	61.49	1443.92	253.44	108.70	342.34	2.63	6.80
Na[2]	75.82	681.06	145.22	105.64	136.95	3.83	15.27
K[1]	1804.47	12334.69	6818.36	5731.00	3178.30	0.05	-1.12
K[2]	3440.42	13648.22	8702.09	8417.91	2968.28	0.00	-0.86
Mg[1]	828.02	8594.53	3715.03	3419.53	1896.92	0.67	0.41
Mg[2]	872.30	5504.87	3467.38	3369.00	1458.04	-0.23	-1.44
Al[1]	9.29	4118.28	528.07	277.09	890.62	3.45	12.96
Al[2]	21.64	4165.67	603.73	321.61	961.04	3.25	11.65
Ca[1]	1941.08	16100.34	7606.94	7370.84	3387.57	0.63	0.51
Ca[2]	1812.82	14285.71	7547.95	7820.90	3221.15	0.19	-0.21
Fe[1]	28.34	1689.66	288.34	154.03	362.06	3.02	10.56
Fe[2]	68.03	3203.59	500.14	305.08	716.79	3.41	12.72
Cu[1]	23.91	584.18	267.33	222.58	137.99	0.82	0.42
Cu[2]	23.98	380.97	196.12	189.16	92.48	0.23	-0.33
Zn[1]	4.67	64.03	33.00	32.08	15.01	0.01	-0.31
Zn[2]	2.07	47.55	25.94	25.63	12.38	-0.39	-0.26
Ba[1]	2.85	134.45	33.14	21.42	32.12	1.93	3.90
Ba[2]	9.45	90.39	34.46	27.37	24.47	1.33	0.60

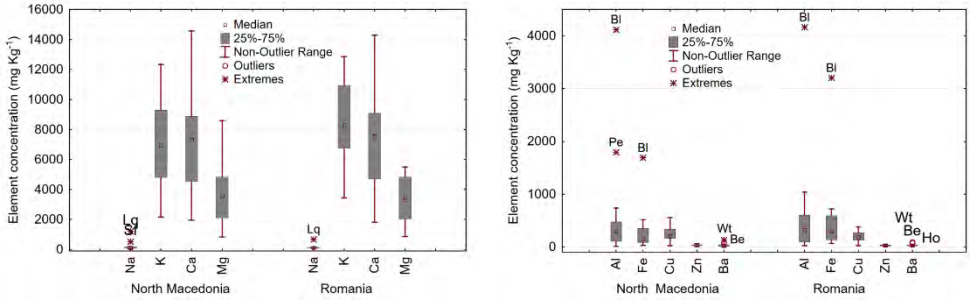

Figure 2. Box and whiskers plot for content of elements in medicinal plant samples. The sample code of medicinal plants is presented in the experimental part, Table 5.

Statistical evaluation of analysed medicinal plants

The correlations between the content of elements found in medicinal plants from North Macedonia and Romania are presented in Table 2.

Table 2. Correlations between content of elements found in medicinal plants from North Macedonia ([1]) and Romania ([2]). Bold values show significant correlations ($p < 0.05$).

Element	Na^1	K^1	Ca^1	Mg^1	Al^1	Fe^1	Cu^1	Zn^1	Ba^1
Na^2	**0.92**	-0.32	0.02	0.35	-0.13	0.00	0.35	-0.08	-0.27
K^2	-0.37	0.62	0.21	0.34	-0.29	-0.36	0.49	0.26	0.41
Ca^2	0.07	0.13	**0.92**	0.66	0.12	0.11	0.53	0.02	0.26
Mg^2	-0.02	0.30	0.50	0.72	0.11	0.10	0.46	0.24	0.13
Al^2	0.07	0.18	0.37	0.36	**0.96**	**0.95**	0.01	0.03	-0.06
Fe^2	0.25	-0.01	0.31	0.31	**0.92**	**0.95**	-0.07	0.02	-0.17
Cu^2	0.01	0.02	-0.13	0.13	-0.16	-0.17	0.35	0.39	-0.16
Zn^2	-0.29	-0.13	-0.18	-0.01	-0.17	-0.21	0.01	0.74	-0.24
Ba^2	-0.21	0.23	0.25	0.16	-0.06	-0.10	0.06	0.02	**0.82**

Statistical significant correlations were observed for Na, Ca, Al, Fe and Ba. For Mg, Cu and Zn (elements with a symmetric distribution in the analysed plants) a lower correlation was observed.

The two-way joining Cluster Analysis and PCA methods were applied to better reveal the variability of profile for content of elements in medicinal plants under study. Heat maps (Figure 3) were depicted by choosing a colour graduation starting with the green tone for the low values below the mean content, up to the red tones above these values. Based on similarity pattern approaches, in both countries the concentration of elements depends on the variety of medicinal plants. Significant differences between medicinal plants from North Macedonia and Romania were observed especially for K, Ca, Mg, Al and Fe content which can be considered as important constituents for originating growth area of the plants. Also, in both countries *Stinging nettle* (Sn), *Horsetail* (Ho), *Peppermint* (Pe), *Bean* (Be) and *Elderberry* (El) have a high content in Ca and Mg while *Blackberry* (Bl) is characterized by high content in Al. Plants as *Elderberry* (El), *Dandelion* (Da), *Valerian* (Va) and *Blackberry* (Bl) from Romania were observed to have a high content in K comparative with content in samples from North Macedonia.

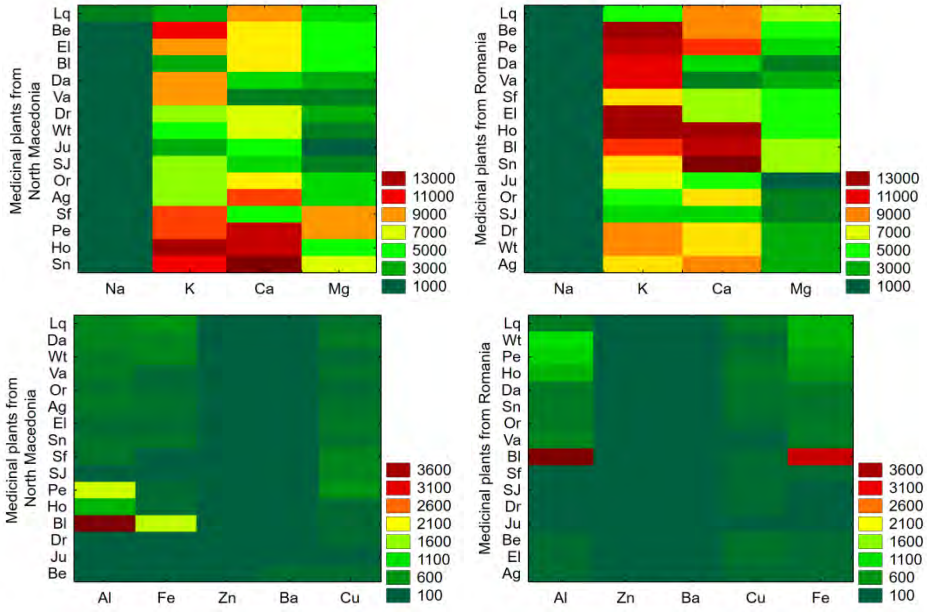

Figure 3. Two-way joining heat map revealing the variation of macroelements and microelements content (mg kg^{-1}) in medicinal plants from North Macedonia and Romania. The sample code of medicinal plants is presented in the experimental part, Table 5.

Based on the heat maps from the auto-scaled values of determinations (Figure 4), some markers were revealed as differentiating the elemental profile of some of the analysed medicinal plants from two countries. Among the analysed elements potassium differentiate *Stinging nettle* (Sn) and *Elderberry* (El), cupper differentiate *Horsetail* (Ho), *St.John's wort* (SJ) and *Sweet fennel* (Sf) while magnesium is an important element that differentiate the elemental profile of *Liquorice* (Lq), *Blackberry* (Bl), *Bean* (Be), *Elderberry* (El) and *Horsetail* (Ho) from North Macedonia and Romania.

The PCA analysis (Table 3) shows that variability of the characteristics in the medicinal plants under study from North Macedonia is described in proportion of 83.4% by four factors with a strong contribution (loadings > 0.700) for Mg, Ca, Al, Fe, Na, Cu, Zn and moderate contribution (0.500 < loadings < 0.700) for K and Ba. The first factor describing 29.4 % of elemental content variation is mainly due to Mg and Ca, but also to K and has been associated with soil carbonates, the main source of Ca and Mg. The second factor (23.3% variability) is due to Al and Fe and has been associated with the hydroxides contained in soil, the main source of these elements.

The third factor (18.0% variability) is mainly due to Na but also to Ba which has a medium influence. Copper and Zn, two essential microelements for plants, describe 12.7% of the characteristics variability of the plants under study.

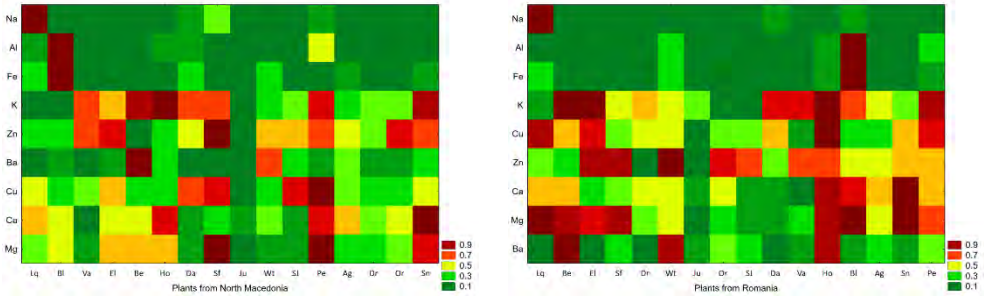

Figure 4. Two-way joining heat map revealing the elemental markers in medicinal plants from North Macedonia and Romania. The sample code of medicinal plants is presented in the experimental part, Table 5.

Table 3. Factor loadings after Varimax rotation of the first PCs with eigenvalue >1.0 reflecting the contribution of each variable in the characteristics of medicinal plants from North Macedonia. (Bold face loadings values > 0.700, strong contribution; Italic loadings values >0.500, moderate contribution).

Essential elements	**Factor 1**	**Factor 2**	**Factor 3**	**Factor 4**
Na	0.12	0.08	**0.92**	-0.09
K	*0.62*	0.31	-0.43	0.37
Mg	**0.92**	-0.15	0.06	0.23
Al	0.14	**-0.96**	-0.03	-0.00
Ca	**0.93**	-0.05	0.05	-0.04
Fe	-0.04	**-0.93**	0.09	-0.18
Cu	0.17	0.07	0.14	**0.82**
Zn	0.07	0.11	-0.06	**0.86**
Ba	0.12	0.18	*-0.66*	-0.41
Total variance (%)	29.4	23.3	18.0	12.7
Cumulative variance (%)	29.4	52.7	70.6	83.4

The variability of medicinal plants in Romania (Table 4) is described in proportion of 70.0% by the first three factors, similar to 70.6% for plants from North Macedonia. Instead of this, there are differences between the contributions of elements on the characteristics variability. Thus, 33.1% is

due to Al and Fe variability associated with the hydroxides contained soil. A variability of 20.3% is due to Ba but also Na, K and Zn, and 16.5% is due to Mg, Cu and Na. In both countries the influence of macroelements in high concentration, as is for example K, was not revealed by a single factor. A similar observation was revealed for Na in case of plants from Romania.

Table 4. Factor loadings after Varimax rotation of the first PCs with eigenvalue >1.0 reflecting the contribution of each variable in the characteristics of medicinal plants from Romania. (Bold face loadings values > 0.700, strong contribution; Italic loadings values >0.500, moderate contribution).

Essential elements	**Factor 1**	**Factor 2**	**Factor 3**
Na	0.02	*-0.65*	*0.57*
K	0.05	*0.64*	0.31
Mg	0.30	0.10	0.81
Al	**0.98**	0.09	0.09
Ca	0.38	0.13	0.66
Fe	**0.97**	-0.04	0.14
Cu	-0.17	0.25	0.85
Zn	0.05	*0.56*	0.00
Ba	-0.03	**0.73**	0.26
Total variance (%)	33.1	20.3	16.5
Cumulative variance (%)	33.1	53.4	70.0

The differences between the factors variability for plants in two countries could be explained by differences between the soils on which they grew, namely a mountainous calcareous soil with higher carbonate content in North Macedonia, and one dominated by Fe and Al hydroxides in Romania. It would also explain the differences between plant varieties in these two countries.

CONCLUSIONS

The existence of a regional pattern of medicinal plants originating in North Macedonia and Romania has been demonstrated based on the macroelements and microelements content. Among the studied elements, the content of K, Ca, Mg, Al and Fe can be considered as a marker parameter for medicinal plants. Medicinal plants such as blackberry and peppermint have been found to bio-accumulate the Al and Fe. The content of Na, Al, Fe and Ba showed an asymmetric distribution while that of K, Ca and Zn showed a symmetric distribution for plants in both countries. Some elements such as Mg showed a symmetric distribution only in plants from Romania. In general, a significant correlation was observed between elements with asymmetric distribution. The

PCA analysis showed that the first four factors and the first three factors describe over 83.4% for North Macedonia and 70.0% for Romania with a strong influence from Ca, Mg, Al and Fe content. These were associated with the different soil composition of these two countries. The first factor in plants from North Macedonia was described by Ca and Mg in accordance with calcareous soil while the first factor in plants from Romania was described by Al and Fe in accordance with presence of hydroxides in the soil.

The PCA analysis showed that indeed the content of Ca, Mg, Al and Fe can be used for discriminating the medicinal plants from these two countries, which was also highlighted by the two-way joining Cluster Analysis. Obviously, the combination of elemental analysis and chemometric methods is an efficient approach in the study of regional pattern and characterization of the medicinal plants from different countries.

EXPERIMENTAL SECTION

Reagents and standards

Nitric acid (69%) and hydrogen peroxide (30%) of analytical reagent grade used for samples digestion were purchased from Merck (Darmstadt, Germany). Double distilled water was used through this study. An ICP multielement standard solution IV (CertiPUR IV, traceable to NIST, Merck, Darmstadt, Germany) contained 23 elements (1000 mg L^{-1}) in diluted nitric acid was used for preparation of calibration standards in the range 0–1.0 mg L^{-1} element (n= 5) in 2% (v/v) diluted nitric acid, necessary for ICP -OES method. The calibration standards in the range 0-5.0 mg L^{-1} Na and K (n=6) in 2% v/v nitric acid were used in FAES method.

Description of medicinal plants and samples

The study was carried out on different vegetal parts (root, leave, flower, fruit and seeds) of 38 medicinal plants from North Macedonia and Romania (Table 5). The plants originated from North Macedonia were collected from the south-eastern part of the country, from three localities in the basin of the Osogovo Mountains. They were identified by determination key using the data from Matevski [15], a specimen being kept in the herbarium at the Department of Plant Production, Faculty of Agriculture, Goce Delcev University in Štip, North Macedonia. Samples of medicinal plants of Romania were purchased from a local specialized market.

Table 5. Description and provenience of investigated medicinal plants.

No.	Common name	Genus (taxonomic rank)	Familly	Part of the plant	Code of sample
1	Liquorice	*Glycyrrhiza glabra L.*	Fabaceae	*radix*	Lq[1a]
				radix	Lq [1b]
				radix	Lq [2]
2	Dandelion	*Taraxacum officinale F.H.Wigg.*	Asteraceae	*radix*	Da[1]
				radix	Da[2]
3	Valerian	*Valeriana officinalis L.*	Caprifoliaceae	*radix*	Va[1]
				radix	Va[2]
4	Sweet fennel	*Feniculum vulgare var. dulcis Mill.*	Apiaceae	*fructus*	Sf[1a]
				fructus	Sf[1b]
				fructus	Sw[2]
5	Dog rose	*Rosa canina L.*	Rosaceae	*fructus*	Dr[1]
				fructus	Dr[2]
6	Juniper	*Juniperus communis L.*	Cupresaceae	*fructus*	Ju[1]
				fructus	Ju[2]
7	Bean	*Phaseolus vulgaris L.*	Fabaceae	*pericarpum*	Be[1]
				pericarpum	Be[2]
8	Elderberry	*Sambucus nigra L.*	Adoxaceae	*flos*	El[1]
				flos	El[2]
9	Wild thyme	*Thymus serpyllum L.*	Lamiaceae	*herba*	Wt[1a]
				herba	Wt[1b]
				herba	Wt[2]
10	Oregano	*Origanum vulgare L.*	Lamiaceae	*herba*	Or[1]
				herba	Or[2]
11	Horsetail	*Equisetum arvense L.*	Equisetaceae	*herba*	Ho[1]
				herba	Ho[2]
12	Peppermint	*Mentha x piperita L.*	Lamiaceae	*folium*	Pe[1]
				herba	Pe[2a]
				folium	Pe[2b]
13	Blackberry	*Rubus fructicosus L.*	Rosaceae	*folium*	Bl[1]
				folium	Bl[2]
14	St.John's wort	*Hypericum perforatum L.*	Hypericaceae	*herba*	SJ[1a]
				herba	SJ[1b]
				herba	SJ[2]
15	Agrimony	*Agrimonia eupatoria L.*	Rosaceae	*herba*	Ag[1]
				herba	Ag[2]
16	Stinging nettle	*Urtica dioica L.*	Urticaceae	*semen*	Sn[1a]
				folium	Sn[1b]
				herba	Sn[2]

[1] - Medicinal plants from North Macedonia; [2] - Medicinal plants from Romania

Samples preparation

Amounts of 0.50 g powdered vegetal material (n = 3 paralel samples) weighed were overnight predigested in 10 mL of HNO_3 (69%), and subjected to microwave-assisted digestion after 2 ml of H_2O_2 (30%) addition. The microwave digestion program is provided in Supplementary material Table S2.

After cooling, the digest was transferred into 100 ml volumetric flask, filtered and stored in polyethylene bottles at room temperature until analysis.

Instrumentation

The SPECTRO CIROS^{CCD} spectrometer (Spectro, Kleve, Germany) was used for the ICP-OES measurements. Instrumental details and operating conditions are summarized in Supplementary material Table S3. Determination of elements was based on external calibration using a 5-point linear calibration curve over the range 0 – 1.0 mg L^{-1} element in 2% HNO_3 (v/v). The emission signals as peak heights were measured using the best signal-to-noise ration SNR strategy for 48 s integration time.

The two points model approach was used for background correction. The most sensitive emission lines free of spectral interferences were selected.

For Na and K determination the FAES instrument using methane-air flame was interfaced with a low resolution microspectrometrer HR 4000 200-1100 nm spectral range Ocean Optix (Dunedin, USA). The flame was operated so that a stable burning was obtained. The emission spectrum was recorded using 500 ms integration time. The selected wavelengths were Na 588.995 nm and K 766.49 nm.

A MW3S+ Berghof model closed-vessel microwave digestion system (Berghof, Germany) with temperature monitoring option up to 210 °C was used for sample mineralization.

Analytical performance and methods validation

The analytical performances of the ICP-OES and FAES methods were evaluated in terms of the limit of detection (LOD), limit of quantification (LOQ), precision and accuracy. LOD was calculated using the (3σ) criterion and parameters of the calibration curve [16].

$$LOD = \frac{3s_b}{m} \quad (1)$$

where (s_b) is the standard deviation of background assessed from 11 measurements of reagent blank 2% V/V HNO_3, while (m) the slope of the calibration curve.

LOQ was considered as 3xLOD. Values of LOD and LOQ in solid sample were calculated taking into account the sample preparation protocol. Statistical evaluation of the linear calibration function was assessed according to SR ISO 8466-1 [17]. The parameters of the calibration curves (LODs and LOQs) for ICP-OES and FAES methods are presented in Supplementary material Table S4.

A good linearity of the calibration curves with determination coefficients in the range 0.9949 – 1.0000 was obtained. The LODs were in the range 0.068 (Ba) – 8.471 (Pb) mg kg^{-1} while LOQs were in the range 0.205 – 25.413 mg kg^{-1} in ICP-OES (Table 1). The LODs in FAES were 10.27 mg kg^{-1} for Na and 0.051 mg kg^{-1} for K.

The ICP-OES and FAES methods were previously validated by analysing a several materials of vegetables and fruits providing recovery in the range 87-108% [18]. The relative expanded uncertainly (k=2, 95%) was in the range 9-25%. The major contribution to combine standard uncertainty come from replicate analysis, fitting and standard preparation.

Statistical analysis

Two-way joining cluster analysis was used to reveal the elements significantly different in medicinal plants samples and to better explore variability in elemental composition on samples from North Macedonia and Romania. Two-way clustering is a common multivariate technique used to analyse complex data matrices and produces a heat map graph (two-way display of a data matrix) ordering cases and variables based on similarity patterns. The individual cells in the heat map are displayed as colored rectangles where the color of a cell is proportional to its position along a color gradient. The elements were shown as column variables of the data matrix while the variety medicinal plants were shown as rows.

The PCA with varimax rotation approach was used to maximize the variation expressed by the principal components (PCs). The varimax rotation algorithm rearrange the amount of variance among principal components, so each new factor has only few variables with significant contribution (large loadings) and many others with no significant contribution (low loadings). In this study only PCs with eigenvalue >1 were retained for varimax rotation method.

Correlations and multivariate statistical analyses were performed using the Software Package Statistica 8.0 (StatSoft inc. 1984-2007, USA).

ACKNOWLEDGMENTS

This work was supported by a grant of Ministry of Research and Innovation, Romania, Project number 33PFE/2018, within PNCDI III.

REFERENCES

1. R.P. Chouldhry; R. Acharyu; A.G.C. Nair; A.V.R. Reddy; A.N. Garg; *J. Radioanal. Nucl. Chem*. **2004**,*120*, 85-93.
2. E.I. Obianjunwa; C. Adeleke; O. Adebajo; O. Omubuwajo; *J. Radioanal. Nucl. Chemistry*; **2004**, *252*, 473-476.
3. A. Łozak; K. Sołtyk; M. Kiljan; Z. Fijałek; P. Ostapczuk; *Pol. J. Nutr. Sci*. **2012**, *62*, 97-102.
4. S.A. Sattar; B.S. Reddy; V.K. Rao; A.S. Pradeep; G.J.N. Raju; K. Ramanarayana; P.V.M. Rao; S.B. Reddy; *J. Radioanal. Nucl. Chem*. **2012**, *294*, 337-341.
5. H. Matsuura; A. Hokura; F. Katsuki; A. Itoh; H. Haraguchi; *Anal. Sci*. **2001**,*17*, 391-398.
6. V.A. Aletor; O.A. Omodara; *Anim. Feed Sci. Technol*. **1994**, *46*, 343-348.
7. A.M. Ebrahim; M.H. Eltayeb; H. Khalid; H. Mohamed; W. Abdalla; P. Grill; B. Michalke; *J. Nat. Med*. **2012**, *66*, 671-679.
8. S.S. Ranđelović; D.A. Kostić; A.R. Zarubica; S.S. Mitić; M.N. Mitić; *Hem. Ind*. **2013**, *67*, 585-591.
9. (2007) WHO (World Health Organization) guidelines for assessing quality of herbal medicines with reference to contaminants and residues. Geneva 2007.
10. (2011) WHO (World Health Organization) The world traditional medicines situation. in Traditional Medicines: Global Situation, Issues and Challenges. WHO, Geneva, Switzerland 3: 1-14.
11. P.S.C. Silva; L.S. Francisconi; R.D.M.R. Gonçalve, *J. Braz. Chem. Soc.*, **2016**, *27*, 2273-2289.
12. D. Casoni; M. Ponta; M.-N. Bibica; I.-V. Lazar; T. Frentiu; *Rev. Roum. Chim.*, **2020**, *65*, 573-578.
13. W. Kathe; S. Honnef; A. Heym; Medicinal and Aromatic Plants in Albania, Bosnia-Herzegovina, Bulgaria, Croatia and Romania. Geography, Social and Political Structure, Biodiversity and Nature Conservation, Wild-Harvesting and Cultivation of MAPs, Bundesamt für Naturschutz, Bonn, **2003**, pp. 30–34.
14. H.M. Sabo; Res. J. Agric. Sci. **2012**, 44, 226–232.
15. V. Matevski; Flora of the Republic of Macedonia, 1st Edition, Macedonian Academy of Science and Arts, Skopje, **2010**.
16. J.N. Miller; J.C. Miller; Statistics and chemometrics for analytical chemistry, 4th Edition, Pearson Education Ltd., Edinburgh Gate, England, **2000**.
17. SR ISO 8466-1:1999. Water quality. Calibration and evaluation of analytical methods and estimation of performance characteristics. Part I. Statistical evaluation of the linear calibration function
18. E. Covaci; M. Senila; M. Ponta; T. Frentiu; *Rev. Roum. Chim*., **2020**, 65, 735-745.

STUDIA UBB CHEMIA, LXVI, 2, 2021 (p. 23-40)
(RECOMMENDED CITATION)
DOI:10.24193/subbchem.2021.2.02

THE INFLUENCE OF ASSORTMENT OF BEER ON THEIR ANTIOXIDANT / PRO-OXIDANT CAPACITY AND PHENOLIC FINGERPRINT

CLAUDIA CIMPOIU[a,b*], ANCA MILNA[a], VIRGIL DANCIU[a], ANAMARIA HOSU[a,b]

ABSTRACT. Different assortments of beers, packed in cans and bottles, exist on the market. Beer has a complex and balanced composition, phenolic compounds being one class of bioactive constituents that are of particular interest due to their essential role in the brewing process, physical stability and aroma of this beverage. The aim of this paper is to integrate antioxidant and pro-oxidant evaluation, total phenolic content (TPC) determination, chromatographic fingerprinting and chemometric methods in order to study the influence of the variety and the packing type for beer assortment recognition. The antioxidant capacity evaluation was done by 2,2-azinobis(3-ethylbenzothiazolyne-6-sulphonic acid) radical cation (ABTS) assay and Folin-Ciocalteu method was used and to determine the TPC. Thin-layer chromatography (TLC) and high performance liquid chromatography (HPLC) were applied to obtain the fingerprints of beers. The results show that antioxidant and pro-oxidant capacities, the TPC and the chromatographic fingerprints were influenced by the packing type, the assortment, the alcoholic content and the colour of beer. Principal component analysis and cluster analysis were applied to study the influence of the variety and bottling type of beers on their characteristics. The results demonstrate that by integrating various methods the classification of beers based on their assortment was enable.

Keywords: *antioxidant capacity, pro-oxidant capacity, phenolics fingerprint, beer assortment, TLC,HPLC, PCA, cluster analysis*

[a] *Babeş-Bolyai University, Faculty of Chemistry and Chemical Engineering, 11 Arany Janos str., RO-400028, Cluj-Napoca, Romania*
[b] *Research Center for Advanced Chemical Analysis, Instrumentation and Chemometrics, 11 Arany Janos, 400028 Cluj-Napoca, Romania*
** Corresponding author e-mail: claudia.cimpoiu@ubbcluj.ro*

INTRODUCTION

Beer is one of the most commonly consumed alcoholic beverages all over the world. The basic ingredients of beer are water, malt, hop and yeast. Therefore, their characteristics together with the brewing technologies are of major importance on beer quality [1]. Beer has a complex and balanced composition and compared with other popular natural alcoholic beverages, including wine, beer has a higher nutritional value given by minerals, amino acids, vitamins, carbohydrates and antioxidants [2]. Moreover, it has a low carbohydrate contents and fewer calories and it does not contain any fat [3].

Considering the great number of beer manufacturers, different criteria such as: the fermentation process (top or bottom fermentation), the color (dark or light), the alcohol content (light or strong), the type of added materials, the origin, etc. could be used for the categorization of beers [4]. Regardless of its type, any beer must satisfy some quality requirements: microbial, flavor, colloidal and foam stability [5]. The main factor affecting the taste and aroma of beer is the presence of oxygen, which is unavoidable despite the filling developed technologies. Antioxidant compounds play an important role in maintaining and extending the stability of beer by reducing the effects of oxidation processes. Therefore, beside the antioxidant compounds which naturally exist in beer, others (ascorbic acid, vitamin E) are sometimes added [6]. The main endogenous antioxidants of beer are phenolic compounds and melanoidins. Melanoidins and precursors of natural polyphenols may also have pro-oxidant properties by involving them in the process of oxidation of alcohols to aldehydes during the storage of beer [7]. Phenolic compounds are derived from malt (70–80%) and hop (20–30%), and include mainly simple phenols, benzoic- and cinnamic acid derivatives, coumarins, catechins, di-, tri- and oligomeric proanthocyanidins, chalcones and various flavonoids [8]. Melanoidins are Maillard reaction products, formed during the malting and brewing process, their content being higher in dark beers than in the light ones [9]. The endogenous antioxidants from beer are of major interest not only for brewers, in order to produce qualitative beer, but also for the nutritionists because they are important bioactive compounds with implications in maintaining and ensuring of human health. This is due to the fact that they have biological activities such as: antioxidant effect, anti-inflammatory action, anti-cancer activity, estrogen antagonistic properties, etc. [8]. Therefore, the moderate consumption of beer is associated with lower incidence of cancer, degenerative and cardiovascular diseases and osteoporosis [2,8].

The analysis of phenolics from beverages can be approached from two different perspectives: the determination of the total phenolic content which is a global assay and the identification and determination of individual phenolic constituents, thus establishing the phenolic profile of a sample. TPC is usually determined by colorimetric methods, based on the reaction between phenolics and different reagents, the commonly used method being the Folin-Ciocalteu assay. An important aspect that must be considered when Folin-Ciocalteu method is applied is that it is not specific for phenolics, these compounds interfering with others with reducing activity (e.g., proteins, Maillard reaction products, sulphite, etc.) [10,11]. Therefore, obtaining the phenolic profile is of major interest. For this purpose, in case of plants or beverage analysis, high performance thin layer chromatography(HPTLC) is often applied [12-14]. Literature shows that only one application of TLC was reported in analysis of beer [15], high performance liquid chromatography (HPLC) with UV [16,17], photodiode array [18-20],electrochemical [21-23] and mass spectrometry [24,25] detection being the most frequent applied technique in order to obtain the phenolic profiles of beers [26,27].

The phenolic content of beer is usually correlated with the antioxidant capacity, which could be determined spectrophotometricaly by various assays based on different reaction mechanisms: electron transfer (ET) of a reduction reaction and hydrogen atoms transfer (HAT). The first mechanism is involved in trolox equivalent antioxidant capacity (TEAC), ferric-ion reducing antioxidant parameter (FRAP), trolox equivalent antioxidant capacity (DPPH), and cupric reducing antioxidant capacity (CUPRAC) assays, the other one being applied in oxygen radical absorbance capacity (ORAC) and total radical trapping antioxidant parameter (TRAP) assays [28]. Also, different constituents of beer with antioxidant activity, such as phenolic compounds and melanoidins, might exhibit pro-oxidant activity in combination with transition metal ions (especially reduced iron and copper ions) involved in the generation of reactive oxygen species which cause the oxidative degradation of beer [29]. Although the pro-oxidant capacity could be evaluated by spectrophotometric measurements, usually by indirect methods [30,31], their application in beer analysis has not been described so far.

Considering the complexity of beer composition and its activities and the fact that from our knowledge there is a lack of information in this direction about beers, the aim of this paper is to study the influence of beer assortments on the antioxidant and pro-oxidant activities, total phenolic content. Also, by integrating spectrophotometric measurements, chromatographic fingerprinting and chemometric evaluation of data a new possibility of beer recognition was obtained.

RESULTS AND DISCUSSION

Spectrophotometric determinations, TLC and HPLC methods were applied in the analysis of five different types of beer, each packed in glass bottles and cans, in order to evaluate the influence of assortment on the antioxidant/ pro-oxidant capacities, on phenolic constituents and on the chromatographic fingerprintings of beer.

All the experimental results obtained by spectrophotometric measurements are presented in Table 1.

Table 1. The antioxidant and pro-oxidant capacities and total phenolic content of analyzed beers.

Beer type		Antioxidant capacity (mg vit C/mL)	Pro-oxidant capacity			TPC (mg gallic acid/mL)
			Equation	R^2	mL	
Premium (1)	B	0.776±0.012	y=1.7661x+0.2277	0.9732	0.437±0.004	1.211±0.003
	C	0.815±0.010	y=2.0499x+0.2433	0.9865	0.369±0.002	1.366±0.001
Non-alcoholic (2)	B	0.637±0.009	y=0.8723x+0.0884	0.9858	0.745±0.002	0.656±0.008
	C	0.782±0.011	y=1.4923x+0.1843	0.9979	0.447±0.003	0.734±0.007
Non-alcoholic Cooler (3)	B	0.859±0.007	y=3.3848x+0.0031	0.9995	0.295±0.002	0.556±0.013
	C	0.943±0.009	y=3.6513x+0.2185	0.9916	0.214±0.003	0.585±0.009
Cooler (4)	B	1.443±0.013	y=2.4624x+0.1567	0.9904	0.342±0.005	0.751±0.005
	C	1.471±0.009	y=2.8173x+0.1832	0.9907	0.290±0.002	0.790±0.006
Black (5)	B	1.243±0.011	y=5.3766x+0.1985	0.9903	0.149±0.001	1.431±0.011
	C	1.359±0.008	y=5.9372x+0.2239	0.9884	0.131±0.002	1.640±0.009

1. Antioxidant and pro-oxidant capacities

Antioxidant capacity of different types of beer was determined using the ABTS assay that measure the ability of antioxidant compounds to act as free radical scavenger agents, in comparison with different standard compounds, such as Trolox, gallic acid, vitamin C [3]. The obtained results presented in Table 1 exhibit that Cooler beers containing alcohol (4), packaged both in bottle (B) or can (C) have the highest antioxidant capacities (1.443 mg vit C/ mL and 1.471 mg vit C/ mL, respectively) followed by the Black beer (5) whose antioxidant capacities are 1.243 mg vit C/ mL in the bottle beer (B) and 1.359 mg vit C/ mL in the can (C) one. The lowest antioxidant capacities are obtained for non- alcoholic beers (2), the values being about 2 times smaller than those of Cooler beers containing alcohol (4) ones. The fact that Cooler beers

have the highest antioxidant capacities can be explained by their composition, because they contain lemon juice, orange juice and ascorbic acid added to prevent the oxidative degradation and to improve their flavor stability, compounds which are known to exhibit high antioxidant activities [6]. Moreover, the Cooler beer (4) contain alcohol (1.9%), which makes their antioxidant capacity higher compared to non-alcoholic beers (2) and even with non-alcoholic Cooler beers (3), whose antioxidant capacities are more than 1.5 times smaller, even if except alcohol, they have the same composition as the last ones. Also, Black beer (5), which have the highest alcohol contents, exert the highest antioxidant capacities among alcoholic beers (1, 4 and 5), while non-alcoholic ones (2) have the lowest antioxidant capacities, showing that the antioxidant capacities increases with the increasing of alcohol content. These findings are in agreement with those reported in literature [3,11,32]. Another remark is that for all the analyzed samples, the antioxidant capacity of can beers are higher than those of bottled beers, maybe due to the packing type, because metallic materials from packing systems such cans preserve the quality of beverages, due to its potential action against reactive oxygen species [33]. Statistical analysis proves that the antioxidant capacity of beer is significantly influenced (p<0.05) by the packing mode (p=0.0268) and by the assortment (p = 0.0006), respectively. Also, antioxidant capacity is also influenced by the color of beer. Thus, in the case of Black beer (5), higher antioxidant capacity is observed than in normal colored beers (1, 2). These results are according to other data presented in literature, showing that raw materials such as dark malt which contains melanoidins and reductones formed in kilning or roasting processes, together with the brewing process might have considerable impacts on the antioxidant capacity of beer [11,26].

The experimental results (Table 1) illustrate that pro-oxidant capacities follow an opposite trend to antioxidant capacities, thus the highest value is exhibited by the non-alcoholic beer packed in glass bottle (0.745 mL) (2, 3), while the can of Black beer have the lowest pro-oxidant capacity (0.131 mL). Also, Cooler beers (3, 4) exhibit pro-oxidant capacities lower than those of beers which does not contain lemonade. It can be observed that irrespective of type, beers packed in glass bottle have higher pro-oxidant capacities than those from cans. Statistical analysis proves that the pro-oxidant capacity of beer is significantly influenced (p < 0.05) by the packing type (p=0.000003) and by the assortment (p=0.000025). From our knowledge, other data regarding the determination of the pro-oxidant capacity of beers have not been reported in literature so far.

2. Total phenolic content (TPC)

The results (Table 2) show that considerable differences in the TPC values of the analyzed beers are obtained, varying from 0.556 mg gallic acid/ mL in non-alcoholic Cooler beer packed in glass bottle to 1.640 mg gallic acid/ mL in can

of black beer. The TPC of the analyzed samples were higher than those reported by Zhao et al. [11] (152.01-339.12 mg gallic acid/ L), Mitić et al. [34] (328.22-545.32 mg gallic acid/ L) and Piazzon et al. [35] (366–622 mg gallic acid/ L). The fact that both non-alcoholic and alcoholic Cooler beers (3, 4) have low TPC values also explain that the high antioxidant capacity of these beers are due to the lemonade containing ascorbic acid that has been added to beer, rather than to the phenolic compounds. Also, the TPC of non alcoholic beers (2, 3) is lower compared with those determined for the alcoholic ones (1, 4).

Regardless of the beer type, it can be observed that for all samples the TPC is lower in bottled beers than in the can ones. Those are supported by the statistical analysis which prove that both the packing type (p=0.0211) and the assortment of beers (p=0.0005) significantly influence (p<0.05) their TPC.

Otherwise, the results from Folin–Ciocalteu method reflect together with phenols the products of Maillard reaction, sulfite or other substance with reducing activity, so in order to reveal the differences on phenolic profiles of beers the separation of individual compounds are of great importance. However, spectrophotometric determination of the phenolic content of beers was useful to assess if the results obtained by chromatographic fingerprinting are following the same trend.

3. Chromatographic analysis

3.1. TLC fingerprinting

In order to optimize the separation of phenolic compounds from beer, several solvent systems were tested on two stationary phases with different polarity (HPTLC Silica gel 60F_{254} and TLC Silica gel 60RP-18F_{254S}). First, some chromatographic systems were tested for the separation of phenols from beers. Thus, the TLC separation were performed either on TLC silica gel 60F_{254} using benzene/ ethyl acetate/ formic acid 6:3:1 v/v/v, toluene/ acetone/ formic acid 9:9:2 v/v/v, ethyl acetate/ acetone/ formic acid/ water 5:3:1:1 v/v/v/v, chloroform/ methanol/ formic acid 44:3:24 v/v/v and n-hexane/ ethyl acetate/ acetic acid 30:14:5 v/v/v. Separation were also done on TLC silica gel 60RP-18 F_{254S} developed with toluene/ ethanol/ formic acid/ n-hexane 30:9:2:9 v/v/v/v and with methanol/ water/ o-phosphoric acid 50:50:1 v/v/v. The best separation of phenols was achieved on TLC silica gel 60 RP-18 F254S plate developed with mixture of methanol/ water/ *o*-phosphoric acid 50:50:1 v/v/v (Figure 1a). The documentation of plate in UV light reveals that at 366nm sufficient information is obtained to fingerprinting and differentiation beers. The fingerprints show that the content of phenols differs from one beer to another, both as composition and concentration. Moreover, even in the case of same beers, it can be observed differences between the separated compounds, depending on the type of packing. Thus, both the intensity of the bands (Figure 1a) and the

chromatograms (Figure 1b) reveal that the content of phenols is higher in case of can beers (C) than in the case of bottle beers (B). Also, the both non-alcoholic and alcoholic Cooler beers (3 and 4) contain specific compounds that are not detected in all the other beers and may be derived from the lemonade. Another remark is that the beers containing alcohol have higher phenolic content than those without alcohol (Figure 1a and 1c). One unpredictably observation is that, though non-alcoholic Cooler beer (3) contains lemonade, it has a lower phenolic content than the non-alcoholic beer (2) (Figure 1d).

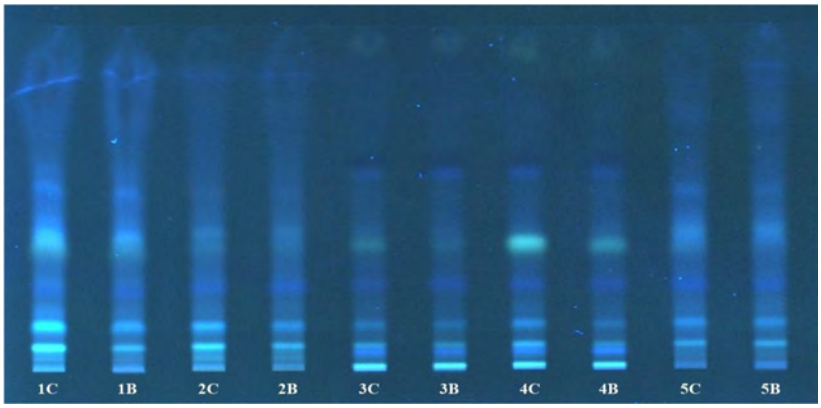

a

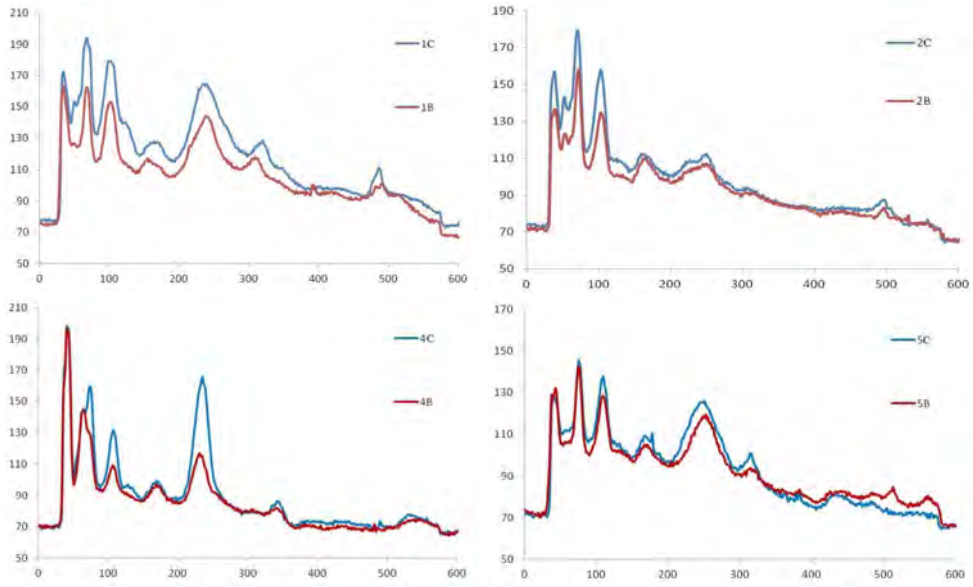

b

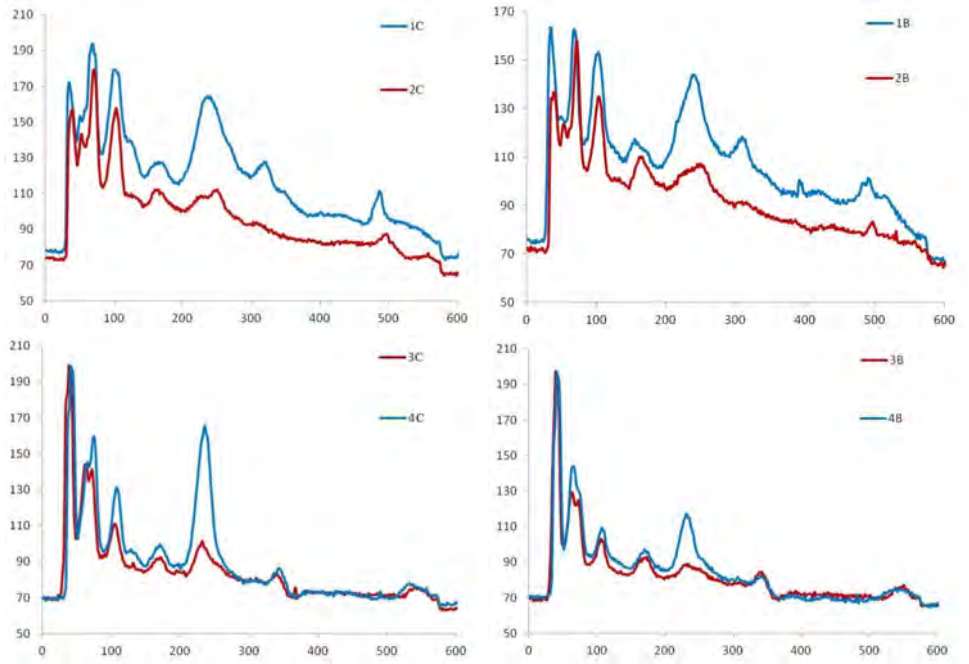

c

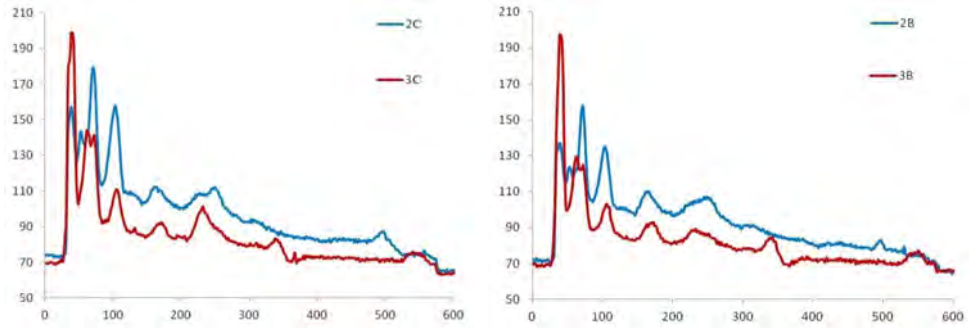

d

Figure 1. The HPTLC phenolic profile of beers: (a) HPTLC fingerprints on silica gel 60RP-18F_{254s} developed with methanol- water- phosphoric acid, 50:50:1 (v/v/v) in UV light at 366nm, after derivatization with NP/ PEG; and the chromatograms of (b) the same beers packed in can and bottle, (c) alcoholic beers and non – alcoholic beers, (d) non – alcoholic beer and non – alcoholic Cooler beer.

This may be due to the fact that non-alcoholic Cooler beer contain only 40% of non-alcoholic beer and 60% of lemonade, the latter having a not- too-high phenolic content. All these findings are in concordance with the spectrophotometric obtained results (Table 2).

3.2. HPLC fingerprinting

Different gradients of mobile phase were tested to find the used one, which allowed obtaining the HPLC fingerprints of beers samples with a relatively high amount of information. It is found mainly in the elution time window between 4 min and 13 min, which represents the most characteristic part of the fingerprint (Figure 2).

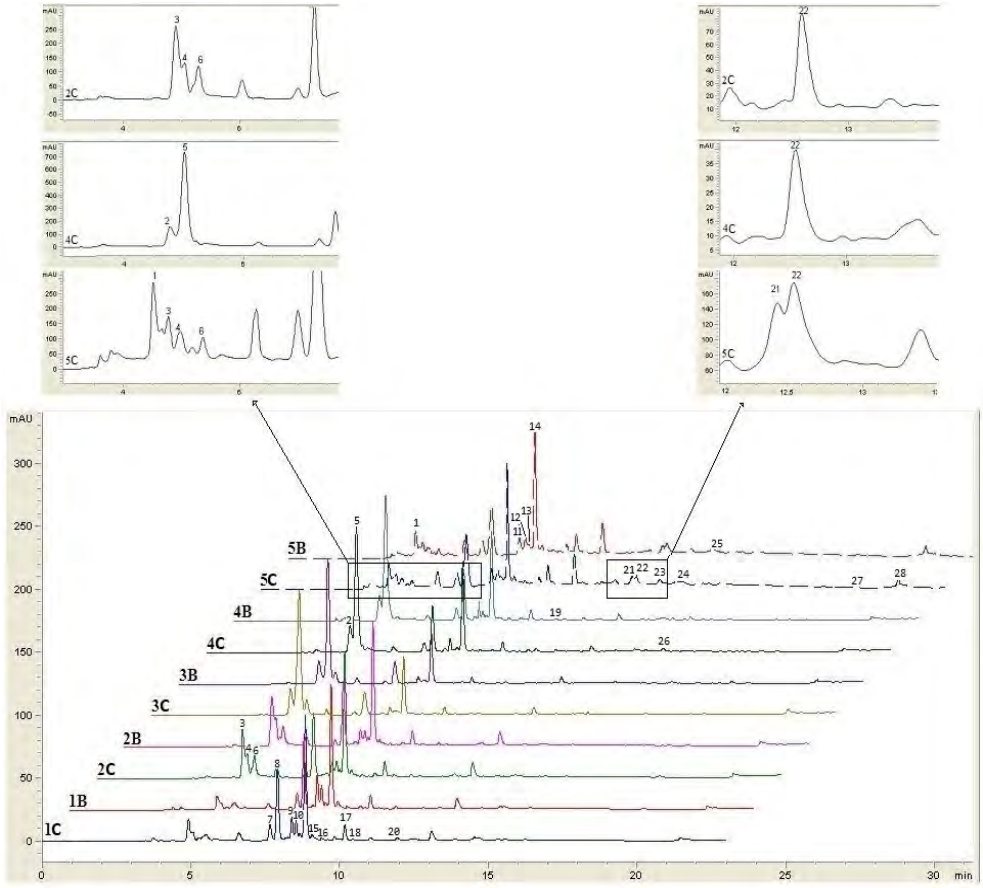

Figure 2. The HPLC chromatograms of beers.

The HPLC fingerprints show that that the absorption intensity and the number of the chromatographic peaks differ from one sample to another, depending on the assortment of beer and on the type of bottling. Visually the fingerprints reveal similar chromatographic profiles and from the twenty-eight chromatographic peaks obtained, fourteen of them could be identified as common peaks in almost all beer samples (Table 2).

Table 2. The areas of the HPLC chromatographic peaks of the analyzed beers.

Comp	Beer									
	1C	**1B**	**2C**	**2B**	**3C**	**3B**	**4C**	**4B**	**5C**	**5B**
1	nd	nd	nd	nd	nd	nd	nd	nd	1377	1391
2	nd	nd	nd	nd	980.6	991.8	1099	1134	nd	nd
3	1899	1093	1872	1789	nd	nd	nd	nd	570.9	544.6
4	505.4	299.7	565.9	549.3	nd	nd	nd	nd	411.5	336.8
5	nd	nd	nd	nd	5449	5862	5371	6188	nd	nd
6	568.2	561.9	668.0	359.0	350.5	254.8	nd	nd	322.4	366.5
7	779.9	463.1	420.3	341.1	207.5	203.2	203.2	208.3	1153	1138
8	1029	845.5	245.1	190.0	112.5	95.7	331.2	395.3	1134	1107
9	4733	3780	2125	1974	991.5	979.2	1534	1623	4787	4701
10	nd	98.67	nd	nd	nd	nd	72.18	63.87	nd	nd
11	869.5	1315	236.8	255.3	178.8	182.9	301.2	380.0	770.6	808.9
12	645.6	732.9	195.9	176.7	81.2	49.8	nd	109.2	573.0	436.3
13	nd	78.3	54.8	48.9	57.1	48.3	53.2	44.6	145.1	159.9
14	7140	6507	3302	3284	1521	1565	2574	2620	6556	6501
15	232.0	316.4	87.7	50.6	nd	nd	nd	nd	190.9	192.8
16	nd	nd	77.2	62.6	nd	nd	nd	nd	423.5	504.9
17	901.1	778.0	369.2	357.4	174.0	170.5	272.9	301.7	958.2	1046
18	209.0	164.2	78.3	76.6	42.4	32.9	67.8	72.6	1980	1936
19	nd	nd	nd	nd	60.3	63.4	91.2	38.8	nd	nd
20	118.8	65.5	nd	nd	nd	nd	nd	nd	nd	nd
21	nd	nd	nd	nd	nd	nd	nd	nd	561.7	628.5
22	797.0	825.1	468.3	432.8	213.9	201.6	206.5	235.5	911.8	838.3
23	79.2	72.1	51.0	46.8	nd	nd	nd	nd	316.8	349.5
24	239.7	179.7	72.6	68.1	46.1	51.6	87.6	83.6	328.1	357.1
25	235.1	186.2	56.5	51.2	30.1	32.8	75.4	80.2	351.1	291.2
26	nd	nd	nd	nd	nd	nd	91.9	87.8	nd	nd
27	83.6	81.1	57.1	49.7	30.2	26.6	35.4	32.3	109.1	117.8
28	196.1	178.0	103.2	119.6	131.8	102.8	91.0	116.2	557.5	620.8

The obtained chromatograms indicate that there are compounds which are characteristic for each beer assortment. Compound 20 is specific for Premium beers (1), compound 1 and 21 are only found in Black beers (5), having a higher concentration in bottled beer than in can one, and also compound 26 is present in Cooler beers (4). In the first part of the chromatogram, until minute 6, compounds 2 and 5 can be observed in beer samples containing lemon juice (3 and 4), with peak areas of approximate 1000mAU and 5500mAU, respectively, which may occur from the lemonade added in beer. Compounds 3 and 4 are found in Premium (1), non-alcoholic (2) and black (5) beer samples, but they are not present in beers containing lemonade (3 and 4). Also, compound 23 is not present in alcoholic and non-alcoholic Cooler beers (3 and 4) and has a high concentration in black beers (5). Moreover, compound 10 is only found in Premium beer packaged in bottle (1B) and in Cooler beers (4).

Significant differences among the contents of the same compounds were observed in different beer assortments, for example, the highest area of compound 14 was 7140mAU in sample 1C and the lowest 1521mAU in sample 3C. Also, compounds 22, 24 and 25 are common in all beers with the highest areas in black beer (5) and lowest in non alcoholic Cooler beer (3). Compounds 27 and 28 are found in all beer samples with highest concentration in black beer (5) and the lowest ones in non-alcoholic and alcoholic Cooler beer 3 and 4, respectively.

The chromatograms of the same beer packaged in glass bottle and in can indicate that, whatever type of beer is considered, the area of almost all chromatographic peaks are higher in case of can beer than in the bottle one. This finding is in concordance with the results obtained both from TLC analysis and also by spectrophotometric determination of TPC (Table 1). There are some differences between samples of the same beer, for example, compounds 10 and 13 being found in sample 1C, but not in sample 1B. Also, the compound 12 is found in all samples, including 4B but it is not present in sample 4C. Moreover, for all types of beer the concentration of compound 14 is higher in can beers than in bottle ones, with the exception of Cooler beers (3, 4), when its concentration is higher in bottle beer (B) than in the can one (C). Compounds 8 and 11 are found in all beer types with lower areas in non-alcoholic beers (2, 3) and lower areas in bottled beers (B) than in can ones (C), with exception of Black beers in which these compounds are in higher concentrations in can beer (C) than in bottle one (B).

4. Statistical analysis

First, PCA and CA were applied separately on data from TLC and from HPLC, but the results show that the beers cannot be classified according to their type only by a single fingerprint. Therefore, it is expected that the use

of data both from the digitized TLC chromatograms and the areas of major peaks from LC chromatograms together with spectrophotometric data in one statistical analysis allow a better classification of beers as a result of the large number of variables.

The PCA of the combined data matrix (676 pixels/row for 10 samples) was performed in order to classify the beers according to their type. It can be seen from the Figure 3 that first two principal components retain a cumulative variance of 93.15% making a clear distinction and classification of beers according to their type.

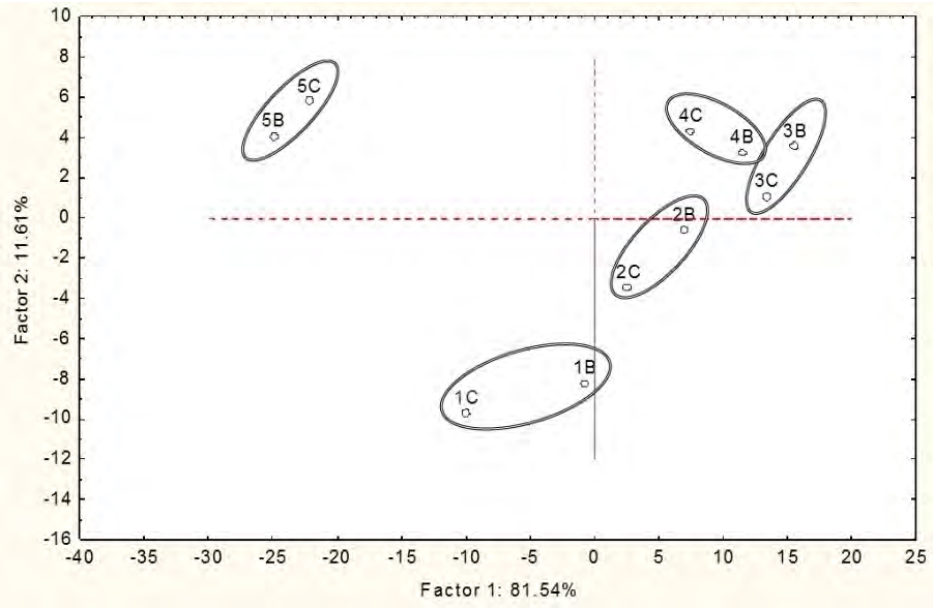

Figure 3. The classification of beers obtained by PC1-PC2 scores plot

Also, the data were subjected to cluster analysis (CA) in order to establish the relationships between beers without using any prior information about these relationships. The samples were grouped according to their similarities using as a clustering criterion Ward's method with Square Euclidian distance as a measure interval between groups. The obtained classification is illustrated by a dendrogram (Figure 4) in which the beers have similar properties within a cluster and different proprieties between clusters.

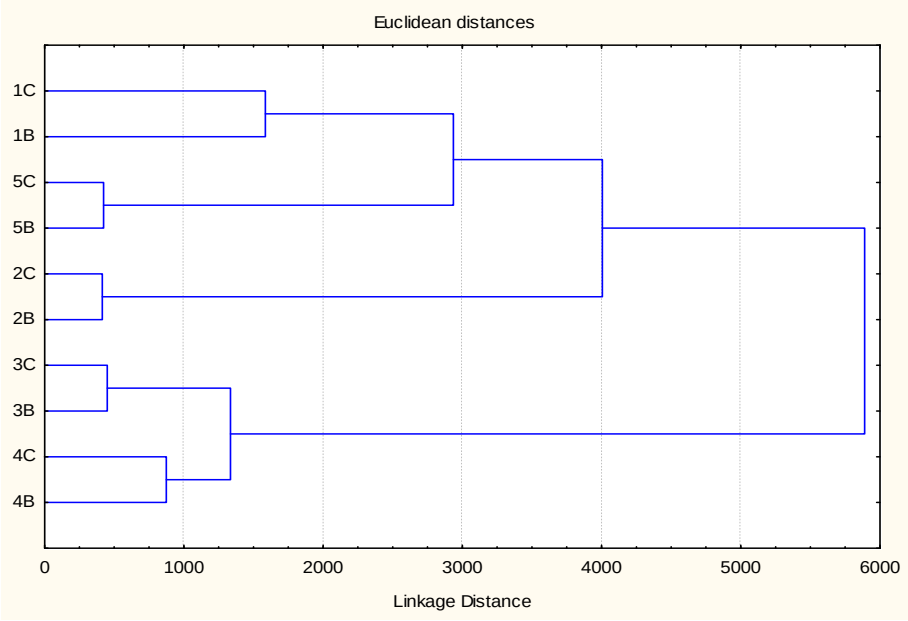

Figure 4. The classification of beers obtained by cluster analysis.

CONCLUSIONS

The results reveal that the antioxidant/ pro-oxidant capacities, the TPC and the chromatographic fingerprints of the analyze beers depend on the assortment, the bottling type, the alcoholic content and the color of the beer. The antioxidant capacity and the TPC follow the same trend in all samples, excepting the Cooler beers, which have high antioxidant capacities but low TPC values, proving that the added lemonade does not improve the phenolic profile of the beer. This fact is also sustained by TLC and HPLC results. The determination of the pro-oxidant capacity of beers is reported for the first time, and the obtained results have an opposite trend than the antioxidant capacities.

The obtained TLC and HPLC fingerprints reveals similar chromatographic profiles, some compounds being present in all beer samples and other being specific for each type of beer. The chromatographic data obtained by two different techniques provide complementary information that allows reliable differentiation of beers. The PCA and CA are successfully used in distinguishing the beers according to their type. The integrated spectrophotometric, chromatographic and chemometric methods enable to study the influence of the type of beers on their properties and to recognize the beer. Moreover, this type of approach can be useful for classification and a further authentication of the beer.

EXPERIMENTAL SECTION

1. Reagents and chemicals

All solvents used were of HPLC grade, acetonitrile, methanol, phosphoric acid and formic acid were purchased from Merck (Darmstadt, Germany) Diphenylborinic acid aminoethylester, polyethylene glycol 400 (macrogol), sodium carbonate ($Na_2CO_{3)}$, 2,2'-azinobis(3-ethylbenzothiazoline-6-sulfonic acid) diammonium salt (ABTS), potassium persulfate (K2S2O8), potassium ferricyanide, trichloroacetic acid, iron chloride (FeCl3), Folin Ciocalteu reagent, gallic acid, vitamin C, ethyl acetate, dichloromethane, toluene, chloroform, ethanol, n-hexane, acetic acid, and the chromatographic plates (TLC Silica gel $60F_{254}$ and TLC Silica gel 60RP-18 F_{254S}) having the size of 20X10 cm were purchased from Merck (Darmstadt, Germany).

The dipping solutions for TLC analysis were prepared as follow: 1 g of diphenylborinic acid aminoethylester was dissolved in 200 mL ethyl acetate for Natural Products (NP) solution and 10 g of polyethylene glycol 400 was dissolved in 200 mL dichloromethane for polyethylene glycol (PEG) solution.

2. Samples

Five commercial beers, namely Premium (1), Non-alcoholic (2), Cooler non-alcoholic (3), Cooler (4) and Black (5), each packed in glass bottle (B) and can (C), produced by Ursus Brewerieswere obtained from the local market, stored in refrigerator at 4°C and analyzed immediately upon opening to avoid loss of phenols by oxidation. The ingredients of beers, as they are declared by the producer on the label, are presented in Table 3.

Table 3. The characteristic and ingredients of the analyzed beers.

Beer assortment	Ingredients	Alcohol content (%, v/v)
Premium (1)	water, barley malt, hop	5
Non-alcoholic (2)	water, barley malt, hop	0
Non-alcoholic Cooler (3)	60% lemonade (water, sugar, lemon juice from concentrate (3%), orange juice from concentrate, natural lemon flavor, natural orange flavor, natural, ascorbic acid, carruba seed gum) and 40% non-alcoholic beer from malt (water, barley malt, hop)	0
Cooler (4)	60% lemonade (water, sugar, lemon juice from concentrate (3%), orange juice from concentrate, natural lemon flavor, natural orange flavor, natural, ascorbic acid, carruba seed gum) and 40% beer from malt (water, barley malt, hop)	1.9
Black (5)	water, barley malt, hop	6

3. Spectrophotometric measurements

All spectrophotometric measurements were done in triplicate, at room temperature, using a double-beam spectrophotometer T80+ (PG Instruments LTD, Lutterworth, UK). For the determination of the antioxidant capacity and total phenolic content, beers were appropriately diluted before spectrophotometric measurements, so the values of the absorbance were between 0.200 and 0.800.

3.1. Antioxidant capacity

The antioxidant capacity was determined by ABTS assay [31] with some modification. The $ABTS^{\bullet+}$ stock solution was prepared by mixing of ABTS solution (7 mM) and $K_2S_2O_8$ solution (2.45 mM) in volumetric ratio of 1:1, 24 h beforeusing. 0.05 mL of sample was mixed with 2.95 mL of $ABTS^{\bullet+}$ solution having an absorbance around 0.800. The absorbance was read after 15 min at 734 nm and the antioxidant capacity calculated using the calibration curve for vitamin C, was expressed as vitamin C equivalents (mg vit C/ mL of beer).

3.2. Pro-oxidant capacity

The determination of pro-oxidant capacity of beer is based on their reducing power of iron ion in a Fenton reaction and was established by method described by [31]. All beers were diluted 2, 5, 10, 20 and 50 times. 2 mL of diluted beer was mixed with equal volume of potassium ferricyanide solution (1 %) and was incubated for 20 min at 50°C. Then 2 mL of trichloroacetic acid solution (10 %) was added and the mixture was centrifuged for 10 min at 3000 rot/min, using a Centurion Scientific centrifuge C2006 (Centurion Scientific Limited, Bosham, UK). After that, 2 mL of supernatant was mixed with 2 mL of $FeCl_3$ solution (1%) and 2 mL of water and the absorbance of obtained solution was read at 700 nm using water as blank. The pro-oxidant capacity was calculated from linear regression curves being expressed as mL of beer for which an absorbance equal to 1.000 was obtained.

3.3. Determination of TPC

TPC was determined using Folin-Ciocalteu method [36] with some modifications. 0.3 mL of diluted beer was mixed with 1.5 mL of Folin-Ciocalteu reagent (0.2 N) and after 5 min, 1.2 mL of Na_2CO_3 solution (0.7 M) were added. The absorbance was measured at 760 nm after the mixture reacted for 2 h in the dark. The results were expressed as mg gallic acid/ mL of beer.

4. Chromatographic analysis

4.1. TLC fingerprinting

5 µL of black beer samples and 10 µL of the other samples were applied as bands (6 mm) onthe chromatographic plates) using a Linomat 5 device CAMAG (Basel, Switzerland). Separation was done on TLC Silica gel 60RP-18 F_{254S} with an optimum mobile phase consisting in methanol- water-phosphoric acid, 10:10:0.2 (v/v/v). After elution, the plate was dried, then heated at 100 °C for 3 min and dipped while still hot in the NP solution, dried in cold air and then immersed in the PEG solution. Documentation was done in UV light (366 nm) using a Reprostar 3 system CAMAG (Basel, Switzerland). The images of the plates were digitally processed using ImageJ computer software to obtain the digitized chromatograms.

4.2. HPLC fingerprinting

HPLC analysis was performed using an Agilent 1200 system (Agilent Technologies Inc.; Santa Clara, CA, USA) equipped with a quaternary pump, column heater and a vacuum degasser. Beer samples were diluted 1:1 (v/v) with 0.1 % v/v formic acid prior to HPLC analysis and filtered through 0.2 µm PTFE membrane filter. Then, 20 µL of each sample were analyzed. Separation was performed on ZORBAX Eclipse XDB-C18 column (150 mm X 4.6 mm i.d., 5 µm). Beer separation was achieved with a binary mixture of (A) 0.1 % v/v formic acid in water and (B) 0.1 % v/v formic acid in acetonitrile. The non-linear gradient elution was: 0 min, 2 % B; 2–16 min, 35 % B; 16–18 min, 23 % - 95 % B; 18–20 min, 95% B; 20–21 min, 95% - 5% B, 21-23 min, 5% B; over a 23 min run time, at a constant flow rate of 0.4 L/min, with column temperature 20°C. Detection was achieved with a UV detector at 254 nm and peak areas were processed with the operating HPLC software (ChemStation, Agilent Technologies Inc.; Santa Clara, CA, USA).

5. Statistical analysis

All spectrophotometric reported data are presented as the mean values ± the standard deviation, obtained from the three replicates. The experimental results were subjected to one-way analysis of variance (ANOVA), principal component analysis (PCA), and cluster analysis (CA), using STATISTICA 7 software (StatSoft Inc., Tulsa, USA). The ANOVA analysis was performed in order to determine if the packing type of beers significantly affect the antioxidant/ pro-oxidant capacities and the TPC of beers. The differences were considered to be significant at the level of $p< 0.05$ for 95% probability. The experimental

results obtained from spectrophotometric measurements andfrom digitized TLC and HPLC chromatograms were subjected to PCA and CA in order to classify the beers according to their assortment.

REFERENCES

1. H.M. Bettenhausen; L. Barr; C.D. Broeckling; J.M. Chaparro; C. Holbrook; D. Sedin; A.L. Heuberger; *Food Res. Int.*, **2018**, *113*, 487-504.
2. G. De Gaetano; S. Costanzo; A. Di Castelnuovo; L. Badimon; D. Bejko; A. Alkerwi; G. Chiva-Blanch; R. Estruch; C. La Vecchia; S. Panico; G. Pounis; F. Sofi; S. Stranges; M. Trevisan; F. Ursini; C. Cerletti; M. B. Donati; L. Iacoviello; *Nutr. Metab. Cardiovas.*, **2016**, *26,* 443-467.
3. P.A. Ribeiro Tafulo; R. Barbosa Queiros; C.M. Delerue-Matos; M. Goreti Ferreira Sales; *Food Res. Int.*, **2010**, *43*, 1702–1709.
4. S. Wunderlich; W. Back; Overview of manufacturing beer: Ingredients, process and quality criteria. In *Beer in health and disease prevention*, V. R. Preedy Ed.; Elsevier Academic Press, Amsterdam, Holland, **2009**; pp. 3–16.
5. H. Zhao; Effects of processing stages on the profile of phenolic compounds in beer. In *Processing and Impact on Active Components in Food,* V. R. Preedy Ed.; Elsevier Academic Press, Amsterdam, Holland, **2015**; pp. 533-539.
6. E. Jeney-Nagymate; P. Fodor; *J. Inst. Brew.*, **2007**, *113*, 28–33.
7. D.O. Carvalho; L.M. Gonçalves; L.F. Guido; *Compr. Rev. Food Sci. F.*, **2016**, *15*, 927-943.
8. C. Gerhäuser; *Eur. J. Cancer,* **2005**, *41,* 1941–1954.
9. D. Rivero; S. Pérez-Magariño; M.L. González-Sanjosé; V. Valls-Belles; P. Codoñer; P. Muñiz; *J. Agric. Food Chem.*, **2005**, *53*, 3637-3642.
10. A. Davalos; C. Gomez-Cordoves; B. Bartolome; *J. Agric. Food Chem.,* **2003**, *51,* 2512−2519.
11. Zhao, H.; Chen, W.; Lu, J.; Zhao, M. Phenolic profiles and antioxidant activities of commercial beers. *Food Chem.* **2010**, *119*, 1150–1158.
12. V. Glavnik; I. Vovk; A. Albreht; *J. Chromatogr. A,* **2017**, *1482*, 97-108.
13. A. Hosu; V. Danciu; C. Cimpoiu; *J. Food Compos. Anal.*, **2015**, *41*, 174–180.
14. M. Ligor; O. Kornyšova; A. Maruška; B. Buszewski; *J. Planar Chromatogr.-Mod. TLC,* **2008**, *21*, 355–360.
15. P.M. Ristivojevic; G.E. Morlock; *Food Chem.*, **2018**, 260, 344-353.
16. A. Alonso Garcia; B. Cancho Grande; J. Simal Gandara; *J. Chromatogr. A,* **2004**, *1054*, 175-180.
17. M.T. Walters; A.P. Heasman; P.S. Hughes; *J. Am. Soc. Brew. Chem*., **1997**, *55*, 83-89.
18. L. Montanari; G. Perretti; F. Natella; A. Guidi; P. Fantozzis; *LWT - Food Sci. Technol.*, **1999**; *32*, 535-539.

19. P.J. Magalhães; S.M. Almeida, A.M. Carvalho, L.M. Gonçalves; J.G. Pacheco; J.M. Cruz; L.F. Guido; A.A. Barros; *Food Res. Int.*, **2011**, *44*, 351–359.
20. J.L. Goncalves; V.L. Alvesa; F.P. Rodrigues; J.A. Figueira; J.S. Camara; *J. Chromatogr. A*, **2013**, *1304*, 42– 51.
21. S. Floridi; L. Montanari; O. Marconi; P. Fantozzi; *J. Agric. Food Chem.*, **2003**, *51*, 1548-1554.
22. N. Whittle; H. Eldridge; J. Bartley; *J.I. Brewing*, **1999**, *105*, 89-99.
23. M. Nardini; A. Ghiselli; *Food Chem.*, **2004**, *84*, 137–143.
24. N. Whittle; H. Eldridge; J. Bartley; *J. Inst. Brew.*, **1999**, *105*,89-99.
25. R. Lang; C. Mueller; T. Hofmann; *J. Agric. Food Chem.*, **2006**, *54*, 5755-5762.
26. C. Leitao; E. Marchioni; M. Bergaentzle; M. Zhao; L. Didierjean; B. Taidi; S. Ennahar; *J. Agric. Food Chem.*, **2011**, *59*, 1249–1255.
27. D.O. Carvalho; A.F. Curto; L.F. Guido; Antioxidants, **2015**, *4*, 563-576.
28. D. Huang; B. Ou; R.L. Prior; *J. Agric. Food Chem.*, **2005**, *53*, 1841-1856.
29. L.R. Fukumoto; G. Mazza; *J. Agric. Food Chem.*, **2000**, *48*, 3597-3604.
30. E. Kondakç; M. Özyürek; K. Güçlü; R. Apak; *Talanta* **2013**, *115*, 583–589.
31. B. Moldovan; A. Hosu; L. David; C. Cimpoiu; *Acta Chim. Slov.*, **2016**, *63,* 213-219.
32. D. Koren; C. Orban; N. Gallo; S. Kun; B. Vecseri-Hegyes; G. Kun-Farkas; *J. Food Sci. Technol.*, **2017**, *54*, 1158-1167.
33. M. Ramos; A. Valdes; A.C. Mellinas; M.C. Garrigos; *Beverages,* **2015**, *1*, 248-272.
34. S.S. Mitić; D.D. Paunović; A.N. Pavlović; S.B. Tošić; M.B. Stojković; M.N. Mitić; *Int. J. Food Prop.*, **2014**, *17*, 908-922.
35. A. Piazzon; M. Forte; M. Nardini; *J. Agric. Food Chem.*, **2010**, *58*, 10677–10683.
36. V.L. Singleton; R. Orthofer; R.M. Lamuela-Raventos; *Methods Enzymol.*, **1999**, *299*, 152-178.

STUDIA UBB CHEMIA, LXVI, 2, 2021 (p. 41-48)
(RECOMMENDED CITATION)
DOI:10.24193/subbchem.2021.2.03

FATTY ACIDS COMPOSITION FROM *ROSA CANINA* AND *PRUNUS SPINOSA* PLANT FRUIT OIL

VANDA BĂBĂLĂU-FUSS[a,b], LACRIMIOARA SENILA[a], ANCA BECZE[a], OANA BOGDANA AL-ZABEN[b], MARCEL DIRJA[b,*], MARIA TOFANĂ[b,*]

ABSTRACT. The objective of this study was to determine the fatty acids content from *Rosa canina* and *Prunus spinosa* plant fruit oil via ultrasound-assisted process. The extracted oil's fatty acids were converted into fatty acid methyl esters (FAME) before gas chromatography analyses (GC) equipped with flame ionization detection (FID). Results showed that *Rosa canina* oils contain mainly polyunsaturated fatty acids with the linoleic acid as the major fatty acids (62.3%) followed by oleic acid (28.6%), whereas *Prunus spinosa* oils contain 46.2% oleic acid and 32.6% linoleic acid. *Rosa canina* oil could be used as potential source of linoleic acid.

Keywords: *Rosa canina, Prunus spinosa, Fatty acids, GC-FID*

INTRODUCTION

In several Romanian regions, traditional uses of wild fruits have become an interesting issue. The data about the medicinal properties of certain plants are often lacking scientific base [1].

In the pharmaceutical market, about 40% of modern monomolecular drugs are derived directly or indirectly from plants [2]. *Rosa canina* and *Prunus spinosa* are among those plants that have been insufficiently explored in terms of scientific research related to human health, irrespective of the fact that it is highly rich in valuable bioactive compounds with protective and beneficial properties [3].

[a] *INCDO-INOE2000, Research Institute for Analytical Instrumentation, ICIA Cluj-Napoca Subsidiary, 400293 Cluj-Napoca, Romania*
[b] *University of Agricultural Sciences and Veterinary Medicine Cluj-Napoca, Faculty of Food Science and Technology, 3-5 Calea Mănăştur Street, 400372, Cluj-Napoca, Romania*
** Corresponding authors: maria.tofana@usamvcluj.ro; marcel.dirja@usamvcluj.ro*

Rosa canina, a member of the Rosaceae family, is a shrub widespread in Europe. Rose hip is a well-known herbal antiphlogistic which has been used in folk medicine for thousands of years due to its anti-inflammatory and pain-relieving properties [4]. Rosehips fruits are typically red to orange in color [5]. The fruits are comprised of 30–35% seeds and 65–70% pericarp. Rose hips are remarkable for their medicinal uses, which may be attributed to their profile of bioactive, especially antioxidant phenolics [6]. The seeds contain high amounts of polyunsaturated fatty acids. The fruits of Rosa canina contain high content of proanthocyanins and ascorbic acid (vitamin C) and can be used as regulator of blood fat caused by obesity, raised serum LDL-cholesterol or physical stress [7]. *Rosa canina* fruits have long been used in food and nutrition due to their antioxidant potential, which is attributed to the presence of ascorbic acid and phenolics. A few studies have been reported on the chemical composition of rose hips essential oil [8]. Rose hips have anti-inflammatory properties because reduce inflammatory cytokines and chemokines, C-reactive protein and matrix metalloproteinases [9].

Plum species belong to genus Prunus, tribe Amygdaleae, subfamily Spiraeoideae of the large Rosaceae family. Blackthorn (*Prunus spinosa*) is the fruit of Prunus genus, in the Rosaceae family [10]. This species is growing in forest margins and open woodlands as part of Mediterranean thermophilus plant communities [11]. The fruits are popularly called ‘‘blackthorn’’ or ‘‘sloes’’ and despite their succulent appearance are far too bitter for human consumption, except as flavoring in home-made liqueurs. Sloes are bluish black, bloomy, globular drupe, 10–15 mm with green astringent flesh [12]. Prunus spinosa is usually 2–3 m tall deciduous shrub with long and sharp thorns. It has plum-like fruits that ripen late. Medicinal usage indicates vasoprotective, anti-inflammatory, diuretic, detoxifying (blood purifying), and spasmolytic activities of the flowers, and document their use as ingredients of herbal prescriptions [13].

Prunus spinosa and *Rosa canina* plants are insufficient explored regarding extraction of lipids and acid composition of extracted lipids.

The oil contains fatty acids (FAs) classified, according to the presence or absence of double bonds, in: saturated fatty acids (SFAs—without double bonds), monounsaturated fatty acids (MUFAs—with one double bond) and polyunsaturated fatty acids (PUFAs—with two or up to six double bonds) [14]. The consumption of SFA must to be less that 10% of total energy intake due to its implications in cholesterol metabolism, according to World Health Organization [15]. The methods used for extraction of oil from different sources are liquid-liquid extraction, microwave assisted extraction, ultrasound assisted extraction, etc. The ultrasound assisted extraction is rapid, has high selectivity and short time of extraction [16, 17].

The present work aims to investigate fatty acids composition of oils extracted from rose hip (*Rosa canina*) and blackthorn plant fruit by ultrasound-assisted extraction. The assess of feasibility of this functional ingredient rich in polyunsaturated fatty acids for improving public health will be also evaluated.

RESULTS AND DISCUSSION

Lipid extraction yield

The lipids were extracted from rose hip and blackthorn plant fruit species in two stages: (1) ultrasound assisted extraction with hexane and (2) conversion of oil into FAMES by transesterification. The yield of extracted lipids from rosehip fruit samples was 31.6% ± 5.6% and 28.6% ± 4.1% for blackthorn, respectively.

Rosa canina and *Prunus spinosa* fruits can be used in food and nutrition due to high lipid content. Other previous studies have reported that the oil content in dog rose (*Rosa canina* L.) from Spain was 9.35% by using Soxhlet extraction with petroleum ether [18]. The quality of oil is affected by the methods of extraction applied. According to Tan et al. (2016), hexane is the best solvent used for extraction of high yield oil from different seed samples [19]. Our experimental results indicate also that the highest yield of oil was extracted from rosehip and blackthorn fruit varieties.

Chemical composition of oil from studied fruits

Some studies have reported the chemical composition of oil extracted from *Rosa canina* and *Prunus spinosa* plant fruit [20, 21].

In the present study, GC-FID analysis of oils extracted from fruits revealed the presence of SFA, MUFA and PUFA fatty acids. The standard FAMES mixtures contain SFA, MUFA and PUFA. Chromatogram of the FAME standard mixture is presented in Figure 1.

The peaks of isomers cis and trans of oleic acid (C18:1 (n-9)) and linoleic acid (C18:2 (n-6) overlap. Also, the peak of cis-11,14,17-eicosatrienoic acid (C20:3(n-6)) overlaps with henicosanoic acid (C21:0) and cis-4,7,10,13, 16, 19-docosahexanoic acid (DHA, C22:6(n-6)) and nervonic acid (C24:1(n-9)) coelute. The fatty acids identified in the compositions of the investigated extracts and separated as FAMES by GC method are revealed in Figure 2.

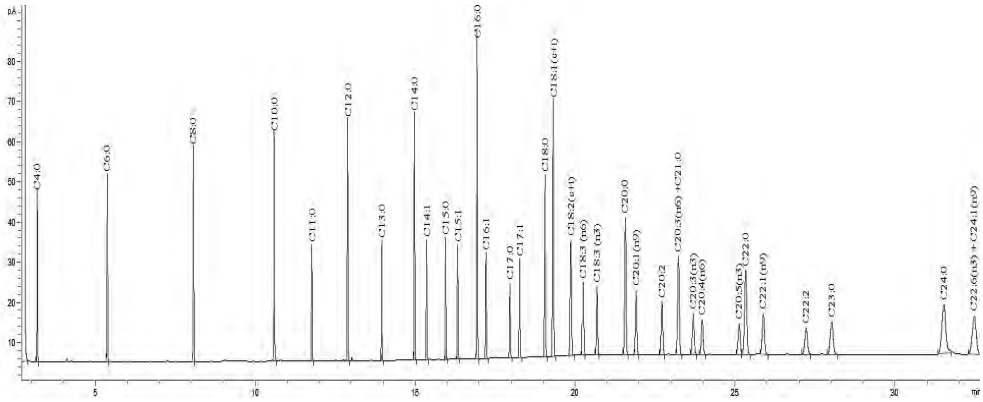

Figure 1. The GC chromatogram of FAMES standard mixture

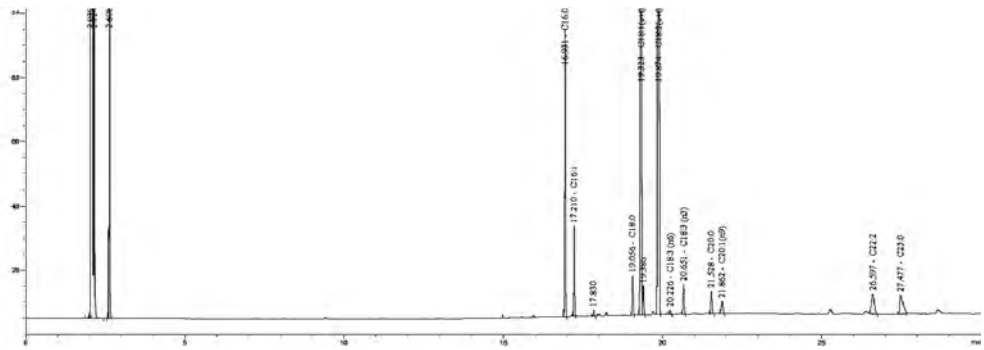

Figure 2. GC chromatogram of rose hip plant fruit oil

The SFAs acids found in studied oil samples are palmitic acid (C16:0), stearic acid (C18:0), arachidic acid (C20:0) and tricosanoic acid (C23:0). Palmitic acid (C16:0) was found to be 6.22 ± 0.04 % in rose hip oil, whereas in *Prunus spinosa* oil was 4.8 ± 0.05%. As can be seen in Table 1, three MUFA acids were found in both oils samples, like palmitoleic (C16:1), oleic acid (C18:1 (*cis*+*trans*)(n-9)) and gondoic acid (C20:1, n-9). The PUFA acids found in studied oils were linoleic (C18:2(*cis*+*trans*) (n-6), linolenic (C18:3, n-3), α-linolenic (C18:3, n-3), cis-13,16-docosadienoic acid (C22:2). The highest value of the linoleic acid (C18:2(*cis*+*trans*) (n-6) was obtained in rose hip oil (62.3% ±0.80%), while in the blackthorn oil was found only 32.6 %± 0.40%. Blackthorn oil contains 46.2 %± 0.85% oleic acid (C18:1 (*cis*+*trans*)(n-9) as majority acid. Linolenic acid content in both varieties was below 1% of the total oil content. Natic et al. reported the following fatty acids compositions for blackthorn from Turkey: 43.9% oleic acid, 37.0% linoleic acid, 5.2% palmitic acid, 2.1% stearic acid and 2.1% arachidic acid [22].

Table 1. The content of SFA, MUFA and PUFA from extracted oil fruits

Fatty acid	Rose hip oil (%)	Blackthorn oil (%)
C16:0	6.22 ± 0.04	4.8 ± 0.05
C16:1(n-7)	0.12 ± 0.03	nd
C17:0	nd	5.1 ± 0.04
C18:0	0.29 ± 0.04	0.05 ± 0.01
C18:1 (*cis*+*trans*)(n-9)	28.6 ± 0.90	46.2 ± 0.85
C18:2(*cis*+*trans*) (n-6)	62.3 ±0.80	32.6 ± 0.40
C18:3 (n-6)	nd	nd
C18:3(n-3)	0.98 ±0.03	0.86 ± 0.04
C20:0	0.5 ±0.02	8.90 ± 0.1
C20:1 (n-9)	0.1 ±0.02	nd
C22:2	0.02 ±0.01	1.08 ±0.06
C23:0	0.03 ±0.01	0.01± 0.01
ΣSFA	7.04 ± 0.8	18.86 ± 0.6
ΣMUFA	28.82 ± 0.88	46.2 ± 0.62
ΣPUFA	63.4 ± 0.56	34.54 ± 0.95
PUFAs/SFAs ratio	9.0	1.83

Values were reported in mean ± standard deviations (n=10). nd- not detected

The results obtained recommended the rose hip oil as a good source of linoleic acid. The obtained results for blackthorn oil varieties revealed a high content of oleic acid (C18:1 cis (n-9)) (46.2 %± 0.85%). The important FAs for health are linolenic and linoleic acids. These FAs are known as essential PUFA since they cannot be synthesized by humans' body and must supplemented from food [23].

Omega-6 has been found in high amount in rose hip oil (62.3% ±0.80%) and 32.6% ± 0.40% in blackthorn. A low quantity of omega-3 was detected in the studied samples (below 1%). The oil obtained from blackthorn has a high content of arachidic acid (C20:0) (8.90%±0.1%). The consumption of oil obtained from blackthorn could prevent cholesterol gallstones by acting as a cholesterol solubilizer, but in reasonable quantities.

The PUFAs/SFAs ratio was very high in rose hip oil (9) and higher than 1 in blackthorn, which recommends their consumption for the prevention of cardiovascular diseases. The PUFA/SFA is an index used for determination of impact of human consumption of fatty acids and their effects on cardiovascular health, according to Chen et al [24]. The PUFA content is much higher in rose hip oil than in blackthorn oil. The dietary guidelines recommend the reduction of SFA intakes [25]. Due to high content of SFA, the oil obtained from blackthorn is recommended for consumption, but with some limitations.

In summary, rose hip oil proves to be a valuable source of linolenic acid and it is recommended for consumption for benefic health.

CONCLUSIONS

In this paper, fatty acids composition of rose hip and blackthorn plant fruit oil were analyzed. The oils were extracted from fruits by ultrasound assisted method with hexane, and analyzed by gas chromatography. The main FA identified in rose hip oil (62.3% ±0.80%) was linoleic acid. Total concentration of mono and polyunsaturated fatty acids in rose hip was 92.22% and 80.74% in blackthorn, respectively. The rose hip oil can be included in food industry due to high linoleic acid content. Due to high percent of SFA found in blackthorn, its limited consumption is recommended. The obtained results could be used for future applications in the field of cosmetics, phytopharmaceuticals and in the food industry.

EXPERIMENTAL SECTION

Chemicals and Reagent

The chemical such as isooctane, potassium hydroxide, methanol, sodium hydrogen sulphate monohydrate of analytic reagent grade, hexane, were purchased from Merck (Darmstadt, Germany). FAME standard mixture (Supelco 37 component FAME mix, CRM47885) was purchased from Sigma–Aldrich (Darmstadt, Germany). All solutions were prepared using ultrapure water (18.2 MΩ/cm, 20 °C) obtained from a Direct-Q3 UV Water Purification System (Millipore, Molsheim, France).

Sample Description

Two different fruit samples (10 samples of each fruit type) were harvested from Cluj-Napoca region, Romania. All the samples were freeze-dried (FreeZone 2.5 LiterBenchtop freeze dry system, Labconco, Kansas, MO, USA) at −40 °C and −25 psi for 24 h to uniform their moisture content. The freeze-dried samples were grounded using an agate mortar and pestle to obtain homogenized powders.

Extraction of Lipids by Ultrasound Assisted Extraction

An amount of 2 g of dried fruit sample was mixed with 10 ml of n-hexane and stirred for 500 rpm. The lipids were extracted in ultrasonic bath for 30 min at room temperature. After extraction, the lipids were separated by filtration, dried by Na_2SO_4 for water removal. The lipid content was determined gravimetrically by using an analytical balance, after hexane evaporation.

Preparation of Fatty Acid Methyl Esters (FAMEs)

Fatty acids methyl esters analysis was performed using the method published by Petrović et al. [26] by conversion of the obtained acids from oils into FAMEs by transesterification with potassium hydroxide. The samples (0.06 g) were dissolved in isooctane, treated with 0.2 mL methanolic potassium hydroxide solution (2 mol/L) and vigorously stirred for 30 s. Finally, the mixture was treated with 1 g sodium hydrogen sulphate to prevent the saponification of the methyl esters and to neutralize excess.

GC Analysis and FAME quantification method

The FAMEs content analysis was carried out using a GC-FID (Agilent Technologies, 6890N GC, Wilmington, DE, USA) equipped with a DB-WAX capillary column with polyethylene glycol stationary phase (30 m × 0.25 mm × 0.25 µm) and a flame ionization detector (Agilent 7683). The gases used for FID analysis were: hydrogen, 40 mL/min; air, 450 mL/min; and make-up helium, 30 mL/min.

The injection volume was 1 µL in 1:20 split mode. The temperature program was as following: the initial oven temperature was set at 60 °C, held for 1 min, from 60 to 200 °C via a ramp of 10 °C/min, held for 2 min and 200 to 220 °C at a ramp of 5 °C/min, held for 20 min). The temperature of the injector and detector was set to 250 °C. The identification of FAs in samples was completed by comparing their retention times with those of the standard mixture. Reference standard of FAMEs (contain 2%-4% relative concentration) are dissolved in isooctane at a 0.01 -0.1% (w/v) to obtain a final concentration 0.2 or 0.4 mg/mL per FAME, before use.

ACKNOWLEDGMENTS

This research and APC was funded by the Competitiveness Operational Program of the Ministry of European Funds, contract no. 7/01.09.2016, code MY SMIS 105654.

REFERENCES

1. W. Guo, E. Kong, M. Meydani, *Nutr. Cancer,* **2009**, *61*, 807–810.
2. M. González-Tejero, M. Casares-Porcel, C.P. Sánchez-Rojas, J.M. Ramiro-Gutiérrez, J. Molero-Mesa, A. Pieroni, *J. Ethnopharmacol.,* **2008**, *116*, 341–357.
3. F. Demir, M. Ozcan, *J. Food Eng.,* **2001**, *47*, 333–336.
4. M. Tabaszewska, D. Najgebauer-Lejko, *NFS Journal*, **2020**, *21*, 50-56.

5. S. Kazaz, H. Baydar, S. Erbas, *Czech J. Food Sci.,* **2009**, *27(3)*, 178–184.
6. C. Chrubasik, B.D. Roufogalis, U. Muller-Ladner, S. Chrubasik, *Phytother. Res.,* **2008**, *22*, 725–733.
7. S.A. Sargin, *J. of Ethnopharmacol.*, **2021**, *265*, 113319.
8. K. Szentmihalyi, P. Vinkler, B. Lakatos, V. Illes, M. Then, *Bioresour. Technol.,* **2002,** *82*, 195–201.
9. J. Gruenwald, R. Uebelhack, M.I. Moré, *Phytomedicine*, **2019**, *60*, 152958.
10. S. Calisir, M. Ozcan, H. Haciseferogullaro, D. Arslan, *J. Food Eng,* **2005**, *66*, 233–237.
11. V. Băbălău-Fuss, A. Becze, A. Moldovan, O.B. Greblă, A.I. Pop, I. Taloș, M. Tofană, *Hop Med. Plants*, **2020**, *1-2*, 218-227.
12. V. Băbălău-Fuss, A. Becze, M. Roman, A. Moldovan, O. Cadar, M. Tofană, *Agriculture*, **2020**, 113, 110-115.
13. T. Murati, M. Miletić, A. Štefanko, I. Landeka Jurčević, I. Elez Garofulić, V. Dragović-Uzelac, I. Kmetič; *S. Afr. J. Bot.,* **2019**, *123*, 36-42.
14. L. Senila, E. Neag, M.H. Kovacs, A. Becze, M. Senila, *Appl. Sci.*, **2020**, *10*, 1589, 1-16.
15. WHO, 2009, Global Health Risks: Mortality and Burden of Diasease Attributable to Selected Major Risks, vol. 20, World Health Organization, Switzerland, Avenue Appia, 1211 Geneva 27.
16. H. Liu, Y. Yao, Y. Ma, X. Wang, *Ultrason. Sonochem.*, **2020**, *63*, 104943.
17. N. Stevanato, C. da Silva, *Ind. Crop Prod.*, **2019**, *132*, 283-291.
18. M. Armenteros; D. Morcuende, S. Ventanas, M. Estévez, *J. Integr. Agric.,* **2013**, *12(11),* 1972-1981.
19. Z. Tan, Z. Yang, Y. Yi, H. Wang, W. Zhou, C. Wang, *Appl. Biochem. Biotechnol.*, **2016,** *179*, 1325-1335.
20. N. Ahmad, F. Anwar, A.-H. Gilani, Rose Hip (Rose canina L.) Oils. Esential oils in Food Preservation, in *Flavor and Safety,* **2016***, Chapter 76,* 667–675.
21. S. Ouerghemmi, H. Sebei, L. Siracusa, G. Ruberto, A. Saija, F.K. Allouche, K. Dhaouadi, F. Cimino, M. Cristani, *Phytochem. Anal.*, **2020**, *31*, 98-111.
22. M. Natić, D.D. Zagorac, I. Ćirić, M. Meland, B. Rabrenović, M.F. Akšić, Cold pressed oils from genus Prunus, in *Cold Pressed Oils*, **2020,** Chapter 56, 637-658.
23. N. Kaur, V. Chugh, A.K. Gupta, *J. Food Sci. Technol.*, **2014**, *51*(10), 2289-2303.
24. J. Chen, H. Liu, *Mol. Sci.*, **2020**, *21*, 1-24.
25. S. Harrison, P. Couture, B. Lamarche, *Nutrients,* **2020,** *12*, 3232, 1-10.
26. M. Petrović, N. Kezić, V. Bolanća, *Food Chem.,* **2010**, *122*, 285–291.

STUDIA UBB CHEMIA, LXVI, 2, 2021 (p. 49-58)
(RECOMMENDED CITATION)
DOI:10.24193/subbchem.2021.2.04

INVESTIGATION OF SYNERGIC/ANTI-SYNERGIC INTERACTIONS OF DIHYDROXIFUMARIC ACID AND ASCORBIC ACID WITH DPPH

CRINA VICOL[a]*, CLAUDIA CIMPOIU[b], GHEORGHE DUCA[a]

ABSTRACT. Reaction of the free-radical 2,2-diphenyl-1-picrylhydrazyl (DPPH) with dihydroxyfumaric acid (DHF) and ascorbic acid (AA) was investigated in ethanolic media and in wine simulated matrix by using a stopped-flow system. The antioxidant activity for both acids were significantly higher in wine matrix, the observed constants (k_{obs}) being about 3 s^{-1} for DHF and 0.66 s^{-1} for AA. Synergic and anti-synergic interactions of DHF and AA against DPPH were also investigated. A strong anti-synergic effect was noticed in ethanol ($k_{obs} <$ 0.35 s^{-1}). In wine simulated matrix the constants were higher than in ethanol ($k_{obs} \approx 1$ s^{-1}), but still too small for a synergic effect. Some explanations concerning the mechanisms of antioxidant action are proposed.

Keywords: *dihydroxyfumaric acid, ascorbic acid, DPPH, wine matrix, stopped-flow*

INTRODUCTION

Dihydroxyfumaric acid (DHF) is a 2-hydroxydicarboxylic acid consisting of fumaric acid having two hydroxy groups at the 2- and 3-positions. Fenton [1] for the first time obtained this compound in 1894 through the oxidation of tartaric acid in the presence of the hydrogen peroxide and Fe (II) [1, 2]. At that time he noticed the reduction power of DHF as long as it could reduce the Ag, Cu, Hg and permanganate salts. DHF is also a very important component in the biosynthesis of the saccharides, uronic acids and vitamin C [3]. Eschenmoser [4] hypothesized that DHF along with the dihydroxymaleic and hydroxyoxalic acids represents the building blocks for the formation of most complex molecules by successive hydrolysis of hydrocyanic acid. The same idea was

[a] *Institute of Chemistry, 3 Academiei, MD-2028, Chisinau, Republic of Moldova*
[b] *Babeş-Bolyai University, Faculty of Chemistry and Chemical Engineering, 11 Arany Janos, RO-400028, Cluj-Napoca, Romania,*
** Corresponding author: crina.smigon@gmail.com*

experimentally supported by Sagi et al. [5]. The authors demonstrated that at the room temperature the Li, Cs and Mg salts of DHF can interact to form more complex molecules.

DHF is also important for its antioxidant properties. Because of the higher reactivity, DHF is instable in the aqueous solutions, being oxidized to the dioxosuccinic acid [5]. It is found to be present in grapes, but in small quantities, being involved in the metabolism of the fruits during the ripening period [6]. Wines contain a low concentration of DHF because of fast decomposition in the aerobic conditions [6]. Added in small quantities (1 – 10 mM), DHF can improve the taste and smell of wines, by inhibiting the oxidation of characteristic polyphenols [7, 8].

DHF and ascorbic acid (AA) are both present in wines mostly by adding them during the wine-making process, as long as their contribution is known to be positive for the quality of the beverage, and respectively, to the total antioxidant capacity of wines [9]. However, not only the presence of the reducing compound is important for the total antioxidant activity of wines. Data reported showed that the species less active as reducing agents have also a significant contribution [10, 11]. For example organic acids like tartaric, malic, citric acids found in big quantities in grapes and wines can enhance the reducing power of the main antioxidants via the synergic interactions.

Many reports [10–13] describe the synergic effect between citric, malic, acetic, tartaric acids with antioxidants from grapes and wines. These results highlight the idea that despite the insignificant antioxidant activity of the organic acids alone, when combined with primary antioxidants, they protect better the main wine compounds.

The assumption of the possible interactions between wine compounds drove the attention of researchers into this area. Thereby, high diversity of studies were performed in a wine model solution, which basically consists of tartaric acid in ethanol-water mixture with an adjusted pH [14–16].

Bearing all this in mind, the aim of this work was to identify the influence of different media on the antioxidant activity of less studied DHF against the free radical DPPH. In addition, the synergic or anti-synergic effect of DHF with AA, both applied at the concentration found in wines, was evaluated.

RESULTS AND DISCUSSION

Absorption spectra of DPPH radical in 98% ethanol and in wine simulated matrix, as well as the spectra for the reduced form of DPPH are reported in Figure 1. The determined value for the molar extinction coefficient of the stock ethanolic solution of DPPH was 11363 $M^{-1}cm^{-1}$, which is in perfect agreement with the data previously reported by others [17–19].

The maximum absorption of the free radical in ethanol is different than in wine matrix. The Figure 1 clearly illustrates this distinction, whereas the absorption maximum in ethanol is found at 517 nm, and in wine matrix at 529 nm. This shifting is due to the changing of solvent and of pH as is described in the literature [17, 20, 21].

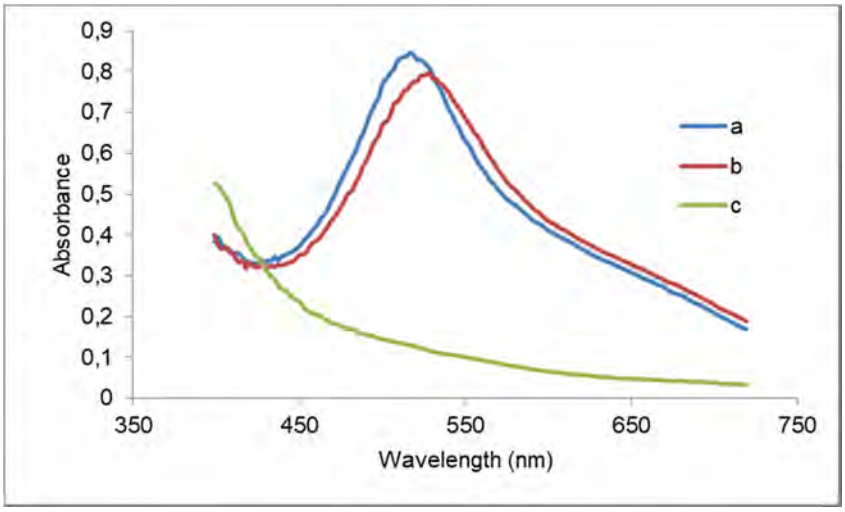

Figure 1. Absorption spectra of DPPH in ethanol (a), DPPH in wine model solution (b) and DPPH-H in wine model solution (c)

The wine simulated matrix as a whole has a small antioxidant activity against the DPPH radical. As depicted in the Figure 2, after the interaction of the DPPH with the wine matrix the decrease in absorbance is minor, the efficiency being of about 3%. Taking into consideration the high concentration of the main constituent of the matrix – tartaric acid, the low DPPH radical scavenging activity of this compound can be underlined. This is in agreement with results obtained by others [10, 11].

A set of spectra were recorder after mixing the solutions of DPPH (0.25 mM) with either 98% ethanol or wine matrix with DHF and AA at different concentrations as displayed in Figure 3. The reaction time was of 2 s. It was found that in ethanol DHF has a low antioxidant activity (Figure 3a), the maximum efficiency being of 16% for the DHF/DPPH molar ratio of 3.2. Contrary to that, in the wine matrix the antioxidant activity of DHF is much higher. The smallest concentration of the acid in the matrix (0.06 mM) reveals the same efficiency (16%) as 0.8 mM ethanolic DHF. The highest concentration of DHF reduces the free radical up to 80% (Figure 3c).

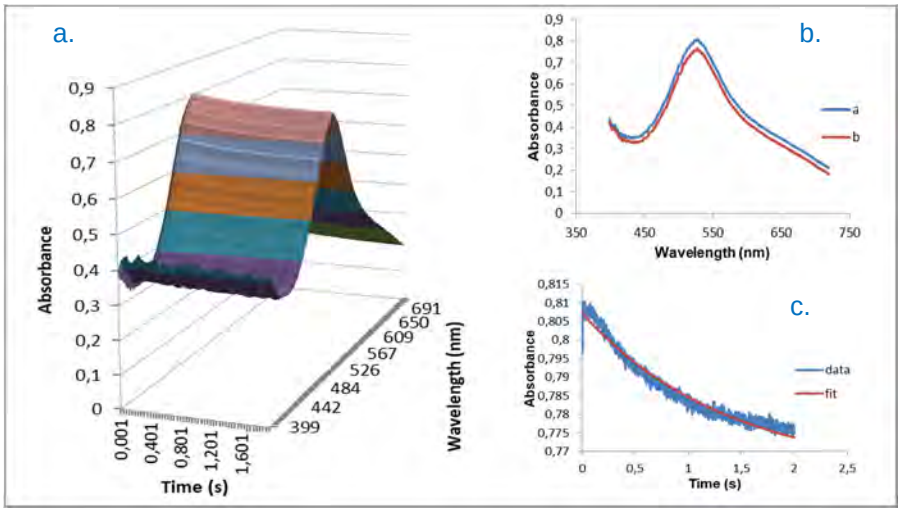

Figure 2. (a) Computed spectra of the interaction of DPPH with the wine simulated matrix. (b) Absorption spectra for the reaction of DPPH with wine simulated matrix at the time 0.001 sec (a) and 2 sec (b). (c) Fitting at the 529 nm for the A→B kinetic model

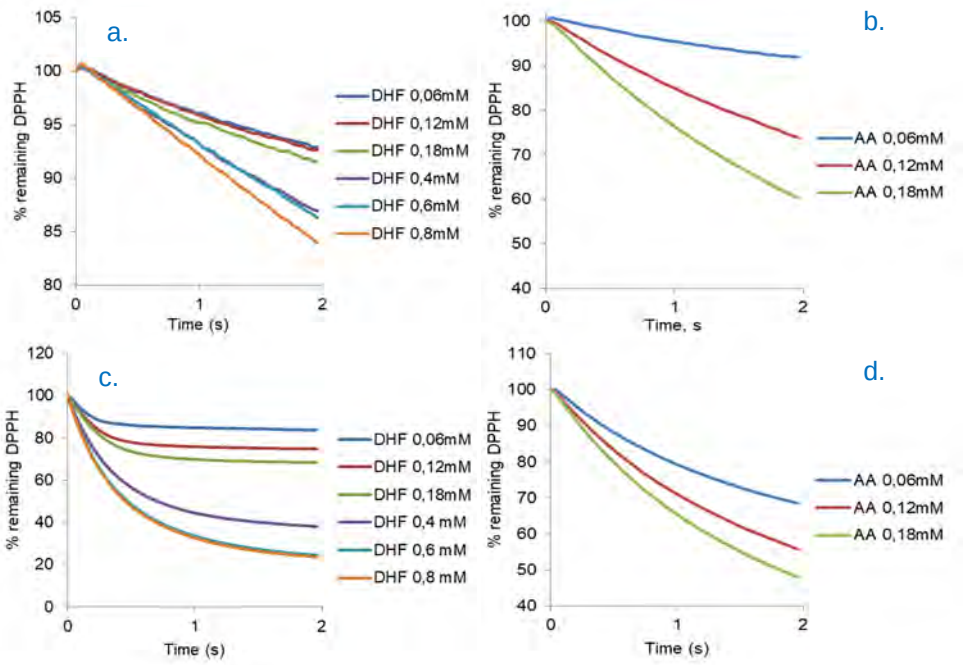

Figure 3. Spectra of the interaction of DPPH with different concentrations of DHF and AA in (a), (b) ethanol, and in (c), (d) wine model solution

As illustrated in Figure 3b, AA has higher antioxidant activity in ethanol comparing to that of DHF in the same solvent, since at the concentration of 0.18 mM AA has the capacity to scavenge 40% of DPPH. The same concentration of AA in the wine matrix reduces more than 50% of the free radical. A considerable change in the antioxidant activity is registered for the smallest concentration of AA (0.06 mM), whose efficiency raises from 10% in ethanol to 30% in wine matrix (Figure 3d). Thus, the DHF show an antioxidant activity almost twice higher than that of AA in both ethanol and wine model solution.

These results are supported by the observed rate constants (k_{obs}) reported in the Table 1. As it can be noticed, in the wine matrix the k_{obs} for the reactions of DPPH with DHF increase 10 times, while the constants for the reactions with AA are twice higher. A similar antioxidant activity of DHF was described by Secara [20]. The author used a methanol – water solution to test the scavenging activity of DHF against DPPH, and obtained a stoichiometric constant of 2.08 for completed reaction. The solvent effect was also reported by Friaa et al. [17], once an important acceleration of the reaction was observed when ethanol–water mixtures were used instead of absolute ethanol, in favor of the electron transfer process.

Table 1. The observed rate constants in ethanol and wine model solution

Sample	Concentration, mM	k_{obs}, s^{-1}	
		Ethanol	Wine model solution
DHF	0.06	0.368 ± 0.049	3.656 ± 0.496
	0.12	0.350 ± 0.030	3.863 ± 0.155
	0.18	0.383 ± 0.054	3.371 ± 0.091
	0.40	0.167 ± 0.024	2.277 ± 0,049
	0.60	0.059 ± 0.062	2.122 ± 0.032
	0.80	0.040 ± 0.016	2.181 ± 0.057
AA	0.06	0.328 ± 0.036	0.654 ± 0.021
	0.12	0.327 ± 0.017	0.653 ± 0.006
	0.18	0.385 ± 0.020	0.681 ± 0.015

In order to determine the presence of synergic or anti-synergic interactions between DHF and AA, a series of experiments were performed using six concentrations of DHF (from 0.06 mM till 0.80 mM) mixed with each of the three concentration of AA (0.06, 0.12 and 0.18 (mM) (see Table 2). The experiments were realized in 98% ethanol and in wine matrix.

The results show the same tendency as described for the antioxidants used alone with DPPH. In 98% ethanol all the mixtures exhibit low antioxidant activity compared to the values obtained in matrix. Figure 4 is well illustrating the influence of the solvent on the kinetics of the reactions. In both examples depicted in the figure the same concentrations of the antioxidants was taken - 0.18 mM for DHF and AA, however in wine simulated matrix the free radical consumption is almost completed after 2 s. For the mixtures with the highest concentrations of the antioxidants, the biggest efficiency in ethanol is of 20%, while in the wine matrix the same combination of antioxidants scavenged 85% of the DPPH.

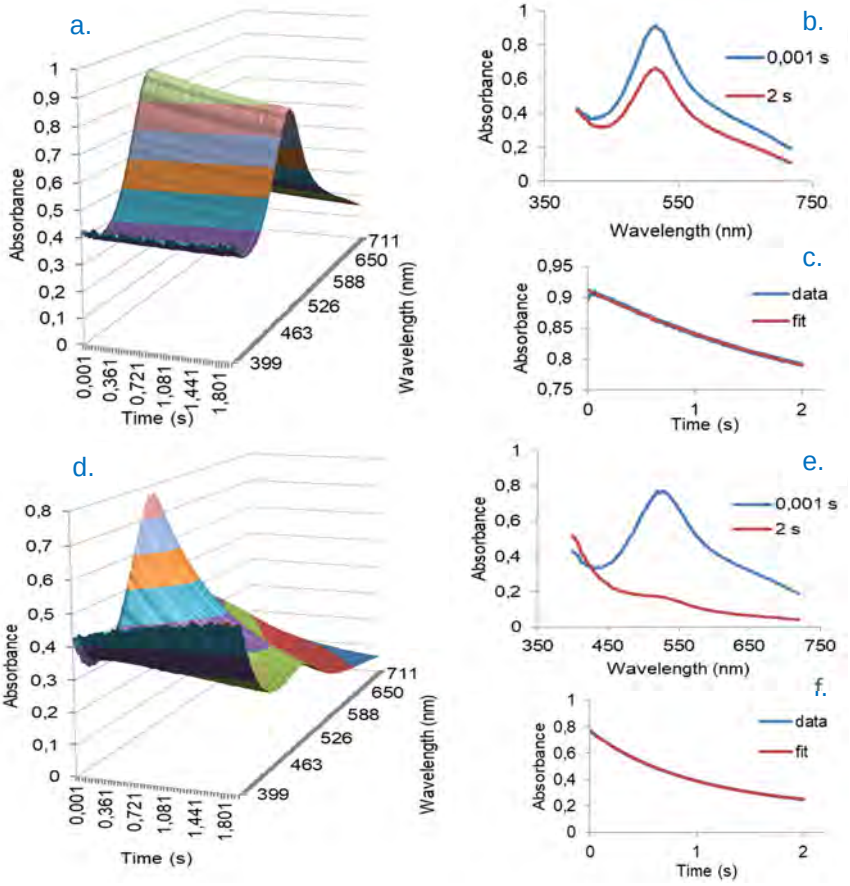

Figure 4. Decrease in absorbance after the interaction of DPPH with the mixture of DHF (0.18 mM) and AA (0.18 mM) in (a) 98% ethanol and (d) wine simulated matrix. Absorption spectra for the reaction of DPPH with mixture DHF - AA at the time 0.001 s. and 2 s. in (b) ethanol and (e) wine simulated matrix. (c), (f) Fitting at the 529 nm for the A→B kinetic model

Data for all the combinations DHF - AA are reported in the Table 2. The values for the k_{obs} obtained reveal a strong anti-synergism between the tested antioxidants in 98% ethanol. The biggest constant of 0.35 s^{-1} is registered for the mixture DHF (0.06 mM) – AA (0,12 mM), this value being smaller than the k_{obs} for DHF alone in ethanol (Table 1).

In the wine matrix the outcomes are improved. The constants range from 0.9 s^{-1} to 1.1 s^{-1}, and are at least three time higher that the k_{obs} in ethanol.

Despite the enhancement in the antioxidant activity of DHF – AA mixtures in the presence of the wine matrix, the anti-synergic effect still remains. This can be noticed by comparing the data in tables 1 and 2. The observed constants for scavenging of DPPH in the wine matrix decrease from values around 3 s^{-1} to values around 1 s^{-1} when DHF is combined with AA in different proportions.

Table 2. The observed rate constants in ethanol and wine model solution for the reaction of DPPH with mixtures of DHF and AA took in different concentrations

Concentration of AA, mM	Concentration of DHF, mM	k_{obs}, s^{-1}	
		Ethanol	Wine model solution
0.06	0.06	0.303 ± 0.040	0.914 ± 0.035
	0.12	0.310 ± 0.032	0.962 ± 0.026
	0.18	0.311 ± 0.021	1.029 ± 0.048
	0.40	0.184 ± 0.015	1.174 ± 0.130
	0.60	0.117 ± 0.008	1.159 ± 0.134
	0.80	0.047 ± 0.011	1.103 ± 0.092
0.12	0.06	0.354 ± 0.010	0.734 ± 0.043
	0.12	0.347 ± 0.022	0.873 ± 0.014
	0.18	0.322 ± 0.035	0.950 ± 0.029
	0.40	0.004 ± 0.000	0.997 ± 0.009
	0.60	0.130 ± 0.007	0.882 ± 0.021
	0.80	0.048 ± 0.008	0.984 ± 0.028
0.18	0.06	0.347 ± 0.016	0.874 ± 0.014
	0.12	0.326 ± 0.009	0.946 ± 0.008
	0.18	0.333 ± 0.017	1.009 ± 0.009
	0.40	0.199 ± 0.018	1.034 ± 0.039
	0.60	0.131 ± 0.011	1.044 ± 0.021
	0.80	0.042 ± 0.030	1.077 ± 0.010

The literature data describes the synergic and anti-synergic effects as being dependent on the nature and concentration of the mixed compounds [22]. It is hypothesized that a combination of two or more antioxidants is considered to be synergetic as one compound can regenerate another [23]. Many authors [24–26] describes as synergetic the combinations of a weak antioxidant with a strong antioxidant, the weaker antioxidant being able to regenerate the strong antioxidant, thus improving overall radical quenching ability of the combination. Contrary to this, the anti-synergic effect assumes that the weak antioxidant is regenerated by the strongest one.

In the present experiment, the large values for the observed constants in the wine matrix can be determined by the presence of tartaric acid as a weak antioxidant that has the capacity to regenerate AA and DHF when the latter ones are used alone against DPPH.

On the contrary, the anti-synergism between these two compounds may be due to the fact that AA is a strong antioxidant, but has to regenerate DHF – at least in the situations when DHF is at higher concentrations. This fact can explain the decrease of the k_{obs} for the mixture of AA with DHF (0.40 – 0.80 (mM)).

CONCLUSIONS

The DPPH method was suitable for determining the antioxidant activity of the less studied compound (DHF) in combination with ascorbic acid in the wine matrix.

Through the stopped flow spectroscopy it was possible to study the fast reactions between DPPH and DHF and AA in 98% ethanol and in wine simulated matrix and to compare the results.

It was found that in the wine matrix the observable constants for the single antioxidants are significantly higher than in ethanol. In the wine matrix, the k_{obs} for DHF are about five times higher than the k_{obs} for AA due to the synergic effect of tartaric acid.

The combination of DHF and AA exhibits a strong anti-synergism in ethanol. Although the antioxidant activity in the simulated wine matrix is higher, the anti-synergic effect remains.

EXPERIMENTAL SECTION

Ethanol (98%) was purchased from Nordic Chemials. 2,2-Diphenyl-1-picrylhydrazyl (DPPH), ascorbic acid (>99%), DHF hydrate (98%) and tartaric acid (99%) were obtained from Sigma-Aldrich.

The wine matrix was prepared by dissolving 5 g/L of tartaric acid in a water – ethanol mixture (12% v/v), then the pH was set at 3.2 by adding sodium hydroxide [16]. The water used for the matrix was ultrapure.

Stock solutions of antioxidants were prepared twice a day, both, in 98% ethanol and in wine matrix. The 0.25 mM DPPH solution was prepared daily only in 98% ethanol. The solutions were sonicated for 5 minutes to increase the rate of dissolution of the antioxidants and the free radical. The same procedure was done in wine simulated matrix for DHF and AA. The working wavelength was chosen based on the absorption spectrum.

UV-Vis spectra were recorded on Cary 50 UV-Vis spectrophotometer (Varian, Inc., Foster City, CA USA), using 1 cm quartz cuvettes. Stopped-flow spectra were collected at room temperature on a Biologic SFM-300 system equipped with three syringes and capable of sequential mixing, with a high-speed diode array detector. All experiments were done in triplicate.

Stopped-flow data were analyzed with SPECFIT32 software package (BioLogic Science Instruments, Seyssinet-Pariset, France) using Singular Value Decomposition (SVD) and global multi-exponential fitting of the SVD treated data, and the spectra were adapted to simple kinetic models using Levenberg - Marquardt or Simplex Algorithms.

ACKNOWLEDGMENTS

The research was carried out within the framework of the Moldavia national project nr. 20.80009.5007.27 and with the financial support of The World Federation of Scientists and Erasmus+ Programme.

Special thanks to PhD student Maria Lehene for her guidance and support in completing the experimental part of the research.

REFERENCES

1. H.J.H. Fenton; *J. Chem. Soc. Trans.*, **1894**, *65*, 899–910.
2. A.C. Clark; *Eur. Food Res. Technol.*, **2008**, *226*, 925–931.
3. L. Hough; J.K.N. Jones; *Nature*, **1951**, *167*, 180–183.
4. A. Eschenmoser; *Chem. Biodivers.*, **2007**, *4*, 554–573.
5. V. Naidu Sagi; P. Karri; F. Hu; R. Krishnamurthy; *Angew. Chemie*, **2011**, *123*, 8277–8280.
6. N. Secara; G. Duca; L. Vlad; F. Macaev; *Chem. J. Mold.*, **2011**, *6*, 29-44.
7. B. García; R. Ruiz; J.M. Leal; *J. Phys. Chem.,* **2008**, *112*, 4921–4928.

8. L. Vacarciuc; *Agricultura*, **2008**, *57*, 1–8.
9. G. Badea; A. Antoce; *Sci. Pap. B, Hortic.*, **2015**, *59*, 123–140.
10. C. Vicol; G. Duca; *Rev. Şt., Inov., Cult. Art. „Akademos"*, **2020**, *56*, 39–43.
11. R. Lo Scalzo; *Food Chem.*,**2008**, *107*, 40–43.
12. W. Piang-Siong; P. De Caro; A. Marvilliers; X. Chasseray; B. Payet; A.S.C. Sing; B. Illien; *Food Chem.*, **2017**, *214*, 447–452.
13. P.R. Quiroga; V. Nepote; M.T. Baumgartner; *Food Chem.*, **2019**, *277*, 267–272.
14. S. Motta; M. Guaita; C. Cassino; A. Bosso; *Food Chem.*, **2020**, *313*, 126045.
15. C. Dallas; J.M. Ricardo-da-Silva; O. Laureano; *J. Agric. Food Chem.*, **1996**, *44*, 2402–2407.
16. P. Comuzzo; F. Battistutta; M. Vendrame; M.S. Páez; G. Luisi; R. Zironi; *Food Chem.*, **2015**, *168*, 107–114.
17. O. Friaa; D. Brault; *Org. Biomol. Chem.*, **2006**, *4*, 2417–2423.
18. J.M. Sendra; E. Sentandreu; J.L. Navarro; *Eur. Food Res. Technol.*, **2006**, *223*, 615–624.
19. D. Villaño; M.S. Fernández-Pachón; M. L. Moyá; A.M. Troncoso; M. C. García-Parrilla; *Talanta*, **2007**, *71*, 230–235.
20. N. Secara; *Chem. J. Mold.,* **2010***, 5*, 83–87.
21. M. Foti; C. Daquino; C. Geraci; *J. Org. Chem*, **2004**, *14*, 2309–2314.
22. U. Cornelli; *Clin. Dermatol.*, **2009**, *27*, 175–194.
23. R. Tsao; *Handbook of antioxidants for food preservation,* Woodhead Publishing, **2015**, pp. 335-347.
24. B.L. Freeman; D.L. Eggett; T.L. Parker; *J. Food Sci.*, **2010**, *75*, 570–576.
25. M.N. Peyrat-Maillard; M.E. Cuvelier; C. Berset; *J. Am. Oil Chem. Soc.*, **2003**, *80*, 1007–1012.
26. P. Pedrielli; L.H. Skibsted; *J. Agric. Food Chem.*, **2002**, *50*, 7138–7144.

STUDIA UBB CHEMIA, LXVI, 2, 2021 (p. 59-66)
(RECOMMENDED CITATION)
DOI:10.24193/subbchem.2021.2.05

EXAMINATION OF (PHENOTHIAZINYL)VINYL-PYRIDINIUM DYE'S CAPACITY OF INTERACTION WITH DNA

BIANCA STOEAN[a]*, LUIZA GAINA[a], EMESE GAL[a], CASTELIA CRISTEA[a], TAMAS LOVASZ[a] and LUMINITA SILAGHI-DUMITRESCU[a]

ABSTRACT. The interaction of (E)-4-(2-(7-bromo-10-ethyl-10H-phenothiazin-3-yl)vinyl)-1-methylpyridin-1-ium (PVP) dyes with calf-thymus DNA was examined by spectrophotometric UV-vis absorption/emission titration and competitive ethidium bromide displacement. The association constant values were situated in 10^6 M^{-1} range, typical to cationic dyes containing the monocyanine chromophore system. The variation of the counterion of the cationic PVP dye from iodide to tetrafluoroborate produced dissimilarities in the interaction pattern with DNA. The PVP iodide competitively displaced the ethidium bromide (EB) from the EB-DNA system, thus suggesting the intercalation ability of the dye, while the PVP tetrafluoroborate did not supported the intercalation of the dye.

Keywords: *cyanine dyes, phenothiazine, DNA binding, association constant*

INTRODUCTION

Synthetic organic compounds which may bind non-covalently to cellular DNA attracted a constantly growing scientific attention [1]. An important group of organic compounds that interact reversibly with the DNA double helix are the intercalators (small molecules inserted within the hydrophobic space between two adjacent DNA base pairs) considered as key compounds for the discovery of new anti-tumor agents based on the assumption that intercalation disrupt replication and/or transcription processes eventually leading to apoptosis of tumor cells rich in DNA. On the other hand, organic

[a] *Babeş-Bolyai University, Faculty of Chemistry and Chemical Engineering, 11 Arany Janos str., RO-400028, Cluj-Napoca, Romania*
** Corresponding author: sba2488@chem.ubbcluj.ro*

dyes which bound specifically to DNA were proved to be very useful in fluorescence microscopy applications designed for visualization of DNA by staining cells of various origins (plants, animals, bacteria and viruses) (*e.g.* ethydium bromide (EB), 4',6-diamidino-2-phenylindole (DAPI) [2]). Relaying on the structural features of the organic compound involved in the intercalation course, the interaction with the DNA macromolecules may occur by three different paths: (i) electrostatic interactions with phosphate groups of nucleotides, (ii) inclusion between base pairs of the two strands (iii) intercalation in the grooves of the double helix [3, 4]. As a consequence, DNA intercalators may exhibit three essential structural features: i) a polyaromatic system involving fused planar rings (chromophore) binding with DNA. ii) Cationic species which increase the efficiency of DNA intercalators by interaction with the negatively charged DNA sugar–phosphate backbone. iii) Groove binding side chains, which can occupy the minor groove of DNA [5, 6]. The experimental methods most extensively used for measuring the DNA binding interactions were: isothermal titration calorimetry (ITC), competition dialysis, ethidium bromide displacement, absorbance and fluorescence titration [5].

Phenothiazine derivatives have a long history behind with leading representatives in pharmaceuticals (bactericides, neuroleptic drugs), dyes and fluorophores. Continuing our preoccupation for the characterization of new phenothiazine-based fluorophores [7-10] and chromophores with binding affinity towards nucleic acids [11-13], in this work we examined the capacity of interaction of (phenothiazinyl)vinyl-pyridinium (**PVP**) dyes [14] with DNA. The selection of the target **PVP** dyes for this study was guided by the presence of prerequisite basic pharmacophoric structural features (as indicated in Figure 1) completed by our previous finding that these dyes display intense fluorescence emission inside the B16-F10 murine melanoma cells [15].

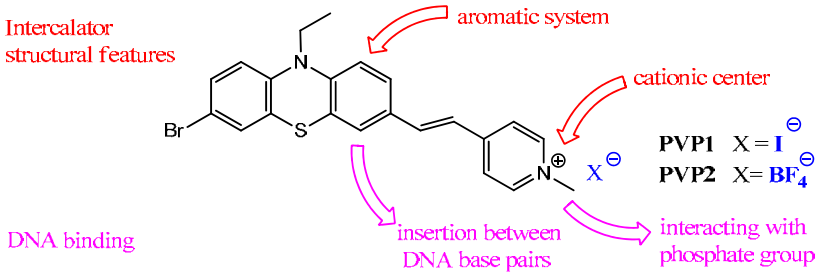

Figure 1. Structural formula of **PVP** dyes in this study and structural features prerequisite for interaction with DNA

RESULTS AND DISCUSSION

The dyes selected for this study, (E)-4-(2-(7-bromo-10-ethyl-10H-phenothiazin-3-yl)vinyl)-1-methylpyridin-1-ium iodide (**PVP1**) and (E)-4-(2-(7-bromo-10-ethyl-10H-phenothiazin-3-yl)vinyl)-1-methylpyridin-1-ium tetrafluoroborate (**PVP2**) contain the same chromophore system belonging to the class of cyanine dyes, but are differentiated by the nature of the counterion. It is known that the presence of iodide anion can induce the quenching of cyanine dyes fluorescence in solution due to photo-induced electron transfer from iodide to the dye's LUMO, a fact which was also observed in the case of **PVP1** which appeared fluorescent only in solid state or in the cytosol where the ion exchange overrides the quenching effect [15]. Upon exchanging the counterion to tetrafluoroborate, **PVP2** displayed an emission maximum situated at 605 nm (10^{-8} M) in DCM solution [15]. Both compounds are stable in the buffer solution used in the CT-DNA titration, fact proven by UV-vis absorption spectra of dye **PVP1** in TRIS-EDTA solution (10^{-5} M) after 0, 30, 60, 90 minutes irradiation with UV radiation λ=365 nm [15].

UV-vis absorption titration

The binding of small molecules to DNA produces a hypochromic effect, a broadening and a red shift of the complex absorption band. These effects are particularly pronounced for intercalators. In order to evaluate the affinity of **PVP** dyes for binding nucleic acids, UV-vis spectra were recorded during **PVP** titration with increasing amounts of Calf Thymus-DNA (ctDNA). As it can be seen in Figure 2, the increase of the ctDNA concentration resulted in a continuous decrease of the intensity of the absorption maxima of **PVP1**. The noticeable hypochromic effect (up to 28%) and the bathochromic shift of the absorption maxima from 450 to 470 nm, are supporting an interaction of **PVP1** with the double stranded helix [16, 17].

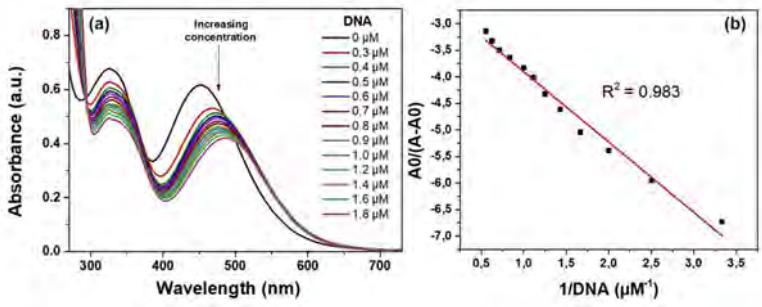

Figure 2. Interaction of PVP with ctDNA a) UV-vis absorption spectra of **PVP1** (5 μM,) in 0.01 M *Tris*-HCl buffer (pH 7.4) in the presence of increasing amounts of ctDNA (0.3-1.8 μM from top to bottom) b) plot of the variation in absorbance of **PVP1** in the presence of ctDNA

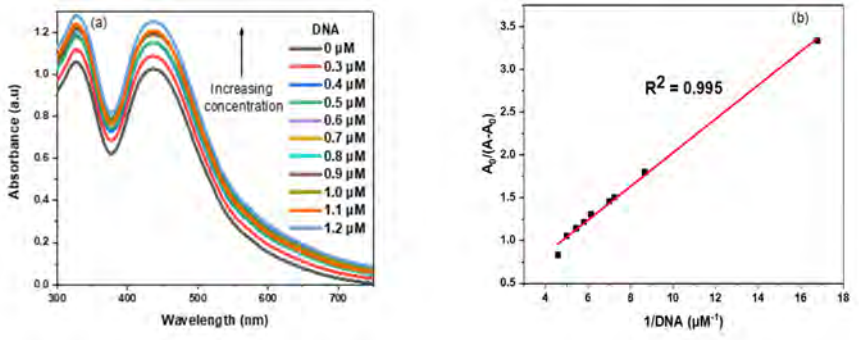

Figure 3. a) UV-vis absorption spectra of **PVP2** (5 μM) in 0.01 M *Tris*-HCl buffer (pH 7.4) in the presence of increasing amounts of ctDNA (0.3-1.8 μM from top to the bottom) **b)** plot of the variation in absorbance of **PVP2** in the presence of ctDNA

From the variation of spectrophotometric absorption of **PVP2** depicted in Figure 3 it can be seen that the change of the counter ion from iodine to the bulky tetrafluoroborate is accompanied by a major change in the way of interaction with the ctDNA. The hyperchromic effect recorded for the molar extinction maxima situated at 436 nm and the 2 nm blue shift are specific for the interaction with the external part of the DNA, most likely through electrostatic interactions [18].

Based on the variation in absorbance of **PVP** in the presence of DNA, the association constants for **PVP**-ctDNA systems were determined according to Benesi–Hildebrand equation (1) from the intercept-to-slope ratio of variation of absorbance *versus* reciprocal DNA concentration plot presented in figures 2b and 3b respectively [3].

$$\frac{A_0}{A - A_0} = \frac{\varepsilon_0}{\varepsilon - \varepsilon_0} + \frac{\varepsilon_0}{\varepsilon - \varepsilon_0} \cdot \frac{1}{K[DNA]} \quad (1)$$

where: K is the association constant, A_0 is the absorbance of **PVP**, A is the absorbances of the **PVP**–ctDNA complex, ε_0 and ε are the molar extinction coefficients of the **PVP** and the **PVP**–ctDNA complex, respectively.

The calculated association constant values depicted in Table 1, are indicating that **PVP1-2** are exhibiting association constants of the same order of magnitude as several monomethine cyanine dyes derived from 2-thiomethylbenothiazolium and 4-methylquinolinium salts [18] and higher than the values reported for phenothiazinium intercalators such as Methylene Blue ($K = 2.13 \times 10^4\ M^{-1}$) [19].

Table 1. Association constants for **PVP**-ctDNA

System	K $\times 10^5$ (M^{-1})
PVP1-ct-DNA	19.5
PVP2-ct-DNA	18.4

Fluorescence emission titration

The direct fluorometric titration of **PVP2** in the presence of increasing amounts of ctDNA was applied. As it can be seen in Figure 4, the increase of the ctDNA concentration produced an increase of the fluorescence intensity but without any shift of the emission maxima. A similar behavior was reported for many cyanine dyes [18].

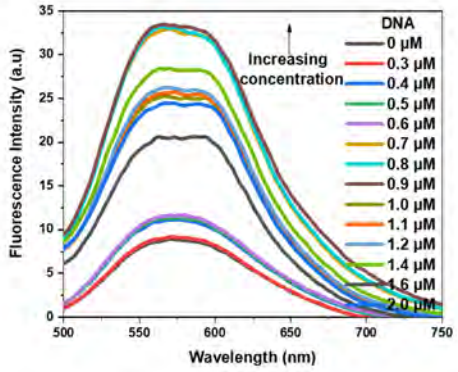

Figure 4. Fluorescence emission spectra of **PVP2** (5 μM) in 0.01 M *Tris*-HCl buffer (pH 7.4) in the presence of increasing amounts of ctDNA (0.3-2 μM from bottom to the top)

Competitive binding between ethidium bromide (EB) and *PVP* for DNA

Ethidium bromide (EB) is a sensitive fluorescence probe with a planar structure that binds DNA by an intercalative mode. The fluorescence of EB increases after DNA intercalation. Due to the fact that **PVP** dye does not display fluorescence emission in solution, its ability to competitively displace the bounded EB-DNA, was explored by fluorescence spectroscopy [18]. **PVP** intercalation into DNA may determine a decrease in the binding sites of DNA available for EB, thus decreasing the fluorescence intensity of the EB–DNA system.

As it can be seen in Figure 5a presenting the fluorescence emission spectrum of EB-ctDNA system upon titration with **PVP1,** the decrease in fluorescence intensity of the emission maxima situated at 606 nm correlates with the increase in the concentration of **PVP1,** suggesting that **PVP1** may interact with EB-ctDNA by displacing the EB fluorophore.

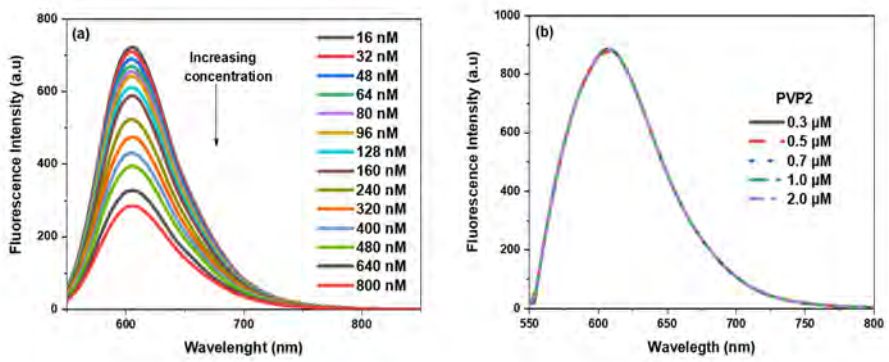

Figure 5. Fluorescence emission spectra of the EB-ctDNA system upon titration with **PVP1** in *Tris*-HCl buffer (pH 7.4), λ_{ex} = 518 nm, [EB] = 8.3 × 10^{-9} mol/L, [ct-DNA] = 2.5 × 10^{-7} mol/L, [**PVP**1] = 16 × 10^{-9} - 800 × 10^{-9} mol/L from top to bottom. **b)** fluorescence emission spectra of the EB-ct-DNA system upon titration with **PVP2** in *Tris*-HCl buffer (pH 7.4), λ_{ex} = 518 nm, [EB] = 8.3 × 10^{-9} mol/L, [ct-DNA] = 2.5 × 10^{-7} mol/L, [**PVP2**] = 0.3 × 10^{-6} - 2 × 10^{-6} mol/L

As it may be seen in Figure 5b, in the presence of increasing amounts of **PVP2** the fluorescence emission spectrum of EB-ctDNA complex does not show any change neither in intensity nor in the position of the emission maximum, therefore, this compound cannot effectively replace EB in the EB-DNA complex, bringing a support that **PVP2** may be faintly bound to DNA.

CONCLUSIONS

The interactions of **PVP** with ctDNA studied by using UV–vis absorbance spectroscopy revealed an association constant **PVP-ctDNA** in the 10^6 range. Based on fluorescence spectroscopic data the interaction of **PVP2** with ctDNA is not of a classical intercalator, further confirmed by EB displacement experiments.

EXPERIMENTAL SECTION

All the materials for experiments, reagents and solvents were obtained from commercial suppliers and used without further purification. **PVP1** and **PVP2** dyes were synthesized according to our previously reported procedure [15].

UV-vis absorption spectra were recorded with a Perkin Elmer Lambda 35 spectrophotometer. UV-vis emission spectra in solution were recorded using a Perkin Elmer LS55 spectrophotometer.

DNA Binding experiments

The ctDNA was purchased from Alfa Aesar, the ethidium bromide 1% water solution and HCl were purchased from Merck. All solutions were prepared using double-distilled water. *Tris*-HCl buffer solution was prepared from (*tris*-(hydroxymethyl)-amino-methane-hydrogen chloride) and pH was adjusted to 7.4 by dropping HCl concentrated solution. The stock solution of ctDNA was prepared by dissolving 1.75 µL of DNA (170 µM) in 3 mL of *Tris*-HCl buffer (pH 7.4). The concentration of nucleotide was determined by UV spectrophotometry at 260 nm wavelength, using the molar extinction coefficient $\varepsilon = 6600\ M^{-1}\,cm^{-1}$.

ACKNOWLEDGMENTS

This work was supported by a grant of Romanian Ministry of Research and Innovation, CNCS - UEFISCDI, project number PN-III-P4-ID-PCCF-2016-0142.

REFERENCES

1. L. Strekowski, B. Wilson, *Mutat Res*, **2007**, *623(1–2)*, 3-13
2. A. Kurutos, I. Balabanov, F.S. Kamounah, K. Nikolova-Ganeva, D. Borisova, N. Gadjevd, T. Deligeorgiev, A. Tchorbanov, *Dyes Pigm.*, **2018**, *157*, 267–277
3. Z. Rehman, A. Shah, N. Muhammad, S. Ali, R. Qureshi, A. Meetsma, I. S. Butler, *Eur J Med Chem*, **2009**, *44*, 3986–3993
4. J.T. Petty, J.A. Bordelon, M.E. Robertson, *J Phys Chem B*, **2000**, *104*, 7221–7227
5. L.V. Smith, J.M. de la Fuente, K.M. Guthrie, A.D.C. Parentya, L. Cronin, *New J. Chem.*, **2005**, *29*, 1118–1120

6. K. El-Adl, M.K. Ibrahim, M.S.I. Alesawi, I.H. Eissa, *Bioorg. Med. Chem.*, **2021**, *30*, 115958
7. E. Gal, B. Brem, I. Pereteanu, L. Gaina, T. Lovasz, M. Perde-Schrepler, L. Silaghi-Dumitrescu, C. Cristea, L. Silaghi-Dumitrescu, *Dyes Pigm.*, **2013,** *99(1)*, 144-153
8. B. Brem, E. Gal, L. Gaina, C. Cristea, A.M. Gabudean, S. Astilean, L. Silaghi-Dumitrescu, *Dyes Pigm.*, **2015,** *123*, 386-395
9. L. Gaina, E. Gal, L. Mataranga-Popa, D. Porumb, A. Nicolescu, C. Cristea, L. Silaghi-Dumitrescu, *Tetrahedron*, **2012**, *68(11)*, 2465-2470
10. L. Gaina, T. Lovasz, I.A. Silberg, C. Cristea, S. Udrea, *Heterocyclic Communications*, **2001**, *7(6)*, 549-554
11. I.H. Filip, E. Gal, I. Lupan, M. Perde-Schrepler, P. Lonnecke, M. Surducan, L. Gaina, E. Hey-Hawkins, L. Silaghi-Dumitrescu, *Dalton Trans*, **2015**, *44*, 615-629
12. L. Gaina, L. Mataranga-Popa, E. Gal, P. Boar, P. Lonnecke, E. Hey-Hawkins, C. Bischin, R. Silaghi-Dumitrescu, I. Lupan, C. Cristea, L. Silaghi-Dumitrescu, *Eur J Org Chem*, **2013**, *2013*, 5500-5508
13. E. Molnar, E. Gal, L. Gaina, C. Cristea, E. Fischer-Fodor, M. Perde-Schrepler, P. Achimas-Cadariu, M. Focsan, L. Silaghi-Dumitrescu, *Int. J. Mol. Sci.*, **2020**, *21*, 3178
14. L. Gaina, I. Torje, E. Gal, A. Lupan, C. Bischin, R. Silaghi-Dumitrescu, G. Damian, G., P. Lönnecke, C. Cristea, L. Silaghi-Dumitrescu, *Dyes Pigm.,* **2014**, *102*, 315-325
15. B. Stoean, D. Rugina, M. Focsan, A-M. Craciun, M. Nistor, T. Lovasz, A. Turza, I-D. Porumb, E. Gal, C. Cristea, L. Silaghi-Dumitrescu, S. Astilean, L. I. Gaina, *Int. J. Mol. Sci.*, **2021**, *22*, 2985-3006
16. D. Jin, B. Wang, Y. Hou, Y. Du, X. Li, L. Chen, *Dyes Pigm*., **2019**, *170*, 107612
17. S. Kashanian, J. Ezzati, N. Dolatabadi, *Food Chem*, **2009**, *116*, 743-747
18. J. Zhao, W. Li, R. Ma, S. Chen, S. Ren, T. Jiang, *Int. J. Mol. Sci.,* **2013**, *14*, 16851–16865

STUDIA UBB CHEMIA, LXVI, 2, 2021 (p. 67-80)
(RECOMMENDED CITATION)
DOI:10.24193/subbchem.2021.2.06

BEHAVIOR OF SILVER AND GOLD NANOPARTICLES IN SIMULATED BIOLOGICAL FLUIDS: NEEDS AND CHALLENGES

ZAMFIRA DINCA[a], TEODORA MOCAN[b,c], LACRIMIOARA SENILA[a], OANA CADAR[a,*]

ABSTRACT. Nanotechnology is an attractive and challenging science focused on the materials at nanoscale level and their employment in a wide variety of applications. Its applications in (nano)medicine are constrained due to the main concerns in understanding and predicting the behavior of nanoparticles (NPs) in complex biological fluids. The properties of NPs can be strongly influenced by the surrounding conditions, such as pH and composition, in terms of aggregation status, chemical reactivity and surface chemistry. In this regard, this review intents to provide some insight into the performance of complex biological fluids associated with nanomaterials. In particular, the behavior of AgNPs and AuNPs in simulated biological fluids that must be addressed to develop an appropriate system for medical applications, from a chemical perspective, mostly related to the physico-chemical characteristics of NPs and simulated biological fluids and their possible interactions (mechanisms) was considered. Furthermore, the fate of AgNPs and AuNPs during the gastrointestinal transit from an *in vivo* experimental perspective, as well as their potential impact on gut microbiota was also systematized.

Keywords: *silver, gold, nanoparticle, simulated biological fluid, gastrointestinal microbiota*

[a] *INCDO-INOE 2000, Research Institute for Analytical Instrumentation, 67 Donath Street, RO-400293, Cluj-Napoca, Romania*
[b] *Iuliu Hatieganu University of Medicine and Pharmacy, Physiology Department, 1 Clinicilor Street, RO-40006, Cluj-Napoca, Romania*
[c] *Regional Institute of Gastroenterology and Hepatology, Nanomedicine Department, 5 Constanta Street, RO-400158, Cluj-Napoca, Romania*
** Corresponding author: oana.cadar@icia.ro*

INTRODUCTION

The metal oxide and metal-based nanomaterials can be considered a fast-growing area due to their wide applications, including (nano)medicine, where nanotechnology has shown a lot of potential in therapeutics and diagnostics. Additionally, Ag and Au are prospective candidates for diagnosis and drug delivery [1]. The physico-chemical characteristics of nanomaterials (*i.e.* small size, large surface area to volume ratio and surface energy) can result in toxicological effects, when nanomaterials enter into biological systems through the adsorption and dissolution, modifying the structure of various macromolecules.

Despite a general acceptance that NPs are persistent as bulk, small nanoparticles (NPs) are normally slightly unstable and short-lived due to their high surface energy. Consequently, there is an increasing concern about the risk of possible pollution and diseases caused by nanomaterials during manufacturing or use. In aqueous solutions, this type of NPs can aggregate, dissolve or remain suspended as single particles depending on the environmental conditions such as pH, ionic strength, temperature, presence of organic matter, etc. [2].

The physico-chemical characteristics of nanomaterials under various conditions are a critical step in order to understand the possible (toxic) effect on the human health and environment. Though, the toxic effect can be higher for nanomaterials, since they can easily penetrate the cell membrane and deliver metal ions in high quantities because of their high surface area [3]. Among various physico-chemical properties of the NPs, the size plays a major role on their solubility in biological media. In this regard, the critical size of NPs is considered 20-30 nm, where they exhibit distinct properties which are absent in case of larger particles with the same chemical composition. The particles tend to reduce their surface energy due to the Gibbs-Thomson effect and consequently, the smaller NPs which own a high surface energy are more reactive and dissolve faster [4].

The full understanding of the behavior of NPs in biological fluids helps to check their biological effects and supports the design of suitable NPs for the desired goal. The NPs used for implantation purpose needs to be bio-persistent, the NPs designed to release ions should be biodegradable, while the NPs administered as contrast agents are preferred to cleared out rather than accumulating inside the body [5]. The *in vivo* experimental data for NPs ingestion should be also considered, in light of elucidating their impact on the gastrointestinal microbiota. To assess the interaction of NPs with the gut microbiome, a better understanding of the ecology, physiology of microorganisms and physico-chemical properties of NPs is needed. The characteristics of NPs

(size, surface chemistry and charge), pH, type of meal and their nutritional characteristics, enzymatic activities, mucosal secretion or host microbiota can affect the fate and bioavailability of NPs during the gastrointestinal transit [6].

This review systematizes the key factors of AgNPs and AuNPs and simulated biological fluids that must be considered to develop a suitable system for medical applications, mainly: (*i*) physico-chemical characteristics of NPs and simulated biological fluids; (*ii*) possible interactions between NPs and simulated biological fluids, (*iii*) the control and change of these characteristics for biomedical applications and *(iv)* the potential impact of NPs to the gastrointestinal microbiota.

RESULTS AND DISCUSSION

Behavior of nanoparticles in simulated biological fluids and their impact on the gut microbiota

The study of dissolution behavior of NPs offers valuable information on their interactions with the biological and environmental surroundings. If the particles release ions at a fast rate, their short-term toxic effect will be similar to that of the dissolved ions, while if the particles release ions at a slow rate, those particles may cause long-term effects in humans [7, 8]. Therefore, the dissolution rate of NPs is a key factor for the assessment of their possible toxic effects. The released ions join in competing reactions, their mobility is high and their concentration is low, the system outlying from the saturation point and, consequently, the NPs tend towards complete dissolution. However, if during the dissolution process, the concentration of available ions brings the system to saturation, the ions will dissolve more slowly.

In terms of *in vivo* experiments, the behavior of NPs in the gastrointestinal environment must also study in the presence of more than 100 trillion microorganisms of human commensal microbes [9, 10]. The human gastrointestinal tract (GIT) is colonized by various species of bacteria, viruses, fungi, archaea and protozoans termed gut microbiota [11]. About 90% of bacteria are belonging to the phyla *Firmicutes* and *Bacteroidetes*, while other 10% species are from the phyla *Proteobacteria, Verrucomicrobia, Actinobacteria, Fusobacteria* and *Cyanobacteria* [12]. The microbial communities play an essential role in the development and differentiation of the intestinal epithelium, contribute to digestion and fermentation of indigestible polysaccharides, produce vitamins, support the host immune defense against pathogens [13] and play an important role in maintaining long-term intestinal hemostasis [14]. The studies on germ-free mice and piglets showed that the

absence of any intestinal flora, leads to underdevelopment of intestinal epithelium in mice or aberrant epithelial surface which causes passage of harmful luminal microorganisms, microbial toxins or foreign antigens [15].

Gut microbiome is a dynamic system that changes depending on factors such as the age, the dietary habits, [16] geographic environment [17] the use of drugs including antibiotics [11, 18] or in response to the disease [19]. Due to the interaction with the environment and external factors, the human microbiota can register imbalances named dysbiosis [20]. The dysbiosis occurs when *Firmicutes/Bacteroidetes* (F/B) ratio, which indicates the health status of the GIT becomes unbalanced [21], and has been associated with the development of inflammatory bowel disease (IBD) [22], irritable bowel syndrome (IBS) [23], cardiovascular diseases [24], neurodegenerative disorders [25], kidney stones [26] or metabolic diseases including obesity and diabetes [27]. Many causes of dysbiosis have been associated with various products and supplements containing NPs. The widespread application of NPs increases the direct human ingestion and access to the host GIT and microbiota [28]. It has been shown that AgNPs accumulate in the stomach, duodenum, ileum, jejunum and colon, with potential negative impact on the gut microbiome and human health [28]. In this context, understanding the microbial communities and their behavior in the presence of NPs is essential to fully assess the potential impact on the human body [29].

Silver nanoparticles

Due to their antibacterial properties, the AgNPs are used in many scientific designs and developments, they enter into the human body or the environment either accidentally or purposefully. The brought biological effects or potential toxicity of AgNPs are highly dependent on their colloidal (aggregation) and chemical (interaction with protein) stability [30].

The specific bactericidal mechanism of Ag is not fully understood, but could result from the interaction of Ag^+ ions with enzymes or generation of free radicals that causes damage bacteria cell membranes [31, 32]. The U.S. Environmental Protection Agency (EPA) suggests a reference dose (RfD) of 0.005 mg/kg/day Ag, a value based on the risk for argyria, a gray or blue-gray discoloring of the skin [33]. The exposure of AgNPs can take place from drinking water, through inhalation or direct skin or organ contact. However, there are still large gaps in understanding AgNPs toxicity [34]. The changes of particle size, surface and charge, purposefully or due to the processing affect the toxicity towards living organisms. In this regard, well-designed *in vitro* and *in vivo* studies were developed to characterize the human exposure to NPs in terms of physico-chemical nature, aggregation state, particle size, functionalization, concentration and potential risk to humans [35].

Generally, the analytical techniques for Ag determination are atomic absorption spectrometry (AAS), inductively coupled plasma mass spectrometry (ICP-MS) and inductively coupled plasma optical emission spectrometry (ICP-OES), while the separation of AgNPs and Ag^+ ions is typically carried-out by centrifugation, dialysis or ultrafiltration. The above-mentioned techniques before the measurements demand the separation of Ag^+ ions from the AgNPs, because they detect total Ag content and not its oxidation state. Also, the above-mentioned techniques cannot distinguish between AgNPs and AgCl, measuring only the dissolved forms of Ag [32, 36]. So, it is a critical step to develop methods in order to differentiate between the toxicities of the metal NPs, the dissolved metal ions and their corresponding ion complexes [32]. Although, several studies on the dissolution kinetics of AgNPs were reported, they are difficult to be compared due to: (*i*) the different physico-chemical properties of NPs (size, charge, surface functionalization) which strongly influence the dissolution behavior, (*ii*) the use of various, complex dissolution media and (*iii*) the released Ag^+ ions in solution are quickly precipitated as AgCl as separate particles, seemingly not on the surface of the initial Ag particles; also, the solubility product (AgCl) and the redox potential of Ag^+ ions strongly depend on the initial (total) concentration [36].

The investigation of AgNPs coated with thick and sub-nanometer range surface layers, in terms of aggregation, sedimentation and dissolution in two biological fluids (artificial interstitial and lysosomal fluids) was conducted to better understand their behavior after inhalation. After introducing into high ionic strength biological fluids, the AgNPs formed aggregates and settled out, independents of surface modification. Furthermore, single NPs and aggregated coexisted in both studied biological media [2].

Treatment of textiles with AgNPs is one of the most commercialized applications due to their anti-bacterial, anti-static and mothproofing properties [37]. Beside the typical study of Ag release into the environment, recently, the researchers have begun to emphasis on the release of Ag into biological fluids and the potential exposure from contact with textile products. In this regard, the used fiber treatment technique was a more dominant exposure factor comparing to physiological properties of artificial saliva or sweat (composition, pH and temperature) [38]. Regarding a possible acting mechanism, the textiles treated with AgNPs release primarily Ag in ionic form when in contact with biological fluids such as sweat, saliva and urine. Although, the product must release sufficient Ag^+ ions to assure efficiency, while the release rate should not pose a dermal or environmental exposure hazard [34]. Hence, the influence of fiber treatment technique is important because, in the absence of acceptable limits for dermal exposure to Ag, it indicates that the obtaining techniques could be tailored to control Ag^+ ion release in order to ensure the product efficacy and diminish the human and environmental exposure [38].

The skin surface fluids and barrier integrity are relevant characteristics when assessing the potential exposure from textiles. Several studies reported that from the physico-chemical characteristics of artificial sweat, NaCl and pH have a minor influence on Ag release (ionic and particulate) from a textile [37, 39]; furthermore, Ag is easily absorbed from suspension through abraded skin compared to intact skin [40].

The Ag release increased with the increase of the exposure time, with a quite different behavior under different pH values, *i.e.* sub-micrometer particles and ionic forms in acid perspiration solution, SL1 (pH≈3), mostly Ag^+ ions in alkaline perspiration solution, SL2 (pH≈8) and NPs in salt perspiration solution SL3 (pH≈8), despite partial aggregation. Moreover, the acidic pH caused the fastest release rate and greatest Ag release [37]. A possible release mechanism was suggested in each case, as follows: (*i*) acid SL-1, the relatively stable dissolved Ag resulted from the aggregation of the particles, while some of them dissolved into the Ag^+ ions, (*ii*) alkaline SL-2, the surface oxide increased, the unstable AgO being transformed into Ag^+ ions in the solution and (*iii*) SL-3, the AgNPs in neutral aqueous solution is relatively stable and only partially converted into an ionic state [37]. The exposure risk of AgNPs was higher in the simulated salt conditions, which indicates that AgNPs may release into in the salt perspiration condition and could further enter the body and the environment.

Generally, the citrate-coated AgNPs are the most popular Ag colloids for various applications, the citrate acting as reducing agent and a stabilizer by decorating the negatively charged particles [41]. In this regard, the Ag dissolution in cell culture medium (DMEM) measured using a simple localized surface plasmon resonance (LSPR) UV-visible absorbance measurement, highlighted a fractional dissolution of different polymer-coated AgNPs (citrate, dextran, poly(vinylpyrrolidone)/ PVP and poly(ethyleneglycol)/ PEG). The dissolution increased at high AgNPs concentrations and PEG coatings, but decreased considerably in case of higher molecular weight coatings. The used absorbance method was recommended as optimal to measure the amount of Ag remained in AgNPs, considering that AgCl do not display a LPSR absorbance [32].

The dissolution kinetics of AgNPs (300 and 600 µg/L) in quarter-strength Hoagland medium revealed a directly relationship between the particle size and concentration, and the Ag release rate. As expected, smaller particles were found to dissolve faster and the used kinetic model using hard sphere theory to define the Ag^+ ions release fitted well the experimental data [41]. Furthermore, the AgNPs dissolved faster in biological media with low pH (gastric acid) comparing to pseudo-extracellular fluid and strongly interacted

with thiol- and selenide-containing biomolecules [42]. Loza et al. also confirmed that thiol-containing compounds (cysteine) can block the particle surface and prevent the dissolution, while the organic molecules complexate the Ag^+ ions and accelerate the dissolution. Reducing sugars (glucose) decreased, but do not totally avoid the oxidative dissolution of Ag [36].

A very interesting study reported that AgNPs did not present any bactericidal effect when *E. coli* were cultivated under strictly anaerobic conditions, meaning no dissolution of the NPs taken place [43]. The surface coatings usually improve the dispersion of NPs, but can also display an acute effect on the solubility of NPsy. For example, when AgNPs are coated with 11-mercaptoundecanoic acid, a thiolated ligand with stronger affinity to the metal surface than Na citrate, no significant decrease in the absorption intensity up to 48 h incubation was remarked [44]. The *in vivo* and *in vitro* behavior of NPs suspended in a fluid can be influenced through the dispersion state or interactions at the surface, resulting in the formation of coatings around NPs.

From the product that contains, AgNPs reach the human body, most often, by oral ingestion and pass through the GIT. The biochemical composition of mouth, stomach and intestine environment can affect the AgNPs bioavailability and toxicological properties [45]. Studies performed on rats and mice using 9 and 10 mg/kg bw/d AgNPs with 28 days exposure time and 14, 20 and 110 nm particle size, revealed no significant alteration in the caecal microbiota composition [46, 47]. A longer exposure of rats for 13 weeks at 9, 18 and 36 mg/kg bw/d concentration with 10, 75 and 110 nm size AgNPs showed an increase of *Bacteroidetes* species and pathogenic gram-negative bacteria, and decrease of *Firmicutes*, *Lactobacillus* and *Bifidobacterium* in ileac microbial populations [48]. Therefore, the doses of exposure and particle sizes are influencing factors on host gene expression [48]. The intestinal microbiota displayed to 1 μg/mL AgNPs *in vitro* batch fermentation models inoculated with human faecal matter and the probiotic *Bacillus* subtilis (BS) revealed that the core bacterial community was not affected but the relative abundance of Firmicutes species was increased and Bacteroidetes species decreased instead. Without BS, single treated AgNPs induces functional differences in cell motility, translation, transport, and xenobiotics degradation [49].

A shifted *Firmicutes*/*Bacteroidetes* (F/B) ratio has been observed in the rats and mice microbiota at 2.5 or 3.6 mg/kg bw/d AgNPs for 7 days or 2 weeks [28, 50] leading to the conclusion that the shape of AgNPs may cause an alteration of the microbiota [50]. A 28 days experiment with mice orally exposed to food pellets supplemented with 0, 460 or 4600 ppb AgNPs (μg Ag NP/kg pellet) revealed microbial alterations in the gut and a shift in the F/B ratio in the fecal microbiota [51]. It was showed that AgNPs treatment reduced *Bacteroides* species and increased the *Coprococcus*, *Lactobacillus*

and *Blautia* taxons [51]. Disturbance in these bacterial populations were observed in the case of obese individuals [52]. Interestingly, the identical exposure of mice to the AgNPs supplemented pellets aged during 4 or 8 months has small or no effect on the F/B ratio due to the Ag sulfidation occurring in this matrix [51]. Another *in vitro* investigation performed with 33 bacterial strains isolated from a healthy human donor stool has evaluated the effects of AgNPs on the microbial communities [53]. The exposure of the bacterial community to 0 to 200 mg/L AgNPs concentrations for 48 h determined a negative impact on the microbial consortium with significant reduction in culture-generated gas production and changes in fatty acid methyl ester profiles [53]. Negative effects were observed in the community structure even at the lowest concentrations, with increasing abundance of species such as *Raoultella* sp. and of *E. coli* which are involved in different pathology or which facilitates the growth of pathogenic bacteria [53].

Even if the complete mechanisms of AgNPs interaction with the intestinal microbiota is not well understood, some studies suggested that alterations of the microbial taxons are explained by the release of Ag^+ ions [54], composition, size, shape surface charge, capping agent used (poly(diallyldimethylammonium)-coated AgNPs, biogenic-Ag and oleate-AgNPs [55] or by forming reactive oxygen species [56].

Gold nanoparticles

The growing interest in AuNPs due to their singular physico-chemical properties, high biocompatibility and opportunity to tailor the size and shape resulted in many applications in the fields of catalysis, imaging, nanophotonics, nanomagnetic, nanoelectronic devices, biosensors, chemical sensors and drug delivery. Among all the properties, the size stability and a good dispersion are required for a high therapeutical performance [57].

The physico-chemical properties of the orally ingested AuNPs are strongly influenced by the composition (pH, salts and enzymes) of gastrointestinal fluid, resulting in unexpected biological outcomes. Recently, some studies reported the biodistribution and accumulation of AuNPs in cell lines and murine models, and the factors that influence their toxicity have been linked to their surface charge and functionalization, size and shape [8, 58]. The dissolution behavior of AuNPs in simulated biological systems *(i.e.* artificial alveolar fluid, weak hydrochloric acid for gastric conditions, ammonium acetate solution for neutral lung fluids) depended mainly on the physico-chemical characteristics of both particles and simulated model (pH and ionic strength) [59].

Beside the characteristics of simulated biological media, the surface charge and functionalization, size and shape of AuNPs can noticeably influence the dissolution of AuNPs [8, 60]. In this regard, the dissolution kinetics of uncoated uncoated citrate-stabilized AuNPs (cit-AuNPs), polyethylene glycol (PEG)-coated AuNPs functionalized with carboxylic acid (COOH-AuNPs) and amine (NH_2-AuNPs) groups were investigated in Gamble's fluid (GF) and phagolysosomal fluid (PSF), gastric fluid (GIF) and intestinal fluid (IF) and blood plasma (BP). Generally, the dissolution of AuNPs in acidic media (PSF and GIF) was greater than that in neutral or alkaline media (Gamble's fluid, blood plasma and intestinal fluids). The cit-AuNPs tended to aggregate resulting in low surface area to volume ratio and low dissolution, while the PEG-coated AuNPs were less disposed to aggregation and displayed higher dissolution. Some possible explanations could be various ligand-promoted processes and the high stability of the cit-AuNPs [8]. Therefore, cit-AuNPs may cause long-term health effects because they are more (bio)durable and show high biopersistence, meaning these NPs might resist chemical or biochemical alteration in biological systems.

Nowadays, the use of AuNPs as therapeutic agents to treat many autoimmune, infectious and neoplastic diseases [61] is of main interest, but the effect of administered AuNPs on gut microbiota is very less studied and not well understood. However, one study has shown that AuNPs with small particle size (5 nm) coated by different agents such as citrate or PVP has proved anti-inflammatory effect in experimental mouse colitis, reducing the cell surface lipopolysaccharide (PLS) receptor and catalytic detoxification of peroxynitrite and hydrogen peroxide [62].

Despite the proven anti-inflammatory effect in macrophages cells, an adverse effect of oral administration of AuNPs against the beneficial probiotic genus *Lactobacillus* was observed in mice microbiota. At the same time, AuNPs coated by 5 nm size tannic acid (Au-5 nm/TA-treated mice) displayed a lower α-diversity of intestinal flora, especially a reduced F/B ratio, the two most abundant phyla in human intestinal microbiota. Similar studies highlighted a markedly decreased species richness of the gut microbiota in mice when AgNPs were orally administrated [28]. *Roseburia*, *Ruminococcaceae*, and *Odoribacter* which are short chain fatty acid (SCFA)-producing bacteria were also reduced in Au-5 nm/TA-treated mice compared to the control. This decrease in the aforementioned bacterial populations, with decreased abundance of *Firmicutes* species was observed in inflammatory bowel disease (IBD) [63]. The taxonomic *Bacteroides* phylum increased instead in Au-5 nm/TA-treated mice compared to the control group. The decrease in the abundance of *Lactobacillus* species responsible for the production of

hydrogen peroxide leads to imbalances of the normal microbiota. Although, the mechanism by which AuNPs cause the decrease of *Lactobacillus* probiotics is not known, the potential of AuNPs to induce intestinal dysbiosis is obvious [62].

Contrary to these findings, 4,6-diamino-2-pyrimidinethiol (DAPT)-coated AuNPs applied as therapy for bacterial infection of *E. coli* in a 28 days oral administration trial on mice showed positive effects against bacterial infections with no disturbances of the intestinal microflora [64].

CONCLUSIONS

A comprehensive understanding of the behavior of nanomaterials when they come into contact with biological fluids and systems is very important to further progress their application in medicine. Sometimes, the balancing between the designed function and desired safety is challenging. This review aimed to explore the stability and chemical reactivity of AgNPs and AuNPs, as well as the evaluation of their persistency in simulated biological fluids, from chemical perspective. In this regard, the dissolution process of Ag and Au is strongly influenced by various intrinsic and extrinsic factors, especially pH and existence of strong binding ligands, being totally different in various biological media. One important aspect is that each study referring to AgNPs should be related to its possible chemical conversion in the experimental medium, in order to provide a more comprehensive understanding of the potential of Ag NPs for further medical applications. The AgNPs and AuNPs can alter the gut microbiota, with serious potential to lead on various diseases. However, some research reported no negative effects for both AgNPs and AuNPs. These contradictory results may be due to the methodological variables, dose, size, coating agent, animal model, methods, the intestinal sampling area, etc. Regarding interaction of AuNPs with the microbiota, there is a lack of data and further systematic research is required to fully assess their potential impact.

ACKNOWLEDGMENTS

This work was supported by a grant of the Romanian Ministry of Research and Innovation, CCCDI-UEFISCDI, project number PN-III-P2-2.1-PED-2019-0844, within PNCDI III.

REFERENCES

1. J.K. Patra; G. Das; L.F. Fraceto; E.V. Ramos Campos; M.P. Rodriguez-Torres; L.S. Acosta-Torres; L.A. Dias-Torres; R. Grillo; M.P. Swamy; S. Sharma; S. Habtemariam; H.S. Shin; *J. Nanobiotechnol.*, **2018**, *16*, 71
2. L.V. Stebounova; E. Guio; V.H. Grassian; *J. Nanopart. Res.*, **2011**, *13*, 233-244
3. Y.N. Slavin; J. Asnis; U.O. Hafeli; H. Bach; *J. Nanobiotechnol.*, **2017**, *15*, 65
4. M. Auffan; J. Rose; J. Y. Boterro; G.V. Lowry; J.P. Jolivet; M.R. Wiesner; *Nat. Nanotechnol.*, **2009**, *4*, 634-641
5. K. Khan; I. Khan; *Arab. J. Chem.*, ***2019***, *12*, 908-931
6. A. Pietroiusti; E. Bergamaschi; M. Campagna; L. Campagnolo; G. De Palma; S. Iavicoli; V. Leso; A. Magrini; M. Miragoli; P. Pedata; L. Palombi; I. Iavicoli; *Part. Fibre Toxicol.*, **2017**, *14*, 47
7. W. Utembe; K. Potgieter; A.B. Stefaniak; M. Gulumian; *Part*. *Fibre Toxicol*., **2015**, *12*, 11
8. O. Mbanga; E. Cukrowska; M. Gulumian; *J. Nanopart. Res.*, **2021**, *23*, 29
9. N. Kamada; S.U. Seo; G.Y. Chen; G. Núñez; *Nat. Rev. Immunol.*, **2013**, *13*, 321-335
10. E. Thursby; N. Juge; *Biochem. J*., **2017**, *474*, 1823-1836
11. R.K. Dudek-Wicher; A. Junka; M. Bartoszewicz; *Prz. Gastroenterol.*, **2018**, *13*, 85-92
12. B. Lamas; N. Martins Breyner; E. Houdeau; *Part. Fibre Toxicol*., **2020**, *17*, 19
13. H.Y. Cheng; M.X. Ning; D.K. Chen; W.T. Ma; *Front. Immunol.*, **2019**, *10*, 607
14. J. Gao; K. Xu; H. Liu; G. Liu; M. Bai; C. Peng; T. Li; Y. Yin; *Front. Cell. Infect. Microbiol.*, **2018**, *6*,13
15. L. Peng; Z.R. Li; R.S. Green; I.R. Holzman; J. Lin; *J. Nutr*., **2009**, *139*, 1619-1625
16. A.M. Sheflin; C.L. Melby; F. Carbonero; T.L. Weir; *Gut Microbes*, **2017**, *8*, 113-129
17. T. Yatsunenko; F.E. Rey; M.J. Manary; I. Threhan; M.G. Dominguez-Bello; M. Contreras; M. Magris; G. Hidalgo; R.N. Baldassano; A.P. Anokhin; A.C. Heath; B. Warner; J. Reeder; J. Kuczynski; J.G. Caporaso; C.A. Lozupone; C. Lauber; J.C. Clemente; D. Knights; R. Knight; J.I. Gordon; *Nature*, **2012**, *222-227*
18. S. Carding; K. Verbeke; D.T. Vipond; B.M. Corfe; L.J. Owen; *Microb. Ecol. Health Dis.*, **2015**, *26*, 26191
19. D. Liang; R.K.K. Leung; W. Guan; W.W. Au; *Gut. Pathog*., **2018**, *10*, 3
20. J.E. Belizário; M. Napolitano; *Front. Microbiol*., **2015**, *6*, 1050
21. M. Ghebretatios; S. Schaly; S. Prakash; *Int. J. Mol. Sci.*, **2021**, *22*, 1942

22. M. Matijašić; T. Meštrović; M. Perić; H. Čipčić Paljetak; M. Panek,; D. Vranešić Bender; D. Ljubas Kelečić; Ž. Krznarić; D. Verbanac; *Int. J. Mol. Sci.*, **2016**, *17*, 578
23. E. Distrutti; L. Monaldi; P. Ricci; S. Fiorucci; *World J. Gastroenterol.*, **2016**, *22*, 2219-2241
24. S. Thomas; J. Izard; E. Walsh; K. Batich; P. Chongsathidkiet; G. Clarke; D.A. Sela; A.J. Muller; J.M. Mullin; K. Albert; J.P. Gilligan; K. DiGuilio; R. Dilbarova; W. Alexander; G.C. Prendergast; *Cancer Res.*, **2017**, *77*, 1783-1812
25. P. Forsythe; W.A. Kunze; *Cell. Mol. Life. Sci.*, **2013**, *70*, 55-69
26. D.W. Kaufman; J.P. Kelly; G.C. Curhan; T.E. Anderson; S.P. Dretler; G.M. Preminger; D.R. Cave; *J. Am. Soc. Nephrol.*, **2008**, *19*, 1197-1203
27. M.D. Schulz; C. Atay; J. Heringer; F.K. Romrig; S. Schwitalla; B. Aydin; P.K. Ziegler; J. Varga; W. Reindl; C. Pommerenke; G. Salinas-Riester; A. Böck; C. Alpert; M. Blaut; S.C. Polson; L. Brandl; T. Kirchner; F.R. Greten; S.W. Polson; M.C. Arkan; *Nat. Cell. Biol.,* **2014**, *514*, 508-512
28. H. Chen; R. Zhao; B. Wang; C. Cai; L. Zheng; H. Wang; M. Wang; H. Ouyang; X. Zhou; Z. Chai; Y. Zhao; W. Feng; *NanoImpact*., **2017**, *8*, 80-88
29. H. Bouwmeester; M. van der Zande; M. A. Jepson; *Wiley Interdiscip. Rev. Nanomed. Nanobiotechnol.*, **2018**,*10,* e1481
30. P. Belteky; A. Ronavari; N. Igaz; B. Szerencses; I.Y. Toth; I. Pfeiffer; M. Kiricsi; Z. Konya; *Int. J. Nanomed.*, **2019**, *14*, 667-687
31. J.R. Morones; J.L. Elechiguerra; A. Camacho; K. Holt; J.B. Kouri; J.T. Ramirez; M.J. Yacaman; *Nanotechnology*, **2005**, *16*, 2346-2353
32. J.M. Zook; S.E. Long; D. Cleveland; C.L.A. Geronimo; R.I. MacCuspie; *Anal. Bioanal. Chem.*, **2011**, *401*, 1993-2002
33. U.S. EPA; Risk assessment guidance for superfund, *Volume I*, **1989**, Human health evaluation manual (Part A). Interim Final EPA/540/1-89/002. Washington, DC
34. Z. Ferdous; A. Nemmar; *Int. J. Mol. Sci.*, **2020**, *21*, 2375
35. G.R. Tortella; O. Rubilar; N. Duran; M.C. Diez; M. Martinez; J. Parada; A.B. Seabra; *J. Hazard. Mater.*, **2020**, *390*, 121974
36. K. Loza; J. Diendorf; C. Sengstock; L. Ruiz-Gonzalez; J.M. Gonzalez-Calbet; M. Vallet-Regi; M. Köller; M. Epple; *J. Mater. Chem. B*., **2014**, *2*, 1634-1643
37. Y. Yan; H. Yamg; J. Li; X. Lu; C. Wang; *Text. Res. J.*, **2012**, *82*, 1422-1429
38. A.B. Stefaniak; M.G. Duling; R.B. Lawrence; T.A. Thomas; R.F. LeBouf; E.E. Wade; M.A. Virji; *Int. J. Occup. Environ. Health.*, **2014**, *20*, 220-234.
39. M.E. Quadros; R.T. Pierson; N.S. Tulve; R. Willis; K. Rogers; T.A. Thomas; L.C. Marr; *Environ. Sci. Technol.* **2013**, *47*, 8894-8901
40. F. Larese-Filon; F. D'Agostin; M. Crosera; G. Adami; N. Renzi; M. Bovenzi; G. Maina; *Toxicology,* **2009**, *255*, 33-37
41. W. Zhang; Y. Yao; N. Sullivan; Y. Chen; *Environ. Sci. Technol.*, **2011**, *45*, 4422-4428

42. J. Liu; Z. Wang; F.D. Liu; A.B. Kane; R.H. Hurt; *ACS Nano*, **2012**, *6*, 9887-9899
43. Z.M. Xiu; Q.B. Zhang; H.L. Puppala; V.L. Colvin; P.J.J. Alvarez; *Nano Lett.*, **2012**, *12*, 4271-4275
44. R.A. Sperling; W.J. Park; *Phil. Trans. R. Soc. A*, **2010**, *368*, 1333-1383
45. A. Abdelkhaliq; M. van der Zande; A.K. Undas; R.J.B. Peters; H. Bouwmeester; *Nanotoxicology*, **2020**, *14*, 111-126
46. N. Hadrup; K. Loeschner; A. Bergström; A. Wilcks; X. Gao; U. Vogel; H.L. Frandsen; E.H. Larsen; H.R. Lam; A. Mortensen; *Arch. Toxicol.,* **2012**, *86*, 543-551
47. L.A. Wilding; C.M. Bassis; K. Walacavage; S. Hashway; P.R. Leroueil; M. Morishita; A.D. Maynard; M.A. Philbert; I.L. Bergin; *Nanotoxicology,* **2016**, *10*, 513-520
48. K. Williams; J. Milner; M.D. Boudreau; K. Gokulan; C.E. Cerniglia; S. Khare; *Nanotoxicology*, **2015**, *9*, 279-289
49. C. Cattò; E. Garuglieri; L. Borruso; D. Erba; M.C. Casiraghi; F. Cappitelli; F. Villa; S. Zecchin; R. Zanchi; *Environ. Pollut.*, **2019**, *245*, 754-763
50. A.B. Javurek; D. Suresh; W.G. Spollen; M.L. Hart; S.A. Hansen; M.R. Ellersieck; N.J. Bivens; S.A. Givan; A. Upendran; R. Kannan; C.S. Rosenfeld; *Sci. Rep.*, **2017**, *7*, 2822
51. S. van den Brule; J. Ambroise; H. Lecloux; C. Levard; R. Soulas; P.J. De Temmerman; M. Palmai-Pallag; E. Marbaix; D. Lison; *Part. Fibre Toxicol.*, **2015**, *13*, 38
52. C. Kasai; K. Sugimoto; I. Moritani; J. Tanaka; Y. Oya; H. Inoue; M. Tameda; K. Shiraki; M. Ito; Y. Takei; K. Takase; *BMC. Gastroenterol.*, **2015**, *15,* 100
53. P. Das; J.A.K. McDonald; E.O. Petrof; E. Allen-Vercoe; V.K. Walker; *J. Nanomed. Nanotechnol*., **2014**, *5*,235
54. C. Levard; E.M. Hotze; G.V. Lowry; G.E. Brown Jr.; *Environ. Sci. Technol*., **2012**, *46*, 6900-6914
55. A.K. Suresh; D.A. Pelletier; W. Wang; J.L. Morrell-Falvey; B. Gu; M.J. Doktycz; *Langmuir*, **2012**, *7*, 2727-2735
56. H. Xu; F. Qu; H. Xu; W. Lai; Y.A. Wang; Z.P. Aguilar; H. Wei; *Biometals*, **2012**, *25*, 45-53
57. A.L. Bailly; F. Correard; A. Popov; G. Tselikov; F. Chaspoul; R. Appay; A. Al-Kattan; A.V. Kabashin; D. Braguer; M.A. Esteve; *Sci. Rep.-UK.*, **2019**, *9*, 12890
58. M.F. Hornos Carneiro; F. Barbosa Jr; *J. Toxicol. Env. Heal. B*, **2016**, *19*, 129-148
59. E.K. Breitner; S.M. Hussain; K.K. Comfort; J. *Nanobiotechnol.*, **2015**, 13, 56
60. M.M. Arnida; A. Ray; C.M. Peterson; H. Ghandehari; *Eur. J Pharm. Biopharm*., **2011**, *77*, 417-423
61. S.J. Berners-Price; A. Filipovska; *Metallomics*. **2011**, *3*, 863-873
62. S. Zhu; X. Jiang; M.D. Boudreau; G. Feng; Y. Miao; S. Dong; H. Wu; M. Zeng; J.J. Yin; *J. Nanobiotechnol.*, **2018**, *16*, 86.

63. I. Khan; N. Ullah; L. Zha; Y. Bai; A. Khan; T. Zhao; T. Che; C. Zhang; *Pathogens*, **2019**, *8*, 126
64. J. Li; R. Cha; X. Zhao; H. Guo; H. Luo; M. Wang; F. Zhou; X. Jiang; *ACS Nano*, **2019**, *13*, 5002-5014

STUDIA UBB CHEMIA, LXVI, 2, 2021 (p. 81-94)
(RECOMMENDED CITATION)
DOI:10.24193/subbchem.2021.2.07

METHOD VALIDATION FOR THE DETERMINATION OF EXCHANGEABLE CATIONS IN NATURAL ZEOLITES USING INDUCTIVELY COUPLED PLASMA OPTICAL EMISSION SPECTROMETRY

MARIN SENILA[a]*, OANA CADAR[a], MARIA-ALEXANDRA HOAGHIA[a], ZAMFIRA DINCA[a], LACRIMIOARA SENILA[a], IOAN ASCHILEAN[b,c], CECILIA ROMAN[a]

ABSTRACT. The paper presents the validation of a method for the determination of exchangeable cations (K^+, Na^+, Ca^{2+} and Mg^{2+}) in zeolites by inductively coupled plasma optical emission spectrometry (ICP-OES), after extraction in ammonium chloride solution. Amongst the analytical techniques that can be used for exchangeable cations measurement, ICP-OES provides rapid, robust, multi-element analysis on a wide range of concentrations. The exchange capacity is one of the most important parameters of zeolites since it indicates their adsorption capacity in different processes. Method validation is an essential requirement for testing laboratories in order to provide trustworthy results in accordance with ISO/IEC 17025:2017 standard. The main figures of merit were studied, and the measurement uncertainty was assessed. The selectivity assay showed no significant non-spectral matrix effect. The linearity study was conducted for the calibration curves in the range of 0.02–20 mg L^{-1} for each exchangeable cation. Limits of quantification were 0.005 mEq 100 g^{-1} for Na^+, 0.011 mEq 100 g^{-1} for Mg^{2+}, 0.002 mEq 100 g^{-1} for K^+, 0.003 mEq 100 g^{-1} for Ca^{2+}. Relative standard deviations of repeatability (RSDr) (n=6 parallel samples) were 4.50 % for Na^+, 4.43 % for Mg^{2+}, 6.55 % for K^+ and 5.53 % for Ca^{2+}. Recoveries (%) estimated using a certified reference material (CRM BCS-CRM 375/1), for total content of cation oxides were in the range 92–103 %. Fourteen zeolite samples from Racos deposit, Romania were analysed, and according to the chemical composition and X-ray diffraction the main mineral in zeolitic tuffs is clinoptilolite-type. The obtained figures of merit demonstrate that the method has a suitable level of precision and accuracy for the intended purpose.

Keywords: *zeolites, exchangeable cations, ICP-OES, method validation, cation exchange capacity*

[a] *INCDO-INOE2000, Research Institute for Analytical Instrumentation, 67 Donath str., RO-400293, Cluj-Napoca, Romania*
[b] *Zeolites Production S.A., Rupea, Brasov, Romania*
[c] *Technical University of Cluj-Napoca, 28 Memorandumului st., 400114, Cluj-Napoca, Romania*
* *Corresponding author: marin.senila@icia.ro*

INTRODUCTION

Zeolites have physical and chemical properties that make them useful in many applications in domains such as ecology, industrial processes, agronomy, cosmetics and medicine. The name 'zeolite' originates from the Greek words 'zeo' (to boil) and 'litos' (a stone) [1]. Zeolites may be natural, of volcanic origin, or synthetic materials. They have a crystalline structure with a three-dimensional framework formed by repeated units of silicon–oxygen (SiO_4) and aluminum–oxygen (AlO_4) tetrahedral units, which forms well-defined cavities negatively charged. To maintain the neutrality for the whole structure, the cavities contain positively charged alkali and alkali earth cations such as K^+, Na^+, Ca^{2+} and Mg^{2+}. The cationic sites of zeolites can be substituted by other cationic species with ionic radius fitting the pore size of internal zeolite framework [2-4].

The exchange capacity is one of the most important properties that influence the zeolites applicability. The higher ability of zeolitic materials to exchange movable Na^+, K^+, Ca^{2+} and Mg^{2+} cations is equivalent with their high adsorption capacity in different processes. The amounts of exchangeable cations within zeolites pores/channels strongly depend on Si/Al ratio in its structure, as it influences the negative charge available to attract cations [5].

The cations naturally contained by zeolites may be replaced with other positive ions such as unwanted heavy metals or ammonia ions from industrial effluents [6]. To increase the cation exchange capacity (CEC), natural zeolites can be modified by single or combined treatments such as thermal or chemical activation using acids, bases or inorganic salts [7,8].

There are different approaches regarding the measurement of CEC for crystalline materials. Munthali and co-workers [9] proposed a method based on the measured amount of Na^+ (sum of retained as Na^+ and free Na^+ as NaCl), following a modified method used for CEC determination in soil clays. Other approaches formerly used to measure CEC are based on methylene blue (MB) absorption in zeolite, but some authors suggested that the size of MB molecule is generally greater than the pores of zeolitic channels, which can lead to inaccurate results [10].

The ammonium acetate saturation (AMAS) method involves the saturation of zeolites channels with ammonium ions (NH_4^+) to replace the exchangeable cations. All NH_4^+ ions adsorbed in zeolite can be considered a measure on CEC [10]. AMAS method was firstly developed to measure the CEC of soil, using for saturation a solution of ammonium acetate 1N. This method involves the subsequent release of NH_4^+ ions from zeolites and measurement of their concentration in the resulted solution.

Although the cation-exchange capacity laid the foundation for applications in different industries, no international standard method is available

for the determination of this exchange capacity of zeolites. Also, the literature is very scarce in presenting methods for CEC determination in zeolites.

A methodology to calculate the CEC of zeolites is based on the measurement of the content of the exchanged cations (K^+, Na^+, Ca^{2+}, and Mg^{2+}) from zeolite samples by NH_4^+ ion [7]. The measurement of these cations in solution can be carried out using spectrometric, ion chromatographic or titrimetric methods. Amongst the spectrometric methods, those using inductively coupled plasma torch as spectral source (inductively coupled plasma optical emission spectrometry (ICP-OES) and inductively coupled plasma mass spectrometry (ICP-MS)) are preferred due to the advantages of multi-element detection capabilities and wide dynamic range [11,12].

In order to produce reliable analytical results, a laboratory should validate the used methods [13]. The purpose of method validation is to ensure that the analytical methodology is accurate, precise, and robust within a specific domain in which the analyte is determined. The methodologies used for the evaluation of performance parameters should take into account the calibration using reference standards, use of certified reference materials, comparison of results achieved by different methods and estimation of the uncertainty of the results [14-16].

The purpose of this study was to perform validation of a method used for the determination of exchangeable cations in zeolites by ICP-OES after their replacement by NH4+ ions from an ammonium chloride solution, and to evaluate the measurement uncertainty for this method. The validation was performed considering the recommendations of the Cooperation for Analytical Chemistry in Europe (EURACHEM) guide [17]. This paper represents a model for the method validation in analytical laboratories in order to check the fit for purpose of spectrometric analytical methods.

RESULTS AND DISCUSSION

Characteristics of the zeolite samples

In order to evaluate the suitability of a zeolite for a specific application as cation exchange material, the determination of its physical-chemical properties is necessary. The chemical formula of zeolites may be presented as $Me_{2/n}O$ Al_2O_3 $xSiO_2$ yH_2O, where *Me* is an atom of alkali or alkaline earth element, *n* represent the charge of *Me*, *x* is the number of Si tetrahedra, while *y* is the number of water molecules [1]. The main cations of alkali or alkaline earth elements present in natural zeolites are K^+, Na^+, Ca^{2+}, and Mg^{2+}. Thus, the measurement of exchangeable cations concentrations will provide a good indication of zeolite cation exchange capacity. Knowing the amounts of each cation released by zeolite during the exchange process offers also useful information for intended use of zeolite.

Fourteen natural zeolites samples (Z1–Z14) from a quarry located in Racos, Brasov County, Romania were collected and analyzed. The samples were preliminary characterized regarding chemical composition for major elements using ICP-OES after microwave assisted digestion. Three parallel determinations including digestion and instrumental measurements were carried out for each sample. The measured concentrations of major elements (Si, Al, Fe, Na, K, Ca, and Mg) were converted to oxides using atomic and molecular masses [8]. Minimum, maximum, mean, median and standard deviation [18] for each oxide, along with skewness, kurtosis values to evaluate normality of distribution calculated using Statistica version 10 Software [19] are presented in Table 1.

Table 1. Major oxides concentrations (%) in zeolite samples from the Racos deposit, Romania

Sample	SiO_2	Al_2O_3	CaO	MgO	K_2O	Na_2O	Fe_2O_3	MnO
Z1	62.95	10.29	2.50	0.72	2.32	0.40	1.39	0.02
Z2	58.98	9.87	2.85	0.59	2.12	0.88	1.12	0.03
Z3	57.09	9.89	2.05	0.65	2.29	0.53	1.23	0.02
Z4	59.09	10.55	2.75	0.54	2.18	0.81	1.04	0.03
Z5	63.84	10.34	2.59	0.55	2.14	0.78	1.10	0.02
Z6	60.17	10.20	2.05	0.73	1.97	0.16	1.36	0.01
Z7	63.75	10.22	2.28	0.72	2.14	0.21	1.15	0.01
Z8	71.79	10.63	2.64	0.66	2.50	0.52	1.55	0.03
Z9	62.68	11.14	2.50	0.70	2.32	0.72	1.44	0.02
Z10	57.32	10.74	2.19	0.71	2.50	0.42	1.41	0.14
Z11	67.50	10.15	2.84	0.59	2.44	0.62	1.59	0.04
Z12	65.36	11.19	2.26	0.82	2.29	0.58	1.59	0.05
Z13	59.30	10.72	2.12	0.73	2.20	0.53	1.43	0.03
Z14	63.43	10.84	2.31	0.80	2.17	0.56	1.70	0.08
Min.	57.09	9.87	2.05	0.54	1.97	0.16	1.04	0.01
Max.	71.79	11.19	2.85	0.82	2.50	0.88	1.70	0.14
Mean	62.38	10.48	2.42	0.68	2.25	0.55	1.36	0.04
Median	62.81	10.45	2.40	0.70	2.25	0.55	1.40	0.03
Stdev.	4.11	0.42	0.28	0.09	0.15	0.21	0.21	0.03
Skewness	0.791	0.231	0.186	-0.185	0.145	-0.346	-0.114	2.356
Kurtosis	0.637	-0.783	-1.431	-0.777	-0.379	-0.214	-1.138	6.025

The concentrations of SiO_2 were in the range of 57.09 - 71.79 %, with a mean value of 62.38 %. The concentrations of the other oxides ranged between 9.87 – 11.19 % Al_2O_3, 2.05 -2.85 % CaO, 0.54 – 0.82 % MgO, 1.97 – 2.50 % K_2O, 0.16 – 0.88 % Na_2O, 1.04 – 1.70 % Fe_2O_3 and 0.01 – 0.14 % MnO. The skewness value indicates the deviation of the distribution from symmetry. When the skewness value significantly differs from 0, the distribution is asymmetrical,

while when this value is less than -1 or greater than 1, the distribution is considered highly asymmetrical [19,20]. Except for MnO, the skewness values within the range of -1 to 1 were calculated, indicating a normal distribution. Kurtosis value is associated with the peakedness of a distribution, and its value increases with peakedness and decreases with flatness [20]. The homogeneity of the oxide concentrations was indicated by the closeness between mean and median values, as well as by low values of the standard deviations. These homogenous distributions of different constituents in the samples can be considered an advantage for the exploitation of the zeolitic tuff from this quarry.

Clinoptilolite mineral has a Si/Al ratio higher than 4 and prevailing alkaline cations (Na + K > Ca) [21]. The content of the alkaline cations are dominant and indicates that the main mineral in zeolitic tuffs collected from Racos deposit is clinoptilolite-type, with Si/Al ratios ranging between 4.70–5.86, and sum of Na + K concentrations higher than Ca concentrations, in all samples. In Figure 1 is presented the XRD pattern of sample Z1.

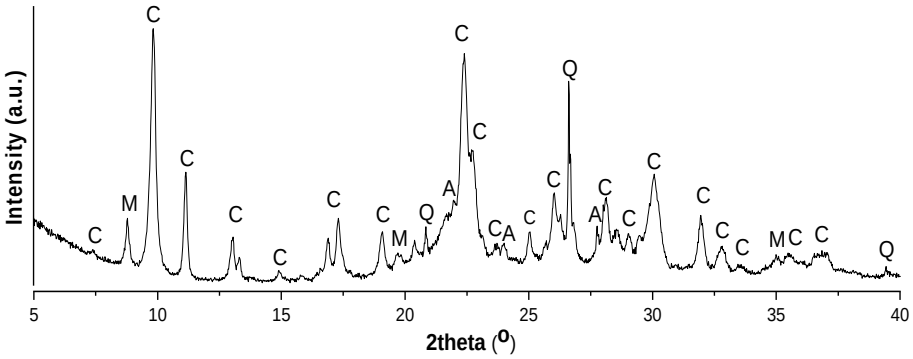

Figure 1. X-ray diffraction pattern of the zeolite sample Z1 from Racos quarry

According to X-ray diffraction analysis, the investigated zeolites from the Racos quarry contain clinoptilolite (*C,* $KNa_2Ca_2(Si_{29}Al_7)O_{72} \cdot 24H_2O$, PDF 00-039-1383) as the main crystalline phase, accompanied by quartz (*Q;* SiO_2, PDF 00-005-0490), muscovite (*M;* $KAl_2(AlSi_3O_{10})(OH)_2$, PDF 00-007-0025) and albite (*A,* $NaAlSi_3O_8$, PDF 00-019-1184) in lower concentrations.

Method validation

The validation of the analytical procedure for determination of exchangeable cations in zeolites by ICP-OES was performed by evaluating the main figures of merit: limit of detection (LoD), limit of quantification (LoQ), working and linear range for each individual cation, trueness/accuracy and

precision according to the EURACHEM guide [17]. The concentrations of exchangeable cations (Na^+, K^+, Ca^{2+} and Mg^{2+}) replaced by NH_4^+ ion from a solution of NH_4Cl 1M were measured by ICP-OES. Inter-cationic exchange capacity was calculated as mEq 100 g^{-1}, taking into account measured concentration for each cation in extraction solution and its corresponding gram equivalent, amount of zeolite sample used for extraction (15 g) and final volume of extract (250 mL).

Selectivity

In the determinations of analytes using spectrometric techniques from samples having complex matrices (in this case, extracts form zeolites), spectral and non-spectral interferences may occur as a result of the other elements present in the solid sample, as well as the matrix of extracting solution. Matrix effects were studied by recovery of spikes in the extract samples, by adding a spike of 10 mg L^{-1} of each element to the original samples. The recoveries were within 90% and 110%, for all the elements.

LoD and LoQ for exchangeable cations

LoD was estimated from the calibration function for an average net signal resulted from measurement of 10 independent reagent blank solutions containing 1M NH_4Cl, measured once each, on the same day and three times its standard deviation. LoQ was estimated from the calibration function for a signal equal to the net signal of blank and ten times its standard deviation [17,22]. In order to experimentally confirm LoQ, six extracting solution with concentrations close to the LoQ were prepared and analysed. The targeted repeatability expressed as relative standard deviation (RSD) and targeted recovery were 20 % and 90-115 %, respectively. Data in Table 2 shows the LoD, LoQ and the measured RSD and recovery for LoQ confirmation.

Table 2. LOD and LOQ for exchangeable cations in extracting solution 1M NH_4Cl by ICP-OES

Element	λ (nm)	LoD (mg L^{-1})	LoQ (mg L^{-1})	RSD at LoQ (%)	Recovery at LoQ (%)
Na	589.592	0.021	0.070	8.84	109
Mg	285.213	0.025	0.083	7.63	94.2
K	766.490	0.014	0.047	10.8	95.6
Ca	317.933	0.011	0.037	8.46	92.5

Considering the LoQ values for cations in extraction solution measured by ICP-OES, the corresponding LoQs expressed as exchange capacity taking into account the extraction procedure were calculated to be 0.005 mEq 100 g^{-1}

for Na^+, 0.011 mEq 100 g^{-1} for Mg^{2+}, 0.002 mEq 100 g^{-1} for K^+, 0.003 mEq 100 g^{-1} for Ca^{2+}, while LoQ for sum of exchangeable cations in zeolite sample was estimated to be 0.021 mEq 100 g^{-1}. Generally the natural zeolites have much higher amounts of exchangeable cations than the calculated LoQs, thus the investigated method is adequate for the intended purpose [22-25].

Working and linear range

In the case of spectrometric techniques, the working range is the domain of concentrations over which the method is linear for a specific analyte. At the lower part of the working range, the limiting factor is given by LoQ, while at the superior part, the limitations are imposed by the instrument analytical response. Linearity was evaluated from the regression function of calibration using 7 standards, the lowest concentration close to the LoQ, and the higher concentration of 20 mg L^{-1} for each element. In order to check the homogeneity of variances, 6 measurements at the lowest and at the highest concentrations of calibration curves were measured, and the standard deviations (s_1) and (s_7) were calculated [26]. Using these values, the PG ratios calculated as s_1^2/s_7^2 or s_7^2/s_1^2 were compared with the critical value Fischer $F_{5;5;0.99} = 11$.

The values for intercept (*a*), slope (*b*), correlation coefficient (*R*), *PG* ratio and standard error of the regression (S_{x0}) are presented in Table 3.

Table 3. Characteristics of the calibration curves for the working range 0.02 – 20 mg L^{-1} using ICP-OES

Element	Intercept (a)	Slope (*b*)	PG	Correlation coefficient (R)	S_{x0}
Na	302536	1082123	7.33	0.9999	0.070
Mg	2036	175305	4.31	0.9999	0.061
K	188793	556877	5.22	0.9999	0.101
Ca	8740	20701	8.64	0.9998	0.120

The experimental data showed that variances are homogenous, and the correlation coefficients are much higher than 0.997, therefore linear regression can be used.

Precision

Internal repeatability for the measurement of exchangeable cations was evaluated by analysis of 6 parallel zeolite samples, including extraction step, performed by a single operator using the same equipment. The set targets were relative standard deviation of repeatability (RSDr) below 10% and limit of repeatability (r) below 28%.

The obtained data, showed in Table 4, indicate that standard deviation of repeatability/limit of repeatability were better than the imposed limits for all the analysed cations.

Table 4. Results from the repeatability study (n=6 parallel zeolite samples) using ICP-OES after microwave assisted digestion

Element	Average (mg/L)	s_r (mg/L)	RSD_r (%)	r (%)
Na^+	154	6.93	4.50	12.6
Mg^{2+}	35.3	1.92	5.43	15.2
K^+	705	46.2	6.55	18.3
Ca^{2+}	742	41.0	5.53	15.5

s_r – standard deviation of repeatability; RSD_r – relative standard deviation of repeatability; r – limit of repeatability (2.8x RSD_r)

Trueness

The most frequent approach to estimate trueness is to evaluate recovery from analysis of CRMs or spiked samples. Since no CRM having certified values for exchangeable cations in zeolites or other silicate materials are available, in our study we evaluated the recovery using a CRM (BCS-CRM 375/1 soda feldspar) with certified values for total content of Na_2O, K_2O, CaO, and MgO. Accurate data for this determination gives indication mainly about reliability of instrumental determination of Na^+, K^+, Ca^{2+} and Mg^{2+} by ICP-OES. The results obtained in the analysis of CRM presented in Table 5 indicate good recoveries in the range of 92 – 103%. These recovery values were in the range of 80 – 120% recommended by Association of Official Agricultural Chemists (AOAC) [27] for spectrometric methods. This shows the lack of systematic errors and proves that the proposed method is reliable and free of non-spectral effects.

Table 5. Certified values of CRM BCS-CRM 375/1 soda feldspar, measured values by ICP-OES (n = 6 parallel determinations) and the recoveries (%)

Components	Certified Values ± U (%)	Measured Values ± U* (%)	Recovery ± U* (%)
Na_2O	8.89 ± 0.11	9.06 ± 0.62	102 ± 7
K_2O	1.47 ± 0.03	1.37 ± 0.12	93 ± 8
MgO	0.180 ± 0.016	0.185 ± 0.018	103 ± 10
CaO	0.78 ± 0.03	0.72 ± 0.07	92 ± 9

*U is the expanded uncertainty for 95 % confidence level (k=2)

In order to evaluate the agreement between certified and measured values in CRM, the combined uncertainty ($U\Delta$) was calculated from the specified uncertainty (U_{CRM}) and measured uncertainty (U_m) expressed as standard deviation, as well as the difference between average measured concentration (C_m) and the certified values (C_{CRM}). The difference between the certified and measured value of each analyte was lower than the combined uncertainty.

Also, an extraction solution of NH_4Cl 1M fortified with 10 mg L^{-1} of each cation was analysed. The recoveries were within 90% and 110% for all the four cations. These results also confirm the lack of non-spectral effects for the proposed method.

Estimation of measurement uncertainty

The main sources of uncertainty of this method are: uncertainty of reference materials used for instrument calibration, uncertainty of dilutions for preparation of reference solutions and samples, uncertainty of the calibration curves, uncertainty of samples weighting, and repeatability of the replicate analysis. The uncertainty budget for each individual cation and the main sources of uncertainty with their contribution to composed uncertainty are presented in Table 6.

Table 6. Uncertainty budget for exchangeable cations and cation exchange capacity (CEC) determination in zeolite samples

Sources / relative standard uncertainty	Unit	Na^+	Mg^{2+}	K^+	Ca^{2+}
Calibration standard	-	0.006	0.006	0.006	0.006
Standards dilution	-	0.013	0.013	0.013	0.013
Weighting	-	0.0001	0.0001	0.0001	0.0001
Sample dilution	-	0.0022	0.0022	0.0022	0.0022
Calibration curve	-	0.0070	0.0061	0.0101	0.0120
Repeatability	-	0.0450	0.0543	0.0655	0.0553
Relative composed uncertainty (u_c)	%	4.8	5.6	6.8	5.8
Relative expanded uncertainty (U) $U=2xu_c$ (95% confidence interval)	%	9.5	11.3	13.5	11.7

Exchangeable cations in zeolite samples

The exchangeable cations measured by ICP-OES in the extracting solution after their replacement by ammonium ion are given in Table 7.

Table 7. Exchangeable cations and cation exchange capacity (CEC) in zeolite samples from the Racos deposit, Romania

Sample	Na^+	Mg^{2+}	K^+	Ca^{2+}	CEC
	mEq 100 g^{-1}				
Z1	13.1	4.2	21.1	67.8	116.2
Z2	28.9	2.7	31.2	79.6	142.4
Z3	15.6	4.0	30.9	59.1	109.6
Z4	25.7	2.5	41.5	82.2	151.9
Z5	25.0	2.5	31.2	79.6	138.2
Z6	4.3	3.7	29.8	63.3	101.2
Z7	7.1	2.6	31.2	51.3	92.1
Z8	15.4	1.9	33.6	53.2	104.1
Z9	20.4	3.7	29.1	77.8	130.9
Z10	11.2	4.8	30.1	61.8	107.9
Z11	17.8	1.7	31.4	69.2	119.9
Z12	15.0	4.4	26.9	66.0	112.3
Z13	15.7	4.4	26.7	67.6	114.5
Z14	15.8	3.8	29.5	69.0	118.1
Min.	4.3	1.7	21.1	51.3	92.1
Max.	28.9	4.8	41.5	82.2	151.9
Mean	16.5	3.4	30.3	67.7	118.5
Median	15.6	3.7	30.5	67.7	115.4
Stdev.	6.8	1.0	4.4	9.6	16.8
Skewness	0.145	-0.268	0.608	-0.086	0.591
Kurtosis	-0.106	-1.661	3.764	-0.756	-0.215

According to the obtained data, showed in Table 7, the total inter-cationic exchange capacity varied in the range of 92.1 – 151.9 mEq 100 g^{-1}, with an average value of 118.5 mEq 100 g^{-1}, which means a high exchange capacity of the studied zeolites. The main contribution to the total inter-cationic exchange capacity is due to the Ca^{2+} (in average 57% of the CEC), K^+ has an average contribution of 25.9% of the IEC, Na^+ 13.5% of the CEC, while Mg^{2+} has an average contribution to CEC of only 2.9%. The release of low amounts of Mg suggests that Mg may be fixed in zeolite, and is not totally released into extracting solution.

Skewness values within the range of -1 to 1 indicate normal distributions for all analysed exchangeable cations. Relatively low values of the standard deviations for the exchangeable Mg^{2+}, K^+, Ca^{2+} (below 30%, if calculated as relative standard deviations) indicate good homogeneity of distributions for these cations. However, in case of exchangeable Na^+ the standard deviation was over 40% (expressed as relative standard deviation), indicating a variable release of this cation into the extracting solution.

An increased inter-cationic exchange capacity is required when using natural zeolites in green decontamination technologies that are based on the ion exchange behavior. In this process, the zeolite exchangeable cations are replaced at the sites by other cations from contaminated media [28]. Thus, zeolites with high exchange capacity are desirable for removal of toxic metals cations (Cu^{2+}, Zn^{2+}, Cd^{2+}, Hg^{2+}, Pb^{2+}, Cr^{3+}, Mn^{2+}, Co^{2+}, Ni^{2+}, etc.) and ammonium cation from wastewaters [29,30].

Belchinskaya et al. [31] reported variable quantities of exchangeable cations desorbed from a natural zeolite form the Sokirnitsa deposit, Ukraine, in the range of 56.7 - 190.1 meq 100 g^{-1}, influenced by concentration of ammonium solution used for extraction. Cerri et al. analysed 20 samples of clinoptilolite-bearing rocks from Sardinia, Italy and reported values in the same order of concentrations (35 - 120 meq 100 g^{-1}) [32].

CONCLUSIONS

Fully validated method for exchangeable cations analysis in zeolites after extraction in NH_4Cl solution is presented. The fast and precise ICP-OES technique allows the quantification of selected cations in this type of samples. The performance parameters (LOD and LOQ, selectivity, working and linear range, accuracy, precision and measurement uncertainty) satisfied the imposed targets. The method was successfully used for the determination of exchangeable cations in zeolite samples. It provides useful data regarding total cation exchange capacity, and also gives information about the amount of each individual cation released in extracting solution. The results attained by physical-chemical methods showed that the zeolitic tuffs from the Racos deposit, Romania is clinoptilolite-type and have high exchange capacity.

EXPERIMENTAL SECTION

Materials

ICP multi-elemental standard solution IV 1000 mg L-1 and mono-element standard solution Si 1000 mg L-1 purchased form Merck (Darmstadt, Germany) were used for ICP-OES calibration. HNO3 65%, HCl 37%, and HF 40%, p.a. obtained from Merck (Darmstadt, Germany) were used for samples digestion or to prepare calibration solutions. Ammonium chloride ≥ 99.5% from Merck (Darmstadt, Germany) was used to prepare the extracting solution NH4Cl 1M. For all dilutions ultrapure water (18 MΩ cm-1) obtained from a Millipore Direct Q3 (Millipore, France) was used. Certified reference material

CRM BCS-CRM 375/1 soda feldspar from Bureau of Analysed Samples Ltd (United Kingdom) was analyzed for the recovery study. Fourteen natural zeolites samples (Z1–Z14) were collected from a quarry located in Racos, Brasov County, Romania.

Sample preparation and instrumentation

For the determination of total contents of elements in zeolites, 0.25 g sample, with grain size <100 µm, was digested with a mixture of 3 mL HNO_3 65%, 9 mL HCl 37%, and 2 mL HF 40%, in a closed-vessel MWS-3+ microwave system (Berghof, Germany). A three steps digestion program was applied: (1) 10 min at 200 ˚C, (2) 30 min at 220 ˚C, (3) 15 min at 100 ˚C. After cooling 2 grams of H_3BO_3 was added and vessels were heat again at 220 ˚C for 30 minutes. The resulting solutions were cooled and diluted to 100 mL with ultrapure water. In order to avoid contamination digestion vessels were pre-cleaned with 10% (v/v) HNO_3.

The mineralogy and crystallinity of zeolite were investigated by X-ray diffraction method using a Bruker D8 Advance diffractometer using CuKα radiation (λ=1.54056 Å) and LynxEye detector, operated at 40 kV and 40 mA.

As no standard method for the determination exchangeable cations in zeolites is available, in this study we used a modification of several methods based on the replacement of K^+, Na^+, Ca^{2+}, and Mg^{2+} ions from zeolite by NH_4^+ from NH_4Cl solution, presented in previous published works [31,32]. A ratio of solid / liquid ratio 1:10 was chosen to ensure enough amount of NH_4^+ to remove in solution the exchangeable cations. For determination of exchangeable cations, 15 ± 0.01 g zeolite sample with grain size <100 µm was weighted in a Berzelius beaker, then 150 mL NH_4Cl 1M were added. The mixture was shaken for 1 h on a magnetic stirrer, and the insoluble part was filtered through 0.45 µm Whatman cellulose membrane filters (Amersham, United Kingdom) and the filtrate was collected in a volumetric flask and diluted up to 250 mL with ultrapure water. The amounts of Na^+, K^+, Ca^{2+} and Mg^{2+} replaced by NH_4^+ ion in this solution were measured using ICP-OES. Three parallel extractions were done for each sample.

Instrumentation

Analyses were carried out using a dual viewing inductively coupled plasma optical emission spectrometer Optima 5300DV (Perkin Elmer, USA). The operating conditions used for ICP-OES determination were 1300W RF power, 15 L min^{-1} plasma Ar flow, 2.0 L min^{-1} auxiliary Ar flow, 0.8 L min^{-1} nebulizer Ar flow, and 1.5 mL min^{-1} sample uptake rate. Axial view and external calibration (7-point linear calibration curve over the range 0 – 20 mg L^{-1} element in 4% HNO_3) were used for metals determination.

ACKNOWLEDGMENTS

The work has been funded by the Competitiveness Operational Programme of the Ministry of European Funds through the Contract No. 7/01.09.2016, code MySMIS 105654.

REFERENCES

1. S. Kraljevic Pavelic; J. Simovic Medica; D. Gumbarevic; A. Filosevic; N. Przulj; K. Pavelic; *Front. Pharmacol*., **2018**, *9*, 1350.
2. B. Calvo; L. Canoira; F. Morante; J.M. Martinez-Bedia; C. Vinagre; J.E. Garcia-Gonzalez; J. Elsen; R. Alcantara; *J. Hazard. Mater.*, **2009**, *166*, 619-627.
3. M. Senila; O. Cadar; L. Senila; A. Hoaghia; I. Miu; *Molecules*, **2019**, *24*, 4023.
4. M. Hong; L. Yu; Y. Wang; J. Zhang; Z. Chen; L. Dong; Q. Zan; R. Li; *Chem. Eng. J*., **2019**, *359*, 363–372.
5. A. Mastinu; A. Kumar; G. Maccarinelli; S.A. Bonini; M. Premoli; F. Aria; A. Gianoncelli; M. Memo; *Molecules*, **2019**, *27*, 1517.
6. M. Mudasir; K. Karelius; N.H, Aprilita, E.T. Wahyuni; *J. Environ. Chem. Eng*., **2016**, *4*, 1839-1849.
7. S.A. Maicaneanu; H. Bedelean; *Studia UBB Chemia*, **2020**, *LXV*, *3*, 89-100.
8. O. Cadar; M. Senila; M.A. Hoaghia; D. Scurtu; I. Miu; E.A. Levei; *Molecules*, **2020**, *25*, 2570.
9. M.W. Munthali; P. Kabwadza-Corner; E. Johan, N. Matsue; *J. Mater. Sci. Chem. Eng.*, **2014**, *2*, 1-5.
10. K. Kitsopoulos; *Clays Clay Miner*., **1999**, *47*, 688-696.
11. E. Covaci; M. Senila; M. Ponta; T. Frentiu; *Rev. Roum. Chim*., **2020**, *65*, 735-745.
12. T. Frentiu; M. Ponta.; M. Senila; A.I. Mihaltan.; E. Darvasi; M. Frentiu; E. Cordos; *J. Anal. At. Spectrom*., **2010**, *25*, 739–742.
13. M. Senila; E. Levei; L. Senila; O. Cadar; G. Oprea; C. Roman; *Studia UBB Chemia*, **2011**, *56*, 27.
14. A. Tudorache; D.E. Ionita; N.M. Marin; C. Marin; I.A. Badea; *Accred. Qual Assur*., **2017**, *22*, 29–35.
15. M. Senila; E. Covaci; O. Cadar; M. Ponta; M. Frentiu; T. Frentiu; *Chem. Pap*., **2018**, *72*, 441-448.
16. T. Frentiu; S. Butaciu; E. Darvasi; M. Ponta; M. Senila; D. Petreus; M. Frentiu; *Anal. Methods*., **2015**, *7*, 747–752.
17. B. Magnusson; U. Ornemark (eds.) Eurachem Guide: The Fitness for Purpose of Analytical Methods – A Laboratory Guide to Method Validation and Related Topics, (2nd ed. 2014), available from https://www.eurachem.org/images/stories/Guides/pdf/MV_guide_2nd_ed_EN.pdf, accessed on 18.03.2021.

18. M. Senila; *J. Environ. Health Sci. Eng*., **2014**, *12*, 108.
19. StatSoft, Inc. (2011). STATISTICA (data analysis software system), version 10. www.statsoft.com.
20. M.K. Cain; Z. Zhang; K.H. Yuan; *Behav. Res*., **2017**, *49*, 1716-1735.
21. D. Bish; J. Boak; *Rev. Mineral. Geochem*., **2001**, *45*, 207-216.
22. A. Drolc; A. Pintar; *Accreditation Qual. Assur.,* **2012**, *17*, 323–330.
23. N. Eroglu; M. Emekci; C.G. Athanassiou; *J. Sci. Food Agric*., **2017**, *97*, 3487–3499.
24. B. Hudcova; M. Osacky; M. Vítkova; A. Mitzia; M. Komarek; *Microporous Mesoporous Mater*., **2021**, *317*, 111022.
25. J.A. Ricardo-Garcia; Y. Enamorado-Horrutiner; G. Rodriguez-Fuentes; M.S. Pomares-Alfonso; M.E. Villanueva-Tagle; *Microchem. J.*, **2021**, *164*, 106064.
26. International organization for standardization (1990) ISO 8466-1 Water quality. Calibration and evaluation of analytical methods and estimation of performance characteristics - Part I: Statistical evaluation of the linear calibration function, Geneva, Switzerland.
27. Chemical Methods for Dietary Supplements and Botanicals. (2002) https://www.aoac.org/aoac_prod_imis/AOAC_Docs/StandardsDevelopment/SLV_Guidelines_Dietary_Supplements.pdf (accessed May 2021).
28. M. Moshoeshoe; M.S. Nadiye-Tabbiruka; V.O. Moshoeshoe; *Am. J. Mater. Sci.*, **2017**, *7*, 196-221.
29. D. Kallo; *Rev. Mineral. Geochem*., **2001**, *45*, 519–550.
30. E. Neag; A.I. Torok; C. Tanaselia; I. Aschilean; M. Senila; *Water*, **2020**, *12*, 1614.
31. L. Belchinskaya; L. Novikova; V. Khokhlov; J.L. Tkhi; *J. Appl. Chem*., **2013**, *789410*, 1-9.
32. G. Cerri; A. Langella; M. Pansini; P. Cappelletti; *Clays Clay Miner*., **2002**, *50*, 127–135.

STUDIA UBB CHEMIA, LXVI, 2, 2021 (p. 95-104)
(RECOMMENDED CITATION)
DOI:10.24193/subbchem.2021.2.08

ACTIVATED NATURAL ZEOLITES FOR PETROLEUM HYDROCARBONS ADSORPTION

MARIA-ALEXANDRA HOAGHIA[a], IOAN ASCHILEAN[b], VANDA BABALAU-FUSS[a,c], ANCA BECZE[a], OANA CADAR[a], CECILIA ROMAN[a], MARIUS ROMAN[a], MARIN SENILA[a], ENIKO KOVACS[a,c*]

ABSTRACT. This study was carried out with the aim of increasing and determining the activated zeolites' adsorption capacity by testing their efficiency on petroleum hydrocarbons. Natural zeolite samples were sequentially studied after thermal and chemical activations. The results indicated that after the activations, the zeolite samples gained an increasing adsorption capacity of petroleum hydrocarbons. Furthermore, the zeolites with small particulate sizes (<10 μm) have a higher adsorption capacity than the zeolites with a granulometry of 1-3 mm. The metal content ranged between 4200-7400 mg/kg Na, 15090-22990 mg/kg Ca, 2670-3950 mg/kg Mg, 19470-19670 mg/kg K, 6140-7210 mg/kg Fe and 149-178 mg/kg Mn. Mineralogical analyzes (X-ray diffraction - XRD and scanning electron microscopy - SEM) were applied for the characterization of the zeolites. According to the XRD results, the zeolites are characterized by a 64 % crystallization level. The main mineral which was determined was Clinoptilolite-Ca. The SEM micrographs indicate the morphology of zeolite surfaces.

Keywords: *zeolites, thermal treatment, chemical activation, adsorption capacity*

INTRODUCTION

Petroleum hydrocarbons are a valuable fuel source, as well as a raw material for a wide range of industrial applications all over the world. On the

[a] *INCDO-INOE 2000, Research Institute for Analytical Instrumentation subsidiary, ICIA Cluj-Napoca, 67 Donath, RO-400293, Cluj-Napoca, Romania*
[b] *Zeolites Production S.A., 359 Republicii, RO-505500, Rupea, Romania*
[c] *University of Agricultural Science and Veterinary Medicine, 3-5 Calea Manastur, RO-400372, Cluj-Napoca, Romania,*
** Corresponding author: eniko.kovacs@icia.ro*

other hand, they are a major environmental polluter, being classified as priority pollutants [1]. Oil and oil products spillages generate considerable damages, thus, more focus is being given to the development of advanced solutions to eliminate these pollutants. Besides the environmental impact of petroleum hydrocarbons, these pollutants cause a major risk to both humans and other forms of life [2, 3, 4, 5]. Ahmed and Fakhruddin [6] provided an overview on the impact of petroleum hydrocarbons on soil, water, and human health, as well as on the use of microorganisms for their degradation.

Different techniques and solutions are being used for the isolation, treatment, removal and control of petroleum-polluted environments. The decontamination technique using zeolites as adsorbents proved to be beneficial to the economy and to the environment [7, 8].

Zeolites are crystalline aluminosilicates composed of three-dimensional structures of AlO_4 and SiO_4 tetrahedra bound together by oxygen ions. Molecular sieves are a term that is often used to describe them. They are expressed chemically by the analytical formula: $M_2/nOAl_2O_3 \cdot ySiO_2 \cdot wH_2O$, where y is 2-200; n is the cation valence and w is the water contained in the voids [9].

Due to their structure, both synthetic and natural zeolites have been used in many industrial processes such as adsorption (gas separation), catalysis (petroleum refining, petrochemical production), separation (detergents, soaps). Many studies focus on synthetic zeolites used as mineral sorbents of diesel fuels and used engine oil [10], as sorbents of benzene, toluene, p-xylene (BTX) [11], as desulfurization sorbents of hydrocarbon fuels, containing benzothiophene and dibenzothiophene [12].

Among the natural zeolites, clinoptilolite has been widely used due to its abundance and ion exchange properties. In a study conducted by Favvas et al [13], clinoptilolite from the area of Drista River (North Greece) was used as a dehydration agent of diesel fuels and their findings indicated an increase in the physicochemical properties of the analyzed fuels. Natural clinoptilolite's potential as a Fenton catalyst in the removal of aromatic hydrocarbons was investigated by Rusoo et al [14]. Al-Jamal et al [15] studied the potential of Jordanian raw zeolitic tuff in adsorbing the oil from oil-contaminated water, by the use of de-alumination and micro-emulsification treatments. Zeolites originated from Romania have been used by different studies in environmental protection and medicine, such as biomonitoring of air pollution, waste water treatment, removal of Fe and Mn from diverse solutions, behavior of zeolites in simulated gastric fluid [16, 17, 18, 19].

In the present study, the determination of the adsorption capacity of a natural zeolite (clinoptilolite) was studied by using two activation methods: (i) thermal activation, and (ii) chemical activation, in order to increase the petroleum hydrocarbons adsorption capacity.

The zeolites were activated with surfactants with the aim of increasing the petroleum hydrocarbons adsorption capacity. After the activation with surfactants, the surface of material is changed from hydrophilic to hydrophobic.

The findings will contribute to the understanding of the potential use of natural zeolites in improving petroleum hydrocarbons spill cleanup.

RESULTS AND DISCUSSION

Zeolite characterization

The physico-chemical and mineralogical characteristics of the zeolites (not activated, thermally activated, and thermally and chemically activated) under this study are indicated as it follows.

X-ray diffraction (XRD) analysis

The XRD patterns of the thermally activated (at 500°C) zeolites are presented in figure 1.

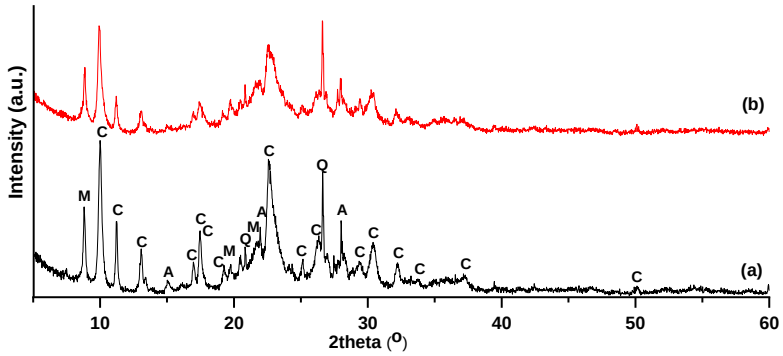

Figure 1. XRD patterns of thermally activated zeolites with particle sizes of *(a)* <10 μm and *(b)* 1-3 mm. Note: A- albite, C- clinoptilolite, Q- quartz, M- muscovite

According to the XRD analysis, the investigated zeolites contain clinoptilolite (00-070-1859) as the major crystalline phase, accompanied by muscovite (00-006-0263), quartz (00-005-0490) and albite (00-020-0548). The non-crystalline components were not quantified by the XRD analysis, but the presence of amorphous volcanic glass in zeolites is indicated by the broad diffraction hump at $2\theta = 20\text{-}25^{o}$. A slight decrease in the degree of crystallinity was remarked for higher particle size (54.6%) comparing with lower particle size (63.6%).

Scanning electron microscopy (SEM) results

SEM was applied for Az1 and Az2 zeolites, with particles dimensions < 10 µm and 1-3 mm, not activated and thermally activated at 500 °C.

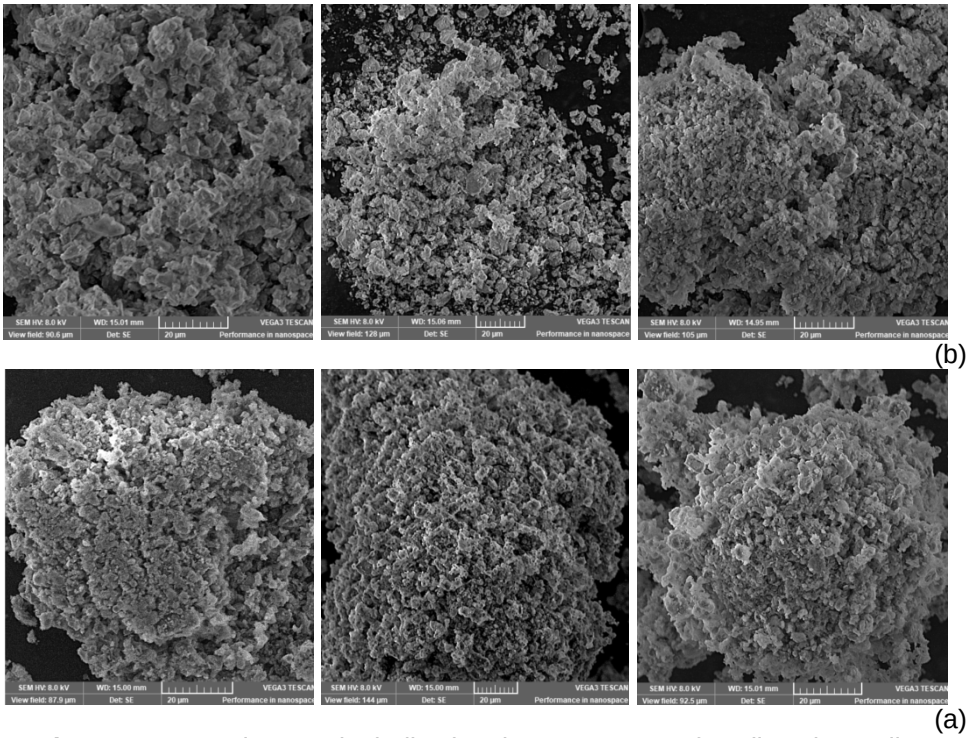

Figure 2. SEM micrographs indicating the occurrence of zeolites thermally activated *a)* Az1 (particle sizes < 10 µm) and *b)* Az2 (particle sizes 1-3 mm)

The Energy-Dispersive X-ray Spectroscopy (EDX) analysis indicate that the zeolites samples are characterized by concentrations of 43.0-61.7 % silicon and 7.10-37.4 % oxygen.

Metals and oxides content

The metals (Al, Ca, Fe, K, Mg, Mn, Na) and major oxides (Al_2O_3, CaO, Fe_2O_3, K_2O, MgO, MnO, Na_2O) contents in the zeolites only thermally activated were determined in a previous study [20]. The results indicate variations of the Al content between 59000-68000 mg/kg, Na, Ca, Mg and K ranging between 4200-7400 mg/kg, 15090-22990 mg/kg, 2670-3950 mg/kg and 19470-19670 mg/kg [20]. Fe and Mn vary between 6140-7210 mg/kg and 149-178 mg/kg. Generally, the metal content is higher in the zeolite with lower particle sizes [20].

In the current study, the results of the metals content in chemically activated zeolites are showed in Table 1.

Table 1. The metal content (mg/kg) in the chemically activated zeolites (Az3-Az8)

Sample	Al	Ca	Fe	K	Mg	Mn	Na
Az3 10	62524	15468	5210	18418	3470	147	4919
Az4 1-3	67886	20983	4204	17736	4207	229	3677
Az5 10	64747	16507	5698	19166	3521	157	4904
Az6 1-3	68875	20873	4607	17636	6298	157	3552
Az7 10	60386	15404	5391	18802	3408	144	4745
Az8 1-3	69882	20362	4594	18413	4669	133	3397
Mean	***65717***	***18266***	***4951***	***18362***	***4262***	***161***	***4199***
Min	***60386***	***15404***	***4204***	***17636***	***3408***	***133***	***3397***
Max	***69882***	***20983***	***5698***	***19166***	***6298***	***229***	***4919***

The Al concentrations vary between 60386 to 69882 mg/kg, with higher values obtained in the zeolites with the particle sizes of 1-3 mm and particularly in Az8. The Ca, Mg and Mn amounts are slightly higher in the not activated samples with particle size of 1-3 mm with values between 15404-20983 mg/kg, 3408-6298 mg/kg and 133-229 mg/kg. For the Fe, K and Na, the highest values were found in the samples that were not activated with particle size < 10 μm. The amounts vary between 4204-5698 mg/kg Fe, 17636-19166 mg/kg K and 3397-4919 mg/kg Na.

No significant variations are observed between the samples activated with different surfactant concentrations.

The major oxides results obtained for the chemically zeolites are indicated in Table 2.

Table 2. The major oxides content (%) obtained in the chemically activated zeolites (Az3-Az8)

Sample	Al_2O_3	SiO_2	CaO	Fe_2O_3	K_2O	MgO	MnO	Na_2O
Az3	11.8	67.3	2.17	0.74	2.22	0.58	0.02	0.66
Az4	12.8	68.1	2.94	0.60	2.14	0.70	0.03	0.50
Az5	12.2	67.0	2.31	0.81	2.31	0.59	0.02	0.66
Az6	13.0	66.4	2.92	0.66	2.13	1.05	0.02	0.48
Az7	11.4	65.7	2.16	0.77	2.27	0.57	0.02	0.64
Az8	13.2	68.2	2.85	0.66	2.22	0.78	0.02	0.46
Mean	***12.4***	***67.1***	***2.56***	***0.71***	***2.21***	***0.71***	***0.02***	***0.57***
Min	***11.4***	***65.0***	***2.16***	***0.60***	***2.13***	***0.57***	***0.02***	***0.46***
Max	***13.2***	***68.2***	***2.94***	***0.81***	***2.31***	***1.05***	***0.03***	***0.66***

The Al_2O_3 content varies between 11.4-13.2 %, SiO_2 65.0-68.2 %, while Na_2O, CaO, MgO and K_2O range between 0.46-0.66 %, 2.16-2.94 %, 0.57-1.05 % and 2.13-2.31. The content of Fe_2O_3 varies between 0.60-0.81%, whereas no significant differences are noticed in the MnO results.

Metals in the thermally activated zeolites were indicated in a previous study [20].

Petroleum hydrocarbon adsorption

In order to increase the petroleum hydrocarbon adsorption, the surface of the zeolites is modified with surfactants. This activation changes the character or the surface from hydrophilic to hydrophobic, increasing the organic pollution affinity of the zeolite which acts like a sorbent [21, 22]. The activated zeolite samples chemically activated with surfactant (methyl dodecylbenzene sulfonate) solutions were tested to study the petroleum hydrocarbon adsorption capacity. The highest petroleum hydrocarbon adsorption capacity is observed at samples activated with the most concentrated surfactant solution (2.0 mmol/L). Results vary between 101-253 mg/g adsorbed hydrocarbons by zeolites (Figure 3).

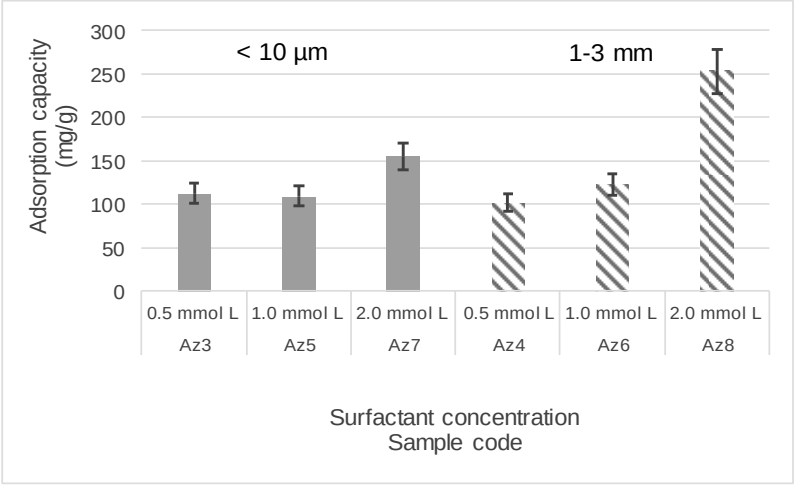

Figure 3. Adsorption capacity (mg/g) in the activated zeolites samples with two granulometries (<10 µm and 1-3 mm) with three different surfactant concentration levels (0.5 mmol/L, 1.0 mmol/L, 2.0 mmol/L)

Samples with the highest granulometry and activated with the 2.0 mmol/L surfactant solution are characterized by the highest petroleum hydrocarbon adsorption capacity. The increasing trend of the zeolite samples is the following Az6<Az4<Az3<Az7<Az5<Az8.

According to the results, an increase of the adsorption capacity was noticed. The zeolite treated with a high concentration of surfactant solution was the most effective (2.0 mmol/L).

The results obtained by Torabian et al [23] also revealed that the zeolite's adsorption capacity is enhanced by the increase of surfactant loading.

Simpson et al. [24] examined the sorption of volatile petroleum hydrocarbons using surfactant modified zeolite and their results showed an increase in the sorption coefficient. The zeolites' affinity for hydrocarbons can be enhanced by transforming their surface from hydrophilic to hydrophobic, under the surfactants' action [25].

CONCLUSIONS

Based on the X-ray diffraction and scanning electron microscopy results, thermally activated zeolites contain clinoptilolite, quartz, muscovite and albite. The SEM micrographs indicate the occurrence of thermally activated zeolites and silicon and oxygen concentrations.

The Al, Ca, Mg and Mn concentrations were slightly higher in the zeolite samples with granulometry of 1-3 mm compared to the samples with lower granulometry (< 10 µm), while the Fe, Na and K amounts were higher in the samples with lower particle sizes. According to the study's results, activated zeolites with 2.0 mmol/L methyl dodecylbenzene sulfonate solution were characterized by the highest petroleum hydrocarbon adsorption capacity. Likewise, the granulometry of samples play an important role in the increasing adsorption capacity.

EXPERIMENTAL SECTION

Sampling, mechanical and thermal treatments

The studied zeolite materials (clinoptilolite tuffs) were provided from the Rupea deposits (Brasov County, central Romania). Clinoptilolite-type minerals represent the predominant zeolite resources in these deposits and generally in the country [26, 27]. After the collection, the samples were crushed and grounded and powdered at two different particle sizes (<10 µm and 1-3 mm). Afterwards, the zeolites were dried at a temperature of 105 °C, using a thermostatic oven INE 200 (Memmert, Germany) for at least 5 h. Then, they were thermally activated at 500 °C for a period of at least 2 h, using an electrical oven model LT9 muffle furnace (Nabertherm, Lilienthal, Germany). Samples were left for cooling in a desiccator, transfused and kept in clean polyethylene bags until the chemical activation.

Chemical activation

The chemical activation consists of treating the zeolites with surfactant (methyl dodecylbenzene sulfonate) solutions. Three different surfactant solutions (0.5 mmol/L, 1.0 mmol/L and 2.0 mmol/L) were prepared. The samples were

immersed (1:10, v:v) and homogenized for 24 h using a magnetic stirrer. Before the separation of the resulted phases, they were left to settle for 45 minutes. The solid phase was washed a coupled of times with distilled water in order to remove the surfactant. The activated zeolites were then dried at 45 °C for 24 h.

After the activation procedures, eight types of materials were obtained as indicated in Table 3.

Table 3. Characteristics for the obtained zeolite materials after three different activations

Sample	Particle sizes	Temperature (°C)	Concentration of methyl dodecylbenzene sulfonate solution (mmol/L)
Az1	< 10 µm	500	-
Az2	1-3 mm	500	-
Az3	< 10 µm	500	0.5
Az4	1-3 mm	500	0.5
Az5	< 10 µm	500	1.0
Az6	1-3 mm	500	1.0
Az7	< 10 µm	500	2.0
Az8	1-3 mm	500	2.0

Characterization techniques

Scanning electron microscopy (SEM)

The SEM was applied with a scanning electron microscope at 8 kV, using a TescanVEGA 3 SBU – EasyProbe model (NanoSystems MC, Czech). The field dimension was 146 µm and the focalization distance at 20 µm.

X-ray diffraction determination

The X-ray diffraction patterns were recorded at room temperature using a D8 Advance (Bruker, Germany) diffractometer operating at 40 kV and 40 mA with CuKα radiation (λ=1.54060 Å).

Metals and major oxides determinations

The metal content (Al, Ca, Fe, K, Mg, Mn, Na) was determined in the activated zeolites (Az3-Az8) after digesting a quantity of 1.0 ± 0.001 g with 28 ml of aqua regia using a closed digestion system DK6 VELP (Velp Scientifica, Usmate Velate, Italy). The solutions were left for at least 12 h at room temperature before the extraction. The extraction took 240 minutes at 120 °C. After the procedure was ended, the samples were filtered through 0.45 µm acetate cellulose filters and brought at a volume of 100 mL with ultrapure water (obtained with a Merck system, Millipore, Merck). The samples were measured using an inductively coupled plasma optical emission spectrometer (ICP-OES), model Optima 5300 DV (Perkin Elmer, Canada).

The obtained concentrations were used for the calculation of the proposed major oxides using conversion factors [19].

The quality assurance was accomplished by measuring soda feldspar BCS-CRM, no. 375/1 (Bureau of Analysed Samples Ltd). For the SiO_2 determination, gravimetric method was applied [19].

Petroleum hydrocarbon adsorption

In order to determine the efficiency of the adsorption capacity, a simulation was caried out on contaminated ex-sites with petroleum hydrocarbons (diesel). Commercial diesel was used in the experiments, that consists of a mixture of hydrocarbons having different carbon number in the range between C10-C22, which are mainly aliphatic and aromatic in nature [28]. Three chemical parameters were used to characterize the diesel: sulphur, sulfated ash content and the acid number.

Sulfur was determined by ICP-OES, as previously described, the sulfated ash content was determined gravimetrically and the acid number by titration with HCl against bromocresol green. The results indicated that the used diesel in the adsorption method was characterized by 3.0 mg/kg S, 0.02 % for the sulfated ash content and the acid number with values below 0.01 mgKOH/g.

The adsorption capacity was gravimetrically determined. The zeolites were weighted and added as a uniform thin layer on the contaminated site. The samples were left for adsorption for 8 h. Afterwards, the contaminated zeolites were carefully and quickly removed and weighed.

After the adsorption of petroleum hydrocarbons, the resulted zeolites-petroleum hydrocarbons mixtures could be used as fuel resources in cogeneration stations. Zeolites could be regenerated, but this implies a serious use of chemicals and/or energy in order to eliminate the amount of petroleum hydrocarbons and to purify the zeolite.

ACKNOWLEDGMENTS

This work was supported by the Competitiveness Operational Programme of the Ministry of European Funds through the Contract No. 7/ 01.09.2016, MY SMIS 105654.

REFERENCES

1. *** Agency for Toxic Substances and Disease Registry (ATSDR), **1999**, Toxicological Profile for Total Petroleum Hydrocarbon, US Department of Health and Human Services, Public Health Service, Atlanta, Ga, USA. https://www.atsdr.cdc.gov/toxfaqs/tfacts123.pdf
2. S.J. Varjani; *Bioresour. Technol*., **2017**, *223*, 277-286.
3. P.W. Sammarco; S.R. Kolian; R.A.F. Warby; J.L. Bouldin; W.A. Subra; S.A. Porter; *Arch. Toxicol*., **2016**, *90*, 829-837.

4. S. Adipah; *JESPH,* **2019**, *3*, 001-009.
5. I.C. Ossai; A. Ahmed; A. Hassan; F.S. Hamid; *Environ. Technol. Innov*., **2020**, *17*, 100526.
6. F. Ahmed; A.N.M. Fakhruddin; *Int. J. Environ. Sci. Nat. Res*., **2018**, *11*, 063-069.
7. T.N. Shchemelinina; L.A. Gomze; O.B. Kotova; J.E.F.M. Ibrahim; D.A. Shushkov; M. Harja; G.V. Ignatiev; E.M. Anchugova; *JSBCM*, **2019**, *71*, 131-137.
8. B. Saremnia; A. Esmaeili; M.R. Sohrabi; *Can. J. Chem*., **2016**, *94*,163-169.
9. E.M. Flanigen; R.W. Broach; S.T. Wilson; Introduction. In Zeolites in Industrial Separation and Catalysis, S. Kulprathipanja Ed.; Wiley-VCH Verlag Gmbh & Co., Weinheim, Germany, **2010**, Chapter 1, pp. 1-26.
10. L. Bandura; M. Franus; G. Jozefaciuk; W. Franus; *Fuel*, **2015**, *147*, 100-107.
11. B. Szala; T. Bajda; J. Matusik; K. Zieba; B. Kijak; *Microporous Mesoporous Mater.*, **2015**, *202*, 115-123.
12. K.X. Lee; G. Tsilomelekis; J.A. Valla; *Appl. Catal. B-Environ*., **2018**, *234*, 130-142.
13. E.P. Favvas; C.G. Tsanaktsidis; A. Sapalidis; G.T. Tzilantonis; S.K. Papageorgiou; A.C. Mitropoulos; *Microporous Mesoporous Mater*., **2016**, *225*, 385-391.
14. A.V. Russo; L.F. Toriggia; S.E. Jacobo; *J. Mater. Sci*., **2014**, *49*, 614-620.
15. N. Al-Jamal; T. Juzsakova; B. Zsirka; V. Sebestyen; J. Nemeth; I. Cretescu; T. Halmagyi; E. Domokos; A. Redey; *J. Environ. Manage*., **2019**, *239*, 333-341.
16. L. Levei; A.I. Torok; O. Cadar; E.A Levei.; A. Ozunu; *20th International Multidisciplinary Scientific GeoConference Proceedings SGEM*, **2020**, 313-320, DOI: 10.5593/sgem2020/4.1/s19.039.
17. A. Moldovan; O. Cadar; E.A. Levei; F. Puskas; M. Senila; *20th International Multidisciplinary Scientific GeoConference Proceedings SGEM*, **2020**, 281-288, DOI: 10.5593/sgem2020/3.1/s12.037.
18. E. Neag; A.I. Torok; C. Tanaselia; I. Aschilean; M. Senila; **2020**, *12*, 1614, DOI: 10.3390/w12061614.
19. O. Cadar; M. Senila; M.A. Hoaghia; D. Scurtu; I. Miu; E.A. Levei; *Molecules*, **2020**, *25*, 2570, DOI:10.3390/molecules25112570.
20. M.A. Hoaghia; E. Kovacs; C. Roman; M. Senila; I. Aschilean; *20th International Multidisciplinary Scientific GeoConference – SGEM*, **2020**, 109-116, DOI: 10.5593/sgem2020/6.1/s24.015.
21. B. Muir; T. Bajda; *Fuel Process. Technol.*, **2016**, *149*, 153-162, DOI: 10.1016/j.fuproc.2016.04.010.
22. L. Bandura; M. Franus, R. Panek; A. Woszuk; W. Franus; *Przem. Chem.*, **2015**, *94*, 323-327, DOI 10.15199/62.2015.3.11.
23. A. Torabian; H. Kazemian; L. Seifi; G.N. Bidhendi; A.A. Azimi; S.K. Ghadiri; *Clean*, **2010**, *38*, 77-83, DOI: 10.1002/clean.200900157.
24. J.A. Simpson; R.S. Bowman; *J. Contam. Hydrol.* **2009**, *108*, 1-11.
25. L. Bandura; A. Woszuk; D. Kołodynska; W. Franus; *Minerals,* **2017**, *7*, 1-25.
26. M. Senila; O. Cadar; I. Miu; *Molecules*, **2020**, *25*, 2591, DOI: 10.339/molecules25112591.
27. A. Maicaneanu; H. Bedelean; M. Stanca; *Natural zeolites. Characterization and applications in environmental protection*; Presa Universitara Clujeana, Cluj-Napoca, Romania, **2008**, 324 p.
28. N. Patel; K.P. Shadangi; *Mater.Today*, **2020**, *33*, 4933-4936. DOI: 10.1016/j.matpr.2020.02.679.

STUDIA UBB CHEMIA, LXVI, 2, 2021 (p. 105-116)
(RECOMMENDED CITATION)
DOI:10.24193/subbchem.2021.2.09

A STRAIGHTFORWARD METHOD FOR DETERMINATION OF Ba AND Sr TOTAL CONTENT IN NATURAL ZEOLITES BASED ON MICROWAVE-ASSISTED DIGESTION AND INDUCTIVELY COUPLED PLASMA OPTICAL EMISSION SPECTROMETRY

MARIN SENILA[a,*], OANA CADAR[a], LACRIMIOARA SENILA[a], ANCA BECZE[a], MARIUS ROMAN[a], BOGDAN ANGYUS[a], GABRIEL BRUJ[b]

ABSTRACT. Ba and Sr may occur in relatively high content in natural zeolites and can contribute to the zeolites ion-exchange properties. In addition, some soluble compounds of Ba and Sr can be toxic, thus their determination is important. The aim of this paper was the development and validation of a method for determination of Ba and Sr in zeolites based on microwave-assisted acid digestion and inductively coupled plasma optical emission spectrometry (ICP-OES). For validation, a certified reference material (BCS-CRM 375/1) was used in the accuracy study, and the obtained recoveries were 92 ± 10 % for Ba and 95 ± 12 % for Sr. A mixture of HNO_3:HCl:HF of 3:9:2 (v/v/v) and a digestion time of 40 min were found to give recoveries in the range of 80-120 %. The obtained LOQs in ICP-OES allowed the quantification of concentrations above 5.0 mg kg^{-1} Ba and 3.8 mg kg^{-1} Sr. The method was applied for the determination of Ba and Sr in five zeolite samples, and concentrations of 422 – 580 mg kg^{-1} for Ba and 115 – 183 mg kg^{-1} for Sr were found. The obtained performance parameters were in agreement with the requirements of international guidelines regarding methods validation.

Keywords: *trace metal, aluminosilicate, barium, strontium, ICP-OES, microwave digestion*

[a] *INCDO-INOE2000, Research Institute for Analytical Instrumentation, 67 Donath str., RO-400293, Cluj-Napoca, Romania*
[b] *ENVIRO NATURALS AGRO SRL, 12A Preciziei str., RO-0622203, Bucharest, Romania*
** Corresponding author: marin.senila@icia.ro*

INTRODUCTION

Zeolites are aluminosilicates materials having porous crystalline structures and well-defined channels or cavities. They have a negative charge in their extended structures, which make them to have strong affinity for cations [1]. Natural zeolites have in their composition significant amounts of Na^+, K^+, Mg^{2+}, and Ca^{2+} that can be substituted by other cations (e.g. cations of heavy metals and radionuclides from contaminated environments), in ion-exchange processes. Due to their occurrence in relatively high amount in nature, zeolites are among the most studied potential inorganic ion-exchange materials [2-4].

The affinity for cations makes natural zeolites useful in many applications, but this property can also conduct to the accumulation in their structure of potentially toxic cations at trace levels [5]. Depending on their origin, the determination of the whole chemical composition of natural zeolites is extremely important mainly when the intended use is human ingestion, animal feed supplements or purification of drinking water. Furthermore, since the zeolites can be used for the removal of different trace elements from contaminated environments, the quantification of elements adsorbed by zeolites is required in order to evaluate their adsorption efficiency [6,7]. Ba and Sr may occur in relatively high content in natural zeolites that can contribute to the zeolites ion-exchange properties. In addition, some soluble compounds of Ba and Sr can be toxic. Therefore, when the zeolite is used as food supplement or as filtrating material it is important to know the content of the two elements.

In several works, zeolites were studied for the removal of radionuclides of barium (Ba) and strontium (Sr) from waters [1,8,9]. The insoluble salts of Ba are nontoxic, being poorly absorbed by organisms, while Sr(II) was reported to be an important mineral for the health of human bones and teeth, thus these elements have no regulated levels in environment [10]. However, the radioisotopes of these elements are of a high concern for human health and their removal from the environment is of high importance [9]. Also, the water-soluble Ba species was reported to affect the mammalian cardiovascular system [11,12]. Sr is an alkaline earth metal naturally occurring in soluble compounds which make it highly mobile and reactive. Sr has four stable isotopes (^{88}Sr, ^{86}Sr, ^{87}Sr, ^{84}Sr), and thirty-one unstable isotopes [13]. Its anthropogenic radionuclides form (^{134}Cs,^{135}Cs and ^{137}Cs) are used in nuclear power plants. Thus, the determination of Ba and Sr both occurring in natural zeolites and those that can be retained by zeolites from contaminated environment is very important.

For the determination of chemical composition of zeolites, instrumental techniques such as X-ray fluorescence spectrometry (XRF), X-ray diffraction (XRD), magnetic resonance spectrometry (NMR), atomic absorption spectrometry (AAS), inductively coupled plasma mass spectrometry (ICP-MS) or inductively coupled plasma atomic emission spectrometry (ICP-OES) can be used [14]. Each of these analytical tools has some particular advantages and disadvantages associated with sample preparation procedures, consuming of time, interpretation of analytical results. ICP-OES is widely accepted technique due to the speed of analysis, multi-elemental capability and wide dynamic range [15].

The determination of elements in solid samples by ICP-OES requires, however, sample preparation to extract the analyte into solution [16]. In this way, a homogeneous solution is obtained, which can be more representative than in case of direct analysis of surface of solid sample. The step of sample preparation is essential in obtaining recovery of the analyte, and thus accurate results.

There are several methods of sample preparation, many of them based on dissolving in a mixture of acids (HCl, HNO_3, HF, H_2SO_4) [17,18]. The chosen acid mixtures, digestion devices, amount of necessary sample may influence the quantitative extraction of analyte in solution. Closed microwave-assisted wet digestion/decomposition based methods have several advantages including fast heating, little risk of contamination, use of low amounts of acids and prevention of loss of volatile elements [19,20].

The present work was initiated with the aim to develop a simple and reliable microwave-assisted extraction method in combination with ICP-OES technique for the determination of Ba and Sr in zeolite samples. The digestion step involves closed microwave extraction using a mixture of concentrated HNO_3, HCl, and HF. The optimum composition of acid mixture for the best recovery of Ba and Sr was established by using a Certified Reference Material (CRM) BCS-CRM 357/1 soda feldspar with known amounts of Ba and Sr. The figures of merit, such as limit of detection, limit of quantitation and precision of ICP-OES were also estimated. Finally, the proposed method was applied to measure Ba and Sr content in five natural zeolites samples.

RESULTS AND DISCUSSION

Optimization of microwave-assisted acid digestion procedure

In order to deliver quantitative results, a spectrometric method should provide recoveries in the range of 80-120% [21]. The dissolution of silicate materials is difficult and time-consuming due to refractory nature of their numerous constituents. Two essentially different approaches were suggested as possible ways to digest this type of samples. One is based on fusion with different salts (e.g. Na_2CO_3, $LiBO_2$), and the other is wet digestion based on dissolution in a mixture of acids (HCl, HNO_3, HF, H_2SO_4) [22].

The wet acid digestion is preferable since, comparing with fusion, is simple and rapid. The recovery in this procedure strongly depends on the solubility of analytes and type of matrix. In the case when the spectrometric method is not used for determination of silica content in this type of samples, the digestion with a mixture of inorganic acids which includes HF is preferable [23]. Insufficient amount of acids or incomplete wetting of solid samples can conduct to an incomplete digestion. The ratio of mineral acids used for digestion may influence the recovery rate. In order to evaluate this factor for the digestion of 0.500 g of sample, mixtures of concentrated HNO_3, HCl and HF were used. The ratio between HNO_3 and HCl was kept at 1:3 (v/v), as in *aqua regia* mixture, but the volume of concentrated HF was varied, in order to have the following HNO_3:HCl:HF ratios: 3:9:1 (v/v/v), 3:9:2 (v/v/v), 3:9:3 (v/v/v), 3:9:4 (v/v/v), 3:9:5 (v/v/v). The applied digestion program was similar for all the experiments. The CRM BCS-CRM 375/1 soda feldspar with known amounts of Ba and Sr was used to evaluate the recovery.

At the end of each microwave extraction process, the sample digest was diluted to required volume with ultrapure water for subsequent determination of Ba and Sr by ICP-OES. The extraction efficiency was evaluated by recovery of each analyte. Three replicates were carried-out for this assay, with an average standard deviation of repeatability of 5%. The results are illustrated in Figure 1.

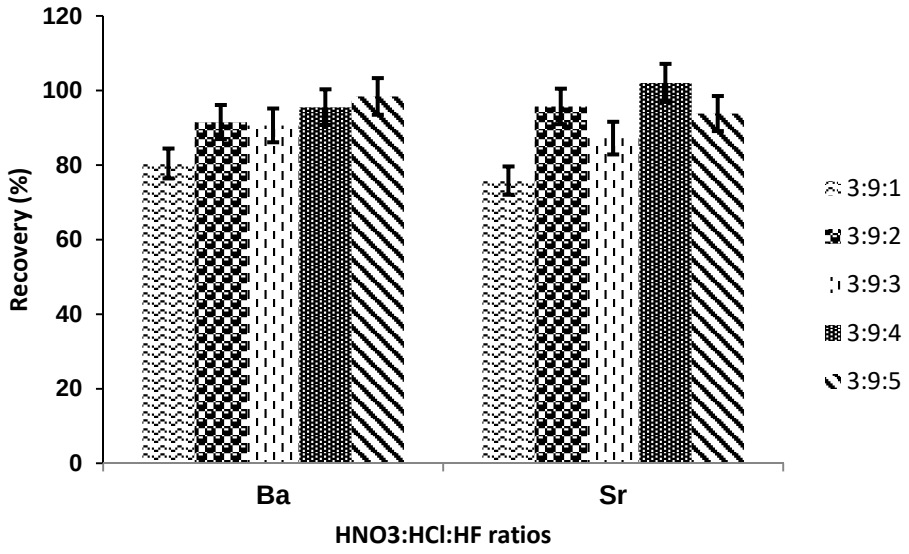

Figure 1. Influence of HNO3:HCl:HF ratios on Ba and Sr recovery (%) from CRM BCS-CRM 357/1 soda feldspar following microwave-assisted digestion. Error bars with CI values are indicated

The recovery of Ba ranged between 80.4 – 98.4 %, with an increase from the ratio HNO_3:HCl:HF of 3:9:1 (v/v/v) to the ratio of 3:9:5 (v/v/v). In all cases, the recovery was in the range of 80-120 %. In case of Sr, for the ratio HNO_3:HCl:HF of 3:9:1 (v/v/v), the recovery rate was of 75.8 %, below 80%, which is an unsatisfactory result, while for the increased HF content, the recovery was in all cases in the range of 80-120 %. Consequently, it was considered that for the quantitative extraction of Ba and Sr from 0.500 g of sample, the use 3 mL of HNO_3 65% (w/w), 9 mL HCl 37 % (w/w) and 2 mL HF 40 % (w/w) is a suitable digestion method.

The validation was performed considering the recommendations of the Cooperation for Analytical Chemistry in Europe (EURACHEM) guide [24].

Selectivity for Ba and Sr measurement by ICP-OES

The emission wavelengths for each metal (Ba – 233.527 nm and Sr – 407.771 nm) which are not affected by spectral interferences according to the recommendation of the instrument manufacturer have been selected. Selectivity was evaluated by recovery of a spike of 1 mg L^{-1} element in the extracted solutions. The recoveries were in the range of 90 –110%, considered as satisfactory [25].

Limits of Detection (LODs), Limits of Quantification (LoQs) and linear ranges

The LODs for both elements were calculated using the $3s_{y/x}/m$ criterion [26] where $s_{y/x}$ is the residual standard deviation of the calibration curve and m the slope of the calibration curve, using the Equation 1:

$$LoD = (3\, s_{y/x} - y) / m \qquad (1)$$

where y is the intercept of the calibration curve.

LoQs were calculated as three times the LoDs. To confirm LoQs, six independent solutions containing Ba and Sr at a level of concentration close to the LoQ (0.10 mg L^{-1}) were analysed, with the targeted relative standard deviation of repeatability (RSD) below 20 % and recovery between 90-115 %. The selected wavelengths, LoDs, LoQs, RSD (%) and recovery (%) at LoQs are presented in Table 1.

Table 1. Selected spectral lines, LoDs, LoQs and LoQ confrmation

Element	λ (nm)	LoD (mg L^{-1})	LoQ (mg L^{-1})	RSD at LoQ (%)	Recovery at LoQ (%)
Ba	233.527	0.008	0.025	5.36	97
Sr	407.771	0.006	0.019	7.73	105

The obtained LoDs were of 0.008 mg L^{-1} for Ba and 0.006 mg L^{-1} for Sr. Lower LoDs of 0.0002 mg L^{-1} for Ba and 0.00007 mg L^{-1} for Sr were reported by Pohl and co-workers [27], but the estimation was based three times standard deviation of blank signal. The performance parameters for LoQs confirmation were well fitted on the targeted values, showing that these values can be measured with good accuracy. Considering the digestion procedure, the calculated LoQs in the solid sample are of 5.0 mg kg^{-1} for Ba and 3.8 mg kg^{-1} for Sr, values that can be lowered by digestion of higher amount of solid sample or by a lower dilution.

Seven-point external calibration curves within the concentration range of 0.02 - 2 mg L^{-1} were used for quantification of studied elements. For concentrations of Sr higher than this value, saturation of the emission signal in axial view of plasma was observed, thus for higher Sr concentrations, sample dilution is necessary. The homogeneity of variances was evaluated by measuring six times the lowest and the highest concentrations of calibration standards. The PG ratios of the standard deviations (s_1) and (s_7), calculated as s_1^2/s_7^2 or s_7^2/s_1^2 were compared with the critical value Fischer $F_{5;5;0.99} = 11$ [28].

The characteristics of the calibration curves for the two elements obtained by ICP-OES are presented in Table 2.

Table 2. Characteristics of the calibration curves over the range 0.02 – 2 mg L^{-1}

Element	Intercept (a)	Slope (*b*)	PG	Correlation coefficient (R)
Ba	235	18830	3.72	0.9999
Sr	230077	12069102	7.32	0.9999

The variances evaluated from the lowest and the highest concentrations of calibration curves are homogenous, and the correlation coefficients are better than the imposed target value 0.995 [29], therefore linear regressions were accepted.

Precision and Trueness

Precision was assessed in term of repeatability for the 6 parallel measurements on a zeolite sample, which included the whole procedure. Relative standard deviation of repeatability (RSD_r) below 10% and limit of repeatability (r) below 28% were the imposed targets for this assay. The standard deviations of repeatability/limit of repeatability, within the imposed limits are presented in Table 3.

Table 3. Repeatability study for a zeolite sample (n=6 parallel determinations)

Element	Average (mg kg^{-1})	s_r (mg kg^{-1})	RSD_r (%)	r (%)
Ba	580	43	7.41	20.8
Sr	170	11	6.47	18.1

s_r – standard deviation of repeatability; RSD_r – relative standard deviation of repeatability; r – limit of repeatability (2.8x RSD_r)

The trueness was evaluated from the recovery study using a CRM (BCS-CRM 375/1 soda feldspar) with indicative values for Ba and Sr content. The calculated recoveries are showed in Table 4.

Table 4. Indicative values of BCS-CRM 357/1 soda feldspar, average measured concentrations (n = 6 parallel determinations) and the recoveries (%)

Components	**Indicative Values** µg g^{-1}	**Average values ± CI** µg g^{-1}	**Recovery (%)**
Ba	95	90.1 ± 11.1	95
Sr	101	92.5 ± 9.6	92

The obtained recoveries were of 95 % for Ba and 92% for Sr, which are in the target range of 80-120 % [30].

Estimation of measurement uncertainty

Two types of sources of uncertainty were identified for Ba and Sr determinations by ICP-OES: those obtained from laboratory experiments (method repeatability and uncertainty of the calibration curves), and those

obtained from certificates of used materials: uncertainty of reference materials, uncertainty of devices used for standards and sample preparations (weighting, dilutions). Composed uncertainties (u_c) were assessed by combining individual uncertainties in the traceability chain. Expanded uncertainties (U_e) were calculated for 95% confidence level (cover factor k=2). The relative expanded uncertainties were of 15.2 % for Ba and 13.3 % for Sr. Replicate analysis was the main contributor to the total uncertainty.

Ba and Sr in zeolite samples

Five natural zeolites samples (Z1–Z5) from a quarry located in Chilioara, Salaj County, Romania were collected and analyzed. The measured concentrations of Ba and Sr are presented in Table 5.

Table 5. Ba and Sr concentrations (mg kg^{-1}) in zeolite samples, n=3 parallel determinations

Sample	Ba Average values ± U_e mg kg^{-1}	Sr Average values ± U_e mg kg^{-1}
Z1	580 ± 88	170 ± 23
Z2	504 ± 77	115 ± 15
Z3	431 ± 66	134 ± 18
Z4	522 ± 79	167 ± 22
Z5	422 ± 64	183 ± 24

U_e – expanded uncertainty, k=2

As showed in Table 5, the content of Ba in the analysed zeolite samples were in the range of 422 – 580 mg kg^{-1}, with an average value of 492 mg kg^{-1}, while the concentrations of Sr ranged between 115 – 183 mg kg^{-1}, with an average value of 154 mg kg^{-1}. In the clinoptilolite zeolite from a qaury from Turkey were reported concentrations of Ba of 454 ± 16 mg kg^{-1} and of Sr of 825 ± 4 mg kg^{-1} [31]. Karapinar [32] reported a concentration of Sr of about 470 mg kg^{-1} in natural zeolite from Germany.

CONCLUSIONS

A microwave-assisted acid extraction method was developed and optimized for the determination of Ba and Sr in zeolite samples. A ratio of HNO_3:HCl:HF of 3:9:2 (v/v) with a total time of digestion of 40 min was found to give recoveries in the target values of 80-120%) for Ba and Sr from a CRM

with silicate matrix. The digestion method based on microwave-assisted wet digestion is simple, faster, and it requires less chemicals than other digestion methods like that based on fusion with salts. The obtained LOQs in ICP-OES allowed the quantification of concentrations higher than 5.0 mg kg^{-1} for Ba and 3.8 mg kg^{-1} for Sr. All the performance parameters (LoD and LoQ, selectivity, linearity, trueness, precision and measurement uncertainty) satisfied the imposed targets. The method was applied for the determination of Ba and Sr in five zeolite samples.

EXPERIMENTAL SECTION

Materials

Standard solutions for external calibration of ICP-OES were prepared by stepwise dilution of a Merck Millipore CertiPur ICP multi-elemental standard solution IV 1000 mg L^{-1}, which contains Ba and Sr, purchased form Merck (Darmstadt, Germany). Emsure® ACS premium grade acids HNO_3 65%, HCl 37%, and HF 40%, purchased from Merck (Darmstadt, Germany) were used for digestion of samples. Ultrapure water (18 MΩ cm^{-1}) obtained from a Millipore Direct Q3 (Millipore, France) was used for dilutions.

For the optimization of digestion procedure and for recovery study a Certified Reference Material CRM BCS-CRM 375/1 soda feldspar from Bureau of Analysed Samples Ltd (United Kingdom) was used.

Five natural zeolites samples (Z1–Z5) were collected from a quarry located in Chilioara, Salaj County, Romania. In this region, the predominant zeolite in tuff is represented by clinoptilolite-type minerals [33]. The samples were crushed and further grounded to a fine powder in a tungsten-carbide swing mill and sieved through a 100 µm mesh sieve.

Preparation of zeolites digest

An amount of 0.500 g of sample, with particulate size <100 µm, was digested with a mixture of 3 mL HNO_3 65%, 9 mL HCl 37%, and 1 - 5 mL HF 40%, for method optimization, in a closed-vessel MWS-3+ microwave system (Berghof, Germany). The three-steps heating program of the microwave system was applied for samples digestion, heating at 160 °C, 200 °C, cooling at 100 °C, in a total time of digestion of 40 min, according to the manufacturer recommendations for similar samples. After cooling at room temperature, 20 mL of saturated H_3BO_3 were added, and then heated again at 160 °C in the microwave system for 15 min. The samples were finally filtered through cellulose filters in volumetric flasks of 100 mL and diluted to final volume using ultrapure water.

Instrumentation

Analyses were carried out using a dual viewing inductively coupled plasma optical emission spectrometer Optima 5300DV (Perkin Elmer, USA). The operating conditions used for ICP-OES determination were 1300W RF power, 15 L min^{-1} Ar plasma support, 2.0 L min^{-1} auxiliary Ar flow, 0.8 L min^{-1} nebulization Ar, and 1.5 mL min^{-1} sample uptake rate, in axial viewing option of the plasma. Axial viewing approach provides an increased sensitivity and lower LoDs in detecting trace elements. 7-point linear calibration curves over the range 0 – 2 mg L^{-1} element were plotted.

Strategy for method validation

The validation of the analytical procedure for quantitative determination of Ba and Sr in zeolites was performed by evaluating limits of detection, limits of quantification, selectivity, linear ranges, trueness and precision. Measurement uncertainty was evaluated based on the bottom-up approach. All the contributions to combined uncertainty were obtained from statistical analysis of repeated measurements and calibration certificates.

ACKNOWLEDGMENTS

The work has been funded by the Competitiveness Operational Programme of the Ministry of European Funds through the Contract No. 7/01.09.2016, code MySMIS 105654.

REFERENCES

1. Y. Li; A. O. Simon; C. Jiao; M. Zhang; W. Yan; H. Rao; J. Liu; J. Zhang; *Microporous Mesoporous Mater*., **2020**, *302*, 110244.
2. S.A. Maicaneanu; H. Bedelean; *Studia UBB Chemia*, **2020**, *LXV*, *3*, 89-100.
3. E. Neag; A.I. Torok; C. Tanaselia; I. Aschilean; M. Senila; *Water*, **2020**, *12*, 1614.
4. M. Senila; O. Cadar; L. Senila; A. Hoaghia; I. Miu; *Molecules*, **2019**, *24*, 4023.
5. M. Tomasevic-Canovic; *J. Serb. Chem. Soc*., **2005**, *70*, 1335-1345.
6. S. Chalupnik; W. Franus; M. Wysocka; G. Gzyl; *Environ. Sci. Pollut. Res.*, **2013**, *20*, 7900-7906.
7. A.K. Mosai; H. Tutu; *Miner. Eng*., **2021**, *161*, 106740.
8. S. Kwon; C. Kim; E. Han; H. Lee; H.S. Cho; M. Choi; *J. Hazard. Mater.*, **2021**, *408*, 124419.

9. D. Alby; C. Charnay; M. Heran; B. Prelot; J. Zajac; *J. Hazard. Mater.*, **2018**, *344*, 511-530.
10. D. Gonzalez-Weller; C. Rubio; A.J. Gutierrez; G.L. Gonzalez; J.M. Caballero Mesa; C. Revert Girones; A. Burgos Ojeda; A. Hardisson; *Food Chem. Toxicol.,* **2013**, *62*, 856-868.
11. I.R. McNeill; K.Z. Isoardi; *Toxicol. Commun*., **2019**, *3*, 88-90.
12. H. Zhang; X. Zhou; L; Wang; W. Wang; J. Xu; *Ecotox. Environ. Safe*., **2018**, *164*, 181-188.
13. Z. Liu; B. Chen; X. Li; L. Wang; H. Xiao; D. Liu; *Sci. Total Environ*., **2019**, *670*, 433-438.
14. Y. Ma; S. Rigolet; L. Michelin; J.L. Paillaud; S. Mintova; F. Khoerunnisa; T.J. Daou; E.P. Ng; *Microporous Mesoporous Mater*., **2021**, *311*, 110683.
15. T. Frentiu; S. Butaciu; E. Darvasi; M. Ponta; M. Senila; D. Petreus; M. Frentiu; *Anal. Methods*, **2015**, *7*, 747-752.
16. M. Miclean; E.A. Levei; M. Senila; C. Roman; E. Cordos; *Rev. Chim. (Bucuresti)*, **2009**, *60*, 1-4.
17. I. Smical; A. Muntean; D. Ciurte; V. Micle; *Studia UBB Chemia*, **2020***, LXV, 4,* 95-107.
18. G.E. Damian; V. Micle; I.M. Sur; *J. Soil. Sediment*., **2019**, *19*, 2869-2881.
19. H. Altundag; M. Tuzen; *Food Chem. Toxicol*., **2011**, *49*, 2800-2807.
20. V.B.K. Mullapudi; K. Chandrasekaran; G. Venkateswarlu; D. Karunasagar; *Microchem. J.*, **2019**, *146*, 807-817.
21. AOAC Guidelines for Single Laboratory Validation of Chemical Methods for Dietary Supplements and Botanicals. (2002). https://members.aoac.org/AOAC_Docs/StandardsDevelopment/SLV_Guidelines_Dietary_Supplements.pdf (accessed Mar 2021).
22. P.K. Srivastava; A.K. Singh; B. Sunilkumar; *At. Spectrosc*., **2003**, *24*, 98-104.
23. M. Balcerzack; *Anal. Sci*., **2002**, *18*, 737-750.
24. B. Magnusson; U. Ornemark (eds.) Eurachem Guide: The Fitness for Purpose of Analytical Methods – A Laboratory Guide to Method Validation and Related Topics, (2nd ed. 2014), available from https://www.eurachem.org/images/stories/Guides/pdf/MV_guide_2nd_ed_EN.pdf, accessed on 22.06.2021
25. A. Drolc; A. Pintar; *Accreditation and Qual. Assur.*, **2012**, *17*, 323–330.
26. E. Covaci; M. Senila; M; Ponta; E; Darvasi; D. Petreus; M. Frentiu; T. Frentiu; *Talanta*, **2017**, *170*, 464-472.
27. P. Pohl; A. Szymczycha-Madeja; M. Welna; *Food Chem*., **2018**, *263*, 171-179.
28. International organization for standardization (1990) ISO 8466-1 Water quality. Calibration and evaluation of analytical methods and estimation of performance characteristics - Part I: Statistical evaluation of the linear calibration function, Geneva, Switzerland.
29. E. Covaci; M. Senila; M. Ponta; T. Frentiu; *Rev. Roum. Chim*., **2020**, *65*, 735-745.
30. M. Senila; E. Covaci; O. Cadar; M. Ponta; M. Frentiu; T. Frentiu; *Chem. Pap*., **2018**, *72*, 441-448.

31. M. Kurudirek; Y. Ozdemir; I. Turkmen; A. Levet; *Radiat. Phys. Chem*., **2010**, *79*, 1120-1126.
32. N. Karapinar; *J. Hazard. Mater*., **2009**, *170*, 1186-1191.
33. A. Maicaneanu; H. Bedelean; M. Stanca; Natural Zeolites. Characterization and Applications in Environmental Protection, Editura Presa Universitara Clujeana, Romania, 2008, pp. 59–78 (in Romanian).

STUDIA UBB CHEMIA, LXVI, 2, 2021 (p. 117-126)
(RECOMMENDED CITATION)
DOI:10.24193/subbchem.2021.2.10

EX-SITU PORTABLE X-RAY FLUORESCENCE SPECTROMETRY FOR THE MAJOR ELEMENTS DETERMINATION IN SILICATE GEOLOGICAL SAMPLES USING MATRIX-MATCHING STANDARDS FOR CALIBRATION

ANAMARIA IULIA TÖRÖK[a], CLAUDIU TĂNĂSELIA[a], CECILIA ROMAN[a], FERENC PUSKAS[b], MARIN SENILA[a,*]

ABSTRACT. An ex-situ method for determining the major elements in the high silicate matrix using portable XRF spectrometry (pXRF) was developed. The calibration is based on the dilution of a matrix-matched certified reference material BCS-CRM No. 376/1 Potash Feldspar with analytical grade SiO_2. Significant correlation coefficients for linear regressions were obtained for all major oxides. This approach of instrument calibration has as the principal advantage the use of a single certified reference material, which reduce the cost of analysis. The limits of detection were evaluated from measurement of SiO_2 considered as blank. The method accuracy of the developed calibration was checked in the recovery study of two certified reference materials (BCS-CRM No. 309 Sillimanite and BCS-CRM No. 375/1 Soda Feldspar), with geological matrix, and the recoveries rate were in the range of 85 – 110 %. The relative expanded uncertainties (*k = 2, P = 95%*) calculated from CRM analysis were of 6.99% for Al_2O_3, 3.56% for Fe_2O_3, 4.82% for CaO and 4.31% for K_2O. The proposed methodology is a green analytical method, allowing fast and accurate analysis of geological samples without use of chemical reagents.

Keywords: *X-ray fluorescence, major element, zeolite, instrument calibration, matrix-matching calibration, ex-situ procedure*

[a] *INCDO-INOE2000, Research Institute for Analytical Instrumentation, 67 Donath str., RO-400293, Cluj-Napoca, Romania*
[b] *Electronic April Cluj-Napoca, 3-5 Pasteur, RO-400349 Cluj-Napoca, Romania*
**Corresponding author: marin.senila@icia.ro*

INTRODUCTION

In general, the laboratory techniques used for the determination of the elements in solid samples require total or partial destruction for extraction of analytes into a liquid solution [1,2]. The sample digestion represents the main drawback of these techniques since it is time-consuming and requires hazardous and expensive reagents [3,4]. For geological sample characterization, usually is needed to know the total amount of constituents. Samples with higher silicate content are difficult to digest and most of the digestion methods are incomplete with an unsatisfactory extraction yield. The wet digestion procedures for silicate samples generally use mixtures of acids containing HF. The resulted solution cannot directly nebulized with the usual sample introduction systems of the spectrometric instruments, being necessary a supplementary neutralization step of HF with high quantities of boric acid [5].

A good alternative to the methods that involve sample digestion is the use of techniques that allow direct determination of elements in solid sample. X-ray fluorescence technique provides compositional data by exciting the sample with X-rays. This technique involves a loss of energy by emitting photons with energy equal to the difference in electron orbitals, specific for the element in question [6]. Energy Dispersive X-ray fluorescence (EDXRF) technique is used to obtain elemental information from different types of materials either in-situ or ex-situ approaches. Measurements made with portable X-ray fluorescence equipment (pXRF) have several advantages: can provide a large number of rapid on-site measurements; are non-destructive and cost-effective. Due to these advantages, the technique got increased attention, being applied to geochemical exploration [7,8] or to assess environmental contamination [9-13].

pXRF is typically used at concentrations between a few mg kg^{-1} to a few percent for elements with medium to high atomic mass (K, Z=19 to Pb, Z=82, and Th, Z=90 and U, Z=92), having more limitations for lightweight elements than laboratory XRF instruments [7], due to higher spectral background in the range of energy of these elements. However, new generation of pXRF have more sensitive X-ray detectors and/or an inert gas flow system (helium) to remove the air between the sample and the detector, that allow simultaneously determination of wide-ranging elements, including Mg (Z=12), Al (Z=13), Si (Z=14), P (Z=15), [7, 14]. Although pXRF has considerable advantages and there are many studies based on this technique [15-17], the obtained results could be influenced by possible matrix effects that can conduct to measurement bias, as quality control being extremely important. On most instruments, pXRF calibration principles differ for trace level elements (soil mode) and major level elements (mining mode).

In order to obtain reliable results, calibrations using matrix-matching CRMs, or techniques based on standard addition of analytes to a corresponding matrix were used [18]. Irenas-Islas and co-workers used for calibration of pXRF equipment a CRM diluted with pure calcium carbonate for analysis of samples with carbonate matrices [19].

In the present study a new calibration strategy using pXRF was established to analyse major elements in silicate samples. Therefore, a calibration scheme that comprises the use of solid calibration standards obtained by mixing of a CRM with pure SiO_2 as diluent was developed. Figures of merit such as limits of detection and limits of quantification, repeatability and accuracy were also evaluated. The proposed methodology is a green analytical method that allows a fast and accurate analysis of complex silicate matrix samples without use of chemical reagents.

RESULTS AND DISCUSSION

Calibration curves for the pXRF

Compared to other more complex laboratory methods (including non-portable XRF analyzers), results obtained through this technique can be susceptible to measurement bias or to matrix effects [6]. To avoid this, the calibration with standards with an appropriate matrix is a more reasonably option than empirical or standardless approaches.

The use of CRMs with different levels of analyte concentrations as calibration standards is possible, although is difficult to find CRMs with similar matrices, and increasing concentrations of all analytes, equally distributed over the calibration range. Moreover, CRMs are expensive materials, which lead to an increased cost of analysis. The approach of standard addition of analyte from liquid solutions to prepare solid calibration standards can conduct to non-homogenous analyte concentrations, and it may not be the best option for calibration in this case. Therefore, in this study we used a different approach based on the dilution of an appropriate CRM (BCS-CRM 376/1 Potash Feldspar) with pure reagent of SiO_2. The study was conducted to evaluate the calibration parameters for Al_2O_3, Fe_2O_3, CaO and K_2O. Five calibration levels were prepared by mixing amounts of SiO_2 and CRM (BCS-CRM 376/1 Potash Feldspar) in order to have 10%, 20%, 40%, 60%, 70%, 80%, 90% and 100% CRM (w/w), with the calculated concentrations presented in Table 1.

Table 1. Concentrations (mg kg^{-1}) of Al_2O_3, Fe_2O_3, CaO and K_2O in the solid calibration standards

CRM content (m/m)	Al_2O_3 mg kg^{-1}	CaO mg kg^{-1}	Fe_2O_3 mg kg^{-1}	K_2O mg kg^{-1}
10%	18630	421	85	11590
20%	37260	842	170	23180
40%	74520	1684	340	46360
60%	111780	2526	510	69540
70%	130410	2947	595	81130
80%	149040	3368	680	92720
90%	167670	3789	765	104310
100%	186300	4210	850	115900

SiO_2 as blank and the calibration standards were measured, and the obtained signals were used to construct the calibration curves. As presented in Table 2, the correlation coefficients of the linear regressions, for the range of 10% – 100 % CRM, were below 0.9 for Al_2O_3, CaO and K_2O, and only in case of Fe_2O_3 the correlation coefficient was better than 0.9 (due to better detection of Fe emission lines, a direct consequence of higher atomic mass of Fe, Z=26). Graphical representation of the calibration curves appeared as a broken line in all cases. The poor linearity of the curves over the entire calibration range can be explained by the possible self-absorption.

Consequently, the calibrations ranges were divided in two different ranges: one for the amounts 10% – 60% CRM (10% CRM; 20% CRM; 40% CRM and 60% CRM), and the second for the range of 70% - 100% CRM (70% CRM; 80% CRM; 90% CRM; 100% CRM), these concentrations were measured, and linear regressions were constructed for the new ranges. The calibration parameters of the linear calibrations for Al_2O_3, Fe_2O_3, CaO and K_2O in the solid calibration standards over the all three ranges are presented in Table 2.

As presented in Table 2, the correlation coefficients for the range 10% – 60% CRM were significantly improved, being in all cases higher than 0.99. Also, the slope values were increased with a factor ranging between 1.60 for Fe_2O_3 to 2.75 for Al_2O_3, which means an increased sensitivity.

Also, the correlation coefficients for linear regressions over the range of 70 – 100% CRM are higher than 0.99 for all the analytes, but with significant lower sensitivity than in the case of lower domain of concentrations.

The significant differences in sensitivity between the two calibration ranges can be explained by different measurement mode of the instrument using different acquisition parameters and calibration coefficients (soil mode for lower concentrations and mining mode for higher concentrations) [7].

The results obtained in the linearity of the calibration curves assay demonstrate that the pXRF can be reliably used to measure major oxides in silicate matrices.

Table 2. Linear calibration curves parameters for the ranges of 10% – 100%; 10% – 60%; and 70% – 100% CRM BCS-CRM 376/1 Potash Feldspar

Element	Intercept (a)	Slope (*b*)	Correlation coefficient (R)
Range 10% – 100% CRM			
Al_2O_3	8980	0.0061	0.792
CaO	11495	1.5985	0.846
Fe_2O_3	4151	6.4965	0.921
K_2O	126122	1.3394	0.838
Range 10% – 60% CRM			
Al_2O_3	8395	0.0168	0.992
CaO	9462	2.9743	0.997
Fe_2O_3	2938	10.368	0.997
K_2O	73235	2.5831	0.996
Range 70% – 100% CRM			
Al_2O_3	9110	0.0048	0.994
CaO	11408	1.4922	0.995
Fe_2O_3	6266	3.4859	0.990
K_2O	199331	0.5557	0.993

Limits of detection (LoDs)

The LoDs for pXRF depend on instrumental characteristics, such as tube and detector specifications, sample matrix and/or emission lines [7]. Thus, each instrument has its own specific element range, for a specific application [17].

The LoD is commonly assessed as three times the standard deviation of replicate analysis of blank standards of the analyte [20, 21]. In our study, we adapted this approach to estimate LoDs of elements in the matrix of SiO_2. For each element of interest, 10 repeated measurements were performed on the pure SiO_2, and the signals were registered. LoDs were calculated as the ratio between three-time standard deviations and slopes of the calibration curves for each element. The obtained LoDs are significant for silicate matrices.

The calculated LoDs were 81 mg kg^{-1} for CaO, 48 mg kg^{-1} for Fe_2O_3 and 161 mg kg^{-1} for K_2O. These values are in the range of those reported by Lemiere et al. [7] for elements as being characteristic for performing pXRF instruments. Also, the LoDs obtained in our study were in similar domains with those reported by Hall et al. [18] for major elements. A higher LoD of about 0.25% was evaluated in our study for Al_2O_3 that can be explained by the high concentrations of this element in the used standards for equipment calibration, in the range of 37260 – 186300 mg kg^{-1}.

Precision and Trueness

BCS-CRM 375/1 Soda Feldspar certified reference material was measured 10 times and the results are listed in Table 3. The concentrations of K_2O were measured on the calibration curve at lower range of concentrations, while Al_2O_3, CaO and Fe_2O_3 were measured on the the calibration curves at high range of concentrations. Since the values for CaO and Fe_2O_3 were higher than those in the most concentrated standard, appropriate dilutions with SiO_2 were used.

Table 3. Repeatability study for CRM sample (BCS-CRM 375/1 Soda Feldspar (n=10 parallel determinations)

Element	Average (mg kg^{-1})	s_r (mg kg^{-1})	RSD_r (%)	r (%)
Al_2O_3	172530	3970	2.30	6.44
CaO	8091	148	1.83	5.12
Fe_2O_3	3044	77	2.53	7.08
K_2O	13995	329	2.35	6.58

s_r – standard deviation of repeatability; RSD_r – relative standard deviation of repeatability; r – limit of repeatability (2.8x RSD_r)

The RSD% for repeatability was in the range of 1.83% - 2.53% indicating a good precision for this method for the analyzed oxides. The trueness was evaluated by analyzing two CRMs with appropriate matrix (BCS-CRM 357/1 Soda Feldspar and BCS-CRM 309 Sillimanite), other that the CRM used for instrument calibration, and the results are presented in Table 4. The concentrations of oxides were measured on the appropriate calibration curves according to theirs concentrations. After the measurement of CRMs the absolute difference (Δm) between the mean measured values and the certified values were calculated. Also, the expanded uncertainty was calculated (for k=2) from the combined uncertainty (UΔ) estimated using Equation (1).

$$U_\Delta = \sqrt{U_m^2 + U_{CRM}^2} \quad (1)$$

where U_m is the measured uncertainty expressed as standard deviation obtained from repeated determinations, and U_{CRM} is the specified uncertainty in the CRM certificate.

To evaluate accuracy, Δ_m was compared with U_Δ. Since $\Delta_m \leq U_\Delta$ there was no significant difference between the measurement result and the certified value.

Table 4. Certified values of CRMs, measured concentrations (n = 10 parallel determinations) and the average recovery degree (%)

Components	Certified Values ± U (mass %)	Average values ± CI (mass %)	Average Recovery ± CI (%)
BCS-CRM 357/1 Soda Feldspar			
Al_2O_3	17.89 ± 0.08	17.25 ± 0.28	96.4 ± 1.6
CaO	0.78 ± 0.03	0.81 ± 0.011	104 ± 1.4
Fe_2O_3	0.291 ± 0.011	0.304 ± 0.006	105 ± 1.9
K_2O	1.47 ± 0.03	1.40 ± 0.024	95.2 ± 1.6
BCS-CRM 309 Sillimanite			
Al_2O_3	61.1 ± 0.2	60.98 ± 0.71	99.8 ± 1.2
CaO	0.22 ± 0.02	0.22 ± 0.003	102 ± 1.2
Fe_2O_3	1.51 ± 0.03	1.45 ± 0.020	96.1 ± 1.4
K_2O	0.46 ± 0.04	0.45 ± 0.004	98.7 ± 1.0

U = expanded uncertainty; CI – confidence interval for repeated determinations

The recovery rates were in the range of 95.2% and 105%. The differences between the certified and measured values for all the analyzed oxides were smaller than the expanded uncertainties (*U*, *k*=2) calculated from the combined uncertainties.

Estimation of measurement uncertainty

Measurement uncertainty was evaluated based on the bottom-up approach. The identified main sources of measurement uncertainty were assumed to come from uncertainty of calibration reference materials, uncertainty of weighted CRMs for standards preparation, uncertainty of measured signals of the calibration standards, bias obtained in accuracy study in CRM analysis, and are presented in Figure 1. In our study for the estimation of measurement uncertainty, it was assumed that two main components affect the method uncertainty: bias in CRM analysis and standard deviation obtained in repeated CRM analysis. The combined uncertainties (u_c) were calculated using Equation (2), then were calculated the expanded uncertainties (*U*) for a cover factor *k* = 2 (P = 95%).

$$u(B) = \sqrt{B^2 + u(C_R)} \tag{2}$$

where *B* is bias from the CRM analysis and $u(C_R)$ is the standard deviation of parallel measurements of CRM.

The pooled expanded uncertainty (*U%*) for the method was calculated by combining the expanded uncertainties (U_1 and U_2) of each CRM analysis, according to Equation (3) [22]:

$$U(\%) = \sqrt{\frac{U_1^2 + U_2^2}{2}} \quad (3)$$

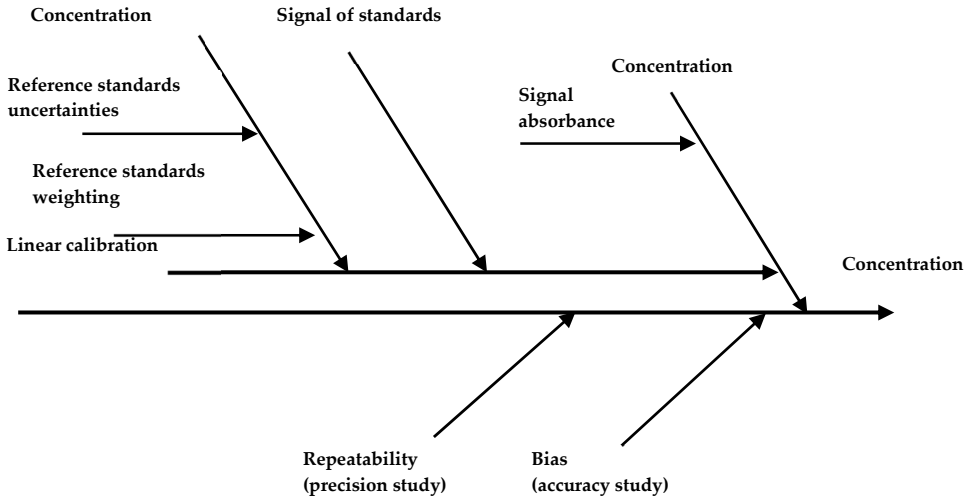

Figure 1. Cause and effects diagram of uncertainties in measurements by XRF

The pooled relative expanded uncertainties (*k = 2, P = 95%*) were of 7% for Al_2O_3, 4% for Fe_2O_3, 5% for CaO and 4% for K_2O, indicating a good confidence for this technique.

CONCLUSIONS

In this study, a new approach for calibration of pXRF for the determination of major elements in geological samples with high silicate matrices was used. Calibration curves were built for determination of Al_2O_3, Fe_2O_3, CaO and K_2O. Correlation coefficients better than 0.9 for linear regressions were obtained for all major oxides. This approach of instrument calibration has as the main advantage the use of a single certified reference material, in a non-destructive way (thus allowing virtually unlimited reuse), which reduces the cost of analysis. The method accuracy of the developed

calibration was checked in the recovery study of two certified reference materials (BCS-CRM No. 309 Sillimanite and BCS-CRM No. 375/1 Soda Feldspar) with good results. The proposed methodology is in the line of green analytical methods, permitting fast and accurate analysis of geological samples without the use of chemical reagents.

EXPERIMENTAL SECTION

Analyses were performed with a Bruker Tracer 5i portable X-ray fluorescence with a 5kV and 4-watt X-ray source, 8 μm Be window and 8 mm spot collimator. The pXRF device was used for all measurements in a desktop stand (laboratory) configuration. Between the instrument's window and the detector, no special conditions were created (air atmosphere). Samples were placed in a Chemplex® container covered with polyester Mylar® film (offering minimal X-ray absorption, but safely separating the sample from the instrument internal volume).

For Fe analysis, a voltage of 50 kV and a current of 6 μA were used, no filters were used. For the rest of the elements (Al, K, Ca), a voltage of 15 kV and a current of 20 μA were used, also with no filter. A 30-minute time was dedicated for signal acquisition for each sample. Data was acquired using Bruker's Artax software (v8.0.0.476) and the signal values (in counts) for each corresponding peaks were exported to Microsoft Excel for further processing.

SiO_2 powdered reagent (Merck, Darmstadt, Germany) was used as diluent for the certified reference material BCS-CRM No. 376/1 Potash Feldspar (Bureau of Analysed Samples Ltd, United Kingdom), with particle size < 60 μm, in order to obtain the calibration standards. Before using, the SiO_2 was dried at 70 °C in an oven for 2 hours, and then the solid mixtures were prepared using different weight percentages of SiO_2 and BCS-CRM 376/1, according to the data presented in Table 1. The final dry weight of each of the 11 mixtures used for the calibration curve was 6.0 g.

Simple linear regression analyses were carried out using Microsoft Excel® program. The detection limits for each element measured with the pXRF were calculated as 3 times the standard deviation (SD) measured in pure SiO_2 (considered as blank).

For the recovery study, two Certified Reference Materials, CRM BCS-CRM 357/1 Soda Feldspar (particle size < 60 μm) and BCS-CRM No. 309 Sillimanite (particle size < 90 μm) from Bureau of Analysed Samples Ltd (United Kingdom) were used. The samples (CRMs) were analysed as powders with the granulation provided by producers.

ACKNOWLEDGMENTS

The work has been funded by the Competitiveness Operational Programme of the Ministry of European Funds through the Contract No. 7/01.09.2016, code MySMIS 105654.

REFERENCES

1. I. Smical; A. Muntean; D. Ciurte; V. Micle; *Studia UBB Chemia*, **2020***, LXV, 4,* 95-107.
2. M. Hlodak; P. Matus; M. Urik; L. Korenkova; P. Mikusova; M. Senila; P. Divis; *Water Air Soil. Pollut.*, **2015**, *226*, 198.
3. T. Frentiu; S. Butaciu; E. Darvasi; M. Ponta; M. Senila; D. Petreus; M. Frentiu; *Anal. Methods*, **2015**, *7*, 747-752.
4. M. Senila; E. Covaci; O. Cadar; M. Ponta; M. Frentiu; T. Frentiu; *Chem. Pap*., **2018**, *72*, 441-448.
5. V.F. Taylor; A. Toms; H.P. Longerich; *Anal. Bioanal. Chem*., **2002**, *372*, 360-365.
6. C.A. Gray; A.D. Van Rythoven; *Minerals*, **2020**, *10*, 431.
7. B. Lemiere; *J. Geochemical Explor.*, **2018**, *188*, 350-363.
8. A. Bourke; P.S. Ross; *Geochem. Explor. Environ. Anal*., **2016**, *16*, 147-157.
9. D.J. Kalnicky; R.J. Singhvi; *J. Hazard. Mater.*, **2001**, *83*, 93-122.
10. E.C. Brevik; C. Calzolari; B.A. Miller; P. Pereira; C. Kabala; A. Baumgarten; A. Jordan; *Geoderma*, **2016**, *264*, 256-274.
11. R. Carr; C. Zhang; N. Moles; M. Harder; *Environ. Geochem. Health*, **2008**, *30*, 45-52.
12. D. Pearson; S. Chakraborty; B. Duda; B. Li; D.C. Weindorf; S. Deb; E. Brevik; D.P. Ray; *J. Hydrol.*, **2017**, 544, 172-179.
13. T. Radu, D. Diamond; *J. Hazard. Mater.*, **2009**, *171*, 1168-1171.
14. A.R. Schneider; B. Cances; C. Breton; M. Ponthieu; X. Morvan; A. Conreux; B. Marin; *J. Soils Sediments*, **2016**, *16*, 438-448.
15. R. Ravansari; S.C. Wilson; M. Tighe; *Environ. Int*., **2020**, 134, 105250.
16. A. Rawal; S. Chakraborty; B. Li; K. Lewis; M. Godoy; L. Paulette; D.C. Weindorf; *Geoderma*, **2019**, *338*, 375-382.
17. A. Turner; K.R. Solman; *Talanta*, **2016**, *159*, 262-271.
18. G.E.M. Hall; G.F. Bonham-Carter; A. Buchar; *Geochem. Explor. Environ. Anal*., **2014**, *14*, 99-123.
19. D. Arenas-Islas; M.A. Huerta-Diaz; C.O. Norzagaray-Lopez; K.G. Mejia-Pina; J.A. Valdivieso-Ojeda; X.L. Otero; F. Arcega-Cabrera; *Sediment. Geol*., **2019**, *391*, 105517.
20. M. Senila, E.A. Levei, L.R. Senila, M. Roman; *J. Chem*., **2015**, *2015*, 762121, 1-8.
21. A. Drolc; A. Pintar; *Accreditation Qual. Assur.*, **2012**, *17*, 323–330.
22. E. Covaci; M. Senila; M; Ponta; E; Darvasi; D. Petreus; M. Frentiu; T. Frentiu; *Talanta*, **2017**, *170*, 464-472.

STUDIA UBB CHEMIA, LXVI, 2, 2021 (p. 127-136)
(RECOMMENDED CITATION)
DOI:10.24193/subbchem.2021.2.11

DEVELOPMENT OF A NON-DESTRUCTIVE METHOD FOR DETERMINATION OF pH OF PAPER ARTIFACTS USING DIFFUSE REFLECTANCE SPECTROSCOPY AND REGRESSION ANALYSIS

BOGDAN M. BOȘCA[a], AUGUSTIN C. MOȚ[a,*]

ABSTRACT. One of the most important factors that influence the quality and resistance to chemical and microorganism degradation of paper, historical artifacts and art works is pH. Despite the simplicity of electrochemical devices that are mostly used nowadays for pH determination, some of them have limitations in terms of precision and time response. In this study, a rapid, simple, and highly precise method for determination of pH of paper was developed using non-destructive reflectance spectroscopy and commercial non-bleeding pH indicator test strips. The calibration curve was constructed using standard Britton-Robinson buffers and was done in the 4.00 – 9.50 pH range. Using univariate regression analysis, the largest linearity domain ($R^2 = 0.9992$, $p < 0.000$) was found to be at 590 nm wavelength, as established from the loadings plot for a PCA analysis. The proposed method, alongside other two known methods, were applied on three real samples, including a 1710 Greek New Testament. No statistical significance ($p > 0.05$, ANOVA) was observed between the three methods, supporting the accuracy of the proposed method. Fischer test reveals a strongly significant higher precision for the tested method ($p < 0.01$). The values of the determined pH for the three real samples were 8.47±0.03, 7.78±0.07 and 7.99±0.08.

Keywords: *non-destructive method, pH determination, reflectance spectroscopy*

INTRODUCTION

Paper represents one of the most used cultural and historical data carrier. [1, 2] It was discovered by the Egyptians in 3000 BC and the papermaking process was developed and improved in China in 105 CE. Over

[a] *Chemometrics and Bioanalytical Chemistry Laboratory, Analytica Research Center, Department of Chemistry, Faculty of Chemistry and Chemical Engineering, Babeș-Bolyai University, 11 Arany János Street, RO-400028 Cluj-Napoca, Romania*
** Corresponding author: augustin.mot@ubbcluj.ro*

the years, scientific, religious, political manuscripts and drawings have been written or drawn on paper such as the Bible, Egyptian hieroglyphs, and others. Preservation of such valuable paper artifacts is a very important aspect in order to improve the communication between generations. [1, 3] Among many natural factors—temperature, humidity, light, presence of microorganisms, oxidative agents—which influence paper degradation in time, pH is one of the most important ones. [1, 2] Moreover, composition of the paper is a determinant factor in the degradation process. The main composite is represented by cellulose fibres. [4] Kaolin, clay, calcium carbonate, lignin represent auxiliary materials which are generally added to improve some physical characteristics of paper such as opacity, mechanic resistance and thickness, to name few. [5, 6] The ratio between these materials depends on the final use of paper, like writing, printing, decoration and others. [5, 7]

Validated analytical methods have been developed for monitoring the relevant parameters of paper—opacity, humidity, pH, thickness —and to discover the optimal conditions for keeping important documents or drawings, in order to avoid or reduce their deterioration in time. [3] As the presence of free radicals—usually detected by electron paramagnetic resonance spectroscopy [8, 9]—or the opacity—frequently studied by diffuse reflectance *UV-Vis* spectroscopy [7]—help us to find the age of the paper, pH values provide useful information regarding the deterioration process. There are already some known analytical tools used in order to obtain information regarding the pH of paper, [4] such as volatile organic compounds determination and flat surface pH electrode. [2, 10, 11] Also, the methods used have to be non-destructive, due to the fact that most of the analyzed papers are of historical importance and some of them are unique, especially old drawings.

The mechanism of the deterioration processes is greatly influenced by pH. An acidic medium produces the degradation of cellulose through acid-catalyzed hydrolysis, whereas autooxidation appears in a more alkaline medium as a degradation path. [4,10] The deterioration process is faster when pH shows a low value and this is why, in general, the paper produced between 1850 and 1900—that has acidic pH—is more susceptible to degradation than the paper produced before 1850—that has alkaline pH. [10]

The aim of this work was to develop a non-destructive method for the determination of the pH of paper artifacts based on diffuse reflectance spectroscopy which is faster and more precise than the classical electrode-based methods. The diffuse reflectance spectra were depending upon the color of the pH indicator strips caused by the change in the pH of the ultrapure water transmitted through the tested paper sample in contact with the pH indicator strips, thus eliminating the acid and alkaline errors typical for electrode-based methods and increasing the number of the calibration points as compared to the classical methods.

RESULTS AND DISCUSSION

The diffuse reflectance spectra of the three-bands non-bleeding pH indicator test strips (band 2 – orange-green and band 3 – yellow-violet) corresponding for all tested pH standard solutions, in the range 4.00 – 9.50 are presented in Figure 1A, alongside the image of the tested strips (Figure 1B). Band 1 – violet-red was not used due to the limited spectral information as revealed by preliminary results carried out on each single band experiments and due to the fact that the reading window of the integrating sphere was limited in size (1x1 cm) and allowed maximum two bands at a time.

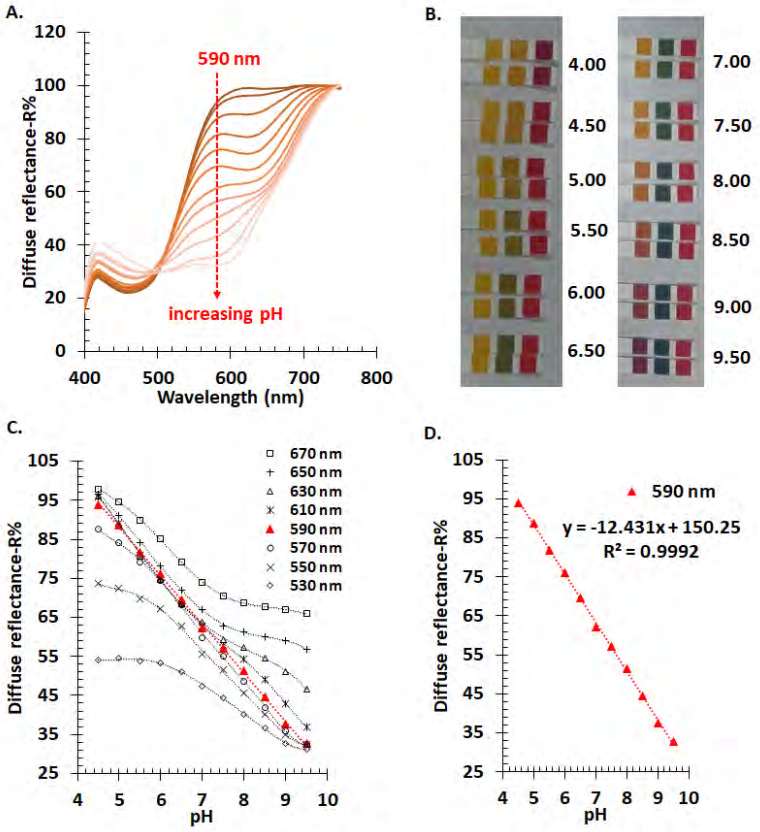

Figure 1. A. Reflectance spectra profile—after min-max normalization—of the non-bleeding pH indicator test strips for pH standard solutions in the range 4.00 – 9.50. Position of 590 nm wavelength is indicated by an arrow, as the pH increases. **B.** Image of the non-bleeding pH indicator test strips used for calibration test, in duplicate, for each tested pH value. **C.** Variation of the calibration curves and their linearity deviation, at various wavelengths. **D.** Selected calibration curve at the optimum wavelength (590 nm).

As the pH increases, a clear gradually decrease in reflectance is observed in the 500 – 700 nm range, with a maximum gradient around 600 nm, as expected by the color of the bands from the tested strips. A minor gradual increase in the 400 – 500 nm range is also observed. In order to construct an optimum calibration curve, univariate regression models were used at various wavelengths. A plot that indicates the variation of the calibration curves at the most important wavelengths is indicated in Figure 1C. Above 600 nm, the calibration curves exhibit a deviation from linearity at alkaline pH values, that gradually enhances as the wavelength increases. A similar behavior was observed at wavelengths lower than 580 nm, but the deviation from linearity is at acidic pH. The coefficient of determination, as well as the bivariate scatterplots were used to assess the linearity and its domain. Following this analysis, the optimum wavelength came out to be 590 nm, as shown in Figure 1D.

Another approach that was used for the determination of the optimum wavelength was the inspection of the loading plot (or correlation circle) obtained after application of PCA on the entire data matrix. The loadings profile indicates two regions of maximum spread of the variation on the first component that takes more than 83% of the information, around 414 nm and 590 nm, as indicated in Figure 2.

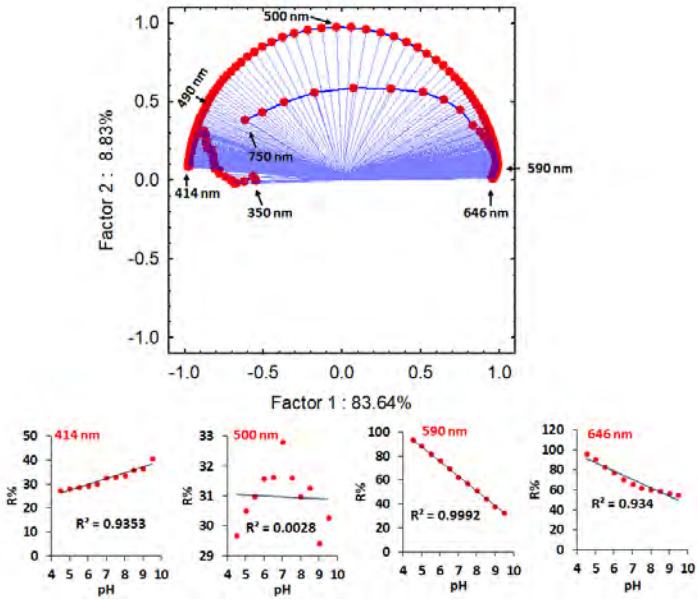

Figure 2. Loadings profile for all the variables (*i.e.* min-max normalized reflectance values) in the 350 – 750 nm spectral domain, at an interval of 1 nm—after application of PCA analysis. Some wavelength points are indicated by arrows, the others are removed for clarity. Univariate calibration curves for some of the indicated wavelengths are presented alongside their corresponding determination coefficient.

A minimum variation is expected around the 500 nm wavelength based on Figure 2. This profile is justified and explained by the original variable profile form Figure 1A. Despite a positive and significant correlation around 414 nm, its strength is quite poor ($R = 0.9665$, $p<0.000$) compared to a highly powerful negative correlation at around 590 nm ($R = -0.9996$, $p<0.000$), as obtained from the first approach.

Following the optimization of the method, it was then tested on real samples using the procedure described in the Experimental section and depicted in Figure 3. The water drop that was applied upon the paper sample diffused through the sample paper and reached the pH test strips changing their color, depending on pH. Using the previously constructed calibration curve at 590 nm, the pH of the paper was then calculated. The statistical results comprising of statistical descriptors and statistical tests results are shown in Table 1. One-way ANOVA reveals no statistical difference between the means of the three analytical methods, supporting the accuracy of the methods. However, the method proposed in this study is about three times more precise, as indicated by RSD% and the Fischer test.

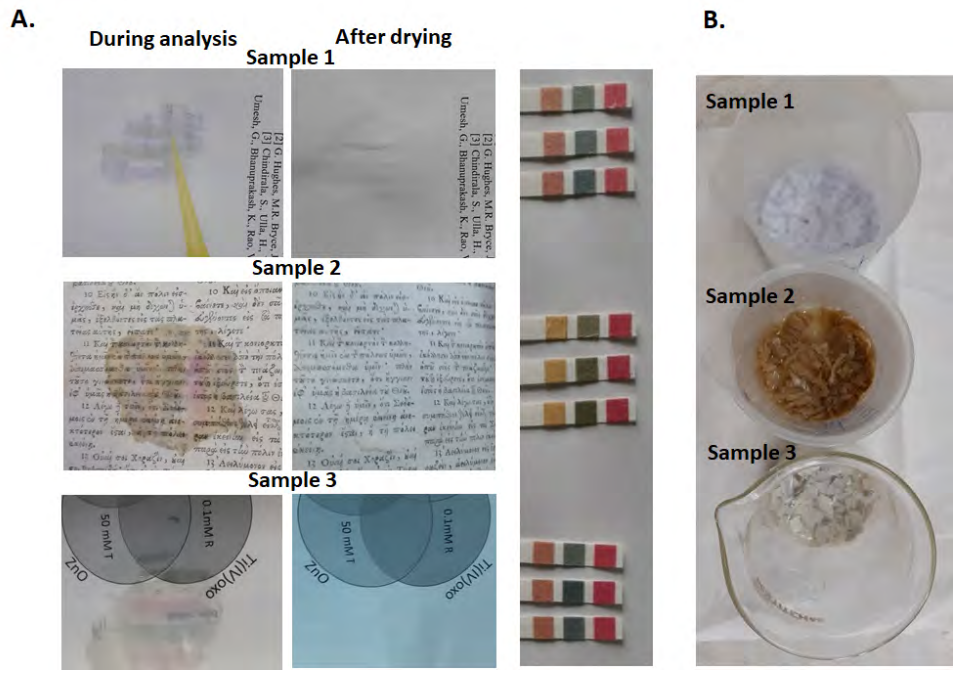

Figure 3. A. Image of the three tested real samples (described in the Experimental section) during analysis and after drying, and their corresponding pH indicator test strips, in triplicates. **B.** Image of the same three real paper samples used in destructive classical cold extraction sample for pH determination.

It is clear that the proposed method is non-destructive as the analyzed paper zone remains intact after drying of the water, since this method requires a small amount of water. The electrochemical pH surface sensors that are commonly used nowadays for monitoring the pH of paper samples also requires a small amount of water. However, they are known to require a long time for equilibration and they also have poor precision and accuracy at short time, which is caused by the gradual diffusion of water away from the measurement region under the electrode. [11] In contrast with these methods, the classical cold extraction method is a destructive method that requires a certain amount of the paper sample to be cut away from the original sample in order to be extracted in water (Figure 3B), followed by pH meter reading. Despite expectance, this method is also not so precise, mostly due to the higher water dilution, and the influence of atmospheric carbon dioxide during extraction. In contrast with these classical methods, the procedure proposed in this work requires much shorter time of analysis (3 minutes water diffusion unto the indicator strips and 1 minute spectrum measurement). Moreover, by working at the optimum 590 nm wavelength, the linearity of the calibration curve is improved and the systematic acidic and alkaline methods that commonly accompany electrode-based methods are eliminated, thus explaining the high precision and accuracy of the method.

Table 1. Statistical results obtained for the three tested real samples

	Sample 1			**Sample 2**			**Sample 3**		
Method[a]	**M1**	**M2**	**M3**	**M1**	**M2**	**M3**	**M1**	**M2**	**M3**
Mean pH	8.43	8.46	8.47	6.02	5.96	5.97	7.78	7.93	7.99
RSD%	3.2	3.4	0.2	4.6	3.2	0.9	3.6	1.6	0.7
Min.	8.00	8.01	8.44	5.75	5.72	5.89	7.43	7.80	7.95
Max.	8.70	8.67	8.49	6.55	6.18	6.02	8.12	8.10	8.07
CI (95%)[b]	0.33	0.30	0.03	0.17	0.24	0.07	0.23	0.15	0.08
p (F test)[c]	-	0.470	0.001	-	0.242	0.003	-	0.071	0.009
ANOVA analysis	F = 0.033, p = 0.967			F = 0.194, p = 0.825			F = 1.661, p = 0.225		

[a]M1 – classical paper cold extraction and pH meter, M2 – pH glass electrode adapted for direct surface analysis, M3 – the method proposed in this study as described in the Experimental section. [b]Confidence interval at 95% probability (n=5). [c]Fischer test for testing the variance compared to the M1 classical method.

It is easily foreseen that the colored, non-bleeding pH indicator test strips that are obtained after water diffusion from the paper samples could be analyzed via other faster and simpler methods, such as image analysis. Therefore, this method is a good candidate for fast image analysis of pH test strips for paper artifacts and integrated in potential smartphone instrument-free applications.

CONCLUSIONS

A non-destructive, simple, rapid, and highly precise method was developed and successfully applied for determination of pH of paper artifacts using univariate regression analysis and diffuse reflectance spectroscopy. The measurements were performed on commercial non-bleeding pH indicator test strips, using a small amount of ultrapure water that quickly dried after analysis. The method was similar in accuracy with classical cold extraction and pH meter-based methods but the precision was improved. The optimum wavelength was found to be 590 nm and this could be directly used for univariate calibration methods (in the pH range 4.00 – 9.50) without the need of multivariate calibration methods. The proposed method could be extended in applicability for pH determination to other types of samples and does not require the mandatory use of standard pH solutions purchased from manufacturers. Calibration standards in the laboratory and the number of the standards used for calibration could be increased without affecting the duration of the analysis, due to the speed of obtaining the reflectance signal.

EXPERIMENTAL SECTION

Reagents and materials

Ultrapure water (18.2 MΩ cm, pH 6.70-7.50) was used for all the solutions that were prepared in this study. A Britton-Robinson universal buffer solution was prepared in a final volume of 1 L by mixing boric acid, acetic acid and phosphoric acid, each at a final concentration of 50 mM. The solution pH was monitored using a three-point calibrated pH meter (Hanna Instruments pH 212 microprocessor) with a two-decimal precision, and the desired pH values was reached using 10 M sodium hydroxide solution that was added dropwise, while stirring continuously. Aliquots of 50 mL solution with pH values from 2.00 up to 10.00—in this order—were drawn from the initial solution and deposited in falcon tubes, at an interval of 0.50 pH units.

Thus, seventeen pH standard solutions were prepared in the 2.00 – 10.00 pH range—at an interval of 0.50 pH units—that were used for calibration curves. Several ranges of non-bleeding pH indicator test strips, with different numbers of bands (Dosatest, VWR Chemicals) were used.

Sample preparation and spectral measurement

For the calibration curve, an aliquot of 15 - 50 µL pH standard solution was evenly spread on a pH indicator test strip and incubated for about two minutes. The excess of standard buffer solution was quickly removed with a clean pure cellulose tissue and the reflectance spectra were recorded in the desired region of the strips, before drying. A maximum of two adjacent bands from a strip could fit in the integrating sphere sample window. Three real samples originating from three books with different textured pages were chosen for the application of the optimized method — a book that used acid-free paper (Advanced Protocols in Oxidative Stress III, Humana Press, Springer 2015 as Sample 1), a New Testament in Greek from 1710 (Η Καίνι Διαθήκη as Sample 2) and a book that used regular modern paper (Book of abstracts 9th ICCSSEEC, Valahia University Press, Targoviste, 2011 as Sample 3). On a certain page of each book, 50 µL of ultra-pure water were placed on the analysed region, using an automatic pipette. Prior to the water application, three pH indicator strips were laid just under the analysed paper zone, as shown in Figure 3A. After an incubation of about 3 minutes, it was checked whether the pH indicator strips were evenly moistened and then the reflectance spectra of the strips were measured. For the validation of the developed method, two other standard methods were used: method 1 (M1) – cold extraction method and method 2 (M2) – a pH electrode adapted for surface analysis. First method is a standard method, in which a modern calibrated pH-meter (Hanna Instruments pH 212 microprocessor) is used to read the pH values of the paper cold extract, after equilibration. The cold extraction was adapted according to ISO 6588-1 [12], that requires 0.2 g of paper sample, cut into 5 x 5 mm pieces and placed in a beaker containing 10 ml ultrapure water at a temperature within the interval 20 to 25 °C for one hour. The beaker was closed and agitated every 10 minutes. The M2 method involves the use of a glass electrode (SenTix 41 Plus connected to a InoLab WTW pH 720 meter) that reads pH directly from the paper that was cut, attached to the tip of the wet electrode, after 5 minutes incubation. The diffuse reflectance spectra in 350 – 750 nm spectral domain were recorded for every type of pH test strips, using a V-550 Jasco spectrophotometer that was equipped with an integrating sphere (Jasco ISV 469). The collection area is 1 cm^2. The scan rate was set at medium, and the reflectance value was recorded every 1 nm. All samples were measured at least in duplicates. White modern paper was used as 100% reflectance reference. The analytical steps form the proposed procedure are presented in Figure 4.

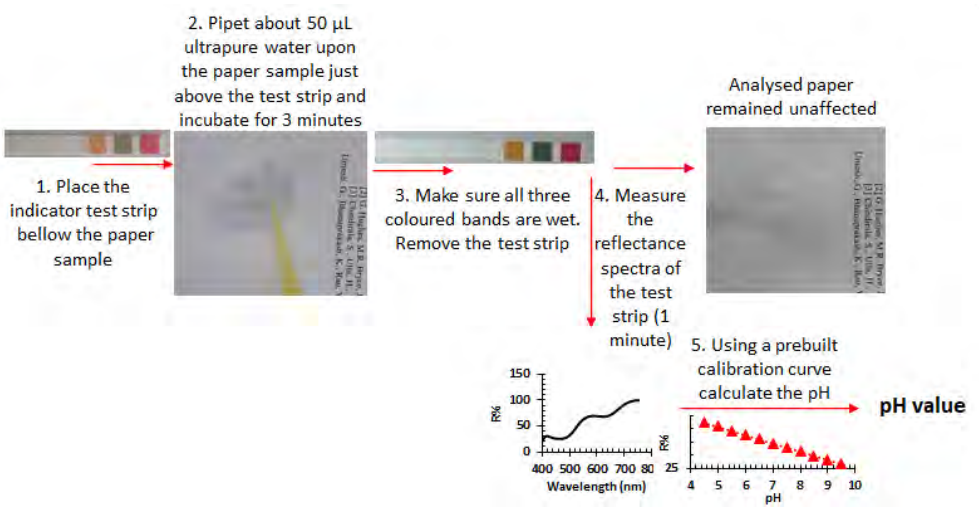

Figure 4. Key analytical steps required for the proposed method

Statistical analysis

The measured spectra of the calibration or testing samples were exported in *txt* format and then were min-max normalized in Excel using the formula:

$$x_i' = \frac{x_i - \min(x)}{\max(x) - \min(x)}$$

The normalized spectra data matrix was further analyzed either using Excel or Statistica software (released by Statsoft, USA) for plotting or for regression analysis and Principal Component Analysis (PCA), that was applied on 350 – 750 nm normalized data matrix. One way ANOVA was used for testing the statistical difference between the three means for the three tested real samples with a significance level of 0.05. Fischer F test was applied for testing the statistical difference between the variances of method 2 and method 3 compared to the classical method 1, with a statistical significance level of 0.01.

ACKNOWLEDGMENTS

This work was supported by UBB-TeMATIC Art P_40_374, project co-financed by FEDR through Competitiveness Operational Programme 2014–2020

REFERENCES

1. M. Kostadinovska; Proc; 3rd Virtual Multidiscip. Conf., **2015**, *3*, 184–189.
2. I. Čabalová; F. Kačík; J. Gojný; B. Češek; M. Milichovský; O. Mikala, T. Tribulová; J. Durkovič; *BioResources*, **2017**, *12*, 2618–2634.
3. F. Coppola; N. Brown; F. Amicucci; M. Strlič; A. Modelli; *Herit. Sci.,* **2020**, *8,* 1–10.
4. M. Strlič; J. Kolar; D. Kočar; T. Drnovesek; V.-S. Šelih; R. Susič; B. Pihlar; *e-Preservation Sci.*, **2004**, *1*, 35–47.
5. R. Kumar; V. Kumar; V. Sharma; Spectrochim. *Acta - Part A Mol. Biomol. Spectrosc.,* **2017**, *170*, 19–28.
6. V. Sharma; J. Kaur; R. Kumar; *Aust. J. Forensic Sci.,* **2020**, *52*, 1–24.
7. R. Kumar; V. Kumar; V. Sharma; *Appl. Spectrosc.,* **2015**, *69*, 714–720.
8. A. Zoleo; F. Vecchia; M. Brustolon; *Appl. Magn. Reson*., **2009**, *35*, 213–220.
9. A. Zoleo; L. Speri; M. Bronzato; *Restaurator*, **2015**, *36*, 269–282.
10. M. Strlič; I. K. Cigić; J. Kolar; G. De Bruin; B. Pihlar; *Sensors*, **2007**, *7*, 3136–3145.
11. A. Beneduci; F. Dalena; B. C. De Simone; I. Lania; G. De Filpo; M. C. Gallucci; G. Chidichimo; *J. Phys. Chem. C,* **2017**, *121*, 25180–25186.
12. https://www.iso.org/standard/77946.html, accessed on 06.05.2021.

STUDIA UBB CHEMIA, LXVI, 2, 2021 (p. 137-149)
(RECOMMENDED CITATION)
DOI:10.24193/subbchem.2021.2.12

SELECTIVE ELECTROEXTRACTION OF BASE METALS FROM LEACHING SOLUTIONS OBTAINED DURING THE RECYCLING OF WASTE PRINTED CIRCUIT BOARDS. II. SELECTIVE POTENTIOSTATIC ELECTRODEPOSITION OF COPPER, TIN AND LEAD

MARIAN-IOSIF FRÎNCU[a], ENIKO COVACI[a], SORIN-AUREL DORNEANU[a,b,*], PETRU ILEA[a,b]

ABSTRACT. This paper presents our results concerning the feasibility of selective potentiostatic electroextraction of copper, tin and lead from leaching solutions obtained during the recycling of base metals from waste printed circuit boards. Applying this protocol, in a first stage, the concentration of Cu ions from the leaching solutions can be lowered, with acceptable efficiency, below 0.5 g/L. To avoid the contamination of Sn-Pb alloys with Cu, an intermediary step of Cu cementation on metallic Sn were proposed and tested. Finally, the potentiostatic selective electrodeposition protocol was successfully applied for the electroextraction Sn-Pb alloys. The experiments were performed in real leaching samples, using a Fisher type electrode as cathode. The obtained experimental results demonstrate that, controlling rigorously the imposed potential and corelating them with the solution composition, high purity Cu and Sn-Pb alloys deposits can be obtained, maximum contents of 99.96%, 99.83% and 82.62% being evaluated for Cu, Sn and Pb, respectively.

Keywords: *waste printed circuit boards, potentiostatic selective electroextraction, copper recovery, tin and lead alloy electrodeposition.*

INTRODUCTION

It is well known that, due to the depletion of mineral resources, the use of different wastes as secondary resources gains increased attention.

[a] *Babeş-Bolyai University, Faculty of Chemistry and Chemical Engineering, Department of Chemical Engineering, 11 Arany Janos Street, Cluj Napoca, RO-400028, Romania*
[b] *Babeş-Bolyai University, Interdisciplinary Research Institute on Bio Nano Sciences, 42 Treboniu Laurian Street, Cluj Napoca, RO-400271, Romania*
** Corresponding author: sorin.dorneanu@ubbcluj.ro*

Currently, consistent researches concerning the recycling of secondary resources are focused on the wasted printed circuit boards (WPCBs) [1], which are the base of the electronics industry. The WPCBs present a potentially high economic value, a serious concern for the environment [2], and an emerging trend towards the circular economy [3].

Copper is the major metal found in WPCBs and its recovery is therefore a top priority [4], followed by tin, lead and other metals [5]. From the ecological and economic point of view, the electrochemical recovery of metals from WPCBs presents significant advantages [6,7], it can apply highly efficient strategies [8] like the electroextraction one [9] or more complex processes [10,11], many of them based on the selective electrodeposition [12,13].

The cathodic electrodeposition represents an efficient method for the electrochemical recovery of the metals from a solution [14], extensive studies presenting different strategies and efficiencies for the Cu electroextraction [15] or the Sn-Pb alloys deposition [16,17], processes that are constantly improved [18]. Electrochemical deposition was used to obtain thin films of Cu and Sn-Pb alloy [19] which have wide applications in the industrial revolution. Starting from the results obtained during our previous research [13,20,21], this paper aimed to evaluate the feasibility of potentiostatic selective electroextraction of copper and Sn-Pb alloys from solutions resulting during the recovery of base metals from WPCBs using the leaching system KBr / HBr / Br_2. Based on the literature data [22], to prevent the contamination of electrodeposited Sn-Pb alloys with Cu, an intermediary step of Cu cementation on metallic Sn were also proposed and tested. For an accurate evaluation of process efficiency, the experiments were divided in several short time tests, the weight and the composition of the intermediary obtained deposits being evaluated. For these steps, the deposits were washed, dried, and detached from the Fisher type working electrode (WE) by mineralization with *aqua-regia* and analyzed by flame atomic absorption spectroscopy (FAAS) and inductively coupled plasma atomic emission spectroscopy (ICP-AES).

RESULTS AND DISCUSSION

The selective potentiostatic electrodeposition of Cu

Our previous results concerning the intense and fast selective electrodeposition of Cu from the leaching solutions demonstrated that high purity Cu deposits can be obtained, in parallel with the regeneration of the leaching solution, at high current densities [13] if the concentration of Cu ions remains over 12 g/L. Continuing the previous work, in the present paper, we

proposed and tested a new protocol for the selective potentiostatic electroextraction of several metals (Cu, Sn and Pb). The main goal of the research was to evaluate the feasibility of the complete extraction of these metals from the leaching solutions.

Based on the information obtained by cyclic voltammetry and galvanostatic electrodeposition, the tests concerning the selective potentiostatic electroextraction of Cu from the leaching solutions started at imposed working electrode potentials (E_{WE}) of -0.25 V *vs.* the reference electrode (RE) [13]. As detailed in the experimental section, the initial concentration of the Cu ions in the real leaching solution sample was 12.89 g/L. When the recorded current through the WE (I_{WE}) decreased at 10% from the initial value, the experiment was stopped and the Fisher type WE was removed from the electrochemical cell, washed, dried and weighted. The obtained deposits were detached from the WE by mineralization with *aqua-regia* and the obtained solutions were analyzed by FAAS and ICP-AES to evaluate its composition. An example of images corresponding to the cleaned Fisher type electrode and of a Cu deposit obtained by electroextraction are presented in Figure 1.A and 1.B, respectively.

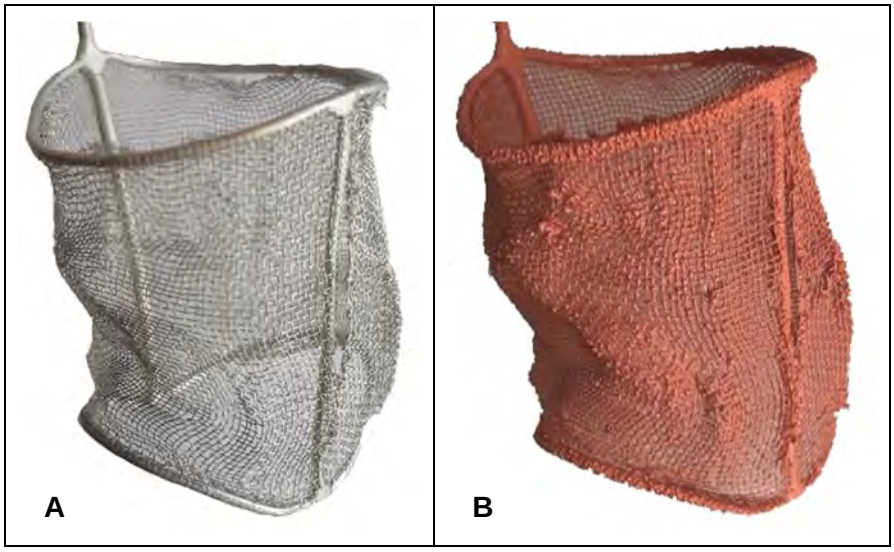

Figure 1. Example of images of the clean Fisher type electrode (A) and of the copper deposit obtained after electrodeposition (B).

Afterwards, the imposed E_{WE} was progressively switched to more negative values of -0.3 and -0.35 V/RE The main electrical parameters recorded during the selective potentiostatic electrodeposition of Cu are

presented in Figure 2, where U_T, E_{CE}, pH and ORP represent the instantaneous values of the voltage at the electrochemical cell terminals, counter electrode (CE) potential, pH and oxidation/reduction potential, respectively. Also, the mean and/or individual values of the operational and efficiency parameters evaluated from the experimental data are presented in Table 1, were C_{EF} and W_S represent the current efficiency and the specific electricity consumption, and $E_{WE,M}$, $I_{WE,M}$ and ORP_M represent the average values of E_{WE}, I_{WE} and ORP, respectively. [Cu] stands for the Cu ions concentration in the leaching solutions.

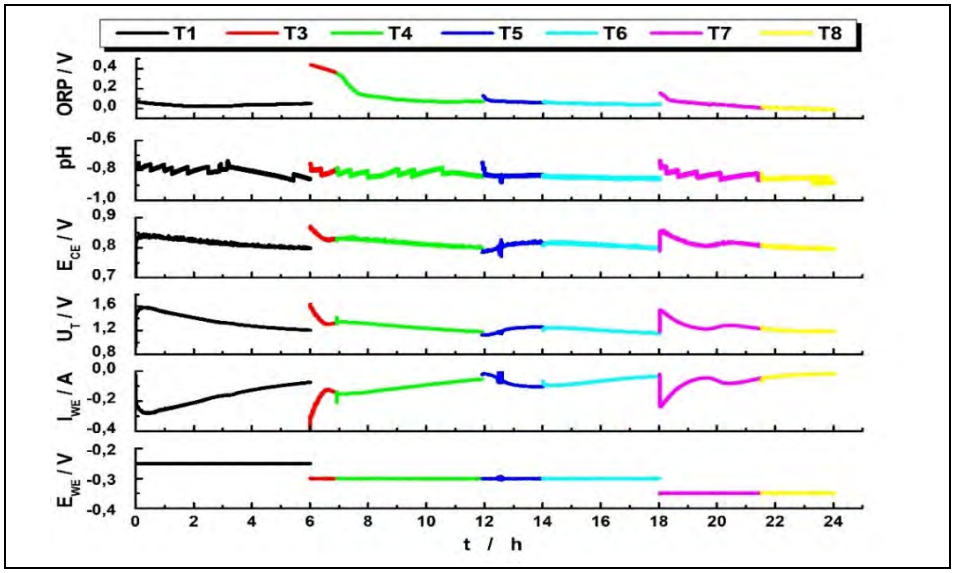

Figure 2. The evolution of the electrochemical and electrical parameters during the potentiostatic selective electrodeposition of Cu from the leaching solution.

Table 1. The evolution of the operational and efficiency parameters for the tests of potentiostatic selective electrodeposition of Cu from real leaching solutions.

Deposit	Test	$E_{WE,M}$ (V/RE)	$I_{WE,M}$ (mA)	t (min.)	[Cu] (g/L)	C_{EF} (%)	W_S (kWh/kg)	ORP_M (V/RE)
D1	**T1**	-0.25	-172	361	5.17	95.9	0.62	0.038
D2	**T2**	-0.25	-1.5	360	5.17	48.6	1.09	0.125
D3	**T3**	-0.30	-173	55	1.63	65.7	0.84	0.397
D3	**T4**	-0.30	-106	300	1.63	65.7	0.84	0.111
D4	**T5**	-0.30	-74	126	1.58	1.7	30.46	0.071
D4	**T6**	-0.30	-67	241	1.58	1.7	30.46	0.048
D5	**T7**	-0.35	-86	211	0.36	41.9	1.32	0.049
D5	**T8**	-0.35	-28	150	0.36	41.9	1.32	0.001

As it can be seen in Figure 2, the U_T, E_{CE}, pH and ORP values remains relatively constant, proving the stability of the electrochemical system during the progressive Cu electroextraction. Contrarily, to maintain a reasonable high value of the I_{WE}, and, consequently, an acceptable rate of Cu electroextraction, the imposed E_{WE} value must be permanently adjusted to more and more negative values, in accordance with the decrease of the Cu ions concentration in the solutions. Otherwise, the reaction of hydrogen evolution (RHE) becomes the main process, wasting electrical energy without any supplementary electroextraction of Cu. These conclusions are in excellent agreement with the C_{EF} and W_S values presented in Table 1.

Finally, it is worth to note that the concentration of the Cu ions in the leaching solution sample decreased from its initial value (12.89 g/L) up to 0.36 g/L, proving the proposed process feasibility. The attempt to continue the process under this value leads to the enhancement of the RHE and increase the risk of Sn and Pb inclusion in the Cu deposits.

For the Cu obtained deposits, their compositions were evaluated analyzing the solution (resulting by mineralization of deposits with *aqua-regia*) by FAAS, the obtained results being presented in Table 2.

Table 2. Percentage of metals (w/w) evaluated by FAAS in the deposits obtained by selective potentiostatic electrodeposition of Cu from the leaching solution.

Test	Cu (%)	Sn (%)	Pb (%)	Fe (%)	Ni (%)	Zn (%)
T1	99.78	0.22	ND	0.00	ND	0.00
T3+T4	99.91	0.00	ND	0.01	ND	0.00
T5+T6	98.76	ND	ND	0.90	ND	0.34
T7+T8	99.96	0.00	ND	0.04	ND	0.00

The data presented in Table 2 reveal that the average purity of the deposits exceeds 99.8%, proving that the selective potentiostatic electrodeposition of Cu from the leaching solution is a feasible and cost-effective technology, leading to products of excellent quality and value.

Extraction of Cu traces by cementation on metallic Sn

To recover completely the existing Cu from the leaching solutions and to avoid the contamination of the Sn-Pb alloys deposit with Cu traces, we decided to implement a step of Cu cementation on metallic Sn between the Cu electrodeposition step and the Sn-Pb alloys electroextraction stage. At this level, in the low pH values, the next reaction takes place:

$$2Cu^{+}_{(aq)} + Sn^{0}_{(s)} \rightarrow 2Cu^{0}_{(s)} + Sn^{2+}_{(aq)} \quad (1)$$

The variation of the measured parameters is presented in Figure 3.

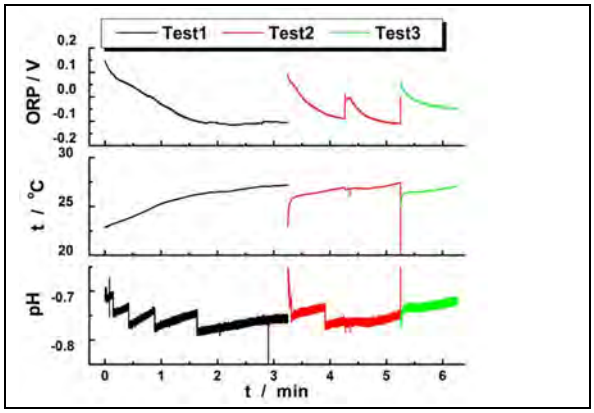

Figure 3. Evolution of pH, temperature and ORP of the leaching solution during Cu cementation on metallic Sn.

During the cementation tests, samples were collected periodically from the chemical reactor and analyzed by FAAS. The evolution of the [Cu] values during this process is presented in Table 3.

Table 3. Evolution of [Cu] during the process of Cu cementation on metallic Sn.

Time (h)	0	1	2	3	4	5	6
[Cu] (mg/L)	266.5	177.7	70.8	57.2	38.5	35.5	7.98

Based on data presented in Figure 3 and Table 3, we demonstrated that the cementation of Cu traces using metallic Sn granules is a feasible, cost-effective, and efficient method to reduce significantly the [Cu] value. Practically, after 6 hours, the [Cu] was diminished from ~250 mg/L to less than 8 mg/L, without altering the pH or the ORP of the leaching solution.

Selective potentiostatic electroextraction of Sn-Pb alloys

The measurements performed by cyclic voltammetry revealed that the electrodeposition of Sn and Pb begins at remarkably close potentials, around -0.5 and -0.55 V/RE, and depends essentially on the concentration of these ions. Consequently, the selective electrodeposition of Sn and Pb is, practically, impossible, but the deposition of the Sn-Pb alloys is favorized.

The electrochemical and electrical parameters recorded during the potentiostatic electrodeposition of Sn-Pb alloys are presented in Figure 4.

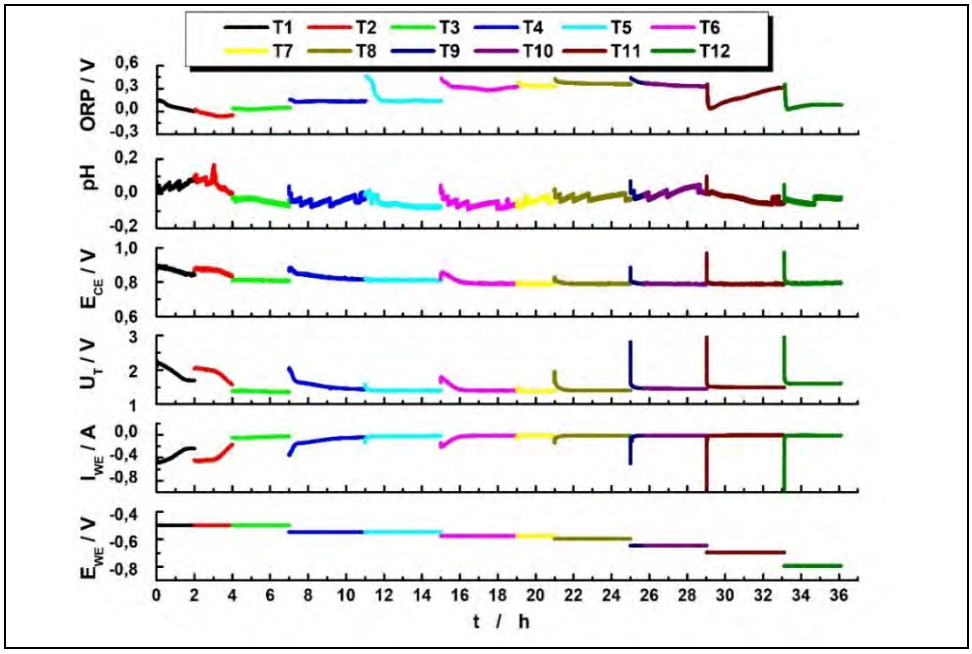

Figure 4. Evolution of electrochemical and electrical parameters during the tests of Sn-Pb alloys electrodeposition from the leaching solution free of Cu ions.

As it can see from Figure 4, the measurements were performed at a starting E_{WE} value of -0.50 V/RE, and initial concentrations of Sn ([Sn]) and Pb ([Pb]) of 7.9 and 3.97 g/L, respectively. Further, the E_{WE} values were shifted progressively, in correlation with the decrease of [Sn] and [Pb] values concentrations, to more negative values of -0.55, -0.58, -0.6, -0.65, -0.7 and, finally, of -0.8 V/RE. As in the case of Cu electrodeposition, the modification of the applied E_{WE} value was made when the instant I_{WE} values decrease to 10% from the initial ones. In addition, the averaged and/or individual values of the operational and efficiency parameters were evaluated based on the experimental data, the obtained results being presented in Table 4.

Supplementary, Figure 4 reveals that the U_T, E_{CE} and pH values remains relatively constant, proving that the progressive electroextraction of Sn and Pb from the leaching solution do not affect the other proprieties of the electrochemical system. Contrarily, to maintain I_{WE} at reasonable high value, the imposed E_{WE} value must be permanently adjusted to more and more

negative values, simultaneously with the decrease of the [Sn] and [Pb] values. Preserving the same E_{WE} for a long period leads to the enhancing of the RHE process, affecting seriously the C_{EF} and W_S values.

Table 4. The evolution of the operational and efficiency parameters evaluated for the tests of potentiostatic selective electrodeposition of Sn-Pb alloys from real leaching solutions with low Cu content.

Deposit	Test	$E_{WE,M}$ (V/RE)	t (min.)	[Sn] (g/L)	[Pb] (g/L)	C_{EF} (%)	W_S (kWh/kg)	$I_{WE,M}$ (mA)	ORP_M (V/RE)
D1	**T1**	-0.50	120	2.95	3.97	45.54	1.93	-353	0.065
D1	**T2**	-0.50	120	2.95	3.97	45.54	1.93	-384	0.038
D2	**T3**	-0.50	180	2.53	3.97	47.06	1.30	-41	0.039
D3	**T4**	-0.55	240	0.55	2.58	94.45	0.81	-100	0.134
D4	**T5**	-0.55	240	0.51	2.54	8.85	5.24	-25	0.176
D5	**T6**	-0.58	240	0.32	1.48	64.24	0.68	-43	0.315
D6	**T7**	-0.58	120	0.30	1.47	12.31	4.99	-15	0.341
D7	**T8**	-0.60	240	0.18	1.45	29.52	1.93	-16	0.369
D8	**T9**	-0.65	44	0.11	1.44	16.22	6.07	-23	0.395
D8	**T10**	-0.65	198	0.11	1.44	16.22	6.07	-11	0.345
D9	**T11**	-0.70	246	0.085	1.44	11.68	6.38	-10	0.197
-	**T12**	-0.80	180	-	-	-	-	-12	0.080

From another point of view, it is worth to note that, applying an optimized protocol for the selective potentiostatic electrodeposition of Sn-Pb alloys, the [Sn] and [Pb] values in the real leaching sample can be lowered, under acceptable efficiency conditions, below 0.1 g/L and 1.5 g/L, respectively. Interestingly, in the tested conditions, at the extremely negative E_{WE} value, of -0.8 V/RE, the deposit was, practically, absent, indicating that, at this polarization level, the entirely quantity of consumed electricity was wasted in the RHE process.

Finally, a series of images showing the obtained Sn-Pb alloy deposits are presented in Figure 5.

For better understand the deposits morphology, they were also mineralized with *aqua-regia* and the resulting solutions were analyzed by ICP-AES, the obtained results being presented in Table 5.

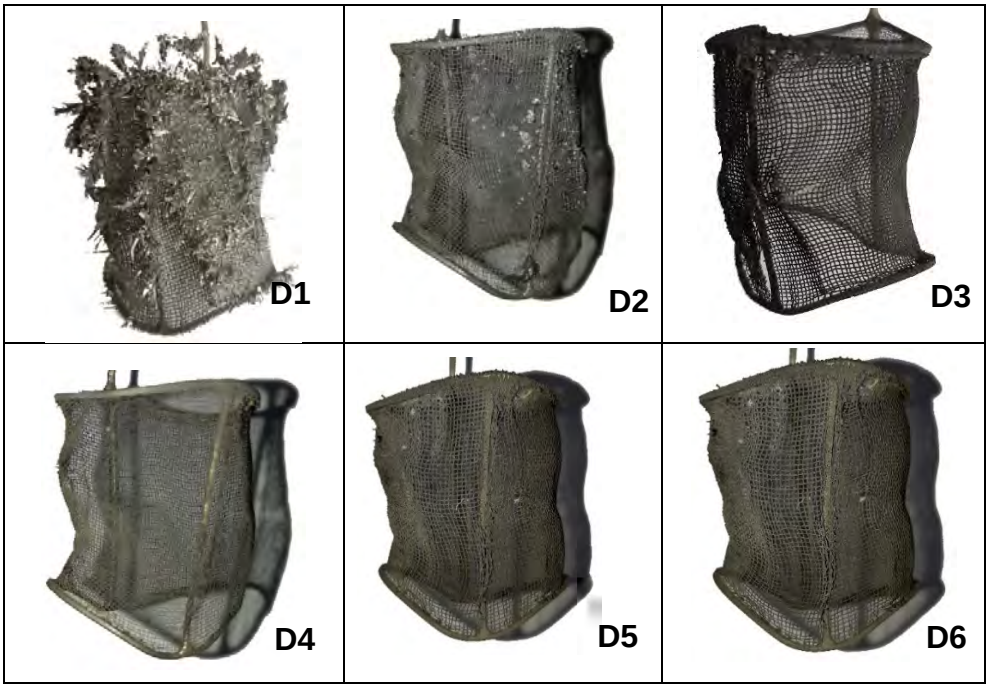

Figure 5. Images of the Sn-Pb alloy deposits obtained by selective potentiostatic electroextraction from real leaching solutions with low Cu content.

Table 5. Percentage of metals (w/w) evaluated by ICP-AES in the deposits obtained by selective potentiostatic electrodeposition of Sn-Pb alloys from the leaching solution with low Cu content.

Deposit	Cumulated tests	Cu (%)	Sn (%)	Pb (%)	Fe (%)	Ni (%)	Zn (%)
D1	**T1 + T2**	0.00	99.8	0.01	0.01	0.01	0.00
D2	**T3**	0.00	99.1	0.06	0.15	0.02	0.09
D3	**T4**	0.00	74.3	25.4	0.02	0.00	0.01
D4	**T5**	0.01	49.3	49.7	0.52	0.02	0.24
D5	**T6**	0.00	14.6	82.6	0.03	0.05	0.01
D6	**T7**	0.03	77.3	20.2	0.26	0.17	0.55
D7	**T8**	0.01	80.6	13.8	0.23	0.19	0.10
D8	**T9 + T10**	0.01	85.1	11.6	0.79	0.91	0.54
D9	**T11**	0.03	91.7	5.6	1.04	0.26	0.48

Corelating the data from Table 3, Figure 5 and Table 4, it is clear that, at high [Sn] in the solution, dendritic deposits (see D1 and D2), with extremely high content of Sn were obtained. Further, simultaneously with the decrease on [Sn] and [Pb] values, the Sn-Pb alloy deposits become smooth and compact, increasing their adherence on the cathode surface. Also, the ratio between Sn and Pb in the deposits changes significantly, depending on [Sn] and [Pb] values and the applied E_{WE}. Additionally, it is worth to note that the major impurities such as Ni, Fe and Zn, which are present in large quantities in the leaching solution and have standard reduction potentials close to the electrodeposition potentials of Sn and Pb, start to be incorporated significantly into the Sn-Pb alloy deposit only when the E_{WE} decrease under -0.65 V/RE

Finally, we conclude that the selective electrodeposition of Sn-Pb alloys, in potentiostatic mode, from leaching solutions with extremely low content of Cu, represents a feasible, efficient and cost-effective technology for the advanced recovery of Sn and Pb from WPCBs.

CONCLUSIONS

Correlating all the recorded data and the evaluated parameters during the experiments concerning the selective potentiostatic electrodeposition of Cu and Sn-Pb alloys from the leaching solution based on the KBr / HBr / Br_2 system, we concluded that the proposed and tested technologies are perfectly feasible, allowing to obtain deposits of high quality and purity, with a good commercial value, comparable with other less ecological and efficient processes cited in the literature [23].

The cost-effectiveness of the proposed processes can be assured by the rigorous monitoring and control of the main process parameters, such as the concentration of Cu, Sn and Pb ions, the pH and ORP of the electrolyte, and the values of the imposed E_{WE} and/or I_{WE} parameters.

In order to increase the performances of the selective potentiostatic electrodeposition of the Sn-Pb alloys, an intermediate step of Cu cementation on metallic Sn must be inserted between the Cu electroextraction and Sn-Pb alloys electrodeposition stages.

Following the presented protocols, final [Cu], [Sn] and [Pb] values below 0.01 g/L, 0.1 g/L and 1.5 g/L, respectively, can be reached under very promising conditions of profitability.

EXPERIMENTAL SECTION

Chemicals

Reagents as KBr and HBr are purchased by Fluka and Sigma-Aldrich and used as received.

The real leaching solution was obtained by mixing equal samples from different solutions resulted by the leaching of the exposed metals from 10 PC motherboards in 2.2 L of 2 M KBr + 0.5 M HBr + 1 M Br_2 solutions [21]. The ORP of the resulting mixture (1 L) was lowered by placing it over 2 kg of WPCBs, after which the solution pH was adjusted to 0.1 by addition of HBr 47%. The concentrations of the main metallic ions in the final starting solution were: 12.89 g/L Cu; 7.9 g/L Sn; 3.97 g/L Pb; 9 g/L Zn; 5.6 g/L Fe; 0.8 g/L Ni [13].

Experimental methods

The selective potentiostatic electrodeposition experiments of Cu and Sn-Pb alloys were performed in an electrochemical reactor divided using a porous ceramic membrane. As anolyte, 0.5 L samples of fresh 2 M KBr + 0.5 M HBr were introduced in the anodic compartment. The cathodic compartment was filled with 0.5 L of mixture of real leaching solutions described in the chemicals part.

The reactor was equipped with a Fisher type electrode as WE, consisting in a cylindrical Pt mesh, with $\varnothing_{EXT} \cong 25$ mm and a height of $\cong 40$ mm, fixed on a Pt wire frame with $\varnothing = 1$ mm. As CE, a rectangular graphite block with dimensions of 80 mm x 70 mm x 20 mm (height x width x thickness), was used. The WE, CE and 2 reference electrodes of $Ag/AgCl/KCl_{sat}$ type (named further as RE) were connected to a computer controlled potentiostat (DXC236, Datronix Computer, Romania).

The measurements concerning the cementation of Cu on metallic Sn were performed in a glass cell with a volume of 400 mL, in which were introduced 300 mL of solution resulting after all the tests of selective potentiostatic electroextraction of Cu. Over this solution 26.04 g of soldering alloy Sn 97% -Cu 3% were added. The initial soldering alloy, with a diameter of 3 mm, was divided into 252 pieces with a length of approx. 5 mm, resulting an estimated grains area of approximately 120 cm^2.

Additionally, 2 laboratory multi-meters (Consort C863, Consort, Belgium) were used as galvanically insulated electrochemical interfaces with high input impedance between the data acquisition board (NI6121, National Instruments,

USA) and the pH and ORP sensors (SP10T and SO50X, respectively, both from Consort, Belgium). During the experiments, the electrolyte from the cathodic compartment was stirred using a magnetic stirrer (FB 15001, Fischer Scientific).

Before each test, the WE was cleaned by immersion during 10 min. in *aqua-regia*, washed with double-distilled water and dried under nitrogen jet, and weighed using an analytical balance (XA110, RADWAG, Polonia).

After each experiment, the Fisher type WE was removed from the electrochemical reactor and the obtained Cu, or Sn-Pb alloy deposits were washed with 2 M KBr + 0.5 M HBr mixture (to avoid the precipitation of Cu, Sn and Pb ions), cleaned with double-distilled water and dried with pure acetone and pure nitrogen jet. Finally, the deposits were weighed using the analytical balance and detached from the electrode by mineralization with 28 mL of *aqua-regia*. The resulted solutions were analyzed by ICP-AES method, using a SPECTRO CIROS CCD spectrometer (SPECTRO Analytical Instruments, Germany). The concentrations of the dissolved metallic ions from the leaching solutions were measured by flame atomic adsorption spectroscopy (FAAS), using an AVANTA-PM spectrometer (GBC, Australia).

ACKNOWLEDGMENTS

The present work has received financial support through the project: Entrepreneurship for innovation through doctoral and postdoctoral research, POCU/380/6/13/123886 co-financed by the European Social Fund, through the Operational Program for Human Capital 2014-2020.

This work was also supported by a grant of the Romanian Ministry of Research and Innovation, CCCDI-UEFISCDI, project number PN-III-P1-1.2-PCCDI-2017-0652 / 84PCCDI/2018, within PNCDI III.

REFERENCES

1. B. Li, D.-A. Pan, Y.-H. Jiang, J.-J. Tian, S.-G. Zhang, K. Zhang, *Rare Metals*, **2014**, *33(3)*, 353-357.
2. A. Kumari, M. Ku. Jha, J.-C. Lee, R.P. Singh, *J. Clean. Prod.*, **2016**, *112*, 4826-4834.
3. R.K. Nekouei, I. Tudela, F. Pahlevani, V. Sahajwalla, *Curr. Opin. Green Sustain. Chem.*, **2020**, *24*, 14-20.
4. Z. Sun, H. Cao, P. Venkatesan, W. Jin, Y. Xiao, J. Sietsma, Y. Yang, *Front. Chem. Sci. Eng.*, **2016**, *11(3)*, 308-316.

5. F. Moosakazemi, S. Ghassa, F. Soltani, Mo. R.T. Mohammadi, J. Hazard. Mater., **2020**, *385*, 121589.
6. S.-A. Dorneanu, E. Covaci, F. Imre-Lucaci, G.L. Turdean, *Studia UBB Chemia*, **2019**, *64(2 T2)*, 555-565.
7. C. Cocchiara, S.-A. Dorneanu, R. Inguanta, C. Sunseri, P. Ilea, *J. Clean. Prod.*, **2019**, *230*, 170-179.
8. L. Pietrelli, S. Ferro, M. Vocciante, *Renew. Sust. Energ. Rev.*, **2019**, *112*, 317-323.
9. S. Akbari, A. Ahmadi, *Chem. Eng. Process.,* **2019**, *142*, 107584.
10. P.K. Choubey, R. Panda, M.K. Jha, J.-C. Lee, D.D. Pathak, *Sep. Purif. Technol.*, **2015**, *156*, 269-275.
11. M.S.B. da Silva, R.A.C. de Melo, A.L. Lopes-Moriyama, C.P. Souza, *J. Environ. Manage.*, **2019**, *246*, 410-417.
12. J.A. Barragan, C.P. de León, J.R.A. Castro, A. Peregrina-Lucano, F. Gómez-Zamudio, E. R. Larios-Durán, *ACS. Omega.*, **2020**, *5(21)*, 12355-12363.
13. M.-I. Frîncu, E. Covaci, S.-A. Dorneanu, P. Ilea, *Studia UBB Chemia*, **2020**, *65(3)*, 33-44.
14. W. Jin, Y. Zhang, *ACS Sustain. Chem. Eng.*, **2020**, *8(12)*, 4693-4707.
15. J. Yang, Y. Wu, J. Li, *Hydrometallurgy*, **2012**, *121-124*, 1-6.
16. S. Fogarasi, F. Imre-Lucaci, M. Fogarasi, A. Imre-Lucaci, *J. Clean. Prod.*, **2019**, *213*, 872-883.
17. H.M. Veit, A.M. Bernardes, J.Z. Ferreira, J.A.S. Tenorio, C. de F. Malfatti, *J. Hazard. Mater.*, **2006**, *137(3)*, 1704-9.
18. R.S. El-Nasr, S.M. Abdelbasir, A.H. Kamel, S.S.M. Hassan, *Sep. Purif. Technol.*, **2020**, *230*, 115860.
19. S. Ghosh, *Thin Solid Films*, **2019**, *669*, p. 641-658.
20. S.-A. Dorneanu, *Studia UBB Chemia*, **2017**, *62(3),* 177-186.
21. S.-A. Dorneanu, A.-A. Avram, A.-H. Mărincaş, N. Cotolan, T. Frenţiu, P. Ilea, *Studia UBB Chemia*, **2018**, *63(4)*, 147-158.
22. R.M. Lamya, L. Lorenzen, *J. South. Afr. Inst. Min. Metall.,* **2005**, 21-29.
23. J. Hao, Y. Wanga, Y. Wua, F. Guo, *Resour. Conserv. Recycl.*, **2020**, *157*, 104787.

STUDIA UBB CHEMIA, LXVI, 2, 2021 (p. 151-161)
(RECOMMENDED CITATION)
DOI:10.24193/subbchem.2021.2.13

OPTIMIZATION OF GOLD SORPTION FROM AMMONIACAL THIOSULPHATE SOLUTION ON ANION EXCHANGE FIBER USING TAGUCHI EXPERIMENTAL DESIGN

EMILIA NEAG[a], ANAMARIA IULIA TÖRÖK[a], ZAMFIRA DINCĂ[a], MARIN SENILA[a], CERASEL VARATICEANU[a], ERIKA ANDREA LEVEI[a], EKATERINA SHILOVA[b], FRANCOISE BODENAN[c]

ABSTRACT. Taguchi experimental design was used to optimize the experimental parameters for Au sorption from ammoniacal thiosulfate solutions containing 2 mg/L Cu complexed as cuprous thiosulfate $[Cu(S_2O_3)_3]^{5-}$ onto anion exchange fiber (METALICAPT® MFH11). An L_9 orthogonal array was chosen to study the effect of three parameters, namely Au initial concentration (10-30 mg/L), fiber quantity (0.05-0.55 g) and temperature (20-30°C). The sorption tests were carried out in batch mode at a stirring rate of 500 rpm and pH of 9.3. The experimental data were processed using signal-to-noise ratio and the analysis of variance was used to determine the most significant parameters. The optimal conditions for Au sorption were found to be 30 mg/L Au concentration, 0.05 g of fiber and temperature of 20°C. The obtained results indicated fiber quantity as the most influential parameter on Au sorption with a contribution of 66%, followed by Au initial concentration with a contribution of 33%. In the optimal conditions, the sorption capacity of the fiber was found to be 16.8 mg/g, in good agreement with the predicted result by Taguchi method (16.7 mg/g). Further investigations are necessary to examine the elution behavior of gold from the fiber.

Keywords: *gold sorption, anion exchange fiber, Taguchi experimental design, ANOVA*

[a] *INCDO-INOE 2000, Research Institute for Analytical Instrumentation, 67 Donath Street, 400293 Cluj-Napoca, Romania*
[b] *AJELIS SAS, 91260 Juvisy-sur Orge, France*
[c] *BRGM, 45100 Orléans, France*
** Corresponding author: emilia.neag@icia.ro*

INTRODUCTION

The technologies for precious metal recovery have gained considerable interest, as gold (Au) resources are limited while Au is frequently used in various fields due to its outstanding thermal and electrical conductivity, high catalytic performance and photothermal conversion efficiency [1,2].

Gold leaching using thiosulfate solutions has emerged as an innovative and eco-friendly alternative to cyanide leaching, for gold containing wastes. However, the recovery of gold thiosulfate complex from pregnant leachate solution proved to be challenging. Thus, development of appropriate methods to effectively recover gold thiosulfate complex are still unavailable [3]. Although there are several papers on gold leaching from wastes, only few studies reported the recovery of Au from pregnant thiosulfate leaching solution. Literature data suggest that activated carbon adsorption, cementation, electrowinning and solvent extraction are likely inapplicable for the separation of gold from thiosulphate solutions, especially in case of the presence of competitive metal ions. Activated carbon presents low affinity for $[Au(S_2O_3)_2]^{3-}$ probably due to weak interaction between carbon active sites and $S_2O_3^{2-}$. The recovery of gold using activated carbon can be improved by the addition of cyanide, which is not environmentally friendly. Through cementation process, gold can be precipitated, yet the recycling solution is difficult. The main disadvantages of electrowinning process for gold recovery are the high energy consumption and the low efficiency. Solvent extraction is a time-consuming process and expensive to achieve a complete solid-liquid separation [4]. Compared to other separation techniques, like electrolysis, solvent extraction and membrane separation, adsorption using ion exchange resins presents several advantages, like fast adsorption, high loading capacity, simultaneous elution and regeneration as well as operation at ambient temperature [4,5]. Moreover, it generates fewer toxic by-products and the adsorbent can be regenerated and reused several times [2]. Although, few information related to resin regeneration is available [6].

The efficiency of gold recovery is dependent on physical and chemical properties of the adsorbent and is influenced by the sorption conditions, such as pH of the solution, contact time, the quantity and initial gold concentration. Weak and strong base anion exchange resins are presently used in gold recovery [5]. In general, the pH of ammoniacal thiosulfate solution used for gold leaching is in the range of 9-11, thus at this pH both the thiosulfate and copper ammonia complexes formed during gold leaching are simultaneously stabilized [4]. Consequently, the weak-base resins are not adequate to recover Au from ammoniacal thiosulfate solution since their ion-exchange ability is damaged at a pH higher than 8. The strong base anion exchange

resins are more resistant to the competing anions and aurothiosulfate complex can be efficiently removed at low concentrations. Nonetheless, these resins have a poor selectivity, $[Cu(S_2O_3)_3]^{5-}$ will strongly compete with $[Au(S_2O_3)_2]^{3-}$ for the active sites on resin surface [4]. The elution of gold and copper from the adsorbent is a two-stage process: in the first stage, Cu is selectively eluted by a solution containing oxygenated ammonia-ammonium sulfate or ammonium thiosulfate and in the second stage, Au is effectively eluted by thiocyanate, polythionates, perchlorate or nitrate containing solutions or by mixtures of thiourea and sulfuric acid or sulfite and chloride [4].

Taguchi method is a simple and effective experimental design technique used for optimizing process parameters [7]. The optimum experimental conditions are determined using an orthogonal array which aims to maximize the experimental results using a small number of experiments. Consequently, the signal-to-noise (S/N) ratio is used to analyze the experimental results and to determine the optimal levels of each parameter [8,9]. S/N represents the ratio of desirable results (signal) to undesirable results (noise) obtained [10]. Thus, using S/N ratio, the control factors that reduce the variability of the Au removal by minimizing the effects of uncontrollable factors can be identified [11]. Through Taguchi method, the effects of multiple parameters and their interaction can be investigated in a time- and cost-effective manner [12].

The objective of the present study was to maximize the total amount of Au as $[Au(S_2O_3)_2]^{3-}$ adsorbed on METALICAPT® MFH11 fiber from a synthetic aqueous solution containing ammonium thiosulfate (0.1 M) and 2 mg/L Cu complexed as $[Cu(S_2O_3)_3]^{5-}$ by optimizing the selected process parameters using Taguchi method. The METALICAPT® MFH11 fiber is a newly developed anion exchange fiber containing ammonium ($-NR_3^+$) and tertiary amine ($-NR_2$) functional groups that has not been previously studied for Au sorption from ammoniacal thiosulphate solution. The research was carried out in four steps. In the first step, three parameters, namely Au initial concentration, fiber quantity and temperature were selected to be optimized in batch experiments due to their significant effect on aurothiosulfate complex sorption. An appropriate orthogonal array was chosen based on the considered parameters and their levels. In the second step, the experiments were performed using the selected 9 experimental trials. For each experiment conducted, the total amount of Au as $[Au(S_2O_3)_2]^{3-}$ sorbed on METALICAPT® MFH11 fiber was calculated. In the third step, the obtained results were processed with larger-the-better equation (S/N output) to determine the optimum conditions for the considered process and to maximize the response in terms of the total amount of $[Au(S_2O_3)_2]^{3-}$ sorbed on METALICAPT® MFH11 fiber. Finally, in the fourth step, confirmation experiments were carried out to verify the experimental conclusions.

RESULTS AND DISCUSSION

Taguchi Experimental Design

The experimental results express in terms of sorption capacity and removal efficiency obtained based on Taguchi's orthogonal array are presented in Table 1. Based on the obtained results, it can be seen that as initial Au concentration increased the q_e values increased and the removal efficiency decreased. The initial Au concentration offers the necessary driving force to overcome the mass transfer resistance of adsorbate [13]. The q_e decreases as the fiber quantity increases because more sorption sites are available. As the temperature increases, q_e decreased suggesting an exothermic process for Au sorption [12]. The Minitab software was used to calculated the equivalent S/N ratio of the experiments based on the obtained q_e values using larger-the-better equation to maximize the response [11].

Table 1. The experimental results obtained based on Taguchi's orthogonal array and the corresponding S/N ratio for each experiment

Experiment number	Experimental result		S/N ratio
	q_e (mg/g)	Au removal (%)	
1	8.1	40.8	18.12
2	2.9	73.3	9.24
3	1.6	88.0	3.98
4	16.8	37.6	23.96
5	6.5	73.0	16.12
6	3.5	87.2	10.83
7	19.9	31.8	25.92
8	8.9	71.5	19.02
9	4.9	85.7	13.75

The S/N ratio response (the average value of S/N ratio of each parameter at levels 1, 2 and 3) for Au sorption onto METALICAPT® MFH11 fiber is given in Figure 1. The greatest S/N ratio represents the optimal level of the considered parameter. Based on the difference between the highest S/N and lowest S/N for each parameter, the delta value can be calculated and compared. The following series was depicted based on the obtained delta values: fiber quantity (13.15) > Au concentration (9.12) > temperature (0.65). Thus, fiber quantity has a strong influence on Au sorption, followed by concentration and temperature has a low influence on Au sorption onto METALICAPT® MFH11 fiber. Consequently, concentration has the highest

effect on the Au sorption at level 3 and fiber quantity and temperature had the highest effect at level 1. The optimum conditions for Au sorption were found to be initial Au concentration of 30 mg/L, fiber quantity of 0.05 g and temperature of 20°C.

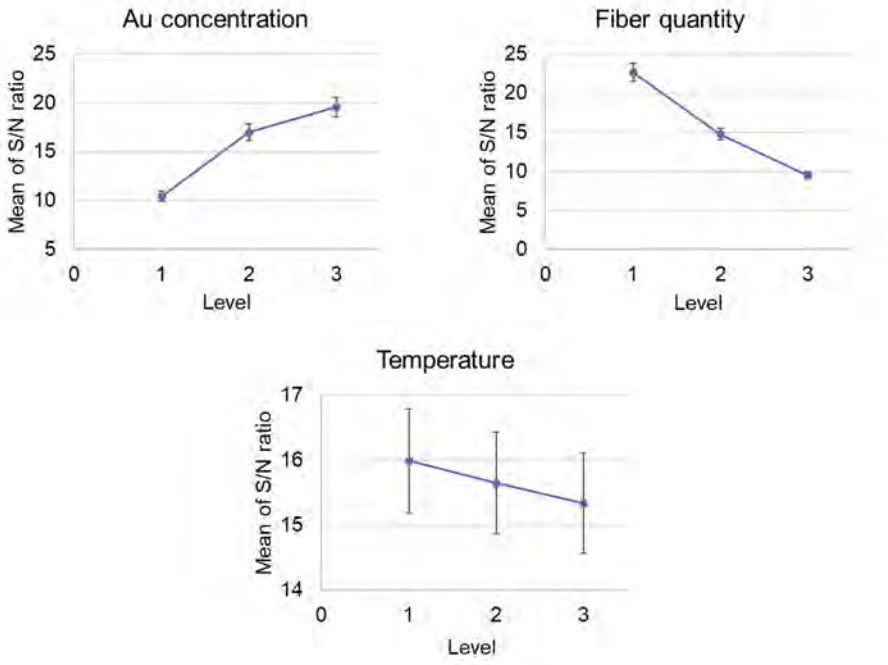

Figure 1. The effects of process parameters on Au sorption onto METALICAPT® MFH11 fiber

Analysis of variance (ANOVA)

ANOVA is one of the statistical models used to distinguish the performance of parameters and their interactions. ANOVA analysis was used to identify the significant parameters for Au sorption onto METALICAPT® MFH11 fiber by the sum of the squared deviations from the total mean of S/N ratio [11].

The degrees of freedom (*DF*), sum of squares (*SS*), mean square (*MS*), distribution of the ratio (*F)* and *p* value are shown in Table 2. Further, the percent contribution (*PC*) of each parameter [14] was calculated and the results are given in Table 2.

Table 2. Analysis of Variance for S/N ratio

Parameter	*DF*	*SS*	*MS*	*F*	*p*	*PC*
Concentration	2	132.48	66.24	197.95	0.005	33.42
Fiber quantity	2	262.65	131.32	392.46	0.003	66.25
Temperature	2	0.64	0.32	0.95	0.512	0.16
Residual Error	2	0.67	0.34			0.17
Total	8	396.43				

The *p* value for concentration and fiber quantity is very small which means that there is significant evidence against null hypothesis (H_0). The most significant parameters ($p<0.01$) for Au sorption are initial Au concentration and fiber quantity (Table 2). The *p* value for temperature was 0.512, thus this parameter can be ignored as it is insignificant for Au sorption. Fiber quantity (PC% = 66.25) was the most important parameter on Au sorption, followed by Au initial concentration (PC% = 33.42). The mean response for larger-the-better used to predict the optimum q_e value is given in Table 3.

Table 3. The mean response for larger-the-better (average q_e values)

Level	Concentration	Fiber quantity	Temperature
1	3.51	**14.24**	**6.17**
2	8.93	6.10	8.19
3	**11.22**	3.32	9.30
Delta	7.71	10.92	3.14
Rank	2	1	3

Three experiments were carried out to validate the obtained results using the levels of the optimal process parameters for Au sorption onto anion exchange fiber. The results obtained are presented in Table 4. As it can be seen in Table 4 the predicted optimal q_e value and the average of confirmation experiment was 16.7 mg Au/g fiber and 16.8 mg/g, respectively. As it can be observed the obtained values are very close. Thus, the results predicted by Taguchi method were validated by the confirmation experiments. Further, the fiber can be burned to obtain Au. Also, the purity of the Au depends on the concentration of other concurrent anions present in the solution subjected to treatment.

Table 4. Predicted optimal q_e values and the results of confirmation experiment

Adsorbent	Predicted optimal q_e value	Mean predicted	Average of confirmation experiment (q_e)
	mg/g	mg/g	mg/g
METALICAPT® MFH11	16.7	18.0	16.8

CONCLUSIONS

In the current study, the Taguchi method was used to investigate the effects of Au initial concentration, fiber quantity and temperature on Au sorption from ammoniacal thiosulfate solutions containing 2 mg/L Cu onto an anion exchange fiber. The experimental results were analyzed using the signal to noise ratio and ANOVA to identify the optimum and to most significant parameters. The most prominent parameter affecting the Au sorption was fiber quantity, followed by initial concentration. The data suggested that temperature was insignificant for Au sorption. The predicted optimal value was confirmed through the confirmation experiments performed using the optimal conditions identified by Taguchi method.

EXPERIMENTAL SECTION

Description and Characteristics of the Sorbent

METALICAPT® MFH11, an anion exchange fiber supplied by AJELIS SAS was used for Au sorption. Its characteristics are given in Table 5.

Table 5. Characteristics of the METALICAPT® MFH11 fiber

Ionic form	Chloride (Cl^-)
Functional group	Ammonium ($-NR_3^+$), Tertiary amine ($-NR_2$)
Total exchange capacity (eq /L)	1.25-2.5 ($-NR_3^+$), 1-1.5 ($-NR_2$),
Maximum operating temperature (°C)	90
Density (kg/dm^3)	~0.2-0.3
Appearance	Staple
Regenerant	1-4%NaOH or Na_2CO_3

Reagents and solutions

Analytical grade reagents, such as copper (II) sulfate pentahydrate ($CuSO_4 \cdot 5H_2O$), ammonium thiosulfate ($(NH_4)_2S_2O_3$) and sodium hydroxide (NaOH) were used for the preparation of the solutions. All used chemicals were of analytical purity and purchased from Merck (Darmstadt, Germany). Au as $AuCl_4^-$ was introduced in 0.1 M ammoniacal thiosulfate solutions, which was reduced to $Au(S_2O_3)_2^{3-}$. The pH of the solution was adjusted to 9.3 with NaOH, and then Cu (2 mg/L) was added to simulate the effluent obtained after leaching of gold from ores.

Taguchi experimental design

Three parameters with three levels each (Table 6) were taken into consideration to identify the optimum conditions for Au sorption using METALICAPT® MFH11 fiber.

Table 6. Selected parameters and their levels used in the Taguchi experimental design

Symbol	Parameters	Units	Levels		
			1	2	3
A	Au initial concentration	mg/L	10	20	30
B	Fiber quantity	g	0.05	0.25	0.55
C	Temperature	°C	20	25	30

Based on the considered parameters and their levels, the Minitab software generated the L_9 orthogonal array (Table 7).

Table 7. Design of experiments using Taguchi orthogonal array

Experiment number	Experiment Design		
	Au **concentration (mg/L)**	**Fiber quantity (g)**	**Temperature (°C)**
1	10	0.05	20
2	10	0.25	25
3	10	0.55	30
4	20	0.05	25
5	20	0.25	30
6	20	0.55	20
7	30	0.05	30
8	30	0.25	20
9	30	0.55	25

Sorption and confirmation experiments

The optimization of gold sorption on METALICAPT® MFH11 fiber using Taguchi experimental design is detailed in Figure 2.

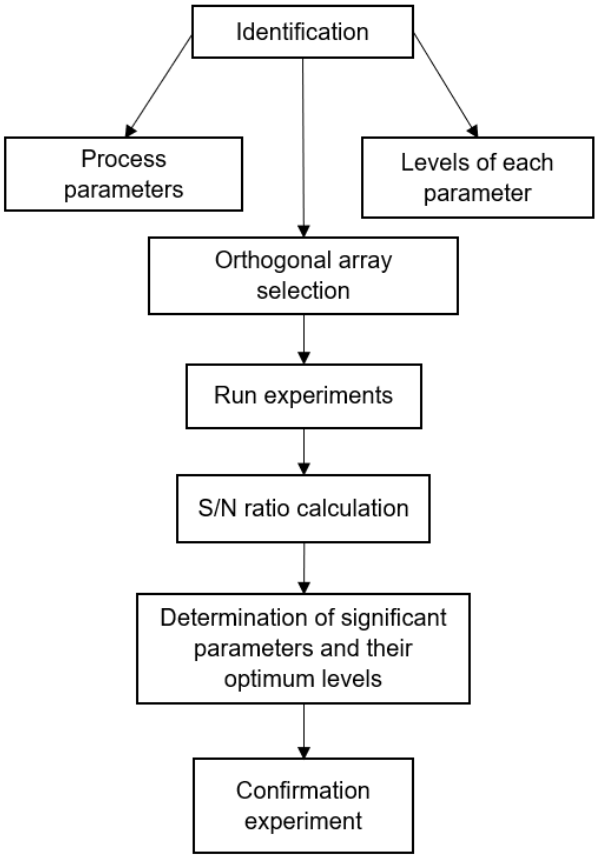

Figure 2. Optimization of gold sorption on METALICAPT® MFH11 fiber using Taguchi experimental design

The sorption experiments were performed in triplicate according to Table 7 for 240 min at a stirring rate of 500 rpm. Preliminary tests showed that equilibrium was reached up to 240 min. The Au concentration was analyzed using an Optima 5300 DV Perkin-Elmer inductively coupled plasma optical emission spectrometer. At the end of each experiment, the sorption capacity of the fiber (q_e) and removal efficiency (percent of sorption, E) were calculated [15] according to Equation 1 and 2, respectively.

$$q_e(mg/g) = \frac{C_o - C_e}{m} \cdot \frac{V}{1000} \quad (1)$$

$$E(\%) = \frac{C_o - C_e}{C_o} \cdot 100 \quad (2)$$

where, C_o, C_e are the initial and equilibrium Au concentrations (mg/L); V is the volume of Au solution (mL) and m is the mass of the fiber (g).

Based on the obtained q_e values, the S/N ratio (using the larger-the-better equation) was calculated to analyze the combined effects of control and noise factors [14]. The larger-the-better equation to maximize the response is given below [11,14].

$$S/N = -10\ log\left[\left(\sum \frac{1}{Y^2}\right)/n\right] \quad (3)$$

where, Y is the value of the response and n is the total number of repetitions in a trial [14].

Further, the ANOVA analysis was conducted to identify the significant parameters of the sorption process. Three confirmation experiment were conducted using the optimal levels of the process parameters. The average value was compared with the predicted value. After determination of the optimum conditions, the mean (μ) was estimated from the significant parameters identified by ANOVA analysis [12,16].

$$\mu = \bar{U} + (A_3 - \bar{U}) + (B_1 - \bar{U}) \quad (4)$$

where, $\bar{U}$ is the overall mean of the response (mean of q_e value of the experiments performed according to L_9) and A_3, B_1 represent average values of response at their optimum levels.

The predicted optimum value of q_e was calculated as follows:

$$\mu_{fiber} = \bar{U}_{fiber} + (A_3 - \bar{U}_{fiber}) + (B_1 - \bar{U}_{fiber}) + (C_1 - \bar{U}_{fiber}) \quad (5)$$

where, μ_{fiber} is the predicted optimum value of q_e for the anion exchange *fiber*, $\bar{U}_{fiber}$ is the overall mean of q_e, and A_3, B_1, C_1, are the average q_e values at their optimum levels [12,16].

ACKNOWLEDGMENTS

This research was funded by a grant of the Romanian National Authority for Scientific Research and Innovation, CCCDI-UEFISCDI, project number 52/2018, COFUND-ERANET-ERAMIN-MINTECO-2, within PNCDI III.

REFERENCES

1. F. Liu; S. Hua; L. Zhou; B. Hu; *Int. J. Biol. Macromol*., **2021**, *173*, 457-466.
2. Z. Chang; F. Li; X. Qi; B. Jiang; J. Kou; C. Sun; *J. Hazard. Mater*., **2020**, *391*, 122175.
3. F.R. Escobar-Ledesma; C.F. Aragón-Tobar; P.J. Espinoza-Montero; E. de la Torre-Chauvin. *Molecules*, **2020**, *25*(12), 2902.
4. B. Xu; W. Kong; Q. Li; Y. Yang; T. Jiang; X. Liu; *Metals*, **2017**, *7*, 222.
5. A. Mohebbi; A. Abolghasemi Mahani; A. Izadi Ion Exchange Resin Technology in Recovery of Precious and Noble Metals. In *Applications of Ion Exchange Materials in Chemical and Food Industries*; M. Inamuddin, T. A. Rangreez, A. M. Asiri Eds. Springer, **2019**, Chapter, pp. 193-258
6. A. Azizitorghabeh; J. Wang; J.A. Ramsay; A. Ghahreman; *Miner. Eng.,* **2021**, *160*, 106689.
7. Y. Javadi; S. Sadeghi; M.A. Najafabadi; *Mater. Des.,* **2014**, *55*, 27-34.
8. G. Zolfaghari; A. Esmaili-Sari; M. Anbia; H. Younesi; S. Amirmahmoodi; A. Ghafari-Nazari; *J. Hazard. Mater*., **2011**, *192*, 1046-1055.
9. B.G. Park; S. Gyeong Kim; J. Soo Ko; *Int. J. Prec. Eng. Man.*, **2019**, *20*, 437-442.
10. S.H. EL-Moslamy; M.F. Elkady; A.H. Rezk; Y. R. Abdel-Fattah; *Sci. Rep.*, **2017**, *7*, 45297.
11. S. Rizal; C.K. Abdullah; N.G. Olaiya; N.A. Sri Aprilia; I. Zein; I. Surya; H.P.S. Abdul Khalil; *Applied Sciences*, **2020**, 10.
12. V.C. Srivastava; I.D. Mall; I.M. Mishra; *Industrial & Engineering Chemistry Research*, **2007**, *46*, 5697-5706.
13. L. Liu, Y. Wan, Y. Xie, R. Zhai, B. Zhang, Jindun Liu, *Chem. Eng. J.*, **2012**, *187*, 210-216l.
14. Ben-Gal; *IEEE Transactions on Reliability*, **2005**, *54*, 381-388.
15. K. Bellir; M.B. Lehocine; A.-H. Meniai; *Desalin. Water Treat*., **2013**, *51*, 5035-5048.
16. V.C. Srivastava; I.D. Mall; I.M. Mishra; *Chem. Eng. J*., **2008**, *140*, 136-144.

STUDIA UBB CHEMIA, LXVI, 2, 2021 (p. 163-170)
(RECOMMENDED CITATION)
DOI:10.24193/subbchem.2021.2.14

GC-MS ANALYSIS OF SOME PLASTIC COMPONENTS FROM 1997-2003 COMPUTER MAIN BOARDS

DALMA KOVACS[a], DORINA SIMEDRU[a], MELINDA KOVACS[a,*]

ABSTRACT. Recycling is one of most important steps toward circular economy. Since the quantity of waste of electrical and electronic equipment (WEEE) is increasing rapidly, it became crucial to know its composition to find adequate recycling solutions. Following this trend, the present study aims to find the major components of plastic components from 1997-2003 computer main boards. A new GC-MS method was developed and used to quantify the main volatile organic compounds of polystyrene PS (benzene, ethylbenzene), acrylonitrile butadiene styrene ABS (acetophenone, styrene, butyldiglycol) and polypropylene PP (n-Tetradecane, n-Hexadecane and n-Heptadecane). The extraction method was carried out using a saline water solution (10 % saline content; w:v) to extract the volatile compounds on SPME fibers under continuous agitation at 55 °C. The analytical method used a complex temperature program and a HP-5ms fused-silica capillary column of 30 m length × 0.25 mm I.D. × 0.25 µm film thickness (Restek, USA) to achieve separation of the compounds. The investigation of the major components of plastic components from 1997-2003 computer main boards using the developed method showed a decrease of ABS and PP major components from 1997 to 2003 and an increase of the major components from PS.

Keywords: *WEEE, polystyrene, acrylonitrile butadiene styrene, polypropylene, GC-MS*

INTRODUCTION

According to European Commission (2019), waste of electrical and electronic equipment (WEEE) is increasing rapidly in EU, with 9 million tons generated in 2005, and expected to grow to more than 12 million tons by 2020 [1]. It is considered that approximately 20% of WEEE consist in different

[a] *INCDO-INOE 2000, Subsidiary Research Institute for Analytical Instrumentation Cluj-Napoca, 67 Donath, 400293, Cluj-Napoca, Romania*
** Corresponding author: melinda.kovacs@icia.ro*

type of plastics [2]. Plastics are the best choice in electrical and electronic equipment (EEE) because they reduce the cost of the product but in the same time, they make a significant improvement of EEE properties. They are used for insulation, noise reduction, sealing, housing, interior structural parts, functional parts, interior electronic components among other uses [3]. From almost 300 different types of plastics that can be found in WEEE, acrylonitrile butadiene styrene (ABS, 30–35%), high impact polystyrene (HIPS, 20–25%) and polypropylene (20–30%) are the most used [4, 5]. These plastics can be recycled using expensive and longtime processes: they are chopped, washed and sorted by type [6].

Acrylonitrile butadiene styrene (ABS) is one of the major components of plastic WEEE [6]. It is a triblock copolymer with attractive mechanical properties and convenient processing conditions [7-9].

Polypropylene is considered to be the lightest and most versatile polymers due to its capacity to undergo various manufactured processes. It is one of the most common types of microplastic found in the marine environment [10].

Polystyrene is a transparent, non-biodegradable polymer which is considered to be relatively chemically inert. It is waterproof and resistant to breakdown by many acids and bases [11].

Due to their intense use and their chemical nature, it is important to know their quantity in order to find adequate techniques for their recycling.

Several analytical methods are mostly used to investigated the presence of polymers in WEEE: Fourier transform infrared (FTIR) [12-14], Raman spectroscopy [15-17] and pyrolysis GC-MS [18, 19]. Even if these methods were proved to be useful in characterization of polymers more accurate methods for their determination are required since these polymers are considered to be environment micropollutants.

The purpose of this study is to develop an GC-MS method suitable for the determination of polymers from WEEE and to establish the chemical profile (the presence of polystyrene (PS), acrylonitrile butadiene styrene (ABS) and polypropylene (PP)) of plastic components from 1998-2003 computer main boards by quantifying the volatile organic compounds present in these polymers.

RESULTS AND DISCUSSION

Plastic components of 4 computer main boards produced between 1997-2003 were analyzed in order to obtain their plastic profile (the quantity of polystyrene (PS), acrylonitrile butadiene styrene (ABS) and polypropylene (PP)).

Figure 1 presents the total ion chromatogram of two samples after GC-MS analysis.

Several volatile organic compounds characteristic to each of these polymers were determined by GC-MS. The results expressed as percentage concentration from the total HS-SPME extracted compounds are presented in Table 1. Since ethylbenzene is a main component of both polystyrene (PS) and acrylonitrile butadiene styrene (ABS) its provenience cannot be precisely established.

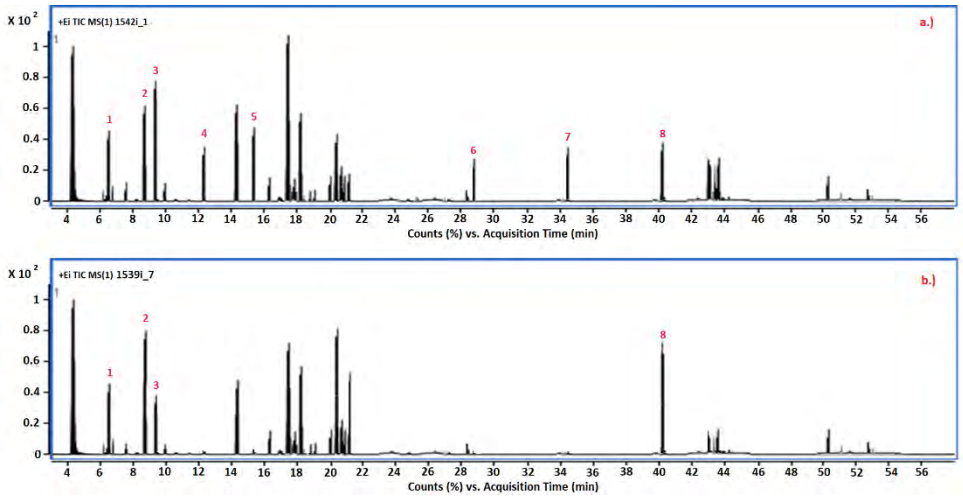

Figure 1. Total ion chromatogram of sample 1542i_1 (a.) and 1539i_7 (b.) after GC-MS analysis. In chromatograms: 1 - benzene, 2 – ethylbenzene, 3 – acetophenone, 4 – styrene, 5 – butyldiglycol, 6 – n-tetradecane, 7 – n-hexadecane, 8 – n-heptadecane.

Analyzing the results obtained for each plastic component the following remarks can be made:

- CPU sockets of 1997 and 2003 computer main boards have similar composition, ABS as main component, followed by PP and PS. Even if PS have closed values for both CPU sockets, a significant decrease of ABS and PS can be observed from 1997 to 2003.
- IDE connectors of 1997 and 1998 computer main boards have similar composition, ABS as main component, followed by PP and PS. Even if ABS have closed values for both CPU sockets, a significant decrease of PP and PS can be observed from 1997 to 1998.

- PCI Connector of 1997 computer main board – the main component is ABS followed by PS and PP.
- Floppy Connector of 1998 computer main board – PS and ABS are the main components having very closed values. Since the value of ethylbenzene, component of both PS and ABS cannot be correctly splinted between the two polymers, it is safer to suppose that ABS is the main component.
- AGP Connector of 1998 and 2003 computer main boards have different composition. The one from 1998 has PP as main component, followed by PS and PP while the one from 2003 has PS as main component, followed by ABS and PP. A significantly decrease of PP from 1998 to 2003 can be observed.
- Power Connector of 1998 computer main board – the main component is ABS followed by PS and PP which have very closed values.
- Socle RAM of 2003 computer main board – the main component is PS followed by ABS and PP.

The results obtained shows that for 1997-1998 computer main boards, in almost all cases, the main component is ABS (namely acetophenone) while for 2003 computer main board the main component is PS (namely benzene) in almost all case. Also, analyzing the results, a decrease of PP usage can be observed.

In this case, the GC-MS method developed proved to be a useful tool to determine the main components of major polymers from WEEE. It is quicker, more accurate and eco-friendly then other methods used previously.

CONCLUSIONS

The GC-MS method developed for characterization of WEEE major polymers proved to be quick, accurate and suitable for the declared purpose. The plastic components of 4 computer main board from 1997-2003 were analyzed, using the new analytical method, in order to establish the main polymer component. Three types of plastic polymers were approximately measured: polystyrene (PS), acrylonitrile butadiene styrene (ABS) and polypropylene (PP). Their percentage in the samples were quantified using the major volatile organic compounds from their composition. The results suggest that for 1997-1998 computer main boards the main component is ABS while for 2003 computer main board the main component is PS. A significantly decrease of PP usage can be observed for 2003 computer main board plastic components comparing with the values obtained for 1997-1998 computer main boards plastic components.

EXPERIMENTAL SECTION

Materials

The extraction was carried out using anhydrous NaCl with ≥99.5% purity purchased from Sigma Aldrich. HiQ Helium 6.0 used as carrier gas was purchased from Linde. Ultrapure water was obtained using a type I ultrapure water system Flex3 Elga Veolia.

Instrumentation

The measurements were carried out using 7890 GC-MS from Agilent. Separation of volatile organic compounds was performed using a HP-5ms fused-silica capillary column of 30 m length × 0.25 mm I.D. × 0.25 µm film thickness (Restek, USA) after their extraction on 50/30 µm Divinylbenzene-Carboxen/Poly(dimethylsiloxane) (DVB-CAR/PDMS) SPME fibre (Supelco).

Table 1. Plastic composition of 1997-2003 computer main boards plastic components

No	Volatile organic compounds	M.U.	Sample identification (code/description)									
			1542i_1 CPU Socket	1542i_2 Ide Connector	1542i_3 PCI Connector	1539i_10 Floppy Connector	1539i_7 AGP Connector	1540i_8 IDE Connector	1540i_9 Power Connector	1541i_4 CPU Socket	1541i_5 Socle RAM	1541i_6 AGP Connector
			Year of fabrication									
			1997			1998		1998		2003		
1.	Benzene	%	3.2	5.1	3.3	12.1	4.2	7.8	7.9	5.3	19.2	15.4
2.	Ethylbenzene	%	2.5	12.2	3.8	5.7	13.7	3.8	3.2	0.8	1.1	0.8
Polystyrene (PS)		%	**5.7**	**17.3**	**7.1**	**17.8**	**17.9**	**11.6**	**11.1**	**6.1**	**20.3**	**16.2**
3.	Acetophenone	%	21.8	17.2	15.2	11.5	5.1	14.2	25.9	12.8	3.4	6.7
4.	Styrene	%	2.9	2.1	1.9	2.8	-	0.7	0.9	1.8	6.2	0.9
5.	Butyldiglycol	%	5.7	2.6	1.8	3.4	-	7.5	7.1	6.7	-	0.8
Acrylonitrile butadiene styrene (ABS)		%	**30.4**	**21.9**	**18.9**	**17.7**	**5.1**	**22.4**	**33.9**	**21.3**	**9.6**	**8.4**
6.	n-Tetradecane	%	2.8	2.2	0.8	0.8	-	1.4	-	1.7	-	-
7.	n-Hexadecane	%	4.7	6.2	-	1.2	-	2.1	0.6	-	-	-
8.	n-Heptadecane	%	3.1	8.6	1.5	5.2	19.2	7.2	10.4	2.9	3.5	7.9
Polypropylene (PP)		%	**10.6**	**17.0**	**2.3**	**7.2**	**19.2**	**10.7**	**11.0**	**4.6**	**3.5**	**7.9**

Extraction and analytical methods

***a. Extraction*.** In order to extract the volatile compounds, plastic samples were chopped (Figure 2). Approximately 2.5 g of sample was placed in headspace vials and 5 mL of saline water solution (10 % saline content; w:v) was added before closing the headspace vials with Teflon/silicone disk and aluminum crimp cap. The SPME fibers were pre-conditioned according to the supplier's instructions in the GC injection port at 270 °C.

The vial and the SPME fiber were then placed into a heating block set at 55 °C and kept at this temperature for 30 min under continuous agitation. Volatiles compounds desorption from SPME fiber was allowed for 7 min in the GC injection port.

Figure 2. Chopped plastic materials (left) and Headspace extraction of volatile compounds from plastics (right)

b. GC/MS analysis. A GC/MS analytical method was developed in order to identify the most important compounds of polystyrene (PS), acrylonitrile butadiene styrene (ABS) and polypropylene (PP): Benzene, Ethylbenzene, Styrene, Acetophenone, Butyldiglycol, n-Tetradecane, n-Hexadecane and n-Heptadecane. Helium was used as carrier gas with a constant flow of 1 mL/min. The split/splitless injector was used in splitless mode and its temperature was maintained at 270 °C. The column oven temperature program for separation of volatile compounds was 40 °C (5 min) to 110 °C (5 min) at 10 °C/min and followed by an increase at 250 °C (5 min) at 10 °C/min. The GC/MS interface was set at 270 °C and the ion source was held at 280 °C. Mass spectra were acquired under electron ionization mode (EI) at 70 eV and recorded in the range m/z 50-650 at one cycle per second. The chromatographic peaks were identified either by direct analysis of the mass spectrum or/and comparison with a reference mass spectral library (US National Institute of Standards and Technology, NIST 02 version 2.0a, 2002). The analytical parameters of the calibration curves are presented in Table 2. For each compounds single component analytical standards were used (Sigma-Aldrich, Darmstadt, Germany). Each concentration was prepared in 5 mL of saline water solution and analyzed after SPME fiber desorption in the same condition as samples.

Table 2. Calibration curves parameters of investigated compounds

Compound	Calibration curve	Range (ug/L)	Correlation coefficient	LOD	LOQ
Benzene	Y=2376.3x+617.97	0.5 - 25	0.9956	0.118	0.354
Ethylbenzene	Y=3321.8x-438.47	0.5 - 25	0.9995	0.215	0.645
Styrene	Y=1831x+2575	0.5 - 25	0.9957	0.145	0.435
Acetophenone	Y=3840.3x-1718	0.5 - 10	0.9977	0.215	0.645
Butyldiglycol	Y=3946.4x+1839.5	0.5 - 10	0.9986	0.321	0.963
n-Tetradecane	Y=741.39x-474.73	0.5 - 50	0.9961	0.115	0.345
n-Hexadecane	Y=1146.7x+285.24	0.5 - 50	0.9988	0.258	0.774
n-Heptadecane	Y=3038x-94.814	0.5 - 50	0.9986	0.082	0.246

ACKNOWLEDGMENTS

The work has been funded by the PNCDI III - Program 1 Complex projects completed in consortia CDI – 2017, TRADE-IT, PN-III-P1-1.2-PCCDI-2017-0652, contract no. 84PCCDI/2018.

REFERENCES

1. https://ec.europa.eu/environment/waste/weee/index_en.htm
2. P.A. Wäger; M. Schluep; E. Müller; R. Gloor; *Environ. Sci. Technol.*, **2012**, *46 (2)*, 628–635.
3. I.C. Nnorom; O. Osibanjo; *Resour. Conserv. Recycl.*, **2008**, *52*, 1362–1372.
4. L.E. Peisino; M. Gómeza; J. Kreikera; R. Gagginoa; M. Angelelli; *Sustain. Chem. Pharm.*, **2019**, *12*, 1-5.
5. C. Guo; Q. Zou; J. Wang; H. Wang; S. Chen; Y. Zhong; *Waste Manag.*, **2018**, *82*,167–176.
6. Y.V. Vazquez; S.E. Barbosa; *Multidiscip. J. Waste Res. Resid.*, **2018**, *2*, 105-111.
7. G. Martinho; A. Pires; L. Saraiva; R. Ribeiro, R., *Waste Manag.*, **2012**, *32*, 1213–1217.
8. E. Maris; P. Botané; P. Wavrer; D. Froelich; *Miner. Eng.*, **2015**, *76*, 28–37.
9. J. Wang; Y. Li, J. Song; M. He; J. Song; K. Xia, K., *Polym. Degrad. Stab.*, **2015**, *112*, 167-174.
10. C.B. Crawford; B. Quinn; Physiochemical properties and degradation, In Microplastic Pollutants, Elsevier Inc., Amsterdam, Holland, **2017**, Chapter 4, pp. 57-100.
11. https://en.wikipedia.org/wiki/Polystyrene

12. F. Wagner, J. Peeters, J. De Keyzer, J. Duflou, W. Dewulf, *Proc. EcoDesign 2017 Intl. Sym.*, **2017**, 1-9.
13. J.C. Arnold, T.Watson, S. Alston, M. Carnie, C. Glover, *Polymer Testing*, **2010**, *29(4)*, 459-470.
14. H. Yan, H. W. Siesler, Identification performance of different types, *Appl. Spectrosc.,* **2018**, *72*, 1362–1370.
15. R. Naushad, M.H. Vijayam, A.M. Hassan, T.S. Rashid, S. Asha, *AIP Conf. Proc.*, **2020**, *2222(1)*, 1-6.
16. V. Allen, J.H. Kalivas, R.G. Rodriguez, *Appl. Spectrosc.*, **1999**, *53(6),* 672-681.
17. A. Tsuchida, H. Kawazumi, A. Kazuyoshi, T. Yasuo, *SENSORS, 2009 IEEE*, **2009**, pp. 1473-1476.
18. F. Puype, J. Samsonek, V. Vilímková, Š. Kopečková, A. Ratiborská, J. Knoop, M. Egelkraut-Holtus, M. Ortlieb, U. Oppermann, *Food Addit. Contam.: Part A*, **2017**, *34(10)*, 1767–1783.
19. W.J. Hall, P.T. Williams, *J. Anal. Appl. Pyrolysis*, **2007**, *79(1-2)*, 375-386.

STUDIA UBB CHEMIA, LXVI, 2, 2021 (p. 171-180)
(RECOMMENDED CITATION)
DOI:10.24193/subbchem.2021.2.15

REMOVAL OF RHODAMINE FROM AQUEOUS SOLUTIONS USING NATURAL ZEOLITE

LACRIMIOARA SENILA[a, 1], EMILIA NEAG[a, 1], DANIELA ALEXANDRA SCURTU[a], OANA CADAR[a], ANCA BECZE[a], CALIN HOREA TOMOIAG[b], MARIN SENILA[a]*

ABSTRACT. The aim of this study was to evaluate the adsorption of rhodamine B (RB) from synthetic water using natural zeolites from Romania. The adsorption capacity of zeolite for RB removal was improved by heat treatment at 200, 400 and 600 °C. The chemical and structural characterization of untreated and thermally treated zeolites was performed using advanced techniques such as X-ray diffraction (XRD), scanning electron microscopy (SEM) and Brunauer-Emmett-Teller (BET) analysis. The adsorption behavior of RB on activated zeolites was studied using Langmuir, Freundlich and Dubinin-Radushkevich isotherms. The thermally treated zeolite at 200°C gave the highest adsorption efficiency (97.9%) for RB adsorption from aqueous solutions. According to the obtained results, it can be concluded that thermally treated zeolite can be used as an effective adsorbent for the removal of RB from wastewater.

Keywords: *zeolites, rhodamine B, thermal activation*

INTRODUCTION

A large quantity of pollutants is discharged in the environment during the textile dying process. Among the chemical pollutants, dyes have carcinogenic and mutagenic effects and are difficult to remove from wastewater [1, 2]. The dye industry is very diverse and heterogenous and the chemical composition of wastewater is very complex due to the use of raw materials and technological processes [3]. Rhodamine B (RB) is used in many textile applications and

[a] *INCDO-INOE 2000, Research Institute for Analytical Instrumentation, Donath 67, 400293, Cluj-Napoca, Romania; Tel: +40-264-420590; Fax: +40-264-420667*
[b] *Tomas Prodimpex SRL,18 B-dul Eroilor Street, Cluj-Napoca, Romania*
[1] *Authors with equal contribution*
* *Corresponding author: marin.senila@icia.ro*

can cause ecotoxicological problems for human health. Consequently, its discharging into water can cause environmental problems. Therefore, it is imperative to effectively remove the RB dye from wastewater due to its polluting effect [4, 5].

Various methods, such as advanced oxidation, biodegradation, coagulation, sedimentation, membrane technology, ozonation and adsorption were applied for the removal of dyes from wastewater. Also, numerous adsorption materials, like active coal, carbon materials, minerals, polymers and zeolites were used for the adsorption of dye from wastewater [6, 7].

In recent years, activation methods, such as acid treatment, base treatment, etc. were investigated in order to improve the adsorption properties of zeolites.

Zeolites are crystalline hydrated aluminosilicates of alkali and alkaline earth cations, usually used for the adsorption of different pollutants (heavy metals, phenols, ammonium, organic pollutants, antibiotics, etc.) from wastewater. The most common mineral of zeolites is clinoptilolite. Clinoptilolite has the capacity to adsorb cations through ion exchange process due to the presence of negative charge of the three-dimensional framework created by silicon, aluminum and oxygen. The factors that affect the adsorption of dyes are Si:Al ratio, ionic potential, size of exchangeable cations, etc. [8, 9, 10].

Generally, natural zeolites are activated physically, chemically or by the combination of both processes in order to increase the adsorption capacity [11]. In the literature, the adsorption of RB into synthesized zeolite or chemically activated zeolites was reported [12, 13, 14].

This paper aimed to study the behavior of natural zeolites from Romania under thermal activation for RB adsorption from aqueous solutions. Also, the mechanism of the RB adsorption process was studied.

RESULTS AND DISCUSSION

Scanning electron microscopy (SEM) of untreated and thermally treated zeolites

The morphological structure and chemical composition of untreated and thermally treated zeolites at 200°C (TZ-200), 400°C (TZ-400) and 600°C (TZ-600) was investigated by using scanning electron microscopy-energy dispersive X-ray (SEM-EDX) analysis (Figure 1). The SEM images showed that the increasing temperature changed the zeolite structure. The morphology of natural zeolite (NZ) showed well-defined agglomerate particles and uniform dispersion, whereas the morphology of thermally treated zeolite presented a

lamellar structure, with the exception of TZ-600, when the alteration of zeolite structure was observed. This can be attributed to the dehydration process and the stress produced by the increase of temperature. According to the study of Cruciani C. [15], the heating treatment of zeolites led to some structural modifications of internal structure. Moreover, a direct correlation between the stability index and Si:Al ratio was established.

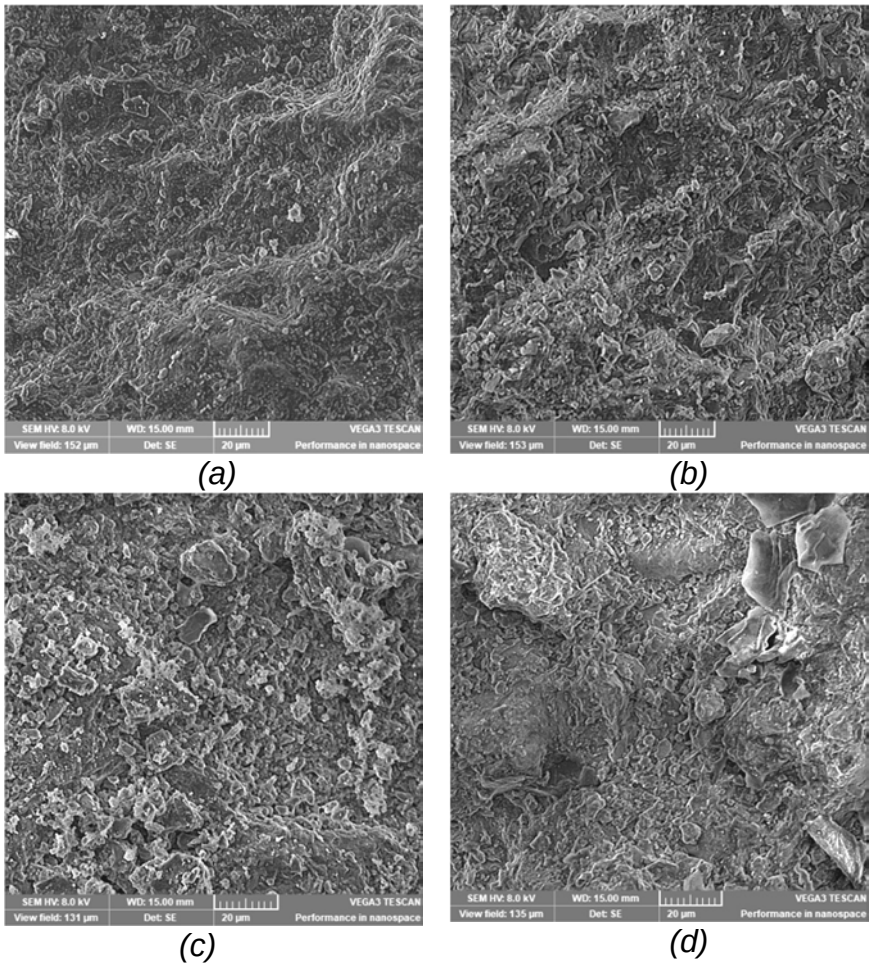

Figure 1. SEM images of zeolites: (a) NZ, (b) TZ-200, (c) TZ-400 and (d) TZ-600

Physical and chemical characteristics of studied zeolites

Table 1. Physical characteristics of the studied zeolites
(Data represents mean ± standard deviation, n = 3).

Element	NZ	TZ-200	TZ-400	TZ-600
pH (pH units)	8.33 ± 0.1	8.25 ± 0.1	8.00 ± 0.2	8.12 ± 0.1
Conductivity (μS/cm)	82.3 ± 0.8	200.4 ± 0.6	301.5 ± 0.5	290.1 ± 0.6
CEC (meq/g)	1.28 ± 0.6	1.18 ± 0.8	0.86 ± 0.7	0.53 ± 0.6
SA (m^2/g)	28.1 ± 0.1	54.2 ± 0.2	40.3 ± 0.1	36.2 ± 0.1

CEC- cation exchange capacity, SA – specific surface area

The physical properties of the studied zeolites are presented in Table 1. The increase of surface area leads to a better adsorption capacity. The Brunauer-Emmett-Teller (BET) surface increased from 28.1 to 54.2 m^2/g (for zeolite activated at 200°C), and slowly decreased for the treated zeolites at 400 and 600°C. This is explained by the modification of the zeolite structure at high temperature, leading to the loss of dyes adsorption sites.

Table 2. Content of oxides (%) from the studied zeolites

Element	NZ	TZ-200	TZ-400	TZ-600
K_2O	3.10	2.42	2.31	2.21
CaO	2.53	2.50	2.40	1.93
MgO	0.84	0.83	0.75	0.70
Fe_2O_3	1.07	1.21	1.18	1.29
SiO_2	65.4	64.3	72.8	77.2
Al_2O_3	13.4	13.8	11.5	10.8
Na_2O	0.67	0.75	0.72	0.68
LOI	12.9	7.30	8.34	5.19

LOI -loss of ignition

The composition of oxides (SiO_2, Al_2O_3, K_2O, CaO, Fe_2O_3, Na_2O and MgO) in the studied samples was presented in Table 2. The chemical analyses indicate low contents of Na_2O, MgO, K_2O and Fe_2O_3. The thermal treatment led to changes in the mineral compositions of zeolites. The Al_2O_3 content gradually decreased with increasing the activation temperature. The results showed that the dealumination process occurred at high temperature.

Adsorption performance of zeolites for RB removal

The removal of RB from the aqueous solution has been investigated using thermally treated clinoptilolite as adsorbent. The adsorption of RB into zeolites was investigated by varying the following parameters: initial dye concentration, dosage of adsorbent, thermal activation of zeolites.

Figure 2 illustrates the removal efficiency E(%) versus the initial concentration for experiments performed for RB adsorption. An increase in zeolite quantity led to an increase in the RB removal.

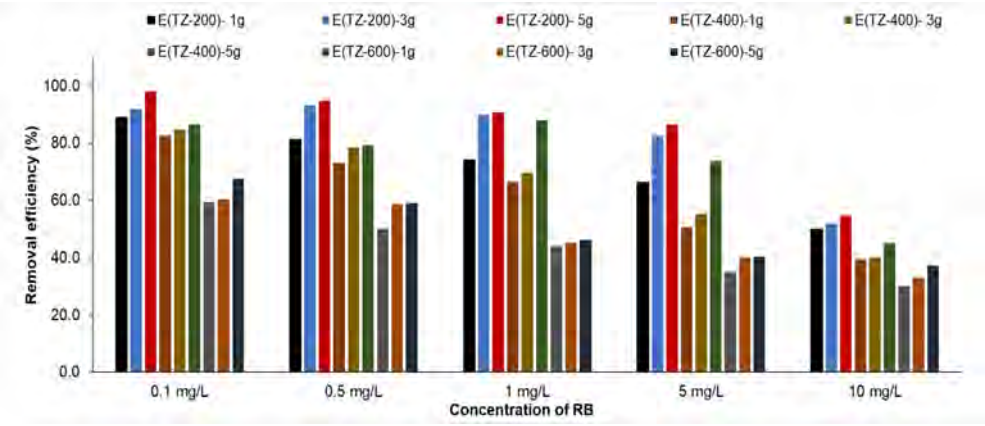

Figure 2. The removal efficiency of RB under different experimental conditions

The temperature used for the activation of zeolites influenced the removal efficiency. As depicted in Figure 2, the RB removal efficiency increased with the increase of zeolite quantity. The highest removal efficiency (98.0 %) was obtained using 5 g of zeolite activated at 200°C. The lowest removal efficiency (30.2%) was obtained using 1 g of zeolite activated at 600°C. The adsorption capacity decreased by increasing initial concentration of RB.

Figure 3 displays the XRD (X-ray diffraction) patterns of the thermally activated zeolite and the TZ zeolite adsorbed with different quantities of RB.

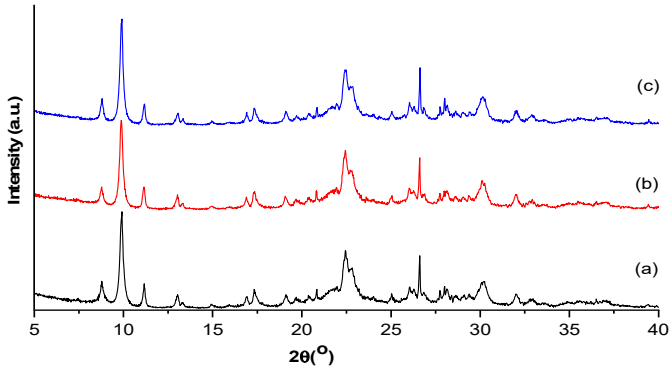

Figure 3. XRD diffraction patterns of zeolites: (a) TZ-200, (b) TZ-200 with 0.1 mg/l of RB, (c) TZ-200 with 10 mg/L of RB

The XRD analysis reveals the presence of clinoptilolite-Na as a major crystalline phase, accompanied by quartz, muscovite and albite. The XRD of the initial sample is similar to those of adsorbed zeolite with different amounts of RB, indicating that the adsorption of dyes did not influence their crystal structure. The obtained results proved that the crystalline structure of zeolites was stable. The following series was depicted based on the degree of crystallinity: 74.2% (TZ-200) > 72.4% (TZ-200, 0.1 mg/L) > 71.6% (TZ-200, 10 mg/L). The degree of crystallinity decreased with the increase of the RB initial concentration, due to the adsorption of RB molecules into the zeolite structure, suppressing the diffraction of the framework atoms of zeolite. The same remarks were observed by Ji et al. [16] and Ertan et al. [17] for the adsorption of methylene blue dye onto synthetized zeolite.

Adsorption isotherms

The Langmuir, Freundlich and Dubinin-Radushkevich isotherm constants and the determination coefficients (R^2) obtained from the slope and the intercept of the linear plots are presented in Table 3.

Table 3. Equilibrium isotherm constants obtained for RB adsorption on treated zeolites.

Isotherm model	Parameters			R^2
	Symbol	Unit of measurement	Value	
Langmuir	q_{max}	mg/g	0.03	0.9667
	K_L	L/mg	41	
Freundlich	s	-	2	0.9689
	K_F	$mg^{(1-1/n)} L^{1/n} /g^1$	0.07	
Dubinin-Radushkevich	β	mol^2/kJ^2	$3 \cdot 10^{-9}$	0.9750
	E_L	kJ/mol	13	

q_{max} is the maximum amount of RB adsorbed per gram of activated zeolite, K_L - Langmuir constant, s - Freundlich constant, K_F - Langmuir constants, β -Dubinin-Radushkevich constant, E_L - mean free energy.

The Freundlich isotherm suggested that zeolite has a heterogenous surface with nonuniform distribution of heat over the zeolite surface. The value s is 2, indicating a favorable adsorption of RB on zeolite.

The Dubinin-Radushkevich isotherm indicated a chemical chemisorption process of adsorption of RB onto zeolite due to the E_L value (< 16 kJ/ mol) according to Sari et al. [18].

CONCLUSIONS

The thermally activated zeolites at three temperatures (200, 400 and 600 °C) were used for RB adsorption. The obtained results indicated that the thermal treatment improved the adsorption performance of zeolites for RB removal, but the activation temperature should be lower than 400°C to prevent the modification of its crystalline structure. It was found that the Freundlich isotherm model described the mechanism of RB adsorption process. The Dubinin-Radushkevich isotherm indicated that RB adsorption onto zeolite was characterized by a chemisorption process. The present study demonstrated that natural zeolites could be used as a promising adsorbent material for the removal of dyes from aqueous solutions.

EXPERIMENTAL SECTION

Chemicals and materials

The NZ obtained from Chiloara quarry; Salaj County, Romania was crushed and sieved in order to obtain 1-3 mm, then washed several times with distilled water to remove the impurities.

All used chemicals were of analytical reagent grade and were purchased from Merck (Darmstadt, Germany). RB was purchased from Sigma Aldrich (Darmstadt, Germany). All solvents used were of HPLC grade. Deionized water used in dilutions was obtained by using a Milli-Q purification system (Millipore, Bedford, MA, USA).

Activation of zeolites

The NZ was activated at 200, 400 and 600°C for 4h obtaining the following samples: TZ-200, TZ-400 and TZ-600.

Physical and chemical characterization of zeolites

The determination of metals was carried-out by the digestion of zeolites with a mixture of 65% HNO_3 and 37% HCl (ratio v:v = 1:3) in closed polytetrafluoroethylene (PTFE) vessels, using a microwave digestion system (Speedwave Xpert, Berghof, Eningen, Germany), followed by inductively coupled plasma optical emission spectroscopy (ICP-OES) [18]. The oxides from zeolites were calculated according to Senila et al. [19] studies. The LOI was determined gravimetrically according to Cadar et al. [11].

The untreated and thermally treated zeolites were characterized by X-ray diffraction (D8 Advance diffractometer (Bruker, Karlsruhe, Germany), SEM analysis with EDX detector (SEM VEGAS 3 SBU, Tescan, Brno-Kohoutovice, Czech Republic), and BET specific area (Sorptomatic 1990 apparatus, Thermo Electron Corporation). The determination of CEC was determined according to Gualtieri et al. method (1999) [20] and the pH was determined using a Seven Excellence multiparameter (Mettler Toledo, Switzerland).

Adsorption experiments

A stock solution of 1 g/L RB was prepared by dissolving the salts in distilled water. The used concentrations (0.1, 0.5, 1, 5 and 10 mg/L) were prepared by diluting the concentrated stock solutions.

The experiments were performed in batch mode, by contacting different quantities (1-5 g) of NZ and thermally TZ at 200, 400 and 600 °C, having particle sizes of 1-3 mm with 100 mL containing RB initial concentrations in the range of 0.1-10 mg/L. All the adsorption experiments were performed at room temperature 20 ± 4°C for 240 min. The samples were centrifuged at 4000 rpm for 10 min. The RB concentrations were determined using Lambda 25 UV-VIS spectrophotometer (Perkin Elmer, Woodbridge, ON, USA) at 552 nm. The adsorption capacity q_e (mg/g) and the removal efficiency E (%) were calculated according to equations (1) and (2), respectively.

$$q_e = \frac{(C_i - C_e)}{m} \frac{V}{1000} \quad (1)$$

$$\%RB\ removal = (C_i - C_e) \times 100/C_i \quad (2)$$

where: C_i is the initial concentration, C_e is the concentration of RB after the adsorbtion of zeolites, m is the mass of dried zeolites, V is the solution volume (mL).

Equilibrium studies

The equilibrium adsorption data of RB on zeolite were analyzed by using the Langmuir, Freundlich and Dubini-Radushkevich isotherms. The linear forms of Langmuir and Freundlich isotherms are given in Egs. (3) and (4), respectively [21]:

$$\frac{1}{q_e} = \frac{1}{q_{max} K_L C_e} + \frac{1}{q_{max}} \quad (3)$$

$$logq_e = logK_F + \frac{1}{s} logC_e \quad (4)$$

where, K_F and s are isotherm constants which indicate the capacity and intensity of the adsorption [22, 23]. If the s value lies between $1 < s < 10$ it indicates a favorable adsorption process [21].

The Dubinin-Radushkevich isotherm suggests that the adsorption process follows a pore filling, having a multilayer character. Its equation is given as follows [24]:

$$lnq_e = lnq_{max} - \beta\varepsilon^2 \quad (5)$$

$$\varepsilon = RTln\left(1 + \frac{1}{C_e}\right) \quad (6)$$

$$E_L = \frac{1}{\sqrt{-2\beta}} \quad (7)$$

where, R is the gas constant (8.314 J mol/K) and T is the absolute temperature (K), ε is the Polanyi potential [24].

The E_L value indicates whether the adsorption process of RB on activated zeolite is chemical ($8 < E_L < 16$ kJ/mol), or physical ($E_L < 8$ kJ/mol) [24, 25, 26].

ACKNOWLEDGEMENTS

This research was funded by the Competitiveness Operational Programme of the Ministry of European Funds, contract no. 7/01.09.2016, code MY SMIS 105654.

REFERENCES

1. R. Pelalak; R. Soltani; Z. Keidari; R.E. Malekshah; M. Aallaei; A. Marjani; M. Rezakazemi; T.A. Kurniawan; S. Shirazian; *J. Mol. Liq.*, **2021**, *322*, 114812.
2. W. Li; B. Mu; Y. Yang; *Bioresour. Technol.*, **2019**, *277*, 157-170.
3. J. Bu; L. Yuan; N. Zhang; D. Liu; Y. Meng; X. Peng; *Diam. Relat. Mater.*, **2020**, *101*, 107604.
4. F. Motahari; M.R. Mozdianfard; M. Salavati-Niasari; *Process Saf. Environ.* **2015**, *93*, 282-292.
5. M. Rahmani; M. Kaykhaii; M. Sasani; *Spectrochim. Acta A: Mol. Biomol. Spectrosc.*, **2018**, *188*, 164-169.

6. S. Mishra; L. Cheng; A. Maiti; *J. Environ. Chem. Eng.*, **2021**, *9*, 104901.
7. M.F. Chowdhury; S. Kladaker; F. Sarker; A. Islam; M.T. Rahman; M.R. Awual; *J. Mol. Liq.*, **2020**, *318*, 114061.
8. M.A. Farghali; M. M. Abo-Aly; T.A. Salaheldin; *Inorg. Chem. Commun.*, **2021**, *126*, 108487.
9. H. Mittal; R. Badu; A.A. Dabbawala; S. Stephen; S.M. Alhassan; *Colloids Surf. A*, **2020**, *586*, 124161.
10. S. Sivalingam; S. Sen; *J. Taiwan Inst. Chem. Eng.*, **2019**, *96*, 305-314.
11. O. Cadar; M. Senila; M.A. Hoaghia; D.A. Scurtu; I. Miu; E.A. Levei; *Molecules*, **2020**, *25*(11), 2570.
12. F. Alakhras; E. Alhajri; R. Haounati; H. Ouachtak; A.A. Addi; T.A. Saleh; *Surf. Interfaces*, **2020**, *20*, 100611.
13. Z. Cheng; Y. Li; Z. Liu; *Ecotoxicol. Environ. Saf.*, **2018**, *148*, 585-592.
14. Z. Cheng; Y. Li; Z. Liu; *J. Alloy. Compd.*, **2017**, *708*, 255-263.
15. C. Cruciani; *J. Phys. Chem. Solids,* **2006***, 67, 1994.*
16. Y. Ji; F. Xu; W. Wei; H. Gao; K. Zhang; G. Zhang; Y. Xu; P. Zhang; *J. Solid State Chem.*, **2021**, *295*, 121917.
17. B. Ertan; S. Gurkok; D. Efe; *Stud U Babes-Bol. Che.*, **2020**, *4*, 109-123.
18. A. Sarı; M. Tuzen; *J. Hazard. Mater.*, **2008**, *152*, 302-308.
19. M. Senila; O. Cadar; L. Senila; A. Hoaghia; I. Miu; *Molecules*, **2019**, *24*(22), 4023.
20. A.F. Gualtierei; E. Marchi; E. Passaglia; *Stud. Surf. Sci. Catal.,* **1999**, *125,* 707-713.
21. I. Langmuir; *J. of Am. Chem. Soc.*, **1916**, *38*, 2221–2295.
22. N. Ayawei; E.A. Newton; D. Wankasi; *J. Chem.*, **2017**, Article lD 3039817.
23. Y. Zhuang; F. Yu; J. Chen; J. Ma; *J. Environ. Chem. Eng.,* **2016**, *4*(1), 147–156.
24. M.M. Dubini; *Chem. Rev.,* **1960**, *60*, 235–241.
25. X. Hu; X. Du; *Molecules*, **2019**, *24*, 1449.
26. N.T. Thanh; T.V. Thien; P.D. Du; C.V.T. Thanh; T.X. Mau; D.Q. Khieu; *J. Environ. Chem. Eng.*, **2018**, *6(2)*, 2269-2280.

STUDIA UBB CHEMIA, LXVI, 2, 2021 (p. 189-196)
(RECOMMENDED CITATION)
DOI:10.24193/subbchem.2021.2.16

ASSESSMENT OF TOXIC ELEMENTS CONTAMINATION IN SURFACE WATER AND SEDIMENTS IN A MINING AFFECTED AREA

ANA MOLDOVAN[a,b], ANAMARIA IULIA TÖRÖK[a]*, OANA CADAR[a], MARIUS ROMAN[a], CECILIA ROMAN[a], VALER MICLE[b]

ABSTRACT. To assess the spatial and temporal contamination with toxic elements (As, Cd, Cr, Cu, Pb, Ni, Zn), surface water and sediments were collected in 2019 and 2020, from Valea Sesii, a contaminated water stream in Romania. The toxic metal contamination of water was assessed using heavy metals evaluation index (HEI), heavy metals pollution index (HPI) and of sediments using contamination factor (C_f) and geo-accumulation index (I_{geo}). The metal concentrations were comparable within the two years, suggesting that the natural attenuation process was inadequate, and treatment technologies are required to improve surface water and sediment quality. The surface water presented high degree of metal contamination in 2019 as indicated by HPI > 100 and HEI < 10. The toxic metal concentrations in sediments were very high for Cd, Ni, Pb and Cu, with highest I_{geo} value for Cd and C_f for Ni. Surface water and sediments showed signs of high level of contamination in the sampling points located downstream of the copper mine discharge point, an improvement of their quality being noticed with distancing from the mining discharge area. This study is a first step for a comprehensive risk assessment and for an integrated environmental management.

Keywords: *metal contamination, river water, sediments, HEI, HPI, contamination index, I_{geo}*

INTRODUCTION

Contamination of surface water due to the wastewater discharge is of major concern, as reported by several previous studies [1-4]. Human activities have an important impact on the environment, including changes in biophysical

[a] *INCDO-INOE 2000, Research Institute for Analytical Instrumentation, 67 Donath Street, 400293 Cluj-Napoca, Romania*
[b] *Technical University, Faculty of Materials and Environmental Engineering, 103-105 Muncii Boulevard, 400641 Cluj-Napoca, Romania*
* *Corresponding author: iulia.torok@icia.ro*

environments, in ecosystems, biodiversity and natural resources, alterations that interfere with the natural processes [5]. In freshwater ecosystems, the metal contamination may result from precipitation, geologic weathering or through the discharge of agricultural, municipal, domestic or industrial waste products [6, 7]. Due to industrialization processes and anthropogenic activities (especially mining, ore processing) conducted in the area, a large number of pollutants were discharged into the surface water, deteriorating the river water quality. Moreover, the hydrology of the river is an important factor in the accumulation and transformation of metals. Also, the river water quality is affected by natural processes such as precipitation and weathering [8].

Contamination in the aquatic systems raises high concerns due to the potential toxicity of metals and their harmful effects on the biota [9, 10]. Heavy metals from natural minerals are more stable, while heavy metals from anthropogenic sources tend to be more mobile and bioavailable, representing greater health and environmental risks [11, 12]. With their long persistence, bioaccumulation, and bio-magnification character, heavy metals from freshwater ecosystems are ultimately adsorbed into the sediments [13] and may bioaccumulate, causing toxic effects at points far from the contamination source [14]. Rivers can act as secondary sources of heavy metals for the adjacent marine environment, being their dominant transport pathway from the source to the environment [15-17]. Therefore, periodic monitoring of the heavy metal concentrations and their spatial distribution in the studied environmental media is required.

The determination of heavy metals concentration in water and sediment is a critical step in defining the level of contamination in the aquatic ecosystems and their potential impact on the environment [18-20]. Thus, environmental quality indicators and pollution indices have been developed for processing and analysing the anthropic inputs and their influence on the environmental quality status [21, 22].

The mining industry is an important waste producer worldwide, with a high influence on environmental quality [23]. Due to the formation of sulphide oxidation, sulphidic mine tailing (pyrite, jarosite, sphalerite, galena) favours metal mobility from mining waste to streams. Minerals with a strong acid reduction potential are an effective waste stabilization strategy for minimizing the sulphide potential of metals dissolving and neutralizing acidic waters. Also, the use of non-reactive materials in the construction of tailing impoundments, compacting the material in order to limit water and oxygen flow and increase stability, and complete water saturation of the impoundment in order to prevent oxidation in the beach area are measures that could reduce the risk of surface water and sediments contamination from mining activities [24-26].

Earlier studies assessed the water quality and contamination risk in catchments near mining areas and their vicinity [24, 25, 27, 28]. Ozunu et al. [24] studied the quality of surface waters in the Aries River, near a mining

area, and their results revealed that the waters discharged by mining tailings considerably impact the environment. The surface water quality from the Aries catchment was also investigated by Levei et al. [27] and increased Mn, Cu, Fe, Pb and sulphates concentrations were found, whereas other metals were only slightly increased. However, to the best of our knowledge, the relationship between the water and sediment quality has been less studied. In this context, the novelty of the present study lies in the integration of individual and synergistic assessment of toxic metals in sediment and water, as well as in the determination of the influence of water contamination on sediment sample quality.

An exhaustive evaluation of spatial and temporal trends of toxic metal contamination in the Valea Sesii rivulet from 2019 and 2020 is presented in this study. Beside the metal concentrations in the surface water and sediment, heavy metal pollution index (HPI), heavy metal evaluation index (HEI), geo-accumulation index (Igeo), contamination factor (C_f) and degree of contamination (C_d) were also used in the assessment of the contamination level of water and sediment samples. The combination of the individual (I_{geo} and C_f) and synergistic (C_d, HPI, HEI) assessments of the seven toxic metals (As, Cd, Cr, Cu, Pb, Ni, Zn) will provide a more comprehensive view on the toxic metal contamination status in the Valea Sesii rivulet. The obtained results will provide a background for future ecological and human health risk assessments and for the development of curatives measures for the river's surface water and sediment quality. In addition, this research can offer the necessary information support for a more comprehensive toxic metal contamination assessment in all the mining affected rivers in the world.

RESULTS AND DISCUSSION

The surface water and sediment were sampled from six different locations among the Valea Sesii rivulet catchment (Fig. 1) in two different years: 2019 and 2020.

1. Toxic metal concentration in surface water

All the studied metals were detected at a level above the method quantification limits in the surface water samples over a two-year sampling campaign (2019–2020) set for six sampling locations (L1–L6), as shown in Fig. 1. Zn, Cu and Ni were the dominant elements in all the locations and years.

Regarding the spatial variation, the metal concentrations from the selected locations were compared. The L1 and L2 results did not differ from each other, having the lowest concentrations of metals among the studied waters, indicating that no anthropogenic interference influenced the water

chemistry. On the other hand, all metals had their highest concentrations in L3, indicating that the contamination source could be situated between L2 and L3. L3 was located downstream of the discharge point of the Rosia Poieni tailing impoundment. Downstream L3, the samples also had relatively high concentration of metals, the only influence among their content's variation seemed to be due to the dilution phenomenon.

Comparing the metal concentrations between 2019 and 2020, most of the metal concentrations (except for Cr, Pb and Zn) reached their highest values in 2020.

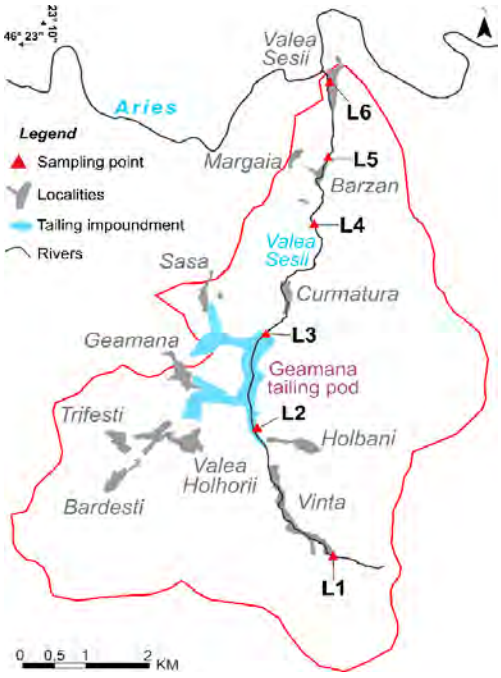

Figure 1. Map of the sampling points in Valea Sesii area

Cu and Zn concentrations had exceeded the quality standards imputed for the V class of surface water quality by the Romanian and European legislation (Minister's Order 161/2006/OD and Directive 2008/32/CE), in four out of the six sampling sites [29, 30]. Downstream L3, Cu concentration ranged between 115 and 159 µg/L in 2019 and between 142 and 214 µg/L in 2020, respectively. In the case of Zn, the concentration ranged from 1813 to 1247 µg/L in 2019, and between 2001 and 1422 µg/L in 2020. The mean value of Ni over the two-year sampling campaigns had a value of 120 µg/L and a standard deviation of 82.5 µg/L. With a mean concentration of 45.7 µg/L and a standard

deviation of 33.8 µg/L, As had its highest value in the water sample from L3 (103 µg/L) in 2020, 2.5 times higher than the quality standards established by legislation limit values for the V class of surface water quality [29, 30]. The water in L3 had poor quality due to the high Cd, Cr, and Pb concentration, with mean concentration values of 1.29 µg/L for Cd, 107 µg/L for Cr, respectively 23.5 µg/L for Pb [30].

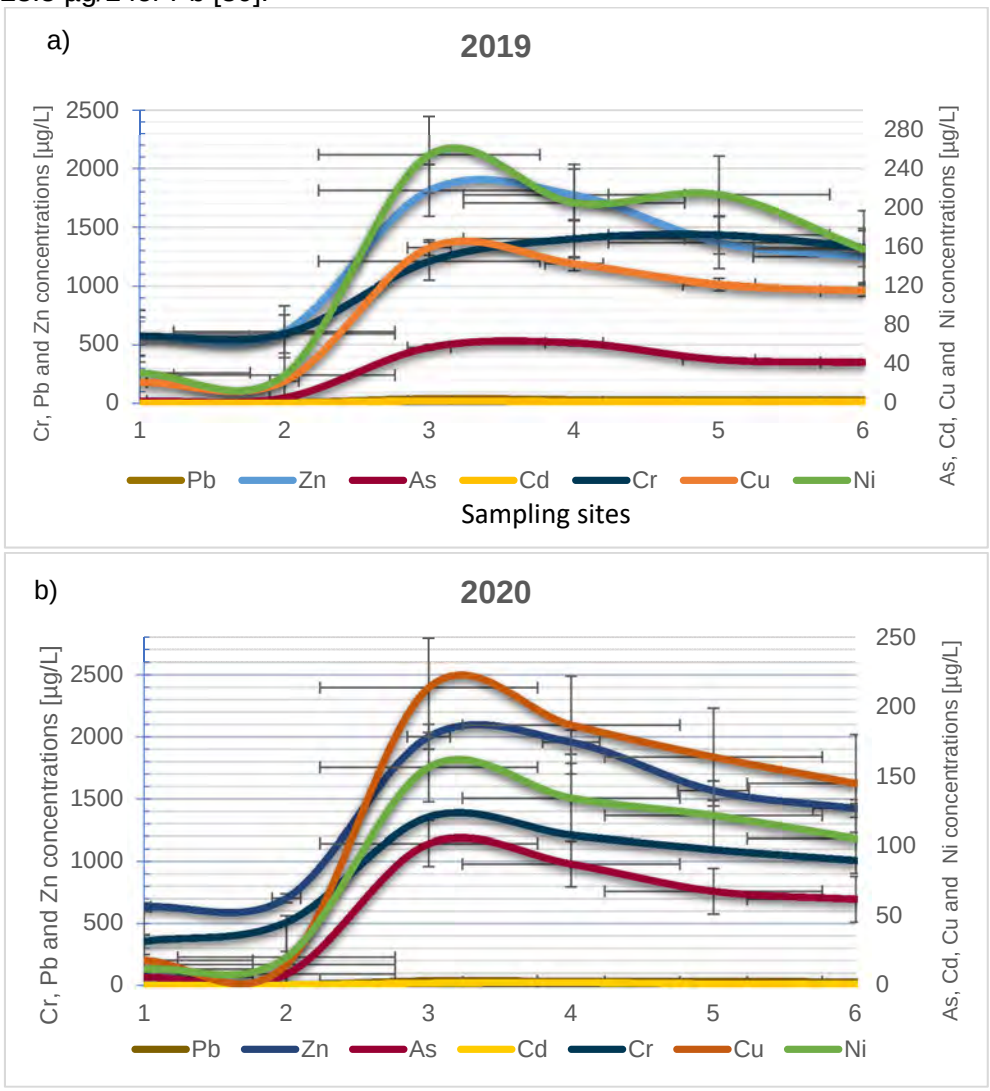

Figure 2. The spatial and temporal variation (a) 2019; b) 2020) of metal concentrations in the Valea Sesii rivulet water samples

The metal concentration trend varied over the two-year duration. This may be due to accidental discharges, annual precipitation, or change in production activities. Thus, an overall conclusion of the toxic metal concentration variation trend was difficult to draw.

The obtained results indicated that Cu, Ni and Zn concentrations were higher than the class V of the national surface water quality standards in the case of L3, L4, L5 and L6, while for Cr and Pb, the metal concentrations were higher than the class III of the national surface water quality standards [30]. Due to Zn and Ni concentrations, L1 and L2 were included in the class II of the national surface water quality standards [30]. As expected, the concentrations of metals decreased as the distance from sources of contamination increased along the flow direction.

A similar study done by Levei et al. (2011) for Aries River catchment has showed that the levels of Ni, Cu, Cd and Zn in Vales Sesii rivulet had exceeded the quality standards established by legislation limit values for the V class of surface water quality [29, 30]. Moreover, our findings were in accordance to Senila results regarding the Cu and Zn concentrations [31]. Similar results were reported by Ning [32] for a water stream near a gold mine area in China, where the metal concentrations were higher than the III or IV class of the national surface water quality standards, indicating, in general, an average quality of the surface water in the study area.

2. Metal concentration in sediment samples

The metal concentrations in sediment samples are presented in Table 1. In general, the metal contents in sediment are higher than in surface water because of their ability to precipitate, accumulate, and bind strongly to sediments [33].

Regarding the spatial variations among sampling sites, the highest metal concentration was measured in the case of L3 and L4, while the lowest in L1 and L2, similar to the metal concentration in the surface water samples, as shown in Fig. 2.

Compared with the samples from 2019, the toxic metal concentrations in sediment presented some variations. While the Cr concentration was notably higher in all the sediment samples, the Zn and Ni concentrations were lower in the case of L3, L4, L5 and L6. Even so, the sediment samples had similar concentration, implying that the sediment quality did not improve over two years. Therefore, the natural attenuation process of the river was proven to be inadequate or insufficient. In order to improve the quality of the river, it is recommended to implement some remediation actions (e.g., employing sediment clean-up operations and enforcing stringent discharge standards).

Table 1. The metal content identified in the sediment samples in mg/kg

	2019							2020						
	As	**Cd**	**Cr**	**Cu**	**Pb**	**Ni**	**Zn**	**As**	**Cd**	**Cr**	**Cu**	**Pb**	**Ni**	**Zn**
L1	2.84	0.040	16.8	6.18	12.10	6.20	6.88	4.12	0.032	22.7	8.12	10.7	12.4	7.18
L2	3.84	0.054	14.5	4.22	14.30	7.22	10.4	4.05	0.048	27.3	7.55	9.45	15.6	7.40
L3	22.70	1.12	97.8	88.3	66.8	233	46.1	19.0	0.812	86.0	72.4	72.1	277	40.8
L4	18.90	0.975	66.3	86.8	75.8	286	52.8	27.3	0.745	96.3	87.4	76.4	218	37.8
L5	17.40	0.827	54.1	67.8	54.3	218	44.3	16.8	0.541	60.8	66.8	60.3	187	32.4
L6	12.00	0.642	60.8	53.8	50.7	177	38.7	12.2	0.42	52.7	48.5	52.4	166	34.2
Average	12.9	0.610	51.7	51.2	45.7	155	33.20	9.04	0.335	30.0	33.8	29.8	109	15.3
SDTV	8.20	0.46	31.7	37.8	26.7	120	19.58	4.05	0.032	22.7	7.55	9.45	12.4	7.18
Min	2.84	0.04	14.5	4.22	12.1	6.20	6.88	27.3	0.812	96.3	87.4	76.4	277	40.8
Max	22.7	1.12	97.8	88.3	75.8	286	52.8	13.9	0.432	57.7	48.5	46.9	146	26.6

Ni, Zn, Cu and Cd had the highest concentration among the studied metals. Downstream L3, Ni and Cu concentrations were 1.2 – 2 times higher than the upper value of the sediment quality guideline established by the Romanian legislation [30]. Zn and Cd had their highest concentration in the sediment samples from L4 and L3, with slightly higher concentration than the sediment guideline for those specific toxic metals, 52.8 mg/kg dry wt. in the case of Zn (L4), respectively 1.12 mg/kg dry wt. in the case of Cd (L3). As, Cr and Pb concentrations were lower than the upper limit of those standards.

3. Assessment of toxic metal contamination trends using pollution indices

The HPI and HEI were used to assess the surface water's level of contamination with heavy metals, which were calculated using the Romanian and European legislation [29, 30] and the concentration level of Cd, Cr, Cu, Pb, Ni and Zn from the analyzed water samples.

The value of HPI ranged from 18.3 to 145, with an average value of 84.6 in 2019, and from 12.4 to 103, with an average value of 62.4 in 2020. In 2019, for four out of six samples, the HPI exceeded the critical value of 100, indicating a high level of heavy metal contamination. As shown in Fig. 3a, the spatial trends of HPI varied as follows: L3 > L4 > L5 > L6 > L1 > L2. L3 had the highest HPI value of 145 in 2019 and 103 in 2020, indicating that the site was highly contaminated with heavy metals, while L2 had the lowest HPI (18.3 in 2019 and 12.4 in 2020), presenting moderately contaminated level of heavy metals.

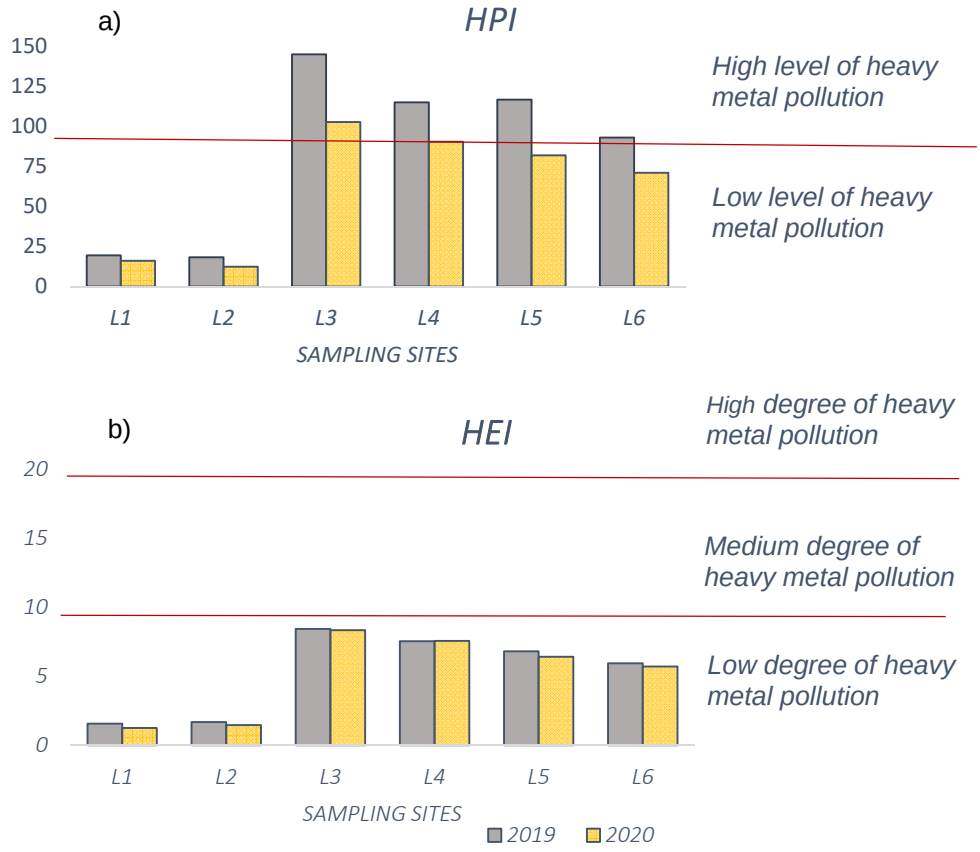

Figure 3. The spatial and temporal variation of heavy metal pollution index HPI (a) and heavy metal evaluation index HEI (b) in the Valea Sesii rivulet

The geo-accumulation index (I_{geo}) and the contamination factor (C_f) were employed for the quantitative measurement of each metal pollution level in the sediment samples. Unlike monitoring data, the individual indices take into consideration the background levels of the heavy metals according to Turekian and Barbieri [34, 35], in the case of I_{geo}, or the maximum allowable heavy metal concentration, in the case of C_d. Fig. 4 shows the I_{geo} values of the heavy metals at different sampling locations.

Most of the heavy metals had their highest I_{geo} at L3 and L4, meanwhile, L1 and L2 had uncontaminated levels of every tested metal, with I_{geo} values lower than 0.

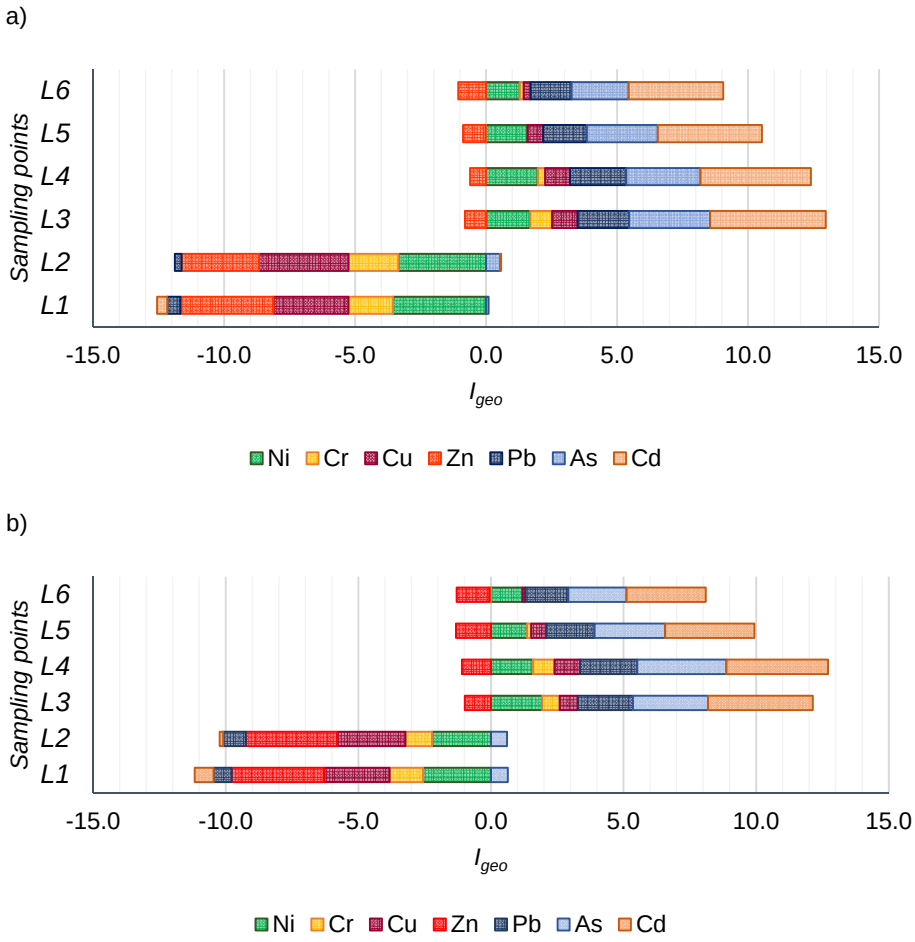

Figure 4. The geo-accumulation index in the Valea Sesii rivulet sediments in 2019 (a) and 2020 (b)

The sediment samples from L3, L4, L5 and L6 were proven to be highly contaminated with As, L3, L5 and L6 moderately to highly contaminated with Pb, L4 heavily contaminated with Pb. In the case of Cd, I_{geo} varied from -0.395 to 4.41 in 2019, -0.714 to 3.95, in 2020, respectively. A heavily to extremely contaminated level with Cd for sediments sample from L3 and L4 and a highly contaminated level for sediment sample from L5 and L6 were assigned, while I_{geo} for L1 and L2 was lower than 0, suggesting a low contamination level for Cd.

Regarding the temporal distributions, in 2019, the highest cumulative I_{geo} value was attributed to L3, while in 2020, to L4.

The highest C_f was in the case of Ni, where a very high degree of contamination was attributed to L3 and L4, and a considerable degree of Ni contamination was allocated to L5 and L6. A moderate degree of contamination with Cu and Cd was assigned to L3, L4 and L5 in 2019, while in 2020, the C_f of Cd was lower, in the case of L4 and L5.

The conclusions about the metal content trends of I_{geo} values are not very similar compared with the heavy metal content trends assessments based on the C_f values. However, both indices suggested high level of toxic metal contamination on sediment, so strategies and technologies to improve sediment quality, such as washing, thermal extraction or bioremediation are necessary and urgent.

The C_d index was employed to assess the synergistic contamination of the seven studied heavy metals in the sediment. The average C_d value of the six locations in two years was 7.94, indicating that, globally, the sediment samples of the Valea Sesii rivulet were moderately to highly contaminated.

The spatial trends varied in the following order: L4 > L3 > L5 > L6 > L2 >L1 in 2019 and L3 > L4 > L5 > L6 > L2 >L1 in 2020, respectively. L4 had the highest C_d value of 14.1 and L3, 13.4, indicating that the investigated sites were highly contaminated with heavy metals, while L1 had the lowest C_d of 0.84.

There are several mitigation measures to reduce the impact of mining activities, among which environmental monitoring; management and remediation schemes depending on the nature of mine; novel biotechnological methods; precipitation and adsorption processes that reduce the transport of contaminants produced by mining with an emphasis on hyporheic zones; the colmation process, which inhibits the flow of mining pollutants; microbiological processes immobilizing metals (manganese and iron); sulphidic mine tailings remediation by soil and water covers which limit the oxidation rate of the tailing; point source remediation [36-39].

CONCLUSIONS

The monitoring data, HEI, HPI, C_f, and I_{geo} indices were used to evaluate toxic metal contamination in the surface water, respectively, in the sediment of the Valea Sesii rivulet, located in an area strongly affected by Cu ore mining activities. Ni, Zn, Cr and Cu were the four dominant metals in the water and sediment samples of the Vale Sesii rivulet. The concentration

of toxic metals in the Cu ores deposit areas depends upon the distance from the pollution source and scalar transport in rivulet flows and decreases along the flow direction. All studied metals had their highest concentration values in L3 and L4, sampling points located downstream of the discharge point of the Geamana tailing impoundment. The heavy metal in the surface water showed signs of contamination, HPI indicating high levels of heavy metal contamination for L3, L4, L5 and L6, in 2019 and for L3, in 2020. For the sediment samples, metal contamination was alarming, especially for Cd, Ni, Pb and Cu, with I_{geo} highest value for Cd and C_f, for Ni, respectively. The metal concentrations in sediments for the two years were quite similar, implying that the natural attenuation process was not adequate to remediate the sediments quality.

The results indicated that immediate and necessary treatment strategies and technologies to enhance surface water and sediment quality are required. Also, the obtained results will be an important step in proposing solutions for improving the water and sediment quality of Valea Sesii rivulet, as well as for establishing the influence of the polluted stream on the quality of its tributaries: Abrud and Aries River.

EXPERIMENTAL SECTION

1. Study area and sampling procedures

The Aries River is one of the most polluted surface waters in Romania, due to the intensive mining activities conducted in the area [40, 41] Rosia Poieni is the largest unexploited porphyry copper deposit in Europe, representing 65% of the total copper reserve of Romania [42]. Annually, 5000 tons of copper are extracted from an open pit mine and the waters from the quarry perimeter are collected by the Aries River tributaries: Valea Strigoi, Valea Sesii, Valea Muscanilor and Valea Fantanilor [41, 43].

Six locations were selected for water and sediment sampling to evaluate the heavy metal contamination in Valea Sesii rivulet (Fig. 1). L1 and L2 were located upstream of the discharge point of the Rosia Poieni tailing impoundment (Geamana tailing pond-L3), situated at ~3.85 km and 1.80 km for L1 and for L2, respectively, from L3, while the rest of them were selected along the downstream watercourse at ~2.00 km, 3.15 km and 4.30 km, for L4, L5 and L6 respectively, from L3, in two sampling campaigns (November 2019 and November 2020). The water samples were collected in pre-cleaned polyethylene bottles that were rinsed three times with ultrapure water (Veolia Environment, France) before sample collection, and kept at 4°C until the analysis. Six samples were collected from the sediment top layer (about 0-20 cm) using a plastic shovel and stored in polyethylene bags [44, 45].

2. Analysis of heavy metals

The sediment samples were dried at 60 °C until constant weight, powdered by an agate mortar and passed through a 200 µm mesh sieve. The fractions <200 µm were stored in polyethylene bags at room temperature until the analysis.

Samples were digested using Speedwave XPERT (Berghof, Germany) microwave digestion system according to the method described by Miclean et al. [46] with HNO_3 65% in the case of water samples and an acid mixture of HNO_3 65% and HCl 37% with a ratio of 1:3 (v/v) in the case of sediment samples, respectively. The digested samples were quantitatively transferred to volumetric flasks and diluted to the mark with ultrapure water. The concentrations of metals (As, Cd, Cr, Cu, Pb, Ni and Zn) in the surface water and sediments were determined using an ELAN DRC II inductively coupled mass spectrometer (Perkin Elmer, Waltham, Massachusetts, US).

Quality assurance and quality control were strictly implemented following the USEPA guidelines to ensure the accuracy of the analysis, using calibration standards, duplicate samples and procedural blank measurements [44]. The accuracy of the metal determination from water was checked by analysing 1643f NIST freshwater certified reference material (National Institute of Standards and Technology, Canada), and from sediments was checked by ERM-CC141 Loam soil certified reference material. Mean recoveries for the determination of metals in CRMs ranged between 94% and 105%, in the case of water and between 88 and 108% in the case of sediments, respectively. The calibrations ranges and limits of detections are presented in Table 2.

Table 2. The metal determination calibration parameters

		Water	*Sediment*
	Range of calibration	**LOD**	
		[µg/L]	*[mg/kg]*
As	1-100 µg/L	0.40	0.013
Cd		0.36	0.012
Cr		0.13	0.004
Cu		0.23	0.008
Pb		0.37	0.012
Ni		0.36	0.012
Zn		0.55	0.018

3. Heavy metal contamination assessments

A combination of individual methods was employed to have a complete assessment of heavy metals contamination trends. Heavy metal pollution index HPI and heavy metal evaluation index HEI were used to

assess the surface water contamination, while contamination factor C_f and geo-accumulation index I_{geo} were used for the sediment quality assessment.

HPI is a rating model that provides the composite influence of individual heavy metals on the overall water quality. The HPI model [47, 48] is given in Eq. (1) and (2):

$$HPI = \frac{\sum_{i=1}^{n} Q_i W_i}{W_i} \quad (1)$$

$$Q_i = \sum_{i=1}^{n} \frac{|C_i - I_i|}{MAC - I_i} \quad (2)$$

where: Q_i is the sub-index of ith parameter, W_i is the unit weightage of the ith parameter and n is the number of parameters considered. C_i, I_i and MAC are the concentration of the ith parameter monitored, the ideal and quality standards concentration of the parameters established for the V class of surface water quality by Minister's Order 161/2006/OD and Directive 2008/32/CE [29, 30].

Regarding the level of pollution with heavy metals, HPI classifies the water bodies contamination levels in two categories: heavy metals low pollution level (HPI<100) and high level of pollution (HPI>100). A HPI value greater than 100 indicates that the water is unsuitable for consumption [47].

HEI provides an insight of the overall quality of groundwater with respect to heavy metals and is computed by Eq. (3) [49, 50].

$$HEI = \sum_{i=1}^{n} \frac{C_i}{MAC} \quad (3)$$

where C_i is the determined concentration of the ith parameter and MAC represents the quality standards concentration of the parameters established for the V class of surface water quality by Minister's Order 161/2006/OD and Directive 2008/32/CE [29, 30]. Classifications of water pollution degree based upon HEI are as follows: <10 low degree of pollution, 10 – 20, medium degree and >20, high degree of pollution.

To identify the contributions of the metals to sediment pollution, contamination index C_d (Eqs. 4-5) and geo-accumulation index I_{geo} (Eqs. 6) were assessed.

$$C_f = \frac{C_{Ai}}{C_{Ni}} - 1 \quad (4)$$

$$C_d = \sum_{i=1}^{n} (c_f) \quad (5)$$

where, C_{Ai} is the value of the concentration of ith metal ions in the analyte and C_{Ni} represents the maximum allowable concentration (MAC) of the elements, according to the national legislation [24]. C_f and C_d results higher than 1.0 indicates a powerful contamination with metals [51]. The values of this index are: low contamination ($C_f \leq 1$, LC); moderate contamination ($1 \leq C_f \leq 3$, MC); considerable contamination ($3 \leq C_f \leq 6$, CC); very high contamination ($C_f > 6$, VHC), according to Arienzo [52].

$$I_{geo} = \log_2\left(\frac{C_m}{1.5 * B_m}\right) \quad (6)$$

where: C_m is the heavy metal measured concentration in sediment; B_m is the concentration of heavy metals in average shale values [34, 35]. Samples may be classified as practically uncontaminated ($I_{geo} \leq 0$, Class 0), uncontaminated to moderately contaminated ($0 \leq I_{geo} \leq 1$, Class 1), moderately contaminated ($1 \leq I_{geo} \leq 2$, Class 2), moderate to heavily contaminated ($2 \leq I_{geo} \leq 3$, Class 3), heavily contaminated ($3 \leq I_{geo} \leq 4$, Class 4), heavily to extremely contaminated ($4 \leq I_{geo} \leq 5$, Class 5), and extremely contaminated ($I_{geo} \geq 5$, Class 6) [52].

ACKNOWLEDGMENTS

This paper was supported by the Project "Entrepreneurial competences and excellence research in doctoral and postdoctoral programs - ANTREDOC", project co-funded by the European Social Fund, Project CEO-TERRA, project co-financed by the European Fund for Regional Development, through the Competitiveness Operational Program 2014-2020, project no. POC-A.1-A.1.1.1- F- 2015-152/2016 and the Core Program, under the support of ANCS, project no. PN 19-18.01.01 (contract no. 18N/08.02.2019). The funder had no role in the design of the study; in the collection, analysis and interpretation of data; in the writing of the manuscript, and in the decision to submit the article for publication.

REFERENCES

1. S. Dash, S.S. Borah; A. Kalamdhad; *Ecol. Indic.*, **2019**, 106.
2. M.S. Bhuyan, M.A. Bakar, A. Akhtar, M.B. Hossain, M.M. Ali; M.S. Islam; *Environ. Nanotechnol. Monit. Manag.*, **2017**, 8, 273-279.
3. M.S. Islam, M.K. Ahmed, M. Raknuzzaman, M. Habibullah -Al- Mamun; M.K. Islam; *Ecol. Indic.*, **2015**, 48, 282-291.
4. M.A. Islam, B. Das, S.B. Quraishi, R. Khan, K. Naher, S.M. Hossain, S. Karmaker, S.A. Latif; M.B. Hossen; *Mar. Pollut. Bull.*, **2020**, 160, 111649.
5. A. Cendrero, L.M. Forte, J. Remondo; J.A. Cuesta-Albertos; *Earth's Future*, **2020**, 8.
6. W. Salomons U. Förstner, Metals in the Hydrocycle. **1984**.

7. M.-A. Hoaghia, A. Moldovan, E. Kovacs, I.C. Mirea, M. Kenesz, T. Brad, O. Cadar, V. Micle, E.A. Levei; O.T. Moldovan; *Water*, **2021**, 13.
8. Y. Zeng, C. Bi, J. Jia, L. Deng; Z. Chen; *Ecol. Indic.*, **2020**, 116.
9. V. Kumar, R.D. Parihar, A. Sharma, P. Bakshi, G.P. Singh Sidhu, A.S. Bali, I. Karaouzas, R. Bhardwaj, A.K. Thukral, Y. Gyasi-Agyei; J. Rodrigo-Comino; *Chemosphere*, **2019**, 236, 124364.
10. O.C. Ihunwo, A.N. Dibofori-Orji, C. Olowu; M.U. Ibezim-Ezeani; *Mar. Pollut. Bull.*, **2020**, 154, 111042.
11. N.U. Benson, A.E. Adedapo, O.H. Fred-Ahmadu, A.B. Williams, E.D. Udosen, O.O. Ayejuyo; A.A. Olajire; *Reg. Stud. Mar. Sci.*, **2018**, 18, 44-56.
12. M. Saleem, J. Iqbal; M.H. Shah; *Environ. Nanotechnol. Monit. Manag.*, **2015**, 4, 27-36.
13. Y. Zhao, M. Xu, Q. Liu, Z. Wang, L. Zhao; Y. Chen; *Mar. Pollut. Bull.*, **2018**, 137, 601-609.
14. P. Weber, E.R. Behr, C.D.L. Knorr, D.S. Vendruscolo, E.M.M. Flores, V.L. Dressler; B. Baldisserotto; *Microchem. J.*, **2013**, 106, 61-66.
15. D. Qiao, G. Wang, X. Li, S. Wang; Y. Zhao; *Chemosphere*, **2020**, 248, 125988.
16. F. Botsou, A.P. Karageorgis, E. Dassenakis; M. Scoullos; *Mar. Pollut. Bull.*, **2011**, 62, 547-63.
17. M.E. Goher, A.M. Hassan, I.A. Abdel-Moniem, A.H. Fahmy; S.M. El-sayed; *Egypt. J. Aquat. Res.*, **2014**, 40, 225-233.
18. V. Kumar, A. Sharma, R. Kumar, R. Bhardwaj, A. Kumar Thukral; J. Rodrigo-Comino; *Human. Ecol. Risk. Assess.*, **2018**, 26, 1-16.
19. M. Li, Q. Zhang, X. Sun, K. Karki, C. Zeng, A. Pandey, B. Rawat; F. Zhang; *Chemosphere*, **2020**, 244, 125410.
20. G. Zhao, S. Ye, H. Yuan, X. Ding, J. Wang; E.A. Laws; *Mar. Pollut. Bull.*, **2018**, 136, 300-308.
21. I. Karaouzas, N. Kapetanaki, A. Mentzafou, T.D. Kanellopoulos; N. Skoulikidis; *Chemosphere*, **2021**, 263, 128192.
22. A.M. Hussein, D. Neama Jabbar; A.R. Ali; *Alex. Eng. J.*, **2020**, 59, 5197-5206.
23. M. Sima, B. Dold, L. Frei, M. Senila, D. Balteanu; J. Zobrist; *J Hazard Mater*, **2011**, 189, 624-39.
24. V. Constantin, L. Ştefănescu; C.-M. Kantor; *Environ. Sci. Policy*, **2015**, 52, 129-139.
25. A. Ozunu, L. Stefanescu, C. Costan, M. Miclean, C. Modoi; S.-N. Vlad; *Environl. Eng. Manag. J.*, **2009**, 8, 809-815.
26. B. Dold; *Minerals*, **2014**, 4, 621-641.
27. E. Levei, M. Senila, M. Miclean, B. Abraham, C. Roman, L. Stefanescu; O.T. Moldovan; *Environl. Eng. Manag. J.*, **2011**, 10, 23-29.
28. A. Moldovan, M.A. Hoaghia, V. Băbălău-Fuss, M. Roman, G. Hognogi, V. Micle; *Agric. Sci.*, **2020**, 113.
29. Directive 2008/32/EC of the European Parliament and of the Council of 11 March 2008 amending Directive 2000/60/EC establishing a framework for Community action in the field of water policy, as regards the implementing powers conferred on the Commission.

30. Ministerial Order no. 161/2006 for the approval of the Norm regarding the classification of surface water quality in order to establish the ecological status of the water bodies. **2006**.
31. M. Senila, E.A. Levei, L.R. Senila; M. Roman; *J. Chem.*, **2015**, 2015, 1-8.
32. L. Ning, Y. Liyuan, D. Jirui; P. Xugui; *Procedia. Environ. Sci.*, **2011**, 10, 914-917.
33. G. Schertzinger, N. Ruchter; B. Sures; *Sci. Total. Environ.*, **2018**, 616-617, 1199-1207.
34. K.K. Turekian K.H. Wedepohl; *Geol. Soc. Am. Bull.*, **1961**, 72.
35. N.A. Barbieri M, Sappa g.; *Senses. Sci.*, **2015**, 2, 94-97.
36. S. Lynch, L. Batty; P. Byrne; *Minerals*, **2014**, 4, 52-73.
37. C.J. Gandy, J.W. Smith; A.P. Jarvis; *Sci Total Environ*, **2007**, 373, 435-46.
38. L. Moreno I. Neretnieks; *Hydrometallurgy*, **2006**, 83, 176-183.
39. W.M. Mayes, E. Gozzard, H.A. Potter; A.P. Jarvis; *Environ Pollut*, **2008**, 151, 165-75.
40. E. Levei, M. Ponta, M. Senila, M. Miclean; T. Frentiu; *J. Serbian. Chem. Soc.*, **2014**, 79, 1019-1036.
41. E. Levei, T. Frentiu, M. Ponta, C. Tanaselia; G. Borodi; *Chem. Cent. J.*, **2013**, 7, 5.
42. E. Luca, Roman, C., Chintoanu, M., Luca, L., Puscas, A., Hoban, A.; *Agricultura –Stiinta si practica*, **2006** 3 -4, 59 –60.
43. P. Rzymski, P. Klimaszyk, W. Marszelewski, D. Borowiak, M. Mleczek, K. Nowinski, B. Pius, P. Niedzielski; B. Poniedzialek; *Environ. Sci. Pollut. Res. Int.*, **2017**, 24, 21445-21458.
44. USEPA, Sediment Sampling. United States Environmental Protection Agency. **2014**: Georgia, United States.
45. USEPA, Surface Water Sampling. United States Environmental Protection Agency. **2016**: Georgia, United States.
46. M. Miclean, E.A. Levei, O. Cadar, M. Senila; I.S. Groza; *Carpathian. J. Earth. Environ. Sci.*, **2013**, 8, 93-100.
47. K. Wątor R. Zdechlik; *Ecol. Indic.*, **2021**, 121.
48. L. Qu, H. Huang, F. Xia, Y. Liu, R.A. Dahlgren, M. Zhang; K. Mei; *Environ. Pollut.*, **2018**, 237, 639-649.
49. M.A. Bhuiyan, M.A. Islam, S.B. Dampare, L. Parvez; S. Suzuki; *J. Hazard. Mater.*, **2010**, 179, 1065-77.
50. A.E. Edet O.E. Offiong; *GeoJournal*, **2002**, 57, 295-304.
51. R. Ullah S. Muhammad; *Environ. Technol. Innov.*, **2020**, 19.
52. M. Arienzo, L. Ferrara, M. Toscanesi, A. Giarra, C. Donadio; M. Trifuoggi; *Mar. Pollut. Bull.*, **2020**, 155, 111149.

STUDIA UBB CHEMIA, LXVI, 2, 2021 (p. 197-212)
(RECOMMENDED CITATION)
DOI:10.24193/subbchem.2021.2.17

PHYSICO-CHEMICAL CHARACTERIZATION OF WATER WELLS FROM REMETI, MARAMURES

THOMAS DIPPONG[a,b], CRISTINA MIHALI[a,b], OANA MARE ROSCA[a,b], MONICA MARIAN[a,b], MARIA MAGDALENA PAYER[b], MARCEL ȚÎBÎRNAC[b], SEBASTIAN BUD[a], GEORGE COMAN[a], ENIKO KOVACS[c,d], MARIA-ALEXANDRA HOAGHIA[c]*

ABSTRACT. This study was conducted with the aim of determining the quality and potential contamination level of water wells. Samples were collected from private water wells used as drinking water sources in Remeți locality, Maramures County, Romania. Remeți is situated near the protected area of the Upper Tisa River. Several physico-chemical indicators were determined, such as pH, electrical conductivity, dissolved oxygen, oxygen saturation, turbidity, temperature, ammonium, nitrate, nitrite, chloride, phosphate, iron, copper, sulphates, carbonate, bicarbonate and total hardness, due to their importance to human health and to the quality of the aquatic systems situated nearby a protected area. The quality status was assessed by using the water quality index (WQI), based on eleven parameters: pH, electrical conductivity, ammonium, total hardness, turbidity, nitrite, nitrate, chloride, sulphate, iron and cooper. The results indicated high amounts of ammonium and nitrate, while the WQI classified the studied water well samples into excellent and good quality categories. The WQI scores ranged between 27.7 and 65.1. The novelty of the study consists in the determination of the chemical composition of water wells from Remeti locality and in identification of some pollution processes which could affect human health if the studied waters are used as drinking water sources.

Keywords: *water quality, physico-chemical parameters, water quality index*

[a] *Technical University of Cluj-Napoca, Faculty of Sciences, Department of Chemistry and Biology, 76 Victoriei Street, 430122 Baia Mare, Romania*
[b] *Heidenroslein Association, 12A/95 Unirii Street, 430122 Baia Mare, Romania*
[c] *INCDO-INOE 2000, Research Institute for Analytical Instrumentation, 67 Donath Street, 400293 Cluj-Napoca, Romania*
[d] *University of Agricultural Sciences and Veterinary Medicine, 3-5 Calea Manastur, 400372, Cluj-Napoca, Romania*
** Corresponding author: alexandra.hoaghia@icia.ro*

INTRODUCTION

The quality of water, an essential factor of the environment, is defined as an assembly of physical, chemical, biological and bacteriological characteristics numerically expressed. These characteristics classify each water sample into a certain category [1-4]. Groundwater is considered the most reliable source of fresh water. Almost 80 % of the Earth's population depend on groundwater resources (used as drinking water sources) due to their quality compared with surface waters, which need chemical treatment and decontamination procedures [5]. Water with an adequate chemical composition is essential for the health and thriving of human life [6]. In order to determine the quality of groundwater, the impact of diverse indicators (pH, electrical conductivity, total dissolved solids, total hardness, chloride, nitrate, sulphate, fluoride, calcium, magnesium, sodium and potassium) of the water's chemistry is assessed [7].

In Romania, a representative part of the population uses groundwater resources from water wells for drinking purposes. Groundwater resources are exploited through centralized water supply systems and by using private and public water wells. The quality of water distributed by public networks needs to follow the quality standards regarding potability. On the other hand, the water wells are characterized by high amounts of various chemical parameters (ammonium, nitrate, nitrite, sulphate, chloride), mostly higher than the maximum allowable limits established by Romanian and international regulations referring to drinking water quality [8, 9]. Anthropogenic activities, as well as natural factors and processes are sources of high concentrations of diverse chemicals and toxic compounds [10]. The variation of the chemical composition depends on physico-chemical processes, such as the interaction between water, soil or rocks, the dilution of various chemical substances or ionic phases, the composition of infiltrated water, precipitation and biochemical reactions [6, 11].

Temperature is an important indicator in determining the quality of natural and residual waters. It influences the chemical composition, since the solubility of chemicals depends on it [1, 3]. The increasing of temperature intensifies the speed of water molecules motion and implicitly of the physico-chemical and biochemical processes [3].

Turbidity is determined by suspended materials (clay, dissolved substances, organic and inorganic materials, plankton and microorganisms) [4]. Water with high turbidity cannot be used for drinking purposes or used as industrial water, due to the unproper appearance and to the potential danger for human health [4].

Electrical conductivity represents the capacity of water to transport electricity, being corelated with the total quantity of dissolved salts and the estimated number of dissolved minerals [1, 12].

The pH indicates the capacity of water to react with acids or alkaline materials. A pH higher than 8.5 generates sulphuric mineralization, imprinting a salty or bitter taste to the water, irritating the eyes and skin, while a pH lower than 6.5 affects the vitamin absorption in the body.

Dissolved oxygen is one of the most important parameters of opened water wells, offering data regarding the nutrients disponibility, the pollution level, the microorganism activities, and the stratification and photosynthesis of water [13]. The concentration of dissolved oxygen depends on the water temperature, air pressure and on the amount of oxidizable substances, microorganisms and hydro-geochemical processes [9,14]. A low amount of oxygen in water well decreases the freshness of water, inducing a vapid taste, reduces the auto purification capacity of water, favouring the persistence of pollution level and making it unsuitable for drinking [5,15].

Total hardness is given by the concentrations of calcium and magnesium and it is a significant parameter in reducing the negative effects of toxic elements, increasing the boiling point of water and preventing the formation of foam as a result of the contact with soaps [12, 13]. Consumption of hard water for a long period of time increases the incidence of anencephaly, cardiovascular disorders and cancer [1].

Total alkalinity represents the quality of all dissolved alkaline substances as carbonates (CO_3^{2-}), bicarbonates (HCO_3^-) and hydroxides (OH^-), influencing the pH and neutralizing acids [2, 12].

A source of chloride (Cl^-) is represented by soluble chloride salts from minerals, which are essential in the activity of metabolism and other main physiological processes [1]. A high amount of chloride influences the content of chloride in groundwater and the amount of rain water and it is an indicator of contamination, causing negative effects (corrodation of pipeline systems, gives a salty taste to the water and causes diverse disorders: arterial hypertension, osteoporosis, asthma and kidney stones) [1,2].

Nitrate (NO_3^-) is related to precarious sanitation conditions, septic tanks situated nearby the water wells, sewage infiltration, fertilizers based on nitrogen [1, 16]. Agricultural practices account for more than 50 % of the total nitrogen spilled into water sources [13]. The antibacterial properties of nitrates play an important role in protecting the gastro-intestinal system against a variety of gastrointestinal pathogens, although a lifetime exposure at high concentrations could lead to health disease, such as diuresis and spleen haemorrhage [13].

A high amount of iron (Fe) in water is a result of geological debris, industrial and household wastes. In order to eliminate the iron from water, is achieved by filtration and drying [1]. High amount of iron has no negative effects on human health, but could generate a series of inconveniences, such as metallic taste and opalescent yellow colour [1, 17, 18].

The aim of the study was to determine the physico-chemical parameters of water samples collected from water wells used as drinking water sources from the Remeți locality (situated in a protected area of Natura 2000). The determined parameters were selected considering their importance to the health of the consumers and also for the well functioning of the aquatic ecosystems nearby the Natura 2000 protected area along the Tisa River. Correlation among the indicators was established and the quality status was determined by applying the water quality index, calculated with the help of the results obtained for eleven physico-chemical parameters (pH, electrical conductivity, ammonium, total hardness, turbidity, nitrite, nitrate, chloride, sulphate, iron and cooper) determined for the studied water samples.

RESULTS AND DISCUSSIONS

Physico-chemical parameters

The results of the analysed indicators (each value was the result of three measurements) present different dissimilarities with low variation coefficients for pH, temperature, turbidity, electrical conductivity, ammonium and iron (Tables 1 and 2).

The measurements were repeteated three times, indicating repetability between the obtained results. Mean values are indicated in Table 1. The statistical analysis indicated normal distributions for the majoriy of the parameters, except for the depth and the water level, dissolved oxygen, carbonates and phospahtes, which indicated deviations from normality according to the standardized skewness and kurtosis from Table 2. The water level, depth, amount of Cu, phosphate, nitrate, nitrite and dissolved oxygen indicated a high variability (65.7 - 105 %), showing the influence of external factors and contamination sources.

The water sample 10 has the highest depth, characterized by the highest dissolved oxygen content caused by the water temperature, air pressure and the content of oxidable substances and the activity of microorganisms. Samples 6, 7 and 8 have the lowest content of dissolve oxygen. Dissolved oxygen is important for the organisms, the high amount determined in sample 10 (9.10 mg/L) is due to the direct air diffusion or it was produced by autotroph organisms through photosynthesis [13]. Dissolved oxygen presents no direct danger for the human health, but could influence the chemical substances from water [13,19-22].

Table 1. Physico-chemical analysis of the studied groundwaters (samples 1-10)

Sample / Parameter	1	2	3	4	5	6	7	8	9	10
Depth, cm	270	320	900	260	345	350	350	430	450	1180
Water level, cm	220	230	800	220	275	280	280	360	310	590
Turbidity, NTU	2.08	1.42	1.53	1.82	1.47	2.03	1.48	0.99	1.08	1.26
Temperature, °C	16.9	19.3	16.6	19.9	19.7	18.1	18.4	16.4	16.0	15.5
Electrical conductivity,µS/cm	654	558	616	572	525	463	639	786	543	590
pH	7.31	7.12	7.71	7.38	7.14	7.53	7.39	7.51	7.68	7.97
Redox potential,mV	-22.5	-11.6	-45.6	-21.2	-12.9	-35.2	-26.9	-34.3	-43.9	-60.4
Dissolved oxygen,mg/L	3.58	3.38	5.56	4.45	4.73	2.79	2.44	2.27	3.66	9.10
Oxygen saturation,%	38.9	37.2	62.3	43.8	52.5	30.1	25.8	23.8	40.1	92.8
Ammonium,mg/L	1.66	1.92	2.38	2.38	1.09	1.49	1.16	1.41	2.22	1.93
Nitrate, mg/L	46.7	36.9	55.6	28.7	26.3	16.2	19.3	24.8	37.6	9.87
Nitrite, mg/L	<QL*	0.001	0.002	0.003	0.002	0.001	0.001	0.003	0.004	0.002
Bicarbonate, mg/L	122	183	232	207	159	195	170.8	305	183	195
Carbonate, mg/L	<QL*	<QL*	<QL*	<QL*	<QL*	<QL*	<QL*	<QL*	58	<QL*
Sulphate, mg/L	0.39	0.65	0.84	0.93	0.55	0.57	0.63	0.63	0.88	0.65
Chloride, mg/L	26.0	19.0	16.0	11.0	18.0	12.0	21.0	13.0	14.0	15.8
Iron, mg/L	0.024	0.025	0.018	0.023	0.024	0.024	0.024	0.028	0.027	0.024
Cooper, mg/L	<QL*	0.01	0.02	0.01	<QL*	0.02	0.01	0.02	0.01	0.02
Phosphate, mg/L	0.15	0.07	0.16	0.11	0.06	0.09	0.12	0.17	0.38	0.78
Total hardness, °G	7.2	8.5	15.5	7.9	9.1	9.5	9.3	11.5	12.4	19.3
**quantification limit of the method*										

In all the studied samples, turbidity is lower than the guideline value (5 NTU). The highest value was obtained in sample 8, due to the household wastes and leakage of chemical substances used in agricultural and beekeeping practices [1]. The turbidity increases during rainfall especially in the case of low depth groundwater [23].

The pH varies between 7.12 and 7.97 and it is related to the predominant soil type or to the accumulation of organic materials, while the degradation of the organic substances is caused by the release of carbon dioxide and by the reaction with the water producing carbonic acid [13].

The low values of electrical conductivity (sample 6) are due to the low content of inorganic substances dissolved in ionized form and due to the dilution effect of groundwater from water wells during precipitation [13, 24]. High electrical conductivity is caused by the presence of high amount of dissolved inorganic substances [12, 25].

The presence of ammonium in water is a result of incomplete degradation of organic substances based on nitrogen and of the water-soil interaction. The obtained results are three to four times higher than the

parametric value (0.5 mg/L) established by the Council Directive 98/83/EC. Nitrate is very mobile in soil and in groundwaters, because it is not adsorbed by the soil or by the geological material, precipitating only in dry conditions as mineral [25]. The amount of nitrate in the environment comes from a variery of sources, including agricultural activities (use of organic and chemical fertilizers based on nitrogen) and household activities (septical tanks and sewage system) [13]. The consumption of water rich in nitrates could induce methemoglobinemia or the blue baby syndrome in infants [25].

Phosphate ranges between 0.06-0.78 mg/L, having an average of 0.209 mg/L. Sources of phosphate are represented by the interactions of water with rocks and soil, the use of phosphorus fertilizers and detergents (phosphates are added as softeners). Sample 10 is characterized by the highest phosphate amount (0.40 mg/L). It was demonstrated that long-term over-application of manure and chemical fertilizer determine the orthophosphate movement into the groundwater system and consequently contaminates the groundwater resources [26]. Low amount of phosphate is observed in samples 2, 4, 5, 6 and 7, while samples 1, 3 and 8 are characterized by a medium amount, possibly due to the leakage of inorganic fertilizers [13]. Rich water in phosphate influences the development of algae, changing and altering the taste and colour of water [13].

The total hardness is influenced by the soil composition and by the presence of undissolved calcium and magnesium [1]. Water samples 1, 2, 6 and 8 have low values for the total hardness, which is corrosive and could dissolve heavy metals [1]. The consumption of water with high amounts of calcium and magnesium (sample 9) could cause deposition of salts (kidney, bones and gallbladder). Likewise, it is characterized by an unpleasant taste, causing indigestion and deposition of calcium oxalate crystals on the urinary tract [1,13,17].

The content of chloride varies between 11.0-26.0 mg/L. Sources of chloride are disinfectants used in water purification, manure and chemical fertilizers used in agriculture, also irrigation, excessive use of groundwater, infiltration of wastewaters, leakage from waste deposits, the interaction of water with the geological layers, degradation of rocks, minerals and soils [6, 13, 19, 20, 24, 27]. High amount of chloride increases the electrical conductivity and implicitly the capacity of water corrosion [12]. Chloride reacts with the metallic ions from the pipeline system forming soluble salts which increases the amounts of metals in the drinking water [18, 24]. Water rich in chloride induces laxative effects [12].

Carbonate varies between 0.01 and 58.0 mg/L. The presence of carbonates in groundwater used as drinking water sources (water well) is due to the interaction of water with degraded granites and gnais or due to the dissolution of carbonate and carbonic acid silicate minerals [27-29].

Sulphate ranges between 0.39 and 0.88 mg/L and it appears naturally in groundwater by sulphide dissolution (pyrites) [13]. The low amount of sulphate is given by the geological profile, the low amount of sulphurous minerals, the interaction of rain water with soil, nitrates reduction, organic matter, household waste and untreated industrial waste [13, 27, 28]. The presence of sulphate in groundwater is due to the dissolution of sulphate rocks, oxidation of sulphurous minerals or decomposition of animal and vegetal substances which contain sulphur [14].

The variation of pH, alkalinity, dissolved oxygen, organic matter, microorganisms and temperature disturbes the solid-liquid equilibrium between the corrosion scale and water phase; this way iron is released into the drinking water [21, 22]. The hydrolysis of Fe(II) in the presence of dissolved oxygen generates $Fe(OH)_3$, causing water slurry [13]. The determined concentrations of iron in the studied samples are low (0.02-0.03 mg/L), having different sources: the chemical decomposition of ferruginous deposits, rocks, minerals and the dissolution of iron minerals [29].

Table 2. Summary statistics of physico-chemical characteristics of the analysed groundwaters

Statistical indicator / Parameter	Average	Standard deviation	Min	Max	Coeff. variation %	Guideline value*	Parametric value**
Depth, cm	485	305	260	1180	62.9	-	-
Water level, cm	356	190	220	800	53.3	-	-
Turbidity, NTU	1.52	0.37	0.99	2.08	24.3	5.0	5.0
Temperature, °C	17.7	1.61	15.5	19.9	9.10	-	-
Electrical conductivity, µS/cm	595	87.7	463	786	14.7	2500	2500
pH	7.47	0.26	7.12	7.97	3.53	6.5-8.5	9.5
Redox potential, mV	-31.4	15.49	-60.4	-11.6	-49.2	-	-
Dissolved oxygen, mg/L	4.20	2.01	2.27	9.10	47.9	-	-
Oxygen saturation, %	44.7	20.6	23.8	92.8	45.9	-	-
Ammonium, mg/L	1.76	0.48	1.09	2.38	27.0	35	0.5
Nitrate, mg/L	30.2	14.1	9.87	55.6	46.7	50	50
Nitrite, mg/L	0.002	0.001	<QL***	0.004	63.0	3.0	0.5
Bicarbonate, mg/L	195	48.4	122	305	24.8	-	-
Carbonate, mg/L	5.80	18.3	<QL	58.0	316	-	-
Sulphate, mg/L	0.67	0.17	0.39	0.93	24.7	250	250
Chloride, mg/L	16.6	4.57	11.0	26.0	27.6	-	250
Iron, mg/L	0.02	0.003	0.02	0.03	11.0	-	0.2
Cooper, mg/L	0.01	0.01	<QL***	0.02	65.7	2.0	2.0
Phosphate, mg/L	0.21	0.22	0.06	0.78	105	-	-
Total hardness, °G	11.0	3.81	7.2	19.3	34.5	-	5.0

**guideline value according to the WHO Guidelines for drinking-water quality [30]*
***parametric value, according to the Council Directive 98/83/EC on the quality of water intended for human consumption [31]*
****quantification limit of the method*

Cluster analysis

Cluster analysis is a useful tool in the analysis of hydrochemical data [17, 32, 33]. According to the physico-chemical characteristics, the level and depth of the groundwater collected from water wells were classified in two homogenous clusters: C1 and C2. Figure 1 indicates the dendrogram of the analysed samples. C1 comprises six samples with low and medium level and depth and also with medium values of the total hardness and HCO_3^-, while C2 contains the samples characterized by higher values of total hardness, PO_4^{3-} and lower dephts. The groundwater samples grouped in C1 are located in the western part of the locality except for sample 3, while cluster C2 comprises mainly the groundwater samples located in the eastern part of Remeți locality (close to Tisa River).

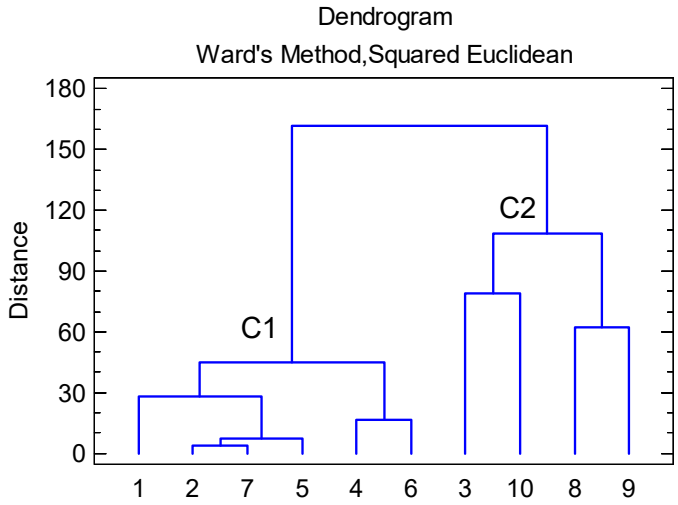

Figure 1. Cluster analysis of groundwater samples based on the physico-chemical characteristics

The Water Quality Index (WQI)

The WQI was calculated for eleven physico-chemical parameters (n=11). The values calculated for the weightage factor corresponding for each indicator are $w_{i\ pH}$=0.11; $w_{i\ EC}$=0.0004; $w_{i\ NH4,\ NO2}$=2.0; $w_{i\ total\ hardness,\ NO3,\ turbidity}$ =0.2; $w_{i\ NO3}$ =0.02; $w_{i\ Cl,\ SO4}$ =0.004; $w_{i\ Fe}$ =5.0; $w_{i\ Cu}$ =10 and $w_{i\ Fe}$ =5.0. According to the WQI results, the studied groundwater samples are characterized with good and excellent quality. Samples characterized by good quality vary between 57.1 and 65.1, while samples characterized by excellent quality range between 27.7 and 49.8 (Figure 2).

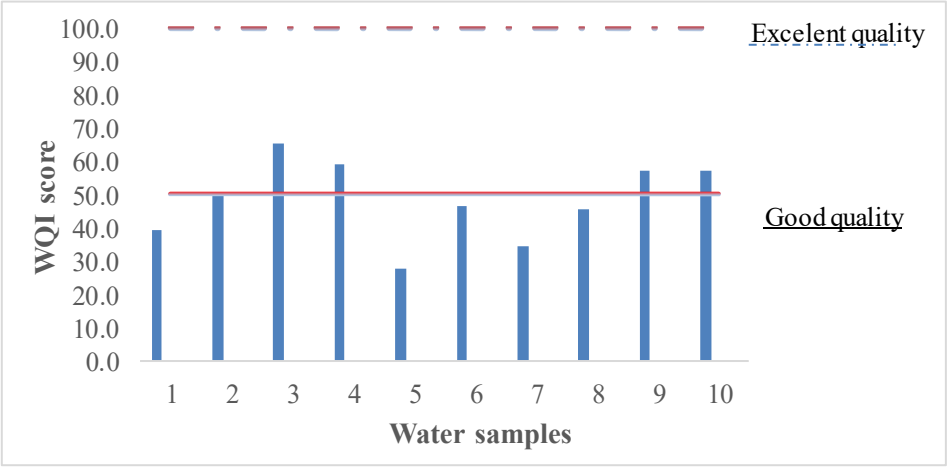

Figure 2. The water quality classification according to the WQI scores

The highest score was obtained for sample 3, followed by samples 4>10>9>2>6>8>1>7>5. The highest score obtained for sample 3 is correlated with the high amount of nitrate (55.6 mg/L) and ammonium (2.38 mg/L); the concentrations exceed the parametric values established by the Council Directive 98/83/EC (50 mg/L NO_3^- and 0.5 mg/L NH_4^+). The WQI scores for samples 4, 9 and 10 are correlated with the high amounts of nitrate, ammonium and values of the total hardness.

Other studies conducted in Romania indicate good to excellent quality as well, with values ranging from 24.1 to 89.8 in the southeastern part of the country (Dobrogea). Excellent, good, poor and very poor quality were determined in the northwestern part of the country (Maramures County) with values ranging from 5.7 to 97.2. The poor quality was due to the high concentrations of nitrates, nitrites and iron [17, 34]. In the central-eastern part of the country, groundwater used as drinking water sources collected from water wells was characterized by excellent and good, poor quality. The WQI scores ranged between 2.4 and 75.0 [35]. At international level, groundwater is characterized by different quality categories, such as poor, good and excellent in Burdur, Turkey (WQI ranging between 17.4-111) [36]. Unsuitable water for drinking, very poor, poor and good quality of waters were determined in Delhi, India (WQI: 50-300) and in Guanzhong Basin, China (WQI: 21.1-967) [37-38].

CONCLUSION

Temperature, dissolved oxygen, oxygen saturation, pH, and phosphate levels all increase with depth, while nitrate levels fall. All water samples have low turbidity with normal total hardness levels (except for sample 9, which has a relatively high total hardness). The chloride, sulphate, iron, and cooper contents and the electrical conductivity values are below the guideline and parametric values.

Cluster analysis indicated two groups of similarity. The first cluster contains the groundwater samples situated in the eastern part of the locality, characterized by low depth. The second cluster consists of the samples localized in the western part of the locality, characterized by high depths and high values of the total hardness (due to the rock weathering processes).

The data regarding the water composition are useful for a more efficient water management. The rise in nutrient levels (ammonium, nitrate and phosphate) could be limited by applying a rational use of chemical fertilizers and by improving the protection areas.

According to the WQI, the studied samples are characterized as waters with generally excellent and good quality. The good quality is correlated with the high amount of nitrate and ammonium.

The novelty of this paper consists in the presentation of groundwater characteristics in relation to the anthropogenic pressure on the water wells situated nearby the Tisa River protected area. A sustainable economic development needs systematic and careful observation of the anthropogenic actions' effects on the environment, especially in protected areas, as a support for rational natural resources management.

EXPERIMENTAL SECTION

Sampling location

Remeți locality is situated in the alluvial plain of Tisa River, a part of this area being protected at national and international level (part of Natura 2000 Tisa Superioara site), as it contains habitats with a significant biodiversity of important fauna and flora. Studying the groundwater quality from this area could protect the health of the inhabitants using it for drinking purposes and the possible anthropogenic pressures on the ecosystems from the site could be minimized or even stopped.

The groundwater samples were collected from Remeți, a village located in the Tisa meadow near the border with Ukraine, presented in Figure 3. Data regarding the depth of the water wells was obtained by measuring the water

well on the levels, while the level of water was determined with the help of a tape meter tool, by measuring the distance from the bottom to the surface of the water.

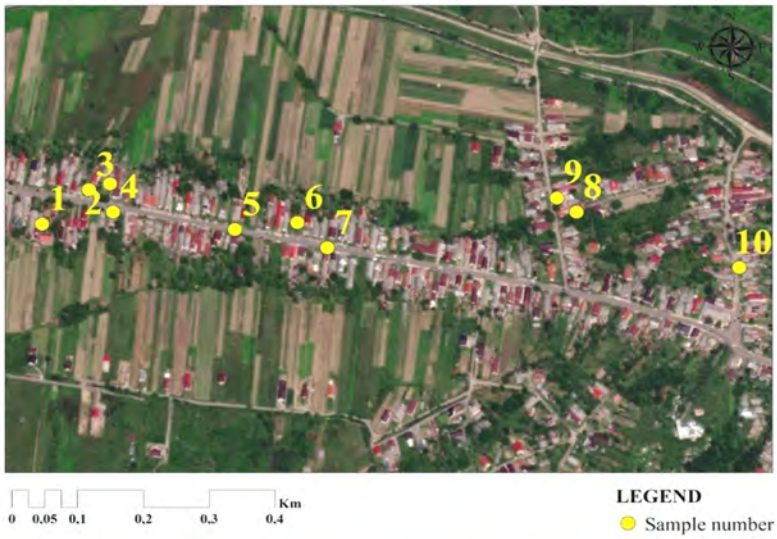

Figure 3. Localization of groundwater samples collected from water wells from Remeți locality

Groundwater bodies in the village of Remeți, which is located in the floodplain of the Tisa river and along its tributary, Remeți, have developed into permeable alluvial deposits of recent age (Quaternary) [23].

Water sample collection and analysis

A number of 10 groundwater samples were collected in September of 2020 from open private water wells.

The sampling was performed in clean polypropylene bottles (500 mL). Part of the physico-chemical analyses were performed on the field (pH, electrical conductivity, redox potential) and part in the laboratory. The determination of pH was performed according to SR ISO 10523/2012, the redox potential according to SR ISO 10523/2012, the dissolved oxygen and oxygen saturation according to SR EN ISO 5814:2013, the ammonium concentration according to SR ISO 7150-1/2001, the nitrate concentration according to SR ISO 7890-3/2000 employing Hach Lange HQ40d portable

equipment. The nitrite concentrations were determined in accordance with SR ISO 6777/2002, the phosphates following STAS 3265-86, the iron following SR ISO 6332:1996, the copper following SR ISO 8288/2001, the total alkalinity with SE EN ISO 9963-1/1996, employing a Hach Lange SL1000 portable equipment [3]. Total hardness of water consists in the joint determination of Ca and Mg cations by their complexometric titration with the sodium salt of ethylenediamine tetraacetic acid (Na_2EDTA) in the presence of the metallochrome indicator Eriochrome Black T and of a pH buffer (to 10.1) according to a standardized method (STAS 7313 – 82). Sulphates are analysed by a turbidimetric method based on the precipitation of sulfate anions (barium sulphates) by adding barium chloride reagent, according to the EPA method [39]. The absorbances of the resulted suspensions are measured at 420 nm with a Perkin Elmer Lambda 25 spectrophotometer. The equipment was calibrated with standard sulphate solutions. Chlorides were determined by precipitation titration against $AgNO_3$, according to the ISO 9297-2001 standard.

Cluster analysis

The data regarding the physico-chemical parameters of groundwater samples are subjected to cluster analysis in order to classify the groundwater samples using the Ward's grouping method and squared Euclidean distance between the observations (the analysed groundwater collected from water wells) considering the depth and level of the water wells as variable. Likewise, the analysed physico-chemical parameters (except the degree of oxygen saturation and the redox potential) were correlated to the dissolved oxygen and pH. Cluster analysis is applyied by using Statgraphic software, used also for the statistical determinations (standardized skewness and kurtosis).

The Water Quality Index (WQI)

The WQI represents a rating, indicating the composition influence of a series of physico-chemical indicators [40]. The calculation of the WQI involves three steps: ***1.*** the calculation of the weightage factor (w_i) for each physico-chemical parameter, ***2.*** the determination of the quality rating scale (Q_i) and ***3.*** the calculation of the WQI [41]. The following equations [eq 1-3] are used in order to determine the WQI, based on the studies of Das Kangabam et al., Babu et al., Srinivas et al. and Goher et al. [41-44]:

$$w_i = \frac{1}{p_v} \quad \text{[eq1]}$$

where w_i and p_v are the weightage factor of each physico-chemical parameter, 1.0 is a proportionality constant, according to Babu et al. (2006), Srinivas et al (2011) and Goher et al. (2014), while p_v is the parametric value established by the Council Directive for the drinking water, indicated in Table 3 [42-44].

$$Q_i = [\frac{C_i - V_i}{p_v - V_i}] \times 100 \quad \text{[eq2]}$$

$$WQI = \frac{\sum_{i=1}^{n}(Q_i \times w_i)}{\sum_{i=1}^{n} w_i} \quad \text{[eq3]}$$

where Q_i is the quality rating scale, C_i is the measured values of each physico-chemical parameters, V_i is the ideal value of the chemical indicator ($V_i=0$ for all applied indicators except for pH, V_{ipH}=7) and n (n=11 in the current study) is the total number of the used indicators [41].

Results are expressed in numerical scores (0-100) indicating the quality status of the studied water. There are five quality classes, namely unsuitable for drinking (WQI>300), water with very poor quality (WQI: 200-300), poor quality (WQI: 100-200), good quality (WQI: 50-100) and excellent quality (WQI<50) [40].

Table 3. The physico-chemical indicators used in the calculation of WQI, the used parametric values, the weight and the variation of the rating scale

Physico-chemical indicator	Unit	Parametric value (p_v)*	Weight (w_i)**	Variation of Q***
pH	-	9.5	0.11	4.80-38.8
Electrical conductivity	µS/cm	2500	$4*10^{-4}$	18.5-31.4
Ammonium	mg/L	0.5	2.00	218-476
Total hardness	°G	5.0	0.20	144-386
Turbidity	NTU	5.0	0.20	19.8-41.6
Nitrite	mg/L	0.5	2.00	0.00-0.80
Nitrate	mg/L	50	0.02	32.4-111
Chloride	mg/L	250	$4*10^{-3}$	4.40-10.4
Sulphate	mg/L	250	$4*10^{-3}$	0.16-0.35
Iron	mg/L	0.2	5.00	9.00-13.5
Cooper	mg/L	2.0	10.0	0.00-20.0

**according to the Council Directive 98/83/EC [31]*
***according to Das Kangabam et. al [41]*
****the rating scale for each physico-chemical indicator [41]*

For the calculation of the WQI in the present study, eleven physico-chemical indicators are considered: pH, electrical conductivity, total hardness, turbidity, ammonium, nitrite, nitrate, chloride, sulphate, iron and cooper and the parametric values proposed by the Council Directive 98/83/EC regarding the quality of water intended for human consumption (Table 3).

REFERENCES

1. A.H. Jagaba; N.M.Y. Almahbashi; *Ain Shams Eng J*, **2020**, *11*, 983-999.
2. O.N. Sila; *Scientific African*, **2019**, *2*, e00018.
3. T. Dippong; C. Mihali; E. Cical; *Metode de determinare a proprietăților fizico-chimice ale alimentelor*, Risoprint Cluj-Napoca, Romania, **2016**.
4. R. Mihaiescu, *Monitoringul integrat al mediului*, Cluj-Napoca, Romania, **2014**.
5. J. Gentry-Shields; J. Bartram; *Sci Total Environ*, **2014**, *468-469*, 306-314.
6. G. Hanrahan; Surface and Groundwater monitoring. In *Key concepts in Environmental Chemistry*, Academic Press, Elservier, Amsterdam, **2012**, pp. 109-152**.**
7. N. Adimalla; H. Qian; M.J. Nandan; *Ecotoxicol Environ Saf*, **2020**, *206*, 111217.
8. O. Iacob; A. Tudor; A. Neamţu; A. Cristea; *Apa de fântână: contaminarea cu nitraţi şi methemoglobinemia Ghid pentru medici de familie, medici igienişti DSP şi populaţie*. Universitara Press, Bucureşti, Romania, **2012**.
9. A. Racariu; A. Urzica; C. Stoleriu; East Europ *J Geograph Info Systems Remote Sensing*, **2018**, *2*.
10. K.P Singh; S. Gupta; D. Mohan; *J Hydrol*, **2014**, *511,* 254-266.
11. V.A. Nemtinov; Y.V. Nemtinov; A.B. Borisenko; K.V. Nemtinov; *J Geochem Explor*, **2014**, *147*, 46-51.
12. I.N. Karthika; K. Thara; M.S. Dheenadayalan; *Mater Today: Proceedings*, **2018**, *5*, 422–428.
13. T.A. Adesakin; A.T. Oyewale; U. Bayero; A.N. Mohammed; I.A. Aduwo; P.Z. Ahmed; N.D. Abubakar; I.B. Barje; *Heliyon*, **2020**, *6*, e04779.
14. H. Çadraku; F. Gashi; A. Shala; O. Fetoshi; *IFAC-PapersOnLine*, **2016**, *49-29*, 200–205.
15. M. Surpateanu; *Elemente de chimia mediului*, MatrixRom, Bucuresti, Romania, **2004**.
16. J. Liu; Y. Peng; C. Li; Z. Gao; S. Chen; *J Clean Prod*, **2021**, *282,*125416.
17. T. Dippong; C. Mihali; M.A. Hoaghia; E. Cical; A. Cosma; *Ecotox Environ Saf*, **2019**, *168*, 88-101.
18. O. Cadar; M. Miclean; S. Cadar; C. Tanaselia; L. Senila; M. Senila; *Environ Eng Manag J*, **2015**, *14*, 2523-2528.
19. M.K. Samantara; R.K. Padhi; M. Sowmya; P. Kumaran; K.K. Satpathy; *Groundw Sustain Dev*, **2017**, *5*, 49–58.

20. M. Kumar; A. Puri; *J Occup Environ Med*, **2012**, *16*, 40.
21. F. Yang; B. Shi; J. Gu; D. Wang; M. Yang; *Water Resear*, **2012**, *46*, 5423-5433.
22. C-Y. Peng; G. V. Korshin; L. Richard; R. L Valentine; A. S. Hill; M. J. Friedman; H. Steve; S. H. Reiber; *Water Resear*, **2010**, *44*, 4570-4580.
23. G. Şerban; D. Sabău; R. Bătinaș; P. Brețcan; E. Ignat;S. Nacu; Water resources from Romanian Upper Tisa Basin. In *Water Resour Manag Romania*, **2020**, 393-436.
24. S. Sargazi; M. Mokhtari; M.H. Ehrampoush; S.A. Almodaresi; H. Sargazi; M. Sarhadi; *Groundw Sustain Dev*, **2021**, *12*, 100509.
25. R. Arulnangai; M.M. Sihabudeen; P.A. Vivekanand; P. Kamaraj; *Mater Today: Proceedings*, **2021**, *36*, 923-928.
26. J.L. Domagalski; H. Johnson; Studies by the U.S. Geological Survey on sources, transport, and fate of agricultural chemicals, U. S. Geological Survey Fact Sheet **2012**.
27. N. Zakaria; G. Anornu; D. Adomako; F. Owusu-Nimo; A. Gibrilla; *Groundw Sustain Dev*, **2021**, *12*, 100489.
28. A. Ramachandran; K. Sivakumar; A. Shanmugasundharam; U. Sangunathan; R.R. Krishnamurthy; *Acta Ecologica Sinica,* **2020**.
29. A.M. Masoud; M.H. Ali; *J African Earth Sci,* **2020**, *172*, 103982.
30. WHO, **2017**, Guidelines for drinking-water quality, 4th ed. Incorporating first addendum. World Health Organization, Geneva, Switzerland. https://www.who.int/publications/i/item/9789241549950 (accessed on 14 January 2021).
31. Council Directive 98/83/EC of 3 November 1998 on the quality of water intended for human consumption. https://eur-lex.europa.eu/legal-content/EN/TXT/PDF/?uri=CELEX:31998L0083&from=EN (accessed on 03 December 2020).
32. J. Wu; P. Li; H. Qian; *Environ Earth Sci*, **2015**, *73*, 8575–8588.
33. A. Nagaraju; A. Thejaswi; Y. Sreedhar; *Earth Sci Resear J*, **2016**, *20*, E1-E7.
34. A. Moldovan; M.-A. Hoaghia; E. Kovacs; I.C. Mirea; M. Kenesz; R.A. Arghir; A. Petculescu; E.A. Levei; O.T. Moldovan; *Water*, **2020**, *12*, 3510.
35. C.A. Roba; I.C. Pistea; E. Neagoe; A.O. Matei; C. Rosu; *Sci Paper Series Manag, Econ Eng Agriculure Rural Dev*, **2019**, *19*, 491-496.
36. S. Varol; A. Davraz; *Environ Earth Sci*, **2014**, *73*, 1725-1744.
37. S. Acharya; S.K. Sharma; V. Khandegar; *Data in Brief*, **2018**, *18*, 2019-2028.
38. Q. Zhang; P. Xu; H. Qian; *Expos Health*, **2020**, *12*, 487-500.
39. US EPA, **1979** Sulfate (turbidimetric). Method 375.4, Methods for the Chemical Analysis of Water and Wastes, EPA/600/4–79/020. US Environmental Protection Agency, Washington DC, USA
40. S. Singh; A. Hussian; *Cogent Eng*, **2016**, *3*.
41. R. Das Kangabam; S.D. Bhoominathan; S. Kanagaraj; M. Govindaraju; *Appl Water Sci*, **2017**, *7*, 2907-2918.
42. R.C. Babu; R. Chandana; O.S.S. Sudarsana, T. Rao; J. Suresh Kumar; *Nat Environ Pollut Technol,* **2006**, *5*, 203-207.

43. P. Srinivas; G.N. Pradeep Kumar; A. Srinivasa Prasad; T. Hemalatha; *Civil Environ Res*, **2011**, *1*, 9-20.
44. M.E. Goher; A.M. Hassan; I.A. Abdel-Moniem; A.H. Fahmy; S.M. El-sayed; *Egypt J Aquat Res*, **2014**, *40*, 225-233.

STUDIA UBB CHEMIA, LXVI, 2, 2021 (p. 213-220)
(RECOMMENDED CITATION)
DOI:10.24193/subbchem.2021.2.18

NUTRIENT AND ORGANIC MATTER REMOVAL FROM CHICKEN MANURE LEACHATE USING *CHLORELLA* SPP.

ZAMFIRA DINCĂ[a], MARIA-ALEXANDRA HOAGHIA[a], ANAMARIA-IULIA TÖRÖK[a], ENIKO KOVACS[a,b], OANA CADAR[a], EMILIA NEAG[a]*, CECILIA ROMAN[a]

ABSTRACT. In the present study, the use of chicken manure leachate (CML) as a nutrient source for the cultivation of *Chlorella* spp. at laboratory scale was investigated. The concentration of total organic carbon (TOC) and biochemical oxygen demand (BOD) was monitored during 15 days of cultivation in CML. The changes of pH, conductivity, Cl^-, PO_4^{3-}, SO_4^{2-}, NO_2^- and NO_3^- concentrations were measured during the growth period. The BOD and TOC reduction was 96.4% and 86.1%, respectively after 15 days of cultivation in CML. The *Chlorella* spp. biomass cultured in CML had a high protein content compared to the biomass grown in the BG-11 medium. The obtained results suggest the potential use of CML as a nutrient source for the growth of *Chlorella* spp.

Keywords: *biomass, chicken manure, microalgae*

INTRODUCTION

The poultry production industry generates large quantities of wastes worldwide. Manure, litter, on-farm mortalities, and hatchery wastes tend to grow if we consider the fivefold increase in poultry production from the last 50 years [1]. With an annual production of 13.3 million tons, the EU is one of the world's leading producers of poultry meat [2]. This exponential growth of the poultry production sector brings into question the issue about the fate of poultry wastes and the disposal ways and strategies [3].

[a] *INCDO-INOE 2000, Research Institute for Analytical Instrumentation, 67 Donath Street, 400293 Cluj-Napoca, Romania*

[b] *University of Agricultural Sciences and Veterinary Medicine, 3-5 Calea Manastur Street, 400372 Cluj-Napoca, Romania*

** Corresponding author: emilia.neag@icia.ro*

Poor waste management in the poultry industry can lead over time to pollution and environmental problems, like eutrophication [4]. Increased GHG emissions, deforestation and biodiversity loss are all significant issues that the intensive poultry industry causes [5]. Leachate from poultry manure reach the soil, surface or groundwater causing nitrates and phosphates pollution and environmental contamination with pathogens, such as *Enterobacteriaceae* or *Staphylococcaceae* [6]. For this reason, the proper treatment of poultry wastes prior to discharge, as well as the environmentally sustainable management of poultry manure are required. Converting chicken manure from a waste product to a resource is one of the environmentally sustainable measures that can be taken [3].

Chicken manure is rich in both organic and inorganic nutrients and contains high concentrations of nitrogen (eliminated in the form of uric acid), high carbon content, phosphate and potassium [6-8]. Moreover, it contains trace elements, such as Fe, Mg, Mn, S and Zn for the growth of microalgae [3]. The nutrient composition of poultry manure depends on the age and diet of the flock, the age of the manure and its moisture content [9]. Because of its complex content, chicken manure has a wide range of applications, from its rational application as biofertilizer or as a culture medium for autotrophic organisms, to the production of biogas or bioethanol [10-12]. The use of nutrients from livestock manure for microalgal biomass production received worldwide interest [4], even if there is a lack of information related to the suitability of chicken manure to sustain microalgae growth [3].

Several microalgae species, such as *Chlorella* spp. or *Scenedesmus obliquus* are considered proper candidates for cultivation in a manure extract medium, due to their rapid adaptation to various nutritional conditions [3]. Many synthetic culture media are expensive and depletable resources. In addition to the nutritional advantage, the growing medium obtained from chicken manure has an economic and eco-friendly impact on the environment [13].

The purpose of this study was to determine the ability of *Chlorella* spp. to grow in nutrient-rich sources, such as chicken manure leachate and to reduce the organic matter concentrations.

RESULTS AND DISCUSSION

Growth of *Chlorella* spp. in CML

Figure 1a and 1b illustrate the pH and conductivity changes, respectively. pH values fluctuate within a tight range during the *Chlorella* spp. cultivation. The obtained data revealed that the pH values (8.2-8.4) slowly increased

during cultivation. The intracellular metabolic fluxes in algal cells increase the pH during their photosynthesis, following the CO_2 assimilation [14]. During the cultivation of *Chlorella* spp., the electric conductivity (EC) values slowly decreased by time (Figure 1b).

The TOC and BOD reduction during the cultivation of *Chlorella* spp. can be observed in Figure 1c and 1d, respectively. The TOC and BOD reduction increased with time. The changes in the TOC reduction ranged between 75% and 86%, while for BOD between 81% and 96% during 15 days of cultivation, showing that the amount of oxidizable pollutants in the water samples was removed with time by the microalgae biomass.

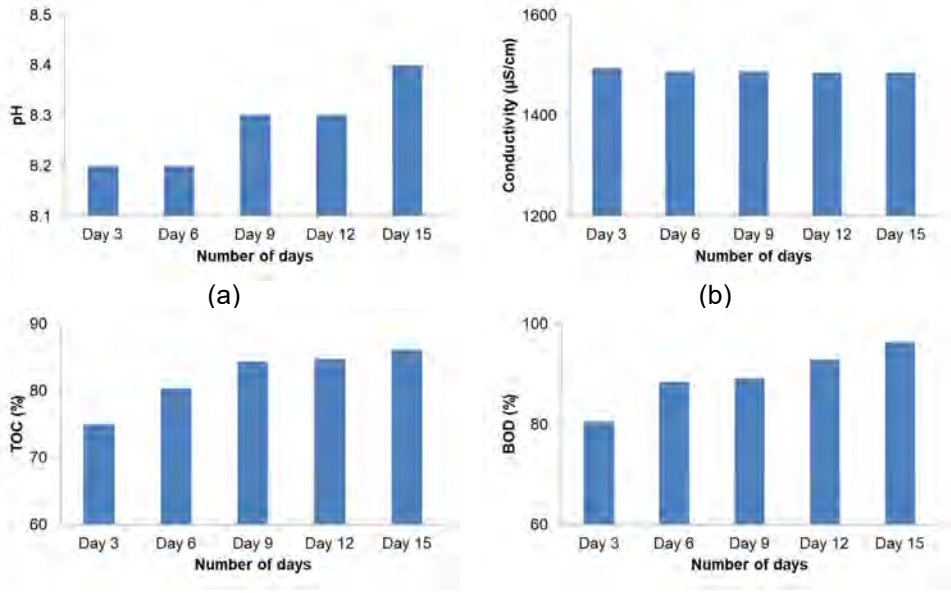

Figure 1. The pH and conductivity changes, and TOC and BOD reduction during the cultivation of *Chlorella* spp. in CML

The variation of Cl^-, PO_4^{3-}, SO_4^{2-}, NO_2^-, and NO_3^- concentrations throughout the growth of *Chlorella* spp. in CML is presented in Table 1.

The Cl^- concentration remained almost constant during the cultivation period. At the beginning of the experiment, the PO_4^{3-} concentration was 109 mg/L. Notably, the PO_4^{3-} concentration decreased considerably to 74 mg/L (3 day of cultivation), and then slowly increased up to 94.2 mg/L (day 15). Similar observations, in the case of phosphorus, were previously reported using activated sludge or bacteria [15]. Some bacteria possess the ability to assimilate and store the phosphate (as polyphosphates) under aerobic conditions. Under anaerobic conditions, the phosphate is released into the medium [15].

Table 1. Variation of Cl^-, PO_4^{3-}, SO_4^{2-}, NO_2^-, and NO_3^- concentrations throughout the growth of *Chlorella* spp. in CML

Element (mg/L)	Day 3	Day 6	Day 9	Day 12	Day 15
Cl^-	34.2	34.2	34.0	33.8	33.4
PO_4^{3-}	74.0	78.0	88.2	90.8	94.2
SO_4^{2-}	40.0	40.2	41.6	42.2	42.8
NO_2^-	<0.05	<0.05	<0.05	<0.05	<0.05
NO_3^-	2.40	1.14	1.16	1.10	1.02

The SO_4^{2-} concentration showed a slight increase from 31.3 mg/L to 42.8 mg/L (day 15). During the microalgae growth, the NO_2^- concentration was below the analytical method's measuring range level (<0.05 mg/L), while the concentration of NO_3^- increased. The increase of NO_3^- concentration during the cultivation period indicates the presence of nitrifying microorganisms [16]. A similar trend was reported previously by Vargas et al. [16], when the capability of a consortium of nitrifying bacteria and microalgae to tolerate low dissolved oxygen concentrations using aerobic sludge from wastewater treatment plants was investigated [16]. Nitrogen is an essential component to living organisms and can be found at different oxidation states. Nitrogen is converted into NH_4^+, which is generated by a reduction process. Further, NH_4^+ is converted to nitrite (NO_2^-) by nitrifying bacteria and then to nitrate (NO_3^-) [17,18].

Elemental composition

The carbon (C), hydrogen (H), nitrogen (N) sulphur (S) and oxygen (O) content of biomass obtained after 15 days of cultivation can be seen in Table 2.

Table 2. The elemental composition of biomass obtained after 15 days of cultivation in CML

		N (%)	C (%)	H (%)	O (%)	C/N	Protein (%)
Control		7.38	42.32	6.04	44.25	5.74	46.12
CML	**day 3**	11.97	42.18	6.32	39.52	3.52	74.79
	day 6	10.77	44.16	6.39	38.66	4.10	67.33
	day 9	9.92	45.16	6.23	38.67	4.55	62.02
	day 12	10.14	44.52	6.47	38.85	4.39	63.38
	day 15	9.99	45.69	6.30	38.01	4.58	62.41

After the treatment of CML, high N and C contents were found in the microalgal biomass when compared with the control biomass. During the cultivation period, the N and C contents ranged from 9.92 to 11.97% and from 42.18 to 45.69%, respectively. The H content remained constant, around 6.0-6.9%, while the S content was below 0.01%. The O content slowly decreased during the cultivation in CML.

Changes in protein contents were observed during the cultivation period. High protein contents were obtained in the biomass grown in CML in comparison with the control biomass (46.12%). A maximum protein content of 74.79% (day 3) was obtained. On days 9, 12 and 15, the protein content of microalgal biomass was in average 62.6%. Nitrogen is mainly associated with proteins [19]. Generally, *Chlorella* contains high protein contents around 42-58 % (dry weight) [20], that are similar to the values found in *Chlorella pyrenoidosa* (57%) and *Chlorella vulgaris* (51-58%) [21]. The C/N ratio is an indicator for bioconversion reactions [22]. The control biomass had a C/N ratio of 5.74, while the biomass grown in CML had poor C/N ratios. The C/N ratio varied from 3.52 to 4.58 in the biomass grown in CML. The obtained results are in good agreement with those reported previously for *Chlorella* sp. (44.5% C, 6.2% H, 9.6% N and a C/N ratio of 4.63) [22].

CONCLUSIONS

Chlorella spp. was grown in a nutrient-rich medium, namely in CML. Preliminary investigations showed that, during the growth period, a decrease of BOD and TOC concentrations was observed, indicating that the microalgal biomass used the carbon source from the CML for their growth, while the aerobic microorganisms were able to break down the organic material from the medium. When compared with the control biomass, cultivation in CML medium increased protein accumulation in the microalgal biomass. Further investigations on the microalgal adaptation to CML conditions are needed in order to better understand the process involved during the assimilation of the nutrients available in the growth medium.

EXPERIMENTAL SECTION

Poultry manure extract

200 g of chicken manure were immersed in 2000 mL distilled water, stirred gently at room temperature for 24 h and filtered using Whatman filter paper to remove the non-soluble particles. The resulting CML was used for the cultivation of *Chlorella* spp. The main characteristics of CML are shown in Table 3.

Table 3. Characteristics of CML used for *Chlorella* spp. cultivation

Parameter	Units	CML
pH		6.80
Conductivity	µS/cm	907
BOD	mgO_2/L	422
TOC	mg/L	448
Cl^-	mg/L	34.2
PO_4^{3-}	mg/L	109
SO_4^{2-}	mg/L	31.3
NO_2^-	mg/L	0.05
NO_3^-	mg/L	0.20

Experiment design

Chlorella spp. was inoculated at 1:10 (v/v) ratio in CML and BG-11 medium. The cultures grown in BG-11 medium were considered the control samples. The cultivation in CLM and BG-11 medium was carried out for 15 days at a temperature of 25±1°C, under artificial illumination of 1200 lux for 12/12 h day/night cycle, at laboratory scale.

Analysis

Prior to the analysis, the samples were filtered to remove the *Chlorella* spp. cells. pH and conductivity of the culture medium throughout the growth period (day 3, 6, 9, 12 and 15) were determined using a Seven Excellence multiparameter, Mettler Toledo, Switzerland. BOD was determined using an oxygen meter WTW, INOLAB 740 electrode with StirrOxG sensor, while TOC values were determined using a multi N/C 2100S Analytik Jena analyzer.

The concentrations of Cl^-, PO_4^{3-}, SO_4^{2-}, NO_2^- and NO_3^- were analyzed with an ion chromatograph (761 IC, Metrohm, Switzerland) after the filtration of the samples with 0.45 µm cellulose acetate membrane filters and dilution with ultrapure water. Quality assurance was performed by measuring the standard solutions with known concentrations supplied by Merck, blanks and two to three replicates. The C, H, N and S content of biomass was determined by a Flash EA 2000 CHNS/O analyzer (Thermo Fisher Scientific, USA). The O content was determined by difference and the protein content was calculated using the nitrogen-to-protein conversion factor.

ACKNOWLEDGMENTS

This work was funded by the Core Program, under the support of ANCS, project no. PN 19-18.01.01 (contract no. 18N/08.02.2019). The funder had no role in the design of the study; in the collection, analysis and interpretation of data; in the writing of the manuscript, and in the decision to submit the article for publication.

REFERENCES

1. FAO, 2018 http://www.fao.org/3/I8153EN/i8153en.pdf
2. Eurostat, 2020 https://ec.europa.eu/eurostat/statistics-explained/index.php?title=Agricultural_production_-_livestock_and_meat&oldid=470510#Poultry
3. X.T. Han; N. Rusconi; P. Ali; K. Pagkatipunan; F. Chen; *Green and Sustainable Chemistry*, **2017**, *7*, 101-113
4. H.M. Singh; V.V. Tyagi; R. Kothari; R. Azam; P.S. Slathia; B. Singh; *Bioresour. Technol.*, **2020**, *316*, 123850
5. P. Smith et al. How much land-based greenhouse gas mitigation can be achieved without compromising food security and environmental goals?, In *Global Change Biology*, John Wiley & Sons Ltd, 2013, Volume 19, Issue 8, pp. 2285-2302
6. Y. Alba Reyes; E.L. Barrera; K.-k. Cheng; *J. Environ. Chem. Eng.*, **2021**, *9*, 104695
7. G. Markou; F. Monlau; Nutrient recycling for sustainable production of algal biofuels, in Biomass, Biofuels, Biochemicals, Biofuels from Algae (Second Edition), A. Pandey, J.-S. Chang, C.R. Soccol, D.-J. Lee, Y. Chisti Eds.; Elsevier, 2019, Chapter 6, pp. 109-133
8. A.J. Ashworth; J.P. Chastain; P.A. Moore Jr.; Nutrient Characteristics of Poultry Manure and Litter, in *Animal Manure: Production, Characteristics, Environmental Concerns, and Management*, Volume 67, H.M. Waldrip, P.H. Pagliari, Z. He Eds.; American Society of Agronomy, Inc. Soil Science Society of America, Inc., 2020, pp. 63-87
9. M.M. Amanullah; S. Sekar; P. Muthukrishnan; *Asian Journal of Plant Sciences,* **2010**, *9,* 172-182
10. R. Li; N. Duan; Y. Zhang; Z. Liu; B. Li; D. Zhang; H. Lu; T. Dong; *Waste Manage.*, **2017**, 70, 247-254,
11. T. Moungmoon; C. Chaichana; C. Pumas; W. Pathom-aree; K. Ruangrit; J. Pekkoh; *Sci. Total Environ.*, **2020**, *714*, 136577
12. R. Malolan; R.S.Jayaraman; S. Adithya; J. Arun; K.P. Gopinath; P.S. Sundar Rajan; O. Nasif; W. Kim; M. Govarthanan; *Chemosphere*, **2021**, *266*,128963

13. M. Altunoz; O. Pirrotta; L. Forti; G. Allesina; S. Pedrazzi; O. Obali; P. Tartarini; L. Arru; *Bioresour. Technol.*, **2017**, *244*, Part 2, 1261-1268
14. S.S.M. Mostafa; E.A. Shalaby; G.I. Mahmoud, *Not. Sci. Biol.*, 2**012**, *4*(1), 56-65
15. S. Zhu; L. Qin; P. Feng; C. Shang; Z. Wang; Z. Yuan; *Bioresour. Technol.*, **2019**, *274*, 313-320.
16. G. Vargas; A. Donoso-Bravo; C. Vergara; G. Ruiz-Filippi, *Electron. J. Biotechnol.,* **2016**, *23*, 63-68.
17. A. Kumar; S. Bera, *Bioresour. Technol. Rep*., **2020**, *12*, 100584.
18. M. Holtappels; G. Lavik; M.M. Jensen; M.M.M. Kuypers; 15N-Labeling Experiments to Dissect the Contributions of Heterotrophic Denitrification and Anammox to Nitrogen Removal in the OMZ Waters of the Ocean, in *Methods in Enzymology;* M. G. Klotz Ed.; Academic Press, 2011, Chapter 10, Volume 486, pp. 223-251
19. A. Sánchez-Bayo; V. Morales; R. Rodríguez; G. Vicente Crespo; L. F. Bautista; *Preprints,* **2019**, 110108, doi: 10.20944/preprints201911.0108.v1.
20. U.D. Enyidi; *Fishes,* **2017**, *2*, 17.
21. T. Bito; E. Okumura; M. Fujishima; F. Watanabe; *Nutrients*., **2020**, *12*, 2524.
22. L. Rendón-Castrillón; M. Ramírez-Carmona; C. Ocampo-López; R. Giraldo-Aristizabal, *Braz. J. Biol*., **2021**, *81*(1), 202-209.

STUDIA UBB CHEMIA, LXVI, 2, 2021 (p. 221-232)
(RECOMMENDED CITATION)
DOI:10.24193/subbchem.2021.2.19

SUBMICRON AIRBORNE DUST PARTICLE MONITORING SYSTEM

CECILIA ROMAN[a], MARIUS ROMAN[a], LUCIAN DORDAI[a], ENIKO KOVACS[a,b], MARIA-ALEXANDRA HOAGHIA[a], FERENC PUSKAS[c,*]

ABSTRACT. The harmful effects of airborne dust have been long known, with numerous studies proving the danger it poses to human health. The paper presents a submicron size airborne dust particle monitoring system, built in collaboration by a laboratory equipment manufacturer and a national research and development institute. The system is designed for the automotive industry, the printed circuit board production lines, and the environmental monitoring. It can measure and record data continuously and the loss of the supply voltage does not lead to the loss of the monitoring history. The key element is the particle sensor itself, consisting of a laser diode assembly - CCD area, a suction pump with continuous operation, with constant electronically controlled flow and an electro-optical detector. The system is designed with the following specifications: the applicable particle size: 0.3 μm; 0.5 μm; 1.0 μm; sampling time: 1…599 sec; programmable (25 sec. by default); average count setting: 2; 4; 8; 16; 32; 64; ambient temperature range: operating at 40ºC; power: 220V / 50 Hz; power consumption: max. 25 VA; ABS housing, IP rating 54; dimensions (L x W x D): 260 x220 x 156 mm; weight: approximately 2.5 kg.

Keywords: *suspended particulate matter, submicron particle monitoring, air quality, analytical instrumentation*

INTRODUCTION

Particulate matter/suspended particles (PM) or particle pollution is a general term for extremely small particles and liquid droplets existing in the

[a] *INCDO-INOE 2000, Research Institute for Analytical Instrumentation, 67 Donath str., RO-400293, Cluj-Napoca, Romania*
[b] *University of Agricultural Science and Veterinary Medicine, Faculty of Horticulture, 3-5 Calea Manastur Street, RO-400372, Cluj-Napoca, Romania*
[c] *SC ELECTRONIC APRIL, Aparatura Electronica Speciala SRL, 3-5 Louis Pasteur, RO-400349, Cluj-Napoca, Romania*
** Corresponding author: april_private@yahoo.com*

atmosphere [1]. Exposure to particles pollution represents a public health hazard, because after inhaling them, they can travel deep into the lungs and cause or aggravate heart and lung diseases [2,3].

Particulate matter represents a complex group of pollutants that vary in size, shape, composition and origin. They are often separated into three classes: coarse, fine and ultrafine particles. Coarse particles have a diameter ranging between 10 μm and 2.5 μm and settle relatively quickly whereas fine (1 to 2.5 μm in diameter) and ultrafine (<1 μm in diameter) particles remain in suspension for longer. It must be mentioned that PM_{10} (coarse) automatically contains $PM_{2.5}$ (fine) and $PM_{1.0}$ (ultrafine). In addition, $PM_{2.5}$ (fine) contains also $PM_{1.0}$ (ultrafine) and submicron and ultrafine particles (UFPs with diameters below 100 nm).

In most countries, both the legislation in force and the regulations define thresholds and require monitoring only PM_{10} and $PM_{2.5}$ particles as air pollution factors. Even if the more recent ambient air quality legislations tend to include and consider submicron and ultrafine particles (UFPs) as particulate matter to be monitored with reference to standardized limit values, no regulatory action has been adopted yet [1, 4].

Particle size is directly related to the potential to cause adverse effects on human health [5-10]. A serious issue is represented by the particles with an aerodynamic diameter of less than 10 μm, which pass through the nose and throat and enter the alveoli of the lungs causing inflammation and poisoning, affecting especially people with cardiovascular and respiratory diseases, children, the elderly and asthmatics [11-22]. Children under the age of 15 inhale more air, and consequently more pollutants. They breathe faster than adults and tend to inhale more through the mouth, virtually bypassing the natural filter of the nose. They are especially vulnerable because their lungs are not developed, and the lung tissue that develops in childhood is more sensitive. Dust pollution worsens the symptoms of asthma, coughing, chest pain and difficulty of breathing. Long-term exposure, even to low concentrations of suspended particles can cause cancer and premature death.

In response to the airborne dust particles issue, the European Commission has proposed the Clean Air Policy Package aiming to reduce the impacts of harmful emissions from sources like industry, traffic, energy plants and agriculture (all representing particulate matter generation sources) on the human health and the environment [17].

Airborne particulates are responsible for many problems: environmental (reducing atmospheric visibility) and medical problems (respiratory problems, cancer, and heart attacks). In addition, airborne particulates can cause corrosion of metals and electrical equipment, as well as soiling of textiles and building materials [2]. In response to these identified problems, the United States Environmental Protection Agency (EPA) recognized the need of developing

techniques and instruments for the continuous measurement of inhalable particulate matter, such as PM_{10} and $PM_{2.5}$ and submicron airborne dust particles [1].

There are cases, such as operating rooms, intensive care units (ATI), where it is necessary to monitor the concentration of smaller, submicron particles, because the size of airborne bacteria that cause nosocomial infections are of this order of magnitude. In the case of highly sensitive electronics manufacturing, the presence of the specks of dust can compromise the quality of a product. The study of submicron particles has become of interest in recent years. Rapid and reliable measurement and counting of submicron particles and UFPs are important for the air quality control (regarding the UFPs presence in the air) in fields such as: environmental study, electronic industries, biomedical research, and drug delivery system development.

The electronics manufacturers must ensure the cleanliness of the manufacturing space in order to ensure the sterility and stability of their highly sensitive electronics manufacturing because the smallest speck of dust can lead to contamination or damage to the product that is often impossible to repair. In the electronic industry, air pollution with particulate matter must be constantly monitored by counting the particles for the compliance with the specific environmental requirements. For this reason, the electronic industry i.e. highly sensitive electronics manufacturing, their production halls must be provided with a low level of polluting factors because the activities must be carried out under pre-established safety standards, carefully controlled and the level of contamination must be fully monitored. To fulfil these goals, the air in the production halls is permanently filtered to remove particles and impurities that can damage the activity. The concentration of particles in the air is controlled and the production halls are built and equipped in order to prevent the introduction, generation and retention of particles is minimal, and to control the relevant parameters (temperature, humidity, particulate matter presence, speed) are also controlled [18,19].

ISO 14644-1:2015, *Clean rooms and associated controlled environments – Part 1: Classification of air cleanliness by particle concentration*, and ISO 14644-2:2015, *Clean rooms and associated controlled environments – Part 2: Monitoring to provide evidence of cleanroom performance related to air cleanliness by particle concentration*, provide the framework for classifying and monitoring the cleanliness of the air in cleanrooms. Cleanrooms are classified by how clean the air is, according to the number and size of particles permitted per volume of air. For classification purposes there are considered only particle populations having cumulative distributions based on threshold (lower limit) particle sizes ranging from 0.1 µm to 5 µm. Table 1 presents the values of maximum number of particles/m^3 according to each class defined by ISO 14644-1.

Table 1. Maximum number of particles/m^3 and cleanrooms – ISO 14644-a

Class	Maximum number of particles/m^3						FED STD 209E equivalent
	>=0.1 µm	>=0.2 µm	>=0.3 µm	>=0.5 µm	>=1 µm	>=5 µm	
ISO 1	10	2					
ISO 2	100	24	10	4			
ISO 3	1,000	237	102	35	8		Class 1
ISO 4	10,000	2,370	1,020	352	83		Class 10
ISO 5	100,000	23,700	10,200	3,520	832	29	Class 100
ISO 6	1,000,000	237,000	102,000	35,200	8,320	293	Class 1,000
ISO 7				352,000	83,200	2,930	Class 10,000
ISO 8				3,520,000	832,000	29,300	Class 100,000
ISO 9				35,200,000	8,320,000	293,000	Room Air

Light scattering (discrete) airborne particle counters (LSAPC) are used for the of airborne particles concentration determination (equal to and greater than the specified sizes, at designated sampling locations), in accordance with ISO 14644-1:2015. When the particle size is smaller than the wavelength of light, the scattering of light energy by particles becomes predominant over reflection or refraction phenomena. There is a nonlinear relationship between the scattered light intensity and the particle size which allows that the particle size to be determined by measuring the intensity of the scattered light.

An LSAPC apparatus is capable to count and classify, *i.e*. sizing, single airborne particles and to report size data in terms of equivalent optical diameter by using a very bright light source (a laser diode) to illuminate the particles. A photodetector converts the burst of light energy from each particle into a pulse of electrical energy. The height of the signal is measured and is compared with the calibration curve. In this way, the apparatus allows the determination of the particle size, and it is also a counter, the number of pulses determining the quantity allocating the particle numbers into size channels.

In recent years, there is an increased demand for submicron dust monitors, but the offer is limited and prices are elevated. There are many companies that sell such monitors for airborne dust particles, at affordable prices and very good quality, like: INCOTECH, MULTILAB, OPTIMUSAT, AEROQUAL, APEXINST, FLUKE (*www.incotech.ro; www.multilab.ro; www.optimusat.ro; www.aeroqual.com; www.apexinst.com, https://www.fluke.com/).*

The paper presents a product built at the request of a major manufacturer of electronic circuits for the automotive industry, namely a system for monitoring submicron airborne dust particles (DUMO) (Fig. 1). DUMO, a system that counts the number of particles and measures their size using the light scattering method, represents a real solution for determining airborne particle concentrations, assuring accurate measurements, even for critical locations requiring ISO Class 6.

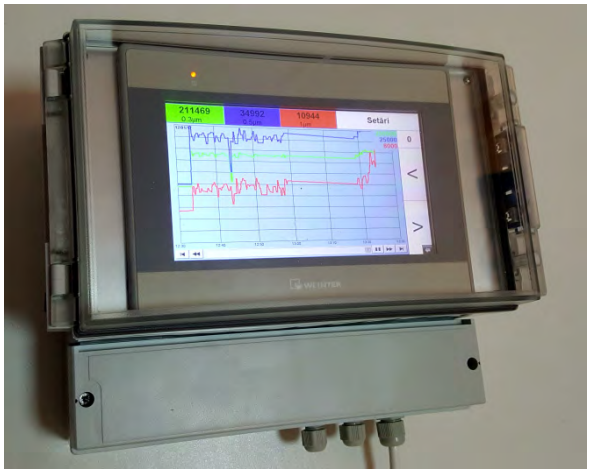

Figure 1. DUMO System for monitoring submicron airborne dust particles (Manufacturer SC ELECTRONIC APRIL, Aparatura Electronica Speciala SRL, Cluj-Napoca, Romania)

RESULTS AND DISCUSSION

The results obtained from the comparative measurements performed with the DUMO and FLUKE devices are presented in Table 2. The notion of measurement uncertainty is inappropriate, and the counting quality will be discussed from the perspective of counting efficacy, which is the subject of these experiments. The results obtained after the measurement with the FLUKE are considered as a reference and the quality of the measurements performed by DUMO is checked according to the FLUKE results for each point.

Table 2. Number of particles counted/recorded in the production hall

Number of sampling points	Number of particles counted >=0.3 µm			Number of particles counted >=0.5 µm		
	Fluke	DUMO	Difference %	Fluke	DUMO	Difference %
1	85789	90345	5.3	4468	4255	4.8
2	67456	71500	6.0	3689	3367	8.7
3	47909	50123	4.6	4322	4266	1.3
4	77566	75849	-2.2	6554	6177	5.8
5	56787	60899	7.2	8777	8655	1.4
6	42577	45788	7.5	5776	5900	-2.1
7	69994	72277	3.3	5432	5444	-0.2
8	49900	52044	4.3	3978	4267	-7.3
9	48678	50398	3.5	4566	4189	8.3
10	85655	86208	0.6	3556	3899	-9.6

By analyzing the results presented in Table 2, the following points can be noticed:

-in all sampling/measuring points, the number of recorded particles values below 102,000 for particles with size> = 0.3 µm (max. recorded 85789 with Fluke and 90345 with DUMO in measuring point no. 1: max. registered 8777 with Fluke and 8655 with DUMO. The results show that, in the production hall, the cleaning requirements class 1000 (Table 2) are met;

-in all sampling/measuring points, the number of recorded particles values below 35,200 for particles with size> = 0.5 µm (max. recorded 8777 with Fluke and 8655 with DUMO in measuring point no. 5) The results show that, in the production hall, the cleaning requirements class 1000 (Table 2) are met;

-the differences recorded between the two devices are less than 10%, which falls into measurement error of the devices and show/demonstrate the high quality of the built devices, both the FLUKE product and the ELCTRONIC APRIL;

-when counting particles with size> = 0.3 µm, the values recorded with DUMO are higher by 0.6…7.5% in 90% of the cases. Only in sampling point no. 4, the DUMO device recorded a smaller number of particles compared to FLUKE (2.2%) (Table 2);

-when counting particles with size >=0.5 µm, the results are different (Table 2). In 40% of the cases, the number of particles recorded with DUMO is higher than with FLUKE and, for the remaining 60%, the number of particles is less than of those registered with FLUKE. The most critical case is recorded in sampling point 9, the difference being 9.6%, but the value is below 10%, i.e. error in the measurement range;

-there is a difference between the values recorded with the Fluke device, which was used as a reference, and the DUMO device due to the wavelengths of the laser diode in the component of the detectors which are different. The scattering on the particles is also affected by the wavelength and the type of component particles of the dust. Because there are various ratios of metallic dust and non-metallic dust at different measurement places, the scattering on the two wavelengths differs, resulting in seemingly uncorrelated data, *i.e*. "heteroskedastic behavior";

-for the two sets of data, a statistic paired t-test was applied and the results showed that for the values recorded in the case of particles with dimensions >= 0.3 microns, the difference between the two data sets, FLUKE and DUMO, is statistically significant ($p<0.05$); for the values recorded for particles with dimensions >= 0.5 microns, the difference between the two data sets, FLUKE and DUMO, is not significant, $p=0.421$, ($p>0.05$).

CONCLUSIONS

Particulate matter, consisting of a mixture of solid and liquid particles suspended in the air, is of particular importance in the electronic industry, where their continuous monitoring is needed in order to maintain the conditions in the cleanrooms. A system for monitoring submicron airborne dust particles, DUMO, was built for the production plants in the electronic industry with an ISO 1,000 cleaning class. DUMO can be used for: cleanrooms monitoring, indoor air quality investigation and particles size distribution monitoring.

The tested and verified system is an easy-to-use instrument, meets the requirements formulated by ISO 14644-1 and has specifications comparable to a FLUKE device, one of the best on the market, all these recommending DUMO for mass production and marketing.

EXPERIMENTAL SECTION

System construction. At the request of a major electronic circuits manufacturer for the automotive industry, a system was designed and built to verify and monitor the air quality in a production hall with ISO 1,000 cleaning class. The beneficiary requested to monitor only the size and not the composition of the airborne particles. Two size categories of submicron dust were of particular interest: 0.3 and 0.5 μm, since these are the size ranges monitored in cleanrooms at his production plant (electronic industry). After studying the specialized literature, it was decided to build a particle counter determining airborne particle concentrations (DUMO), device that meets all the requirements specified by ISO 14644-1:2015, taking into account that it also specifies the standard method of testing to determine the cleanliness class, including the selection of sampling locations. DUMO, a light scattering (discrete) airborne particle counter, was designed for: high accuracy, on-screen data presentation, the ability to perform more experiments rapidly and the ability to access and analyze data anytime. DUMO is an LSAPC and the measurement principle is based on the detection of light scattered by a particle which passes through an incident light beam. The particle size is determined from the intensity of scattered light and the number of light pulses scattered by individual particles. DUMO can quantify the number of particles as particle number concentration per volume of air in different size range categories.

The key element of the DUMO is the particle sensor itself, consisting of a laser diode assembly - CCD area, suction pump with continuous operation with electronically controlled constant, and the electro-optical detector. The

DUMO operation is based on the scattering of a laser beam on air samples taken from the environment, with illumination at 90 degrees with a semiconductor laser diode. The laser beam is scattered on the dust particles and reaches the CCD area, where the concentration and size of the particles can be determined using the electrical signals received. The measurement principle is illustrated in Fig. 2.

The ZN-PD03 sensor, air particle sensor for in-line measurement produced by Omron Corporation, was used due to the unique advantages it offers [20]:

- robust, compact construction, with magnetic levitation suction pump
- coarse dust filter, for particles larger than 1 micron
- calibrated from the factory for applicable particle size 0.3-0.5-1.0 microns
- providing additional modules for signal processing
- simple wiring
- very good resistance to vibrations: 10 to 55 Hz, 0.7-mm double amplitude 80 min each in X, Y, and Z directions
- very good resistance to shocks: 150 m/s^2 three times each in six directions (up/down, left/right, forward/backward

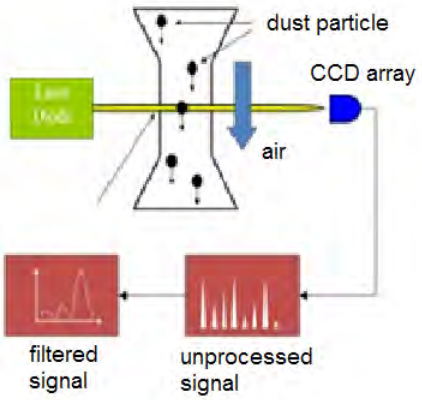

Figure 2. DUMO measurement principle

The sensor connects to the ZN-PDA11 type amplification module (Omron Corporation), which processes the analog signals sent by the sensor, and displays the measured values from a miniaturized numerical display [21]. The measurement conditions are also established on this module, such as:

- sampling time
- number of mediated samples
- the unit of measurement in which the values will be indicated
- scaling the obtained values, offset correction and amplification

The amplifier module forwards digital signals to another Omron module, the ZN-SFW11, the serial transmission module, which processes and transforms information for the standard RS232 serial interface. The block diagram of the assembly can be seen in Fig. 3.

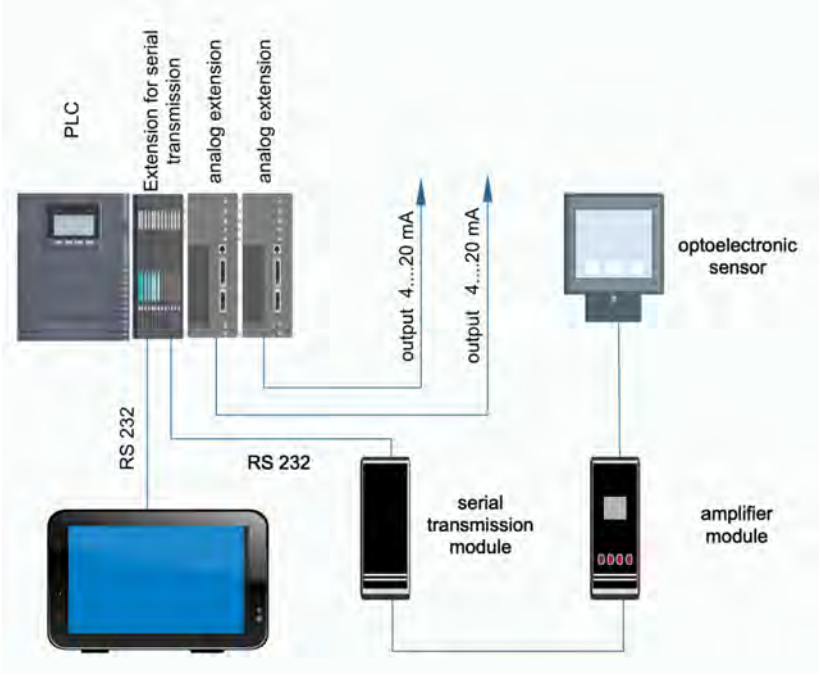

Figure 3. Block diagram of the DUMO system

The costumer requested that the results be displayed graphically, the 8-hour trend at the device installation point, the 30-day measurement history be downloadable to a USB memory, readable in Excel, and the measured values will be transmitted remotely as a unified signal 4…20 mA. For this purpose, a computing unit was built around a DirectLogic25 programmable controller with serial communication module extensions and two 4...20 mA analog output modules. Attached to this computing system is a 7” color touch-screen display that acts as a human-machine interface. The communication between the PLC and the display takes place through the RS232 serial interface.

Experiments performed. The experiments aimed at verifying the accuracy of measuring submicron particles. The experiments were performed in the production hall of the customer for whom this system was built. The measurements were conducted in the PCB manufacturing and implantation hall of the beneficiary at the points identified by his representative.

The ISO 14644 standard was used for the determination of measurement points, their positioning in the production hall, number and duration of sampling at each point, calculation of the average concentration value for each measurement point, total average, standard deviation of the average value for each measurement/sampling point [18]. The sampling locations within each segment were chosen to be “representative of the characteristics” of each section of the production hall, taking into account that ISO14644-2:2015 Sample Point Placement ISO 14644-1/2:2015 is also a beneficial tool to use in achieving mature cleanroom environmental control. The aim of the experiments was to identify critical areas, if they exist and to understand the contamination sources and their impact on the activity in the production hall.

To evaluate the measurement accuracy, 10 systems were placed in the customer's production plant, at critical points for air quality (selected according to ISO 14644), and the values indicated by DUMO in parallel with a Fluke 985 laboratory particle measuring device for sizes between 0.3 and 0.5 microns were recorded. At each point, 8 measurements were performed, and the averages were recorded, which were then analyzed and interpreted.

DUMO Specification and Key features:

- particle size rage: 0,3 µm; 0,5 µm; 1.0 µm
- sampling time: 1……599 sec
- programmable (25 sec. by default)
- average count setting: 2; 4; 8; 16; 32; 64
- operating temperature: 0…….40 ºC
- power: 220V/50 Hz
- power consumption: max. 25 VA
- housing: ABS
- IP rating: IP 54
- dimensions: 260 x220 x 156 mm
- weight: approx. 2,5 kg
- channels: 6; simultaneously measures and displays 6 channels of particle size, ambient temperature and humidity
- the loss of the supply voltage does not lead to the loss of the measurement history.

ACKNOWLEDGMENTS

This work was supported by a grant of the Romanian Ministry of Research and Innovation, CCCDI –UEFISCDI, contract number 65PTE/2020, within PNCDI III.

REFERENCES

1. *** https://www.epa.gov/pm-pollution, online source accessed in 08 January 2021.
2. C.A. Pope, *Inhal. Toxicol.*, **2007**, *19*, 33-38. doi.org/10.1080/08958370701492961
3. C.A. Pope, D.W. Dockery, *J. Air Waste Manag. Assoc.*, **2006**, *56*, 709-742. doi.org/10.1080/10473289.2006.10464485
4. C.A. Pope, R.T. Burnett, M.C. Turner, *Environ. Health Perspect.*, **2011,** *119*, 1616–1621. doi: 10.1289/ehp.1103639
5. R. Zhang, G. Wang, S. Guo., M.L. Zamora, Q. Ying, Y. Lin, W. Wang, M. Hu, Y. Wang, *Chem. Rev*., **2015**, *115*, 3803–3855. doi: 10.1021/acs.chemrev.5b00067
6. P. Kumar, A. Robins, S. Vardoulakis, R. Britter, *Atmos. Environ*, **2010**, *44*, 5035–5052. doi:10.1016/j.atmosenv.2010.08.016
7. P. Paasonen, M. Peltola, J. Kontkanen, H. Junninen, V.M. Kerminen, M. Kulmala, *Atmos. Chem. Phys*., **2018**, *18*, 12085–12103. doi: 10.5194/acp-18-12085-2018
8. M. Manigrasso, M. Vitali, C. Protano, P. Avino, *Environ. Int*., **2018**, *118*, 134-145.
9. C. Nguyen, L. Q. Li, C.A. Sen, E. Ronquillo, Y.F. Zhu, *Atmos*. *Environ.*, **2019**, *211*, 159–169.
10. M.R. Heal, P. Kumar, R. Harrison, *Chem. Soc.,* **2012**, *41*, 6606. https://doi.org/10.1039/c2cs35076a
11. *** US - EPA, National Ambient Air Quality Standards for Particulate Matter; Final Rule. Federal Register 78, **2013**,*10*, 3086–3287.
12. *** WHO, Review of evidence on health aspects of air pollution – REVIHAAP Project. Copenhagen, Denmark, **2013**, https://www.euro.who.int/__data/assets
13. *** Joint Research Centre. Particle Measurement Programme (PMP): Inter-laboratory correlation exercise with Condensation Particle Counters (CPCs). **2018**, (Publications Office of the European Union).
14. B. Giechaskiel, B. *Combust. Engines*, **2018**, *174*, 3–16.
15. *** https://www.health.ny.gov/environmental/indoors/air/pmq_a.htm, online source accessed in 08 January 2021.
16. H.-S. Kwon, M. H. Ryu, C. Carlsten, *Experim. Mol. Med*., **2020**, *52*, 318–328.
17. *** https://www.consilium.europa.eu/en/policies/clean-air/
18. *** ISO 14644:2019, Cleanrooms and associated controlled environments, www.iso.org/iso/foreword.htm

19. *** ISO 14698-1:2003, Cleanrooms and associated controlled environments — Biocontamination control — Part 1: General principles and methods, https://www.iso.org/obp/ui/#iso:std:iso:14698:-1:ed-1:v1:en
20. *** Omron Corporation-Instruction Sheet for Zn-PDA air particle sensor, https://www.omron.com/global/en/
21. *** Omron Corporation-Instruction Sheet for air particle amplifier unit, https://www.omron.com/global/en/

STUDIA UBB CHEMIA, LXVI, 2, 2021 (p. 233-246)
(RECOMMENDED CITATION)
DOI:10.24193/subbchem.2021.2.20

DEEP EUTECTIC SOLVENTS FOR CO_2 CAPTURE IN POST-COMBUSTION PROCESSES

ELIZA GABRIELA MIHĂILĂ[a,b], DIANA CONSTANTINESCU ARUXANDEI[b], SANDA MARIA DONCEA[b], FLORIN OANCEA[b], CRISTIAN DINCĂ[a]*

ABSTRACT. CO_2 emissions represent an actual problem for the environment. Additionally, the new demands for all chemical and physical processes request to be more eco-friendly. In this work, deep eutectic solvents (DESs), a relatively new class of solvents, were used for CO_2 capture and desorption. DESs are more environmentally friendly than classical solvents. Two choline chloride-based DES – ethaline (ChCl:EG, 1:2 molar ratio) and reline (ChCl:U, 1:2 molar ratio) were prepared and characterized before studying their CO_2 absorption – desorption capacity. The formation of eutectics was confirmed by FT-IR analysis and DESs were characterized in terms of pH, density, viscosity, refractive index, and electrical conductivity. The tests showed that ethaline had better CO_2 absorption and desorption capacity than reline, which could be explained by several parameters.

Keywords: *CO_2 capture, deep eutectic solvents, green solvents*

INTRODUCTION

The demand for energy in the world market presents a complex transition, compartmentalized by several dimensions: geopolitical, economic, technological and climatic. These developments lead to new strategic partnerships with security, investment, trade, and technology. From the perspective of the latest EU documents, environmental security becomes the fundamental idea of sustainable development.

[a] *University POLITEHNICA Bucharest, Power Engineering Faculty, Department of Energy Generation and Use, Romania*
[b] *National Institute for Research and Development in Chemistry and Petrochemistry ICECHIM, Romania*
** Coresponding author e-mail: crisflor75@yahoo.com*

The EU has already made a first step in the Spring European Council since 1990, setting an ambitious target for the whole Union, to reduce greenhouse gas emissions (GHG) by 20% by 2020. Another objective consisted in a contribution of 20% of renewable energy resources to the European Union's from the total energy consumption by 2020. In 2016 GHG emissions had a value of 88 million tons CO_2 equivalent, representing a decrease by 54% compared to the emissions of 1990 (226 Mt eq. CO_2). At present time, Romania contributes to the total GHG emissions at European Union level by approximately 2.5% of the total emissions, which is lower than in 1990 when the contribution was higher than 4% [1].

The most important contribution to climate change results from CO_2 emissions, due to the large quantities released in the atmosphere especially by the energy sector, over 30 billion tons yearly. In 2016 the CO_2 level raised 50% faster than the average in the previous decade, leading to its level rising by 45% above pre-industrial levels, i.e. the highest concentration in the last 800,000 years [2].

In 2018, 66.3% of the total world electricity production was generated by using as combustible fuels: coal and coal products, oil and oil products, natural gas, and biofuels – (i) solid biomass and animal products, (ii) gas/liquids from biomass, industrial waste and municipal waste. Worldwide, 38% of the electricity is obtained by burning coal, 23% by using natural gas, 16.2% hydropower and 10.1% nuclear power. The newer solutions (wind, solar, biofuel and waste) are used for 9.1% energy production [3]. Abruptly halting the use of fossil fuels risks leading to the collapse of the current society. Therefore, the decision was to gradually give up coal, oil, and natural gas while looking for solutions to capture CO_2 emissions from fuel processing.

Reducing the pollution generated by the fossil fuels combustion is possible through technologies such as *CCUS (Carbon Capture, Utilization and Storage)*. CO_2 could be stored at large depths, in rock layers or even in the oceans (but with high risks to the aquatic area), could be injected to extract oil or methane, and could be used, but in small amounts, in various activities (industry food, chemical, agriculture, and carbon fiber manufacturing) [4]. Another method of storage would be the natural one in the biosphere, but there is the disadvantage of slow absorption of CO_2 by plants and the need for large areas for forest rehabilitation [5]. This method, however, is seized for the storage of excess CO_2 from the atmosphere.

The CO_2 post-combustion capture is the most advanced technology that can be easily adapted to the large capacities installed in the thermoelectric power plants. The principle of the method consists in the chemical absorption of CO_2 from the flue gas using a solvent (amine or cooled ammonia) with an approximately 95% efficiency. Unfortunately, the energy penalty for chemical absorption process integration in a coal fired power plant is around 10-15 % [6].

Recently, deep eutectic solvents (DESs) were proposed as an efficient and more environmentally friendly alternative to classical methods for the absorption of post-combustion CO_2 from combustion gases [7].

DESs consist of two or three components (ideally non-toxic and cost-effective), which are associated via hydrogen bonds forming eutectic mixture with a melting point below the melting temperatures of each component in part. One of the great advantages of DESs is the possibility to tailor them so that they are specific to individual applications. Most DESs are mixed systems of Lewis or Brønsted acids and bases, generally obtained by binding quaternary ammonium salts acting as hydrogen bond acceptor (HBA) to a salt of metal or another hydrogen bond donor (HBD) [8]. There are also other possible combinations, for example between carbohydrates. Deep eutectic solvents are made up of large, asymmetric molecules, with low network energy, thus explaining the low melting temperatures. The dislocation of the electrical charge that may occur in a hydrogen bond (e.g. between a halogen ion and a donor hydrogen molecule) is responsible for decreasing the melting point of the mixture from the individual temperatures of components.

The most investigated DESs are those based on choline chloride, which is biodegradable, nontoxic, cost-effective and which can be extracted from biomass. These DESs were also found to be the most effective in CO_2 absorption. Most of the studies reported until now investigated the absorption / solubility of CO_2 in DESs [9-13]. There are only few reports dealing with CO_2 desorption from DESs and most of them are based on theoretical simulation. Experimental investigation of desorption is scarce, to the best of our knowledge.

In this paper, we set out to prepare and characterize 2 deep eutectic solvents: choline chloride: urea with 1:2 molar ratio – also called reline; and choline chloride: ethylene glycol, 1:2 molar ratio, respectively ethaline, and to determine their CO_2 absorption and desorption capacity under several conditions.

The process of CO_2 separation by absorption into DES is similar to the other solvents (ammonia, amines, etc.) [14], consisting in a typical absorber unit followed by a desorption unit configuration. A compressor pumps the CO_2-rich flue gas into the absorption column, where it meets the DES, and releases the CO_2-poor flue gas. After that, the CO_2-rich solvent is moved into the desorption column, where, using a reboiler, pure CO_2 is discharged for further utilization and/or storage, and the regenerated solvent is recycled back to the absorption unit. As operating parameters, the temperature and pressure in the two columns, the absorbent mass, the solvent regeneration energy, and the pressure required for the compressor must be taken into account.

RESULTS AND DISCUSSION

Preparation and characterization of DES

As part of a new class of solvents, the mechanism of formation of eutectic mixtures is not fully known. The following "molecular cage" structures [15] are proposed as illustrated by the schemes 1-2

A) Choline chloride, together with two ethylene glycol molecules, forms ethaline (scheme 1).

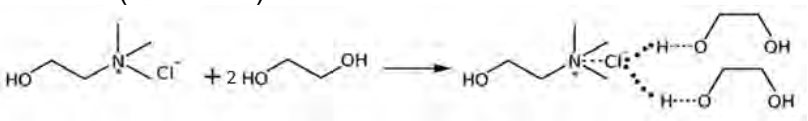

Scheme 1

B) Choline chloride, together with two urea molecules, forms reline (scheme 2):

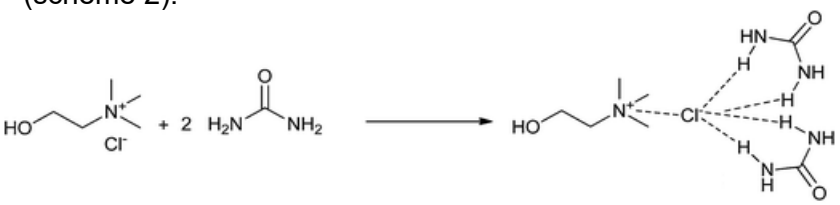

Scheme 2

The change in the FT-IR spectral response between pure substances and the formed eutectic due to the physico-chemical interaction between ChCl-EG and ChCl-U is highlighted in Figure 1.

Between 3600 and 3000 cm^{-1} the vibrations of hydrogen bonds of the type O-H N-H, and / or O-H·O and/or N-H·O are observed [16], which denotes the existence of molecular aggregates specific to eutectic mixtures. In the case of reline, this spectral band has a maximum at 3329-3328 cm^{-1}, specific to hydrogen bonds and a maximum at 3198-3197 cm^{-1}, specific to the –NH group. These are correlated also to vibration bands at 1660 cm^{-1}, 1656 cm^{-1} and 1607cm^{-1}. The presence of the HO HN group from 924 cm^{-1} is also noteworthy (Fig. 1A).

Ethaline has a very wide and high intensity band, specific to intramolecular –OH bonds, and indicates the formation of new hydrogen bonds and/or molecular aggregates, with a maximum at 3321-3322 cm^{-1}. Relevant is also the formation of new hydrogen bonds with absorption band at 3035 cm^{-1}, specific to the O-H·N-H and/or N-H·O type bonds, correlated also with the vibration band at 1653 cm^{-1}. It is also worth noting the appearance of bands specific to the C-C-O- group from 1084 cm^{-1} and from 1038-1039 cm^{-1} and the HO···HN group from 925 cm^{-1}, (Fig. 1B).

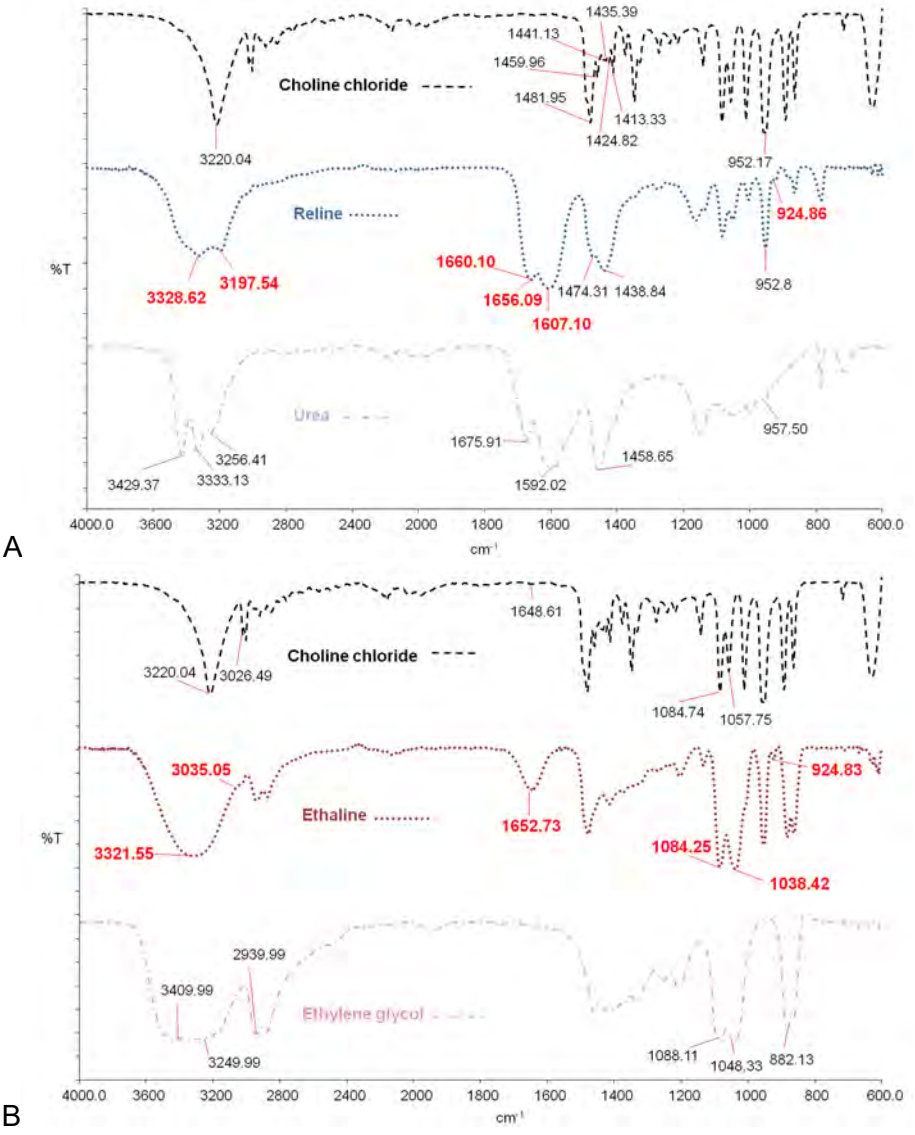

Figure 1. FT-IR spectra of reline (A), ethaline (B) and the individual components

The pH of our prepared reline was found to be moderately alkaline due to urea and that of ethaline was close to neutral. The values are similar to those of commercial DESs (Table 1) and are close to the values reported in the literature, at this molar ratio [17]. A special equipment was used, a pH-meter electrode for viscous samples from Mettler Toledo *InLab® Viscous Pro-ISM*.

Table 1. pH values of reline and ethaline samples

Sample	pH	Standard deviation
Commercial reline	*9.74*	*0.0153*
Prepared reline	*9.14*	*0.0252*
Commercial ethaline	*7.57*	*0.0404*
Prepared ethaline	*7.27*	*0.0265*

The densities were also close to the values of the commercial reline and ethaline. The density of reline was lower than reported in the literature [18], probably due to residual humidity. The results are shown in Table 2.

Table 2. Density values of reline and ethaline samples

Sample	Density g/cm^3	Standard deviation	In literature
Commercial reline	*1.1926*	*0.0005*	
Prepared reline	*1.1988*	*0.0008*	*1.25* [18]
Commercial ethaline	*1.1167*	*0.0007*	
Prepared ethaline	*1.1186*	*0.0007*	*1.12* [18]

Ethaline is 20 times less viscous than reline. The viscosity values obtained for our prepared DESs were similar to the commercial DESs and to the values reported in the literature (Table 3). Most eutectic solvents have high viscosities, more than 100 cP, attributed to the extensive network of hydrogen bonds, which do not allow the free movement of chemical species. Other explanations could be the large ions that give small free volumes in the structure of DES or the existence of other electrostatic forces, such as Van der Waals. High viscosity solvents would increase the cost of CO_2 absorption process and it is therefore not desirable for CO_2 capturing. In our case the difference between ethaline and reline is probably due to the higher flexibility of the ethylene glycol molecule compared to urea and the liquid character of ethylene glycol [19].

Table 3. Viscosity of reline and ethaline samples

Sample	Viscosity cP 25°C	Standard deviation	In literature
Commercial reline	*739.7*	*0.7750*	
Prepared reline	*735.5*	*0.5508*	*750* [18]
Commercial ethaline	*38.8*	*0.3512*	
Prepared ethaline	*36.0*	*0.2082*	*37.0* [18]

Electrical conductivity is correlated with viscosity. Reline has much lower conductivity due to its higher viscosity compared to ethaline (Table 4). Due to high viscosities, the electrical conductivity of DESs does not exceed 2 mS/cm at room temperature in general [20]. Ethaline is one of few DESs with higher conductivity, so better electron transfer which should theoretically influence the CO_2 absorption positively. Increasing the temperature should lead to an increase in electrical conductivity, as it decreases viscosity.

Table 4. Electrical conductivity – reline and ethaline samples

Sample	Electrical conductivity mS/cm	Standard deviation	In literature
Commercial reline	*0.187*	*0.0031*	*0.2* [21]
Prepared reline	*0.193*	*0.0036*	
Commercial ethaline	*7.39*	*0.0208*	*7.61* [21]
Prepared ethaline	*7.54*	*0.0603*	

The refractive index determined for DES samples, both commercial and prepared in this work is slightly different from the data already reported [22]. This is probably related to the experimental method used. The refractive index is a measure of the electronic polarizability and intermolecular interactions between DES components [21].

Higher refractive index of reline compared to ethaline suggests stronger interactions between choline chloride and urea than between choline chloride and ethylene glycol (Table 5). Reline is characterized by a “H-bound soup”, wherein different types of H-bond (NH···O=C; OH···O=C; OH···Cl; NH···Cl; OH···NH; CH···Cl; CH···O=C; NH···NH and NH···OH) are possible to be formed [21, 22]. Different types of complex ionic species are formed in reline, such as $[Cl(urea)_2]^-$ complexed anion and urea[choline]$^+$ complexed cation [22]. Most probably, these strong intermolecular interactions are responsible for the high reline viscosity.

Table 5. Refractive index – reline and ethaline samples

Sample	Refractive index	Standard deviation	In literature
Commercial reline	*1.5035*	*0.0005*	*1.4826* [23]
Prepared reline	*1.5034*	*0.0004*	
Commercial ethaline	*1.4625*	*0.0004*	*1.3326* [23]
Prepared ethaline	*1.4635*	*0.0002*	

***CO_2 Absorption tests*.** The tests started with the following parameters: temperature 25°C, pressure 1-30-60 bar, flow 200 ml/min, 30 minutes, until the second flowmeter showed the same debit as the first one (fig. 2). The CO_2 absorption value is up to 6% per ethaline and 2% for reline, at the highest tested pressure, 60 bars, in line with the reported data. Slightly higher solubility of CO_2 in ethaline compared to reline was obtained by Mirza et al., at low pressure [13].

Recently, Chhotaray et al. correlated the CO_2 capture capacity to the free volume (V_f) of solvent [24]. We have also calculated the free volume of the two DESs and determined the value 117.30 cm^3/mol for reline and 130.66 cm^3/mol for ethaline. The higher V_f of ethaline compared to that of reline could also contribute to the higher CO_2 absorption observed for ethaline. Most probably, the stronger intermolecular interactions in reline, compared to ethaline, hamper CO_2 sorption.

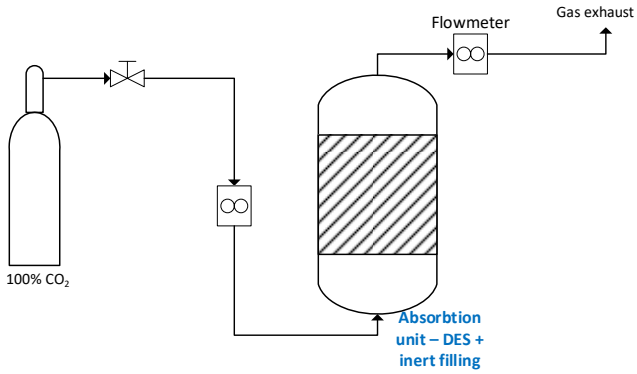

Figure 2. Absorption scheme of the $scCO_2$ system reactor

Two types of desorption methods were tested: in the vacuum oven (-0.75 bar) with heat and the classic way, thermal heating at normal pressure (1 bar). The vacuum did not help the desorption at room temperature, but it did at 60ºC.

***CO_2 Desorption in vacuum oven*.** The data are presented in Table 6. These data demonstrate that the absorbed CO_2 could be partially desorbed from the tested DES by vacuuming. Ethaline performed better than reline in sorption and desorption of carbon dioxide. For ethaline, the desorption rate could reach 3.75 g per 100 g of DES (62.5% from the solubilised CO_2, compared to only 34.5% in the case of reline after absorption at 60 bar).

Table 6. Amount of CO_2 desorbed after vacuuming at 60°C

	Solvent	***Reline***	***Ethaline***
Absorption at 1 bar	*Desorbed CO_2 mass – 100g DES*	0.0003	0.0024
	g CO_2 / g DES	0.3×10^{-5}	0.24×10^{-4}
	Molar fraction	2.63×10^{-6}	2.068×10^{-5}
Absorption at 30 bars	*Desorbed CO_2 mass – 100g DES*	0.23	2.12
	g CO_2 / g DES	0.0023	0.0212
	Molar fraction	0.002	0.0179
Absorption at 60 bars	*Desorbed CO_2 mass – 100g DES*	0.69 g	3.75 g
	g CO_2 / g DES	0.0069 g	0.0375 g
	Molar fraction	0.006	0.031

Thermal desorption. The results are illustrated in fig. 3. Ethaline proved slightly better desorption than reline in absolute values, but not statistically significant. The slightly higher absolute desorption values could be related to the higher sorption capacity.

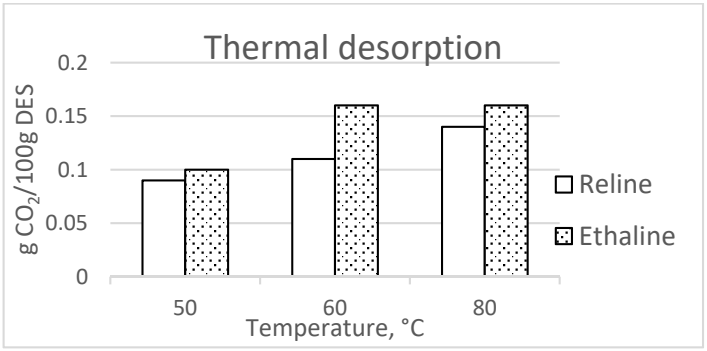

Figure 3. Thermal desorption of CO_2 - quantity of gas desorbed from ethaline and reline.

In the case of introduction of CO_2 at 1 atm pressure into the system, the pH decreases from 10.86 to 6.25. After removing CO_2 using inert N_2, the pH returns to its initial value, which means that these DES have reversible acidity/basicity.

The results presented indicate that ethaline could be used for further improvement of CO_2 sorption and desorption by adding amine and /or super-strong basis.

CONCLUSIONS

This study aimed to prepare, characterize and evaluate two deep eutectic solvents, reline and ethaline for CO_2 absorption and desorption, the comparison of desorption capacity for the two DESs being performed for the first time, to the best of our knowledge. The prepared solvents were compared with their commercially available variants in order to have standard references. The four samples (commercial and prepared reline, and commercial and prepared ethaline) were confirmed by FT-IR and characterized for their physical and chemical properties: pH, density, viscosity, refractive index, electrical conductivity.

The values obtained for commercial and prepared solvents are similar. The data are reproducible, confirmable in other specialized works.

Ethaline had 3x better CO_2 absorption (6% versus 2%) and up to 2x better desorption capacity (62.5% versus 34.5%) than reline due to weaker intermolecular interactions, which lead to larger free volume, lower density and viscosity compared to reline.

Normal conditions are not applicable as an "ultra-green" method. Increasing the values of the reaction conditions (temperature and pressure), the absorption capacity of the two eutectics is increased due to physical changes (decreases viscosity and density), allowing easier penetration of the CO_2 molecule into the "eutectic cage". The same applies in the reverse process, desorption. Further studies are necessary to better exploit the DESs potential for CO_2 absorption and desorption.

EXPERIMENTAL SECTION

Materials

Choline chloride was purchased from Sigma-Aldrich, ethylene glycol and urea were purchased from Fluka and used without further purification, but after drying in a vacuum oven. Commercial DES, reline and ethaline, were purchased from Scionix Ltd (U.K.) and used as standard.

Preparation of DES

Choline chloride and urea for reline and choline chloride and ethylene glycol for ethaline were precisely weighed using an analytical balance with 5 decimals [25] [26], thus respecting the molar ratio of 1:2. The preparation took place in a system consisting of a glass round-bottomed vessel, to which a vertical refrigerant was attached (to minimize gas losses in the vessel), an

oil bath (for uniform heating), an electric heating plate with magnetic agitator and a magnetic bar, and a thermometer. The temperature of 40°C was found to be the optimal temperature in order to keep DES liquid at room temperature. The substances were incubated at 600 rpm magnetic stirring for two hours. No release of ammonia from the composition of urea was noticeable. After the reaction was completed, a transparent, colorless, viscous, perfectly homogeneous solution was obtained.

The new eutectic solvents were placed in hermetically sealed plastic containers in desiccators, due to the high hygroscopic character of ChCl. Subsequently, these solvents were characterized for chemical and physical properties and CO_2 absorption and desorption.

DES characterization

The formation of deep eutectic was confirmed by FT-IR and the physico-chemical properties such as pH, density, viscosity, refractive index, and electrical conductivity were determined for the prepared and commercial DESs.

***FT-IR*.** The equipment used was an FT-IR Spectrophotometer - Spectrum GX Perkin Elmer. The FT-IR spectral analysis was performed throughout the wavelength range, from 4000 to 600 cm^{-1}. The samples of ethaline and reline scans were also compared with pure component substances, i.e., choline chloride, ethylene glycol and urea, all three standards being of high analytical purity.

***pH*.** In this study, the pH of the 4 samples was measured using an electrode dedicated to viscous solutions attached to a Mettler Toledo Seven Compact pH meter. Measurements were done at 25°C, with the ATC (automatic temperature correction) function active.

Density. The operating principle of modern appliances is based on the technology of the U(U-tube) glass oscillating tube. A window monitors the existence of gas bubbles which can give measurement errors. The density was determined using a Mettler Toledo EasyD40 densimeter.

Viscosity. Viscosity was determined with a Brookfield DV-II+ Pro viscometer. This parameter is calculated from the resistance encountered by the rotor immersed in the eutectic.

***Refractive index*.** The absolute refractive index is defined as the refractive index of a vacuum medium, which represents the ratio between the speed of light in a vacuum (c) and the speed of light in that environment (v).

The refractive index of a substance depends on the wavelength of the light. The phenomenon is called the dispersion of light. For transparent and colorless environments, such as the solvents studied, reline and ethaline, the variation of the refractive index in the visible domain is given by Cauchy's relationship:

$$n(\lambda) = a + \frac{b}{\lambda^2} + \frac{c}{\lambda^4} \quad (3)$$

Different standard refractive indices are used to characterize the dispersion: n_F - the index for the blue line of hydrogen ($\lambda_F = 486.1$ nm); n_D - the index for the yellow line of sodium ($\lambda_D = 589{,}3$ nm); n_C - the index for the red line of hydrogen (656,3 nm). The refractive index was measured with a Bausch & Lomb Abbe Refractometer.

Electrical conductivity was measured with the conductometer WTW 2FA311 Multi 3320, at room temperature.

CO_2 absorption and desorption

Two experiments were carried out by bubbling a flow of 100% CO_2 (SIAD) in 100 g of DES, at atmospheric pressure with a flow rate of 200 ml/min. Absorption took place in a bubbling vessel fitted with ceramic frieze for better gas dispersion from a supercritical CO_2 equipment – SFT-150-SFE System – Supercritical Fluid Technologies Inc.

The captured CO_2 desorption was performed by two methods, vacuum desorption and thermal desorption. The vacuum desorption took place in a Thermo Scientific Heraeus vacuum oven. Degassing took place at -1bar pressure, 60°C, for 24 hours. The amount of CO_2 desorbed was determined gravimetrically [10]. The thermal desorption system consisted of a thermostatic bath, a round-bottomed balloon, and a magnetic agitator. A fixed amount of solvent was introduced into the flask, the temperature of each sub-experiment was set at 50, 60 or 80°C, at atmospheric pressure, after less than an hour no gravimetrical changes were noticeable).

Free volume calculation

The free volume calculation was performed according to Chhotaray et al. [25], using equations 4 and 5.

$$V_f = V_m - R_r \quad (4)$$

where, V_m is the molar volume (Molar mass/density) and R_m is the molar refraction calculated as follows:

$$R_m = \frac{M}{\rho}\left(\frac{n_D^2 - 1}{n_D^2 + 2}\right) \quad (5)$$

where M is the molar mass, ρ is the density, and n_D is the refractive index.

ACKNOWLEDGMENTS

The study has been funded by the UEFISCDI within the International project NO Grants 2014 - 2021, under project contract no. 13/2020, National Project number PED296/2020 with the title: “New Amine based DES’s Solvent development for CO_2 capture in a demonstrative pilot Installation by Chemical Absorption Technology” – ASOCIAT, and The Operational Programme Human Capital of the Ministry of European Funds through the Financial Agreement “Developing the entrepreneurial skills of the PhD students and postdoctoral students - key to career success (A-Succes)” contract number 51675/ 09.07.2019 POCU/380/6/13, SMIS code 125125.

REFERENCES

1. Government of France, “Integrated National Energy and Climate Plan for France,” **2020**
2. N. US Department of Commerce, Global Monitoring Laboratory. "Global Monitoring Laboratory - Carbon Cycle Greenhouse Gases https://www.esrl.noaa.gov/gmd/ccgg/trends/history.html
3. EA, World gross electricity production, by source, **2018**, IEA, Paris, https://www.iea.org/data-and-statistics/charts/world-gross-electricity-production-by-source-2018
4. J. Bae, Y. Chung, J. Lee, and H. Seo, J. Clean. Prod., **2020**, *246*, 119003
5. C. Hepburn, E.Adlen, J. Beddington, E.A. Carter, S. Fuss, N.M. Dowell, J.C. Minx, P. Smith, C.K. Williams, *Nature*, **2019**, *575*, 7781, 87–97
6. Y. Wang, L. Zhao, A. Otto, M. Robinius, D. Stolten, *En. Proc*. **2016**, *114*, 650-665
7. A. Paiva, R. Craveiro, I. Aroso, M. Martins, R.L. Reis, and A.R.C. Duarte, *ACS Sustain. Chem. Eng.*, 2, 5, 1063–1071
8. Y. Zhang, X. Ji, and X. Lu, *Renew. Sustain. Energy Rev.*, **2018**, *97*, 436–455
9. R.B. Leron, A. Caparanga, M.-H. Li, *J. Taiwan Inst. Chem. Eng.*, **2013**, *44*, 6, 879-885
10. B. Leron, M.-H. Li, *Thermochim. Acta*, **2013**, *551*, 14-19
11. X. Li, M. Hou, B. Han, X. Wang, L. Zou, *J. Chem. Eng. Data,* **2008**, *53*, 548–550
12. A. Malik, H.S. Dhattarwal, H.K. Kashyap, *The J. of Phys. Chem. B*, **2021**, *125*, 7, 1852-1860
13. N.R. Mirza, N.J. Nicholas, Y. Wu, K.A. Mumford, S.E. Kentish, G.W. Stevens, *J. of Chem. & Eng. Data*, **2015**, *60*, 11, 3246-3252

14. E. Ali, M.K. Hadj-Kali, S. Mulyono, and I. Alnashef," *Int. J. Greenh. Gas Control*, **2016**, *47*, 342–350
15. M. Hayyan, T. Aissaoui, M.A. Hashim, M.A.H. AlSaadi, A. Hayyan, *J. Taiwan Inst. Chem. Eng.*, **2015***, 50*, 24–30
16. T. Aissaoui, *Pharm. Anal. Acta*, **2015**, *6*, 11, 11–14
17. W. Li, Z. Zhang, B. Han, S. Hu, J. Song, Y. Xiea, X. Zhou, *Green Chem.*, **2008,** *10*, 1142–1145
18. Q. Zhang, K. De Oliveira Vigier, S. Royer, and F. Jérôme, *Chem. Soc. Rev.*, **2012**, *41*, 7108–7146
19. A.P. Abbott, R.C. Harris, K.S. Ryder, *J. Phys. Chem. B*, **2007**, *111*, 18, 4910–4913
20. K. Shahbaz, S. Baroutian, F.S. Mjalli, M.A. Hashim, and I.M. Alnashef, *Thermochim. Acta*, **2012**, *527,* 59–66
21. A.P. Abbott, G. Capper, S. Gray, *ChemPhysChem*, **2006**, *7,* 4, 803–806
22. M. Taherzadeh, R. Haghbakhsh, A.R.C. Duarte, and S. Raeissi, *J. Chem. Eng. Data*, **2020**, *65*, 8, 3965–3976
23. C.R. Ashworth, R.P. Matthews, T. Welton, and P.A. Hunt, *Phys. Chem. Chem. Phys.*, **2016**, *18*, 27, 18145–18160
24. R.B. Leron, A.N. Soriano, and M.H. Li, "*J. Taiwan Inst. Chem. Eng.*, **2012**, *43*, 4, 551–557
25. P.K. Chhotaray, S.K. Biswal, and S. Pandey, *J. of Molec. Liq.,* **2020**, *312*, 113477
26. S. Sarmad, Y. Xie, J.P. Mikkola, and X. Ji, *New J. Chem.*, **2016**, *41*, 1, 290–301
27. J. Naser, F. Mjalli, B. Jibril, S. Al-Hatmi, and Z. Gano, *Int. J. Chem. Eng. Appl.*, **2013**, *4*, 114–118

STUDIA UBB CHEMIA, LXVI, 2, 2021 (p. 247-254)
(RECOMMENDED CITATION)
DOI:10.24193/subbchem.2021.2.21

POWER CONSUMPTION FOR MIXING OF SHEAR-THINNING FLUIDS

ADINA GHIRIŞAN (MICLĂUŞ)[a] and VASILE MICLĂUŞ[a*]

ABSTRACT. The mixing/agitation of time independent non-Newtonian fluids can be a challenge in many technological processes. In the present study, the influence of rheological parameters, K and n, on Reynolds number, power number and power consumption, for different concentration of carboxymethyl cellulose (CMC) solutions, 1%, 2%, 3%, 4 % and 5%, with shear-thinning behaviour, was analysed. The power consumption obtained by theoretical model and by an appropriate curve Po = f(Re) from experimental data, found in literature, was compared. The results have shown good agreement between calculated power number and the graphically determined values, and also minimal power consumption values comparable with those founded for the agitation of non-Newtonian liquids.

Keywords: *mixing, agitation, Reynolds number, power number, power consumption, non-Newtonian fluids, shear-thinning fluids.*

INTRODUCTION

Agitation/mixing is one of the most common operations in the chemical, biochemical, polymer processing, and other industries. Almost all manufacturing processes entail some sort of mixing, and the operation may constitute a considerable proportion of the total processing time. Mixing is a physical process which aims to reduce the gradients of concentration, temperature and other properties in fluids.

In mixing, there are two types of problems to be considered – how to design and select mixing equipment for a given duty and how to assess whether an available mixer is suitable for a particular application. In both cases, the following aspects of the mixing process must be evaluated: the

[a] *Babeş-Bolyai University, Faculty of Chemistry and Chemical Engineering, 11 Arany Janos str., RO-400028, Cluj-Napoca, Romania,*
** Corresponding author: vasile.miclaus@ubbcluj.ro*

mechanisms of mixing, mixing time, scale-up or similarity criteria, specific power consumption, shear rate distribution and flow characteristics [1, 2].

From a practical point of view, power consumption is one of the most important parameter in the design of stirred vessels.

Mixing power for non-aerated Newtonian fluids depends on stirrer speed, N, the impeller diameter and geometry, D, and fluid properties such as density ρ, and viscosity η, Equation 1 [3].

$$Po = \frac{P}{\rho \cdot N^3 \cdot D^5} \qquad (1)$$

$$P = Po \cdot \rho \cdot N^3 \cdot D^5$$

where: Po is the power number (-), and P - power consumption (W).

The power number Po, a dimensionless group, has a significant effect on the definition of power consumption.

The hydrodynamics is strongly dependent on the nature of the fluids involved in the mixing system. Shear-thinning fluids are a class of non-Newtonian fluids, as in the present study, carboxymethyl cellulose (CMC) solution with different concentrations [4].

Carboxymethyl cellulose (CMC) is a water-soluble cellulose derivative with many applications in food, pharmaceutical, cosmetics, detergent, textile, paper and many other industries. It is a white to off-white, non-toxic, odourless and biodegradable powder. CMC is used to enhance the viscosity, to control the rheology of a solution, to avoid separation of water from a suspension, and to improve the surface barrier properties [5].

The rheological properties of CMC depend on the concentration of polymer and the degree of substitution, which varies from 0.5-1.2 [6].

The prediction of power consumption for agitation of time-independent non-Newtonian fluid, at a desired impeller speed, may be evaluated considering the dependence of power number on Reynolds and Froude number, Po = f(Re, Fr).

The value of the Reynolds number is given by:

$$Re = \frac{\rho \cdot N \cdot D^2}{\eta_{eff}} \qquad (2)$$

The corresponding apparent viscosity η_{eff} can be evaluated, either from a flow curve, or by means of the appropriate viscosity model (e.g. power law model).

Depending on the value of Reynolds number it was considered the laminar regime for Re < 10, when $\mathrm{Po} \cong 1/\mathrm{Re}$, turbulent regime Re > 10^3-10^4, when Po becomes independent of Reynolds number, and between them, the transition regime, when both density and the viscosity affect power requirements [1]. The influence of Froude number was neglected in the present estimation; do to the fact that it is generally important only when vortex formation occurs and Reynolds number is higher than 300.

It is known, that as the liquid viscosity or constancy increases, the tendency for vortex formation decreases.

The aim of the present work is to evaluate the fluid rheological parameters on Reynolds criteria, power number Po and specific power consumption P, using different types of stirrers for mixing of CMC solutions with shear-thinning behaviour.

RESULTS AND DISCUSSION

In the present study, the Reynolds number was calculate with the corresponding effective viscosity, η_{eff}, evaluated by means of the power viscosity model:

$$\eta_{eff} = \mathrm{K} \cdot \dot{\gamma}_{avg}^{n-1} \tag{3}$$

The mean shear rate was for the first time estimated by the Metzner and Otto [7] and correlated with rotational speed by Equation (4):

$$\dot{\gamma}_{avg} = \mathrm{k_s} \cdot \mathrm{N} \tag{4}$$

where: k_s is the shearing constant, normally dependent on the type of the stirrer and vessel configuration, and N is the rotation speed of stirrer (rot/s).

The Metzner-Otto method is a widely used method to design impellers for non-Newtonian fluids applications.

For the agitation of shear-thinning liquids by turbines, propellers and paddles, Skelland [8] suggest that the shearing constant k_s lies approximately in the range 10 – 13.

Based on the Godfrey [9] and Wang [10] observations, there are no scale-problems, k_s is independent on the equipment size, and fluid properties.

In the present study, three types of stirrers, paddle, propeller and turbine, are analysed. For each type, the value of k_s is chosen in agreement with the literature data, 10.0 for 2-badles paddle, 10.0 for propeller and 11.5 for turbine [1, 11].

Table 1 contains the obtained values of rheological parameters, K and n, for CMC solutions with 1, 2, 3, 4 and 5, weight %, based on measured data.

The obtained values of flow index, n smaller than 1, indicate the shear-thinning or pseudo-plastic behaviour of all CMC solutions. The values are closer to those founded in literature [12]. As it was expected, with the increase of CMC concentration the index flow n decreases and the material constancy K increases.

Table 1. Rheological parameters of CMC solutions

CMC (%)	K (Pa.s^n)	n (-)
1.00	0.110	0.9000
2.00	0.910	0.7400
3.00	3.035	0.6300
4.00	9.250	0.5626
5.00	28.000	0.5200

The influence of the rheological parameters K and n on the Reynolds number, calculated with the Equation (2), is shown in Figure 1.

For all types of stirrers evaluated in this article, paddle, marine propeller and turbine (Figure 1), the decrease of the Reynolds number with the increase of material constancy K and the decrease of flow index n, is correlated with CMC concentration.

The agitation of non-Newtonian fluids is recommended to be done at low Reynolds, in laminar or creeping-flow region. In the present study, the Reynolds number was calculated as for laminar model up to Re < 50, obtained for CMC concentration higher than 2%.

The prediction of power consumption for agitation of our solutions is evaluated by the Equation (5):

$$P = k_1 \cdot \eta_{eff} N^2 \cdot D^3 = k_1 \cdot K \cdot (k_s \cdot N)^{n-1} \cdot N^2 \cdot D^3 \quad (5)$$

The values of power number determined directly as a function of Reynolds number, $Po = k_1/Re$, and the power consumption P mathematically calculated by Equation 5, are compared with those obtained by graphically method from literature [1] in Table 2.

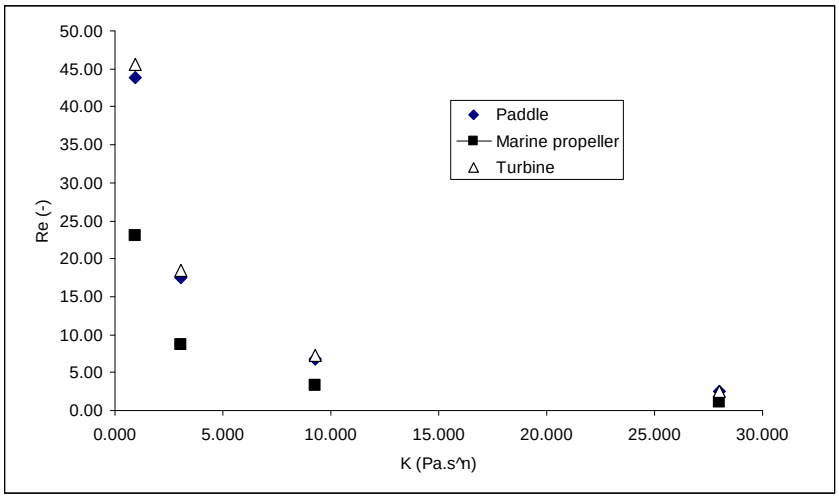

a.

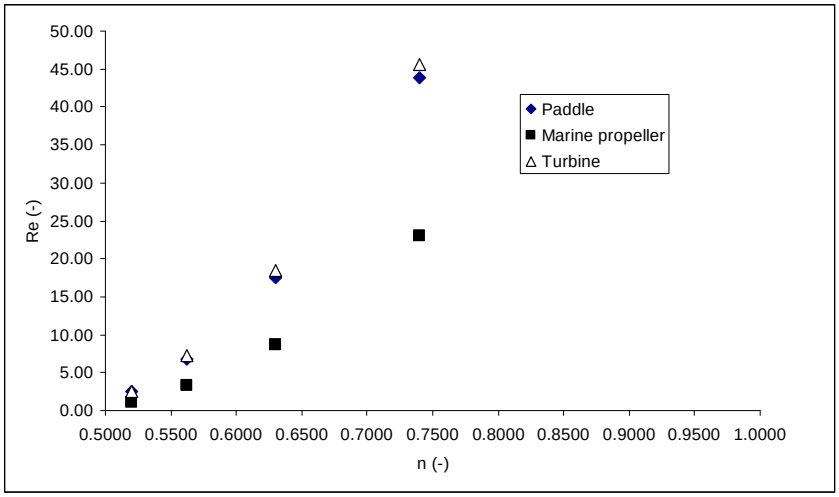

b.

Figure 1. The influence of the material constancy K (a) and flow index n (b) on Reynolds number

The constant k_1 dependent only on the impeller type has the values presented in Table 2 [8].

Table 2. Values of power number and power consumption

CMC (%)	N (rot/s)	D (m)	k_1 (-)	Re (-)	Po math (-)	P math (W)	Po graph (-)	P graph (W)
2-blades Paddle								
2	1.00	0.15	35	43.88	0.80	0.06	1.00	0.08
3	1.00	0.15	35	17.58	1.99	0.15	2.00	0.15
4	1.00	0.15	35	6.76	5.18	0.40	6.00	0.46
5	1.00	0.15	35	2.47	14.15	1.10	15.00	1.16
Marine propeller with 3 blades								
2	0.60	0.15	40	23.06	1.73	0.03	1.70	0.03
3	0.60	0.15	40	8.73	4.58	0.08	4.00	0.07
4	0.60	0.15	40	3.24	12.33	0.21	12.00	0.20
5	0.60	0.15	40	1.16	34.45	0.58	30.00	0.50
Single turbine with 6 flat blades								
2	1.00	0.15	70	45.51	1.49	0.12	2.00	0.15
3	1.00	0.15	70	18.51	3.78	0.29	4.00	0.31
4	1.00	0.15	70	7.19	9.74	0.75	9.50	0.73
5	1.00	0.15	70	2.47	28.31	2.19	30.00	2.32

In order to analyse the dependence of power number Po on Reynolds number for shear-thinning CMC solutions it was plotted the graph in Figure 2.

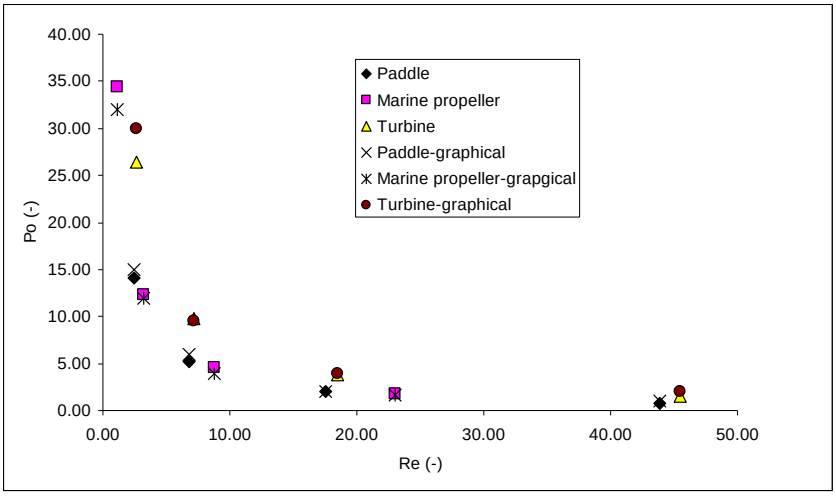

Figure 2. Dependence of Power number on Reynolds number

The results from Figure 2 show the decrease of the power number Po with the increase of Reynolds number, as in the case of Newtonian fluids. Thus means an increase of power number and power consumption with the increase of material constancy K, and decrease of flow index n, in order to keep constant the impeller speed.

Although the values of power consumption are small, they are comparable with other values founded in literature [13, 14].

There are no high differences between values obtained by theoretical and graphical interpretation of the power number, the standard error $\varepsilon < 10$ %.

CONCLUSIONS

Based on the Metzner and Otto method, it was possible to estimate the mixing power requirements with reasonable accuracy in laminar regime, for CMC solutions, inelastic non-Newtonian fluids.

The value of Reynolds number has shown a decrease with the increase of material constancy K and with the decrease of flow index n for CMC solutions.

Power number and power consumption values were influenced by Reynolds number, especial by the apparent or effective viscosity.

The results have shown good agreement between theoretically calculated power number and the graphically determined values.

The obtained values of power consumption are small, but comparable with other values founded in literature.

EXPERIMENTAL SECTION

CMC solutions were prepared by dissolving carboxymethyl cellulose powder in an appropriated hot water and waiting sometime for it to swell, in order to obtain the desired concentration of each solution.

The rheological measurements were performed with a Rheotest-2 rotary rheometer with an S/S1 cylinder system, at an increasing and decreasing shear rate, ranging between 2.0 - 900 s–1. The measurements were conducted at room temperature, 21±1 ^{0}C.

The flow curves were analyzed by power law or Ostwald de Vaele model in order to estimate the rheological parameters of CMC solutions, with a shear-thinning behaviour.

REFERENCES

1. R.R. Chhabra; J.F. Richardson, *Non-Newtonian Flow in the Process Industries. Fundamentals and Engineering Applications*, 2nd ed.; Publisher: Butterworth Heinemann, Linacre House, Jordan Hill, Oxford, Great Britain, **2008**; Chapter 8, pp. 325–358.
2. M. Cortada-Garcia; V. Dore; L. Mazzei; P. Angeli; *Chem. Eng. Res. Des.*, **2017**, *119*, pp. 171-182.
3. G. Ascanio; B. Castro; E. Galindo; *Chem. Eng. Res. Des*., **2004**, *82*, 1282–1290.
4. A. Ghirisan; C.I. Anghel; S. Dragan; In Proceedings of the 41st International Conference of Slovak Society of Chemical Engineering, Editor: J. Markoš, Slovakia, **2014**, pp. 863–872.
5. C. Chang; L. Zhang; *Carbohyd. Polym.,* **2011**, *84*, 40-53.
6. C. Barba; D. Montane; X. Farriol; J. Desbrieres; M. Rinaudo; *Cellulose*, **2002**, *9*, 327-335.
7. A.B. Metzner; R.E. Otto; *AIChEJ*, **1957**, *3*, 3-10.
8. A.H.P. Skelland; in *Handbook of Fluids in Motion*, Edited by N. P. Cheremisinoff and R. Gupta, Ann Arbor Science, Ann Arbor, **1983**, Chapter 7, pp. 623-860.
9. J.C. Godfrey; Static mixers, in *Mixing in the Process Industries*, Edited by N. Harnby, M.F. Edwards and A.W. Nienow, Butterworth-Heinemann, Oxford, 2nd edition, **1992**, Chapter 12, pp. 225-249.
10. J. Wang; L. Feng; X. GU; et al.; *J. Chem. Eng. Sci*., **2000**, *55(12)*, 2339–2342.
11. D. Patel; F. Ein-Mozaffari; M. Mehrvar; *Chem. Eng. Res. Des.,* **2015**, *100*, pp. 126-134.
12. Z.Y. Nor; A.A. H. Zafarizal; E.A.O. Nur; A.M. Yusrabbil, *J. Oil Palm Research*, **2020**, in press Published online: 9 December 2020
13. D. Luan; Q. Chen; S. Zhou; *Chin. J. Mech. Eng*., **2014**, *27(3)*, 635-640.
14. K. Yapici; B. Karasozen; M. Schaefer; Y. Uludag; *Chem. Eng. Process: Process Intensification*, **2008**, *47*, 1340–1349.

STUDIA UBB CHEMIA, LXVI, 2, 2021 (p. 255-264)
(RECOMMENDED CITATION)
DOI:10.24193/subbchem.2021.2.22

NATECH HAZARD IDENTIFICATION AT NATIONAL LEVEL FOR SEVESO SITES AFFECTED BY FLOODS AND EARTHQUAKES

ZOLTÁN TÖRÖK[a], ALEXANDRU OZUNU[a,b] *, ANDREI RADOVICI[a], CRISTIAN MALOȘ[a], ADRIANA CALAPOD[a], FRANCISC SENZACONI[c]

ABSTRACT. The intensity of disasters is on an upward trend and inhabited areas are expanding into various risk areas, threatened by natural, technological or complex multi-hazards. The present study focuses on the analysis of Seveso-type economic operators whose activity is regulated by Law 59/2016 on the control of major-accident hazards involving dangerous substances. In Romania, the natural hazards that can trigger technological accidents in these sites are largely represented by earthquakes and floods. The analysis presented in this study was performed for a recurrence period of 475 years for earthquakes and 500 years for floods. The results of the analysis highlighted the sites in Romania that present specific Natech risks. Also, the possible technological accidents that may occur as a result of the manifestation of natural hazards have been identified for each site while a more detailed analysis was performed for the selected processes based on qualitative criteria. Finally, a ranking of these sites for Natech risks is presented considering the two natural hazards.

Keywords: *Natech, Seveso, earthquake, flood*

INTRODUCTION

Although the Romanian chemical industry is no longer as well represented as before 1989 [1] there are a number of companies that still manage large quantities of hazardous substances [2]. In the context in which

[a] *Babeş-Bolyai University, Faculty of Environmental Science and Engineering, ISUMADECIP Institute, 30 Fântânele str., RO-400294, Cluj-Napoca, Romania;*
[b] *Disaster Management Training and Education Centre for Africa (DiMTEC), University of the Free State, Bloemfontein, South Africa*
[c] *General Inspectorate for Emergency Situations, Ministry of Internal Affairs, Romania*
** Corresponding author: alexandru.ozunu@ubbcluj.ro*

the intensity and complexity of disasters is on an upward trend [3]–[6] and inhabited areas are expanding into various risk areas, a reference point in terms of impact on the health of the population and the environment is represented by technological accidents [7]. It is this complex nature of disasters that has led to the study of Natural hazard triggered technological accidents (Natech) and multi-hazard events. Natechs involving the release of hazardous materials were studied for the first time at the end of the 1970s and were mainly focused on earthquakes as the main triggering event, only later they were focusing on other types of natural hazards such as floods [8]. The basic concept, which was later developed, refers to the natural hazards capacity to determine the loss of containment (LOC) in affected industrial facilities causing pollution, toxic dispersions, fires or explosions [9], [10].

Even though Natechs are low probability events, the linked consequences are significant enough to determine a comprehensive analysis which can fall outside traditional risk assessment and management practices [11]. An overview article on advances in Natech research [8], showed that the peer reviewed papers were grouped in three major categories based on the type of hazards (geological, hydrometeorological and multi-hazards) and referred to four stages in the risk management process: accident analysis and return of experiences, risk assessment, risk treatment/risk reduction, risk communication and risk perception.

Numerous examples of Natech disasters and their investigation, such as the Kocaeli earthquake in Turkey which destroyed the Tupras refinery [12], or the Tohoku earthquake and consequent tsunami in Japan causing multiple Natech disasters at the Fukushima nuclear plant, Chiba and Sendai refineries etc. [13] are presented in the scientific literature. Lessons learned from these disasters are key elements to consider in future risk mitigation strategies and plans.

A study developed by Campedel [14] of Natech accidents reported in the main chemical accident databases, such as ARIA, MARS, DFC, MHIDAS, NRC, FACTS etc., shows an average of 2-3% of Natech events out of the total registered accidents. The author concludes that the very low number of these events is mostly due to the improper reporting of accident data in terms of causes and consequences. The results of the study reveal that in case of floods the most affected equipment were atmospheric storage tanks, floating roof storage tanks, pipelines and pressurized tanks, mostly involving the release of oil, diesel and gasoline and leading to water and ground contamination, fires or explosions. In case of earthquakes the most affected equipment were pipeworks and atmospheric storage tanks leading to releases followed by fire, explosion, dispersion and ground contamination [14].

The first disaster risk assessment at national level in Romania was conducted under the coordination of General Inspectorate for Emergency Situations (GIES) within the “RO-RISK” project and aimed both natural and anthropic related risks. Although the results of the project indicated a generally lower level of technological risks than that represented by earthquakes or floods [2], one of the conclusions was that the main direction of future research should be determined by a more detailed analysis of the interaction between natural and technological hazards [15].

In Romania the prevention and control of major industrial accidents involving dangerous substances is regulated by Law 59/2016 [16], being the Seveso III Directive of the EU Commission transposed into the national legislation. The law stipulates that in the risk analysis the possible internal and external events, such as natural hazards, must be considered as accident initiating factors [16].

The earthquake risk in Romania, determined by the Vrancea seismic region, is one of the highest in Europe and has caused many casualties and extensive damage in the past centuries. Natech risk analyses have been carried out for Romanian Seveso-type sites, such as the study conducted by Gheorghiu et.al for a petroleum product storage tank farm, within Vega refinery, affected by a possible seismic event [17], or the case study developed in “RO-RISK” project considering earthquake induced chlorine release from a storage tank, within Oltchim site [2]. The results of these studies have reflected an increase of the overall risk with one order of magnitude when considering the earthquake induced Natech events in the risk analysis, compared to pure technological risks [2], [18]. Due to the above presented aspects, a national level analysis of possible Natech accidents is with high importance.

In what follows, this study aims to provide an overview of the situation of Seveso operators from Romania, located in earthquake and flood prone areas and the possible outcomes of the interaction between natural and technological hazards. The study presents a starting point for the future national multi-risk assessments. A ranking of these sites have been made for both Natech types, based on qualitative criteria and expert judgement. The study presents a starting point for the future national multi-risk assessments.

RESULTS AND DISCUSSION

The results of the exposure analysis of Seveso sites to the flood hazard highlighted that a number of 20 sites, out of the total 245, are located in floodable areas where water depth can reach values that varies from 0.1 up to 11.2 meters for flood events with a recurrence period of 500 years (Figure 2).

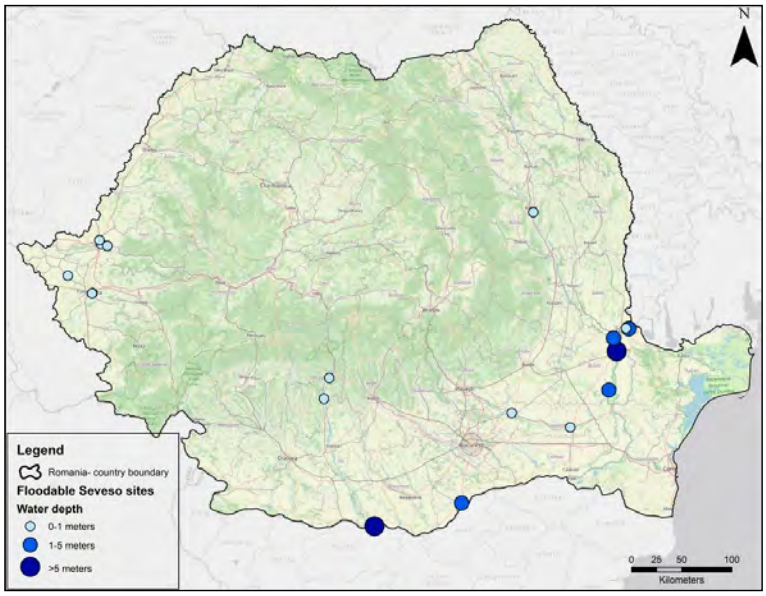

Figure 1. Seveso sites exposed to floods in Romania

From the point of view of activities carried out within these sites, it can be mentioned that 5 operators have petroleum products / fuel storage activities, followed by the compression and distribution of LPG and the production of technical gases. The other sites operate in the field of agriculture or production of fertilizer, vehicles and energy. The most common hazardous substances found on these sites, and in the largest quantities, are derived petroleum products like diesel oil, gasoline or naphtha stored in atmospheric or floating roof tanks, which are highly vulnerable to floods. Ammonium nitrate, its precursors and liquefied gases are the following hazardous materials when considering degree of occurrence and quantities stored within the sites. The information extracted from the hazard sheets specific to each of the operator, developed within RO-RISK Project, indicates the following types of possible events: toxic dispersions in air, fires, explosions and BLEVE. To these scenarios the water contamination can also be added as the main outcome of a release in case of floods.

The analysis regarding the number of Seveso sites located in earthquake prone areas highlighted a number of 4 active sites in zones with PGA values higher than 400 cm/s^2 and a number of 38 sites in areas with PGA values between 300-400 cm/s^2.

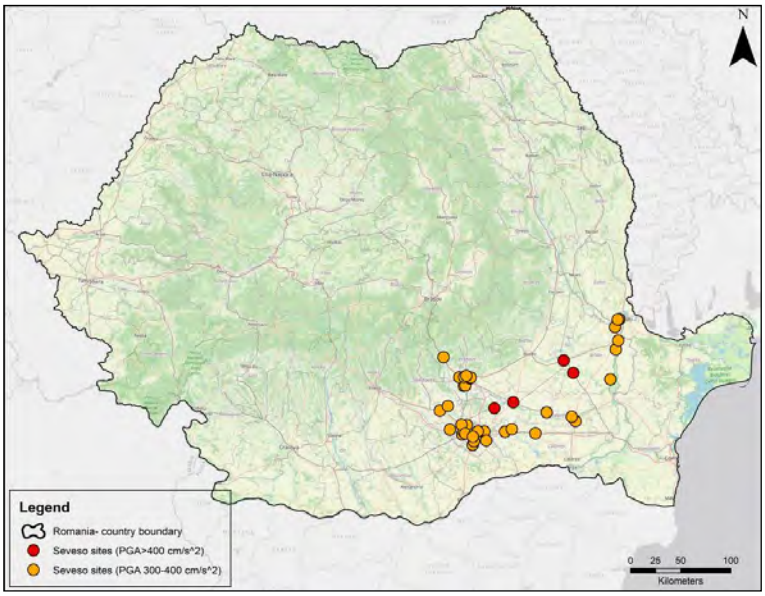

Figure 2. Seveso sites exposed to earthquakes in Romania (PGA >300 cm/s^2, recurrence period-475 years)

Two of the sites located in the areas where PGA reach values higher than 400 cm/s^2 operates in the field of storage, compression and distribution of LPG, and the other two are involved in the storage activity of the fossil fuels. Thus, the substances present on these sites are mostly represented by liquid or liquefied gas fuels, the most probable scenarios can be fires, explosions, BLEVEs and ground contamination.

Regarding the field of activity of the sites located in area where PGA can reach values between 300-400 cm/s^2, the results of the analysis indicate that the largest number of these sites operate in the field of compression and distribution of LPG (6 sites) on par with storage of petroleum derived fuels. Significant activities of the operators are also found in the oil refining, energy production and agriculture sectors. As this area largely corresponds to the oil extraction fields in Romania, explains the fact that most operators carry out related activities and the most common hazardous substances at the sites are petroleum derivatives. The hazard sheets prepared for these sites indicate the possibility of four types of technological hazards: toxic dispersions, fires, explosions and BLEVEs, to which the ground contamination can be added.

The situation of the sites exposed to the two types of natural hazards analyzed, from the point of view of the worst-case scenarios for technological accidents, is presented in Table 1. The values presented in the table refer only

to the scenarios resulting from the inherent characteristics of the materials and processes, not being influenced by the possible action of natural hazards and further cascading events.

Table 1. The number of occurrences for possible worst-case scenarios in case of Natech accidents

		Toxic dispersion in air	**Fire**	**Explosion**	**BLEVE**	**Water/ ground contamination**
Sites exposed to:	Floods	4	14	8	8	20
	Earthquake	19	27	18	19	42

Using RO-RISK Project data, hazard and vulnerability identification and expert judgement a qualitative Natech ranking index of the sites has been calculated, based on the criteria evaluation described above.

The list of the top 5 sites for flood, respectively top 4 sites for earthquake induced Natech (presented only for PGA > 400 cm/s2), are presented in Table 2.

Table 2. List of the top Natech prone sites from Romania

Ranking	**Flood**	**Index value**	**Earthquake**	**Index value**
1	Donau Chem – Teleorman county	15	Romgaz – Prahova county	12
2	Unicom Oil Terminal – Galați county	15	Conpet – Braila county	11
3	City Gas – Galați county	10	Panebo Gaz – Braila county	9
4	Padova Agricultura – Brăila county	10	Delta Gaz – Ialomița county	9
5	Air Liquide Romania – Brăila county	8		

It can be noticed that all sites from the Flood category are located in the immediate vicinity of the Danube river, which can produce high water levels in case of a 500 years flood event.

In case of the Earthquake category Romgaz site took the 1st place, because of the very high quantities of natural gas stored underground. Normally, in case of an earthquake, only damages at the pipeworks pipelines

of the separate wells are expected with the release of much lower quantities of gas than the total stored. Therefore, a correction in the ranking is necessary, placing Conpet site in the top of the list.

CONCLUSIONS

The study aimed to create a rapid methodology for the ranking of Seveso-type chemical plants in Romania, from the perspective of Natech risks induced by floods and earthquakes.

A qualitative criteria evaluation was performed using RO-RISK project data combined with GIS technique. Among the limitations of the study, we can enumerate the lack of better resolution flood maps; the lack of flood water speed estimations and the qualitative way of Natech hazard identification and risk analysis.

In conclusion, this study is serving as a starting point for more detailed Natech risk assessments, using quantitative risk analysis methodologies. Furthermore, the importance of such studies in disaster risk reduction activities, land-use and emergency planning is highlighted due to the increased risk and complexity of Natech events.

EXPERIMENTAL

In order to determine which Seveso sites are located in flood and earthquake prone areas the list of the 300 operators analyzed within the national risk assessment [2] was verified and updated, aiming to identify the operators that still carry out their activity or are still under the provisions of Romanian Law 59/2016 [19].

The characterization of flood impact on equipment is based on frequency (recurrence period) and severity quantified by water depth and speed [14], [20].

The database on flood prone areas in our country, used within this study, was developed by the European Commission's Joint Research Centre (JRC) at global scale for flood events with 500-year recurrence period [21]. The limitations of this database are consisting mostly on spatial data resolution of approx. 1km or 30 arcseconds and the fact that it is only available for large watercourses [22], [23] and representing only the water depth. Therefore, this study analyses the possible Natech events only from the perspective of the water depth, without quantifying the potential impact of floods on specific equipment.

Using Geographic Information System (GIS) specific techniques, the raster dataset was accessed in order to retrieve the values of water depth (in

meters) characteristic for each cell. The data on Seveso sites located in floodable areas were obtained by overlapping the layer consisting in Seveso sites locations with the raster provided by JRC.

For the study of Seveso operators in earthquake prone areas, it was necessary to retrieve information related to the expected seismic effect, expressed in terms of earthquake ground-motion parameters. In this regard the peak ground acceleration (PGA) values calculated by Sokolov et al. [18] were used in order to identify the Seveso sites in high seismic prone areas. Again, the collocation information was obtained based on GIS techniques for areas with PGA higher than 300 cm/s^2 for events with a recurrence period of 475 year, this period being recommended in "Eurocode 8: Seismic design of buildings" and typically used in Natech risk assessments for Importance class II buildings, such as most of the Seveso establishments [3].

The schematic representation regarding the identification of the Seveso sites located in the area of manifestation of natural hazards can be consulted in Figure 1.

Along with the selection of sites that are located in flood prone areas or with high seismicity, specific data was extracted from safety reports or major accident prevention policies regarding the types and maximum quantities of substances possible to be present on sites, type of storage/processing and maximum distances calculated for the accident scenarios involving: fires, explosions, boiling liquid expanding vapor explosions (BLEVE), toxic dispersions in air or soil and water pollution.

Considering the above-mentioned data and the hazardous properties of the substances and their classification according with Annex 1 of Law 59/2016, ranking criteria were created for the following factors:

- Fire/explosion hazard: 1–low (P5c liquids, for ex. Crude oil); 2-medium (P5b liquids – Gasoline etc., P3b aerosols); 3-high (P1a,b explosives, P2 flammable gases, P3a flammable aerosols, P5a flammable liquids);
- Pollution hazard: 1-low (without major environmental effects, harmful health hazards); 2-medium (E2 chronic environmental effects; H2 acute toxicity); 3-high (E1 acute environmental effects; H1 acute toxicity);
- Storage/processing vulnerability: 1-low (underground storage of natural gas; pressurized process equipment); 2-medium (pressurized storage in high quantities); 3-high (atmospheric storage in high quantities);
- Quantity: rounded value of the logarithm base 10 of the maximum quantity of substance possible to be present;
- Distance between first vulnerable elements dV (human settlements identified using GIS software) and radius of potential impact ri (calculated in the safety reports): 1-low (if $(dV - ri) > 100$ m); 2-medium (if $100 \text{ m} \geq (dV - ri) \geq 0$ m); 3-high (if $(dV - ri) < 0$ m).

The total ranking score of each site is calculated by summing up the individual criteria scores.

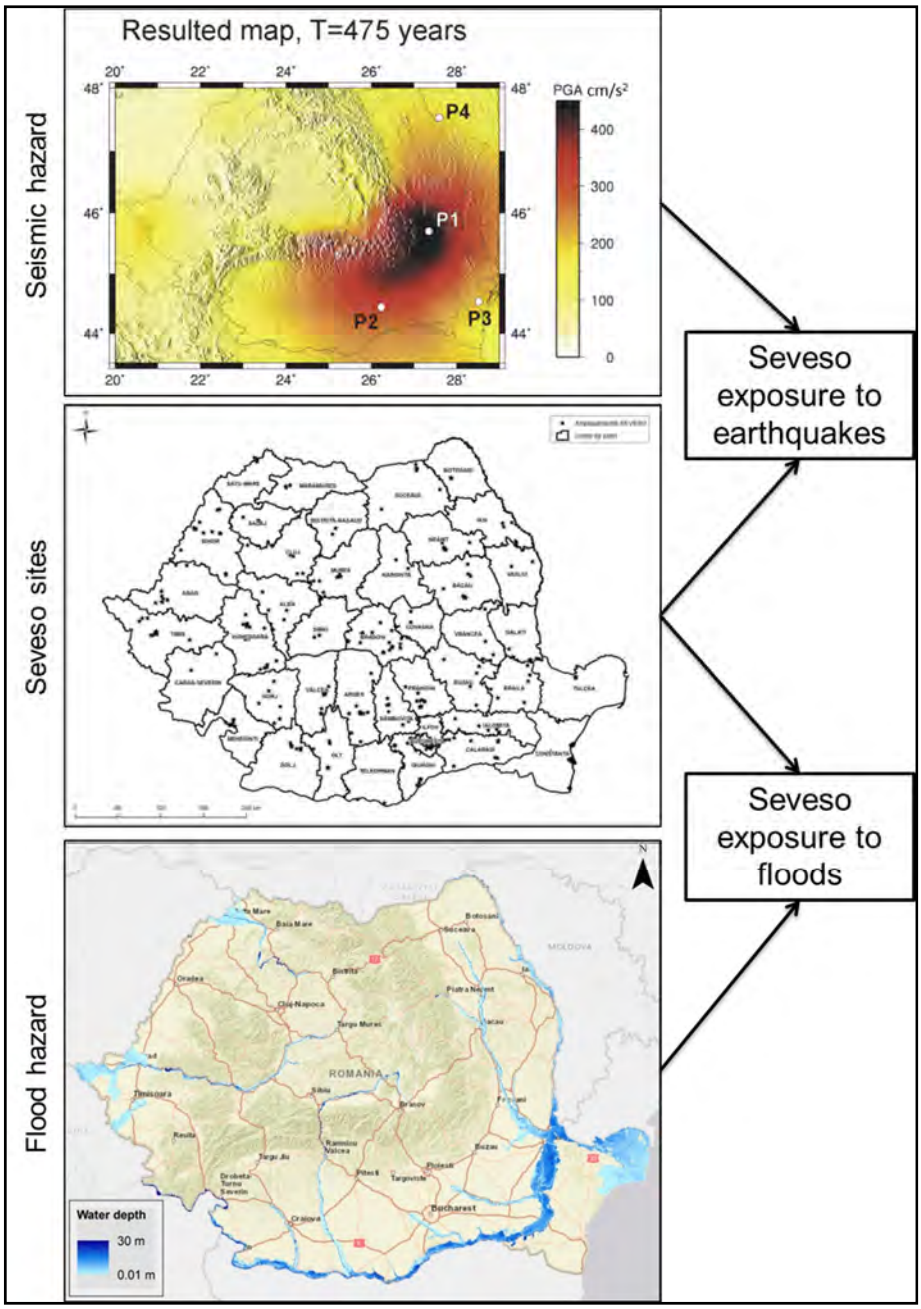

Figure 3. GIS workflow diagram for determining the exposure of Seveso sites to earthquakes [18] and floods [21]

REFERENCES

1. A. Ozunu; Safety hazards and risks in Romania. *SSCHE Conference proceedings*, **2019**
2. Romanian General Inspectorate for Emergency Situations (IGSU); National Risk Assessment- Country Report, **2016**
3. A.M. Cruz; L.J. Steinberg; A. Lisa; V. Arellano; J.-P. Nordvik; F. Pisano; State of the Art in Natech Risk Management (NATECH: Natural Hazard Triggering a Technological Disaster), **2004**
4. M.K. Lindell; R.W. Perry; *J. Hazard. Mater.,* **1996***, 50,* 31-46
5. K. Rasmussen; *J. Hazard. Mater.,* **1995***, 40, 43-54*
6. H. Sengul; N. Santella; L.J. Steinberg; A.M. Cruz; *Disasters,**2012**, 36, 4,* 723-743
7. A. Ozunu; *Elemente de hazard şi risc în industrii poluante*; Editura Accent, Cluj-Napoca, **2000**, pp. 7-12
8. A.M. Cruz; M.C. Suarez-Paba; *Prog. in Dis. Sci.*, **2019**, *1*, 100013, 1-4
9. J. Casal; Introduction. In *Evaluation of the Effects and Consequences of Major Accidents in Industrial Plants*, Elsevier Ltd., **2018,** pp. 1-24
10. A. Mesa-Gómez; J. Casal; F. Muñoz; *JLPPI*, **2020**, *64*, 104071, 1-14
11. V. Cozzani; G. Antonioni; G. Landucci; A. Tugnoli; S. Bonvicini; G. Spadoni; *JLPPI*, **2014**, *28*, 10-22
12. S. Girgin; *Nat. Hazards Earth Syst. Sci.*, **2011**, *11*, 4, 1129-1140
13. E. Krausmann; A.M. Cruz; *Loss Prev. Bull.*, **2021**, *277*, 10-14
14. M. Campedel; Analysis of Major Industrial Accidents Triggered by Natural Events Reported in the Principal Available Chemical Accident Databases, *JRC Publications Repository*, Luxemburg, **2008**, pp. 17-29
15. Romanian General Inspectorate for Emergency Situations (IGSU); Summary containing the conclusions of the study within component 1 of RO-RISK research, **2016,** pp. 11-17
16. Law No. 59/2016 of 11 April 2016 on the control of major accident hazards involving dangerous substances; In Romanian Official Gazette no. 290, **2016**
17. A.D. Gheorghiu; Z. Török; A. Ozunu; G. Antonioni; V. Cozzani; *Chem. Eng. Trans.*, **2014**, *36*, 439-444
18. V.Y. Sokolov; F. Wenzel; R. Mohindra; *Soil Dyn. Earthq. Eng.*, **2009**, *29*, 364-381
19. Romanian General Inspectorate for Emergency Situations (IGSU); List of economic operators classified in accordance with the provisions of Law 59/2016, 2019, Available at: https://www.igsu.ro/Resources/Seveso/Lista operatorilor economici clasificati in conformitate cu prevederile Legii 59_2016 la 30.12.2019 pentru site IGSU.doc
20. A.M. Cruz; N. Okada; *Nat. Haz.*, **2008,** *46*, 2, 199-220
21. F. Dottori; L. Alfieri; P. Salamon; A. Bianchi; L. Feyen; F. Hirpa; Flood hazard map of the World - 500-year return period, *Eur. Comm. Jt. Res. Cent. [Dataset]*, **2016**
22. L. Alfieri; P. Salamon; A. Bianchi; J. Neal; P. Bates; L. Feyen; *Hydrol. Process.*, **2014**, *28*, 13, 4067-4077
23. F. Dottori; P. Salamon; A. Bianchi; L. Alfieri; F.A. Hirpa; L. Feyen; *Adv. Water Resour.*, **2016**, 94, 87-102

STUDIA UBB CHEMIA, LXVI, 2, 2021 (p. 265-275)
(RECOMMENDED CITATION)
DOI:10.24193/subbchem.2021.2.23

FISH ROE SAMPLE PREPARATION FOR SYNTHETIC FOOD DYES DETERMINATION BY HPTLC

DORINA CASONI[a], MIHAELA BADEA[b], SIMONA CODRUTA AURORA COBZAC[a]*

ABSTRACT. Food dyes are widely used in food products to offset the colour loss. To prevent fraud in the food industry, to ensure food safety and consumer health protection, it is necessary to implement fast, accurate and reliable methods for the analysis of dyes. A relatively fast method based on high-performance thin-layer chromatography (HPTLC) - photodensitometry was developed and applied to determine two synthetic food dyes (Sunset Yellow – E 110 and Ponceau 4R – E 124) in fish roe. TLC separation was carried out on silica gel plates, using the mixture isopropyl alcohol-ammonia (2:1, V/V) as mobile phase. Good separation of the dyes was achieved, the R_f values being 0.39 for E110 and 0.12 for E124, respectively. Due to the complexity of the matrix, sample preparation was performed into two steps: (i) extraction by ultrasound-assisted extraction with methanol-ammonia (1:1, V/V) and (ii) purification of the extract by ion-pair solid phase extraction (IP-SPE) on ChromaBond RP-18E cartridges. For both dyes, the overall recovery for the sample preparation step was higher than 91%, the relative standard deviation being less than 3.5%. The procedure was applied for E110 and E124 determination from a “red caviar” sample with the declared content of dyes.

Keywords: *Food synthetic dyes, roe fish, ultrasound-assisted extraction (UAE), ion-pair solid phase extraction (IP-SPE), HPTLC*

INTRODUCTION

The evolution of human society has caused increasing consumer complaint regarding food quality. The long experience on food demonstrates

[a] *Babeş-Bolyai University, Faculty of Chemistry and Chemical Engineering, 11 Arany Janos str., RO-400028, Cluj-Napoca, Romania*
[b] *Transilvania University of Brasov, Faculty of Medicine, 29 Eroilor Blvd, 500036, Brasov, Romania*
** Corresponding author e-mail: simona.cobzac@ubbcluj.ro*

that the nutrition problem is more complex than the simple food-consuming act. The scientific studies have pointed out that the concept of food quality should be improved by taking into account all of its four aspects: energetic, biological, hygienic and psycho-sensorial [1]. One of the most important sensory qualities of a food product is the colour, frequently related to freshness and good taste. This aspect determines the producers to find solutions to produce more and more attractive food. Due to their instability, the natural dyes were replaced with synthetic food dyes (SFDs), which are cheaper, brighter, and stable. Food synthetic colorants are complex organic compounds derived from coal tar and petroleum that are classified according to their chemical structure (azo, triphenylmethane, indigo, etc.) and colour (yellow, orange, red, etc.).

Recent studies concerning the influence of SFDs on human organism revealed their neurotoxicity, genotoxicity and carcinogenicity. Azo dyes can be decomposed in the intestine to aromatic amines causing headaches and hyperactivity, and also they may have immunomodulatory effects even at a non-cytotoxic dose [2]. Due to these toxic effects, EU legislation has elaborated regulations that establish a list of food additives, which include the approved SFDs and their conditions of use [3, 4].

As there is a growing need for fast, sensitive and accurate analytical methods to determine SFDs in different types of food, researchers have also focused on this topic [5]. Due to their spectral properties, dyes can be easily determined by spectrophotometric methods [6]. Complex dyes mixtures can be resolved by multivariate calibration [7] or spectra interpretation with the aid of chemometric computations such as classical least squares (CLS), principal component regression (PCR), partial least squares (PLS) and hybrid linear analysis (HLA) [8]. Spectrophotometric improved instruments for SFDs determination were also reported [9]. The most used technique for SFDs determination is chromatography which allows separation, identification and quantification in one single run. Usually, high-performance liquid chromatography with diode array detection (HPLC-DAD/PAD) [10, 11] and high-performance liquid chromatography coupled with mass spectrometry (HPLC-MS) [12, 13] are used. Another employed technique for SFDs determination is thin layer chromatography (TLC). The difficulty of this technique consists in optimization of chromatographic conditions regarding the selection of the stationary phase and an appropriate mobile phase. Usually, silica gel plates were used for separation. Various mobile phases were reported in the literature [14-16]. Plate evaluation was performed classical by scanning the plate at an appropriate wavelength or digital image processing [17-19].

Sample preparation is the bottleneck of an analysis. In the TLC technique, partial removal of the interferences (sugars, fats) can cause the blurring of chromatographic spots. Preconcentration and purification of liquid samples can be achieved by liquid-liquid microextraction [20] or dispersive liquid-liquid microextraction [21]. Solid-phase extraction is another technique usualy applied for preparation of liquid sample. The retention of SFDs is performed by using different sorbents such as alumina [22, 23], polyamide [10,19, 22], C18 [14, 19], aminopropyl modified silica [6], hydrophilic-lipophilic balanced polymers (HLB) [12] and anion exchangers [22]. Different liquid-solid extraction techniques were also employed to extract SFDs from solid matrices, ranging from classical ones such as magnetic stirring to modern ultrasound-assisted extraction [24] and accelerated solvent extraction [25], respectively. The touchstone is the selection of those extraction conditions that can assure an exhaustive extraction of the analytes.

According to our knowledge only few studies have been published for SFDs determination in samples with high content of protein and lipid [26, 27]. Based on the above consideration the aim of this paper is development of a new method fpr determination of Sunse Yellow – E110 (SY) and Ponceau 4 R – E124 (P4R) in fish roe and red caviar using ultrasound-assisted extraction (UAE) and ion-pair solid phase extraction (IP-SPE) for sample preparation followed by high-performance thin-layer chromatography (HPTLC) analysis.

RESULTS AND DISCUSSION

Evaluation of the analytical performance of the chromatographic method

The chromatographic analysis of the dyes, carried out on HPTLC Silica gel G60 plates using the mixture isopropyl alcohol - ammonium hydroxide (2:1, v/v) as mobile phase, revealed a good separation of the analysed SFDs with a R_f value of 0.39 for E110 and 0.12 for E124. The analytical performance of the chromatographic method was evaluated in terms of linearity range, limit of detection (LOD) and quantification (LOQ) (Table 1).

Table 1. Calibration curve equation for the studied food synthetic dyes

SFD	Calibration range (ng/spot)	Equation	R^2	LOD (ng/spot)	LOQ (ng/spot)
E 110	81.65 – 489.9	Y=97127X + 5912.3	0.9959	36.8	69.9
E 124	117.45 – 704.70	Y=59669X + 7454.5	0.9935	24.3	46.5

Recovery studies

The fish roe samples are very complex solid matrices considering their high content in lipids, proteins and salt. Moreover, in this particular case, sample preparation is more difficult due to the high affinity of synthetic food dyes for proteins [28]. Usually, sample preparation of a solid matrix is performed in two steps: (i) analyte isolation from the solid using a solvent or a mixture of solvents which should ensure exhaustive extraction of the analytes and (ii) extracts purification to remove the interferences using liquid-liquid extraction or solid-phase extraction (SPE). As the number of processing steps increases, the sample preparation has a larger contribution to the overall analysis error. Anyhow, each step must be carefully optimized because only in those conditions the error and the relative standard deviation can be diminished. Moreover, to obtain reliable and robust sample preparation, it is preferable to carry out the studies on the different sample and at various concentration levels of the analytes.

Taking in account the general considerations mentioned above, the recovery studies were carried out on two types of fish roe - herring and trout, selected based on their properties: herring roe having a white colour it was easier to observe the extraction of the dye by visual observation, and trout roe because of the similar aspect with the red caviar sample. On the other hand, the recovery studies were carried out on two different concentration levels.

SPE recovery study

For the recovery studies, liquid matrices obtained by extraction from fihs roe (herring) free of dyes were used. These extracts were spiked with E110 and E124 at a concentration level of 40.825 µg/mL and 58.725 µg/mL. Two approaches for extract purification using SPE were studied. The first one consists of dyes retention from acidic solution (acetic acid aqueous solution 2%). Good recoveries values were obtained (Table 2), but when the extract was evaporated, a lipids residuum was observed.

The second procedure was based on the retention of the ion-pair compound formed by the SFDs with CTAB. By applying this procedure, several advantages have been achieved. First, the retention of the dyes on C18 sorbent, through a hydrophobic retention mechanism, was improved. Narrow adsorption zone was obtained because of the strong interaction between hexadecyl radical of the ion-pair compound and the octadecyl chains of the sorbent. Second, during retention, CTAB was also adsorbed on the sorbent surface. This imparts a charged character to the sorbent surface, and lipids were no longer retained. All these contribute to obtaining a cleaner extract and high recovery values (Table 2).

Table 2. Recovery values of dyes obtained by SPE

Sample	Purifying method	Recovery (%)		RSD (%)	
		E110	E124	E110	E124
Spiked extract of herring roe	SPE (acid environment)	97.42	97.09	1.06	1.31
	SPE (ion-pair with CTAB)	98.53	97.78	0.70	0.94

Overall recovery study for sample preparation

The studies of SFDs recovery were carried out on spiked roe samples at two concentration levels using ultrasound-assisted extraction. The mixtures water-ammonium hydroxide (Method I and II) and methanol-ammonium hydroxide (Method III and IV) were used as extraction system. Two purification techniques, liquid-liquid and SPE using a C18 sorbent, were evaluated. The extraction agent used for method I and II was selected considering that SFDs are very soluble in water and that ammonium hydroxide can break the bond analyte-substrate. After centrifugation, when the removal of the residual lipids was attempted by liquid-liquid extraction (Method I), a three-phase system was formed. When SPE was employed for purification (Method II) the cartridge becomed quickly clogged. It is possible that during sonication, when high shear forces are present, the cell membrane to be advanced fragmented. Consequently, the extraction system was changed; water being replaced with methanol (Method III). Due to a lower value of the heating capacity ratio, the pressure produced by the acoustic waves in the new extraction system was smaller. The complete extraction was achieved after three extraction cycles. After HPTLC separation, tailed spots were observed. These could be explained by the presence of interferences. A purification step by SPE was implemented in the sample preparation protocol (Method IV). Based on the recovery values obtained using extraction Method IV (Table 3) the IP-SPE variant was chosen for pre-treatment of the red caviar sample.

Synthetic food dyes determination from red caviar sample

The determination of dyes content was performed using ultrasound-assisted extraction with methanol:ammonia mixture as extraction system followed by IP-SPE (Method IV). The extraction was carried out on non-spiked red caviar samples (C0) and also on spiked samples at two concentration levels (C1; C2). The analytes were identified by comparing the retention factor

R_f and spot colour with those of the SFDs standard spots. The calibration curve method was used for the determination of dyes amount in red caviar. The initial amount of SFDs for spiked samples was computed as diference between the determined quantity and the added one.

Table 3. Recovery of the dyes extracted from spiked fish roe samples by Method IV (extraction agent methanol-ammonia (1:1, v/v) and extract purification by SPE)

Sample (spiking level)	Purifying method	Recovery (%)	
		E110	E124
Herring roe (L1)	SPE	91. 47	91.20
Herring roe (L2)	SPE	87.56	85.98
Trout roe	SPE	87.24	86.66
Herring roe (L1)	SPE	98.98	96.26
Herring roe (L2)	SPE	93.48	91.87
Trout roe	SPE	97.49	95.37

Table 4. Quantitative estimation of the synthetic dyes content in red caviar by using standard addition method at two concentration levels

No	Red caviar sample	Determined amount (mean value ± SD) (mg/kg)	
		E110	E124
1	C0	195.51(±7.96)	197.65(±5.18)
2			
3			
4	C1	192.46(±6.41)	194.82(±7.2)
5			
6			
7	C2	191.90(±8.36	193.69(±7.47)
8			
9			

C0 – non-spiked sample; C1 – spiked sample (40.825 µg/mL E110; 58.725 µg/g E124); C2 – spiked sample (81.65 µg/mL E110; 117.45 µg/g E124); the determined amount was expressed as mean value ± SD

In order to decide if there are significant differences between the determined concentration of SFDs in non-spiked (C0) and spiked (C1, C2) t-test was used for the statistical comparation of the mean values (Table 5).

Table 5. Statistical parameters for comparison of results in non-spiked and spiked caviar samples

Grup	C0		C1		C2	
	t-value	**p**	**t-value**	**p**	**t-value**	**p**
SY						
C0	-	-	1.5750	0.1904	1.6462	0.1750
C1	-	-	-	-	0.2760	0.7961
P4R						
C0	-	-	2.2921	0.0837	1.6838	0.1675
C1	-	-	-	-	0.5699	0.5992

C0 – non-spiked sample; C1 – spiked sample (40.825 µg/mL E110; 58.725 µg/g E124); C2 – spiked sample (81.65 µg/mL E110; 117.45 µg/g E124)

At a confidence interval of 95%, a significance level of 0.05 and 4 degree of freedom, the critical t-value is 2.78. Since the experimental t-value is smaller than critical value, null hypothesis (no significant differences) is accepted.

CONCLUSION

A fast, simple, and economically method was developed for the determination of SFDs from the fish roe. Sample preparation was achieved by using ultrasound-assisted extraction with methanol-ammonia (1:1, v/v) as extraction agent followed by IP-SPE extract purification using CTAB as an ion-pairing reagent. TLC analyses were carried out on HPTLC Silica gel plates and isopropyl alcohol-ammonia (2:1, v/v) as mobile phase. The extraction studies on SFDs in spiked roe samples showed an overall recovery value at least of 91.87% and a maximum relative standard deviation of 3.49%. The proposed method was used for the determination of E110 and E124 in a red caviar sample, 193.29 mg Kg^{-1} and 195.39 mg Kg^{-1} being determined for E 110 and E 124, respectively. Considering the studied dyes as a III-rd category food additive that permit a maximum combined limit of 300 mg Kg^{-1}, the red caviar product cannot be considered adequate for consumers.

EXPERIMENTAL SECTION

Reagents and chemicals

Methanol (PubChem CID: 887), iso-propanol (PubChem CID: 3776), hexane (PubChem CID: 8058), acetic acid (PubChem CID: 176) and ammonium hydroxide (25%) (PubChem CID: 14923) were purchased from Chemical Company

(Iași, România). Sunset yellow (PubChem CID: 6093232) and Ponceau 4R (PubChem CID: 54604869) were purchased from Fluka (Buchs, Switzerland). Cetyltrimethylammonium bromide (CTAB) (PubChem CID: 5974) was purchased from Merck (Hohenbrunn, Germany). All reagents were analytical grade. HPTLC Silica gel 60 plates (20x10) and ChromaBond C18 (6 mL/500mg) cartridges were purchased from Macherey-Nagel (Duren, Germany).

Standard solutions of Sunset Yellow-E110 (163.3 µg/mL) and Ponceau 4R-E124 (234.9 µg/mL) were prepared by dissolving the appropriate amounts of dyes in methanol. For calibration curve, a 1:5 dilution of standard solution was used. The standard solutions were stored in darkness at 4^{o}C until use. Acetic acid 2% and CTAB 0.02% aqueous solution were also prepared.

Experiments were carried out on two different samples of fish roe (herring and trout) free of dyes and on a red caviar sample with the declared content of synthetic colorants on the label. All these samples were purchased from the local supermarket.

Equipments

Sample preparation was performed by using an Elma Transsonic T310 sonication bath (Singen, Germany), a Hettich EBA20 centrifuge (Tuttlingen, Germany) and a drying stove Venticell BMT (Brno, Czech Republic). An IST VacMaster vacuum manifold was used for solid-phase extraction (Lund, Sweden). The samples were applied on the Silica gel plates using a Linomat 5 semiautomatic TLC applier (Camag, Switzerland). Plate evaluation was performed using a Dual-wavelength flying spot scanner Shimadzu CS-9000 (Shimadzu Scientific Instruments, Inc. Columbia, MD, USA).

Sample preparation

A blank extract* of *fish roe was obtained by ultrasound extraction of 2 g of herring roe three times with 10 mL of methanol-ammonium hydroxide (25%) (1:1, v/v). The collected extracts were centrifuged 10 minutes at 4500 rpm, and the supernatant was evaporated and brought to 10 mL with methanol-water (9:1, v/v). This extract spiked with E110 and E124 at a concentration level of 40.825 µg/mL and 58.725 µg/mL, respectively was further used for solid phase extraction purification studies.

Solid-phase extraction was performed using two different retention conditions, in an acid environment (acetic acid) and in the presence of ion-paring reagent CTAB (IP-SPE). The sample (1 mL) subjected to SPE was diluted to 50 mL with acetic acid (2%) or CTAB (0.02%) solution. The SPE cartridge was conditioned with 5 mL methanol and washed with the aqueous solution of acetic acid or CTAB. The dyes retention was carried out at a flow

rate of about 5 mL/min. After a washing step with acetic or CTAB solution, the cartridge was dried up for 10 min by passing an airflow. Elution was performed with 5mL methanol-ammonium hydroxide (25%) (10:0.1, v/v) at low flow rate (1mL/min). The extract was dried up and redissolved in 1 mL methanol-water (9:1, v/v). Triplicate samples were obtained with each procedure.

Dyes extraction from the spiked sample of roe was carried out both on herring and trout roe at two concentration levels L1 (163.3 µg/g E110; 234.9 µg/g E124) and L2 (81.65 µg/g E110; 117.45 µg/g E124). There were investigated four different methodologies.

Method I consists of sonication with water-ammonia (1:1, v/v) mixture as the extraction agent. Three successive extractions with 15 mL extracting agent were carried out for 10 minutes at room temperature. The collected extracts were centrifuged at 4500 rpm for 10 minutes, and the supernatant was purified by liquid-liquid extraction with hexane (3x15 mL).

Method II was similar to that described before, except for the purification step, which was carried out by solid phase extraction instead of liquid-liquid extraction.

Method III consists of sample sonication with methanol-ammonia (1:1, v/v). The extraction was repeated three times with 15 mL extraction agent. The collected extracts were centrifuged for 10 minutes at 4500 rpm. The supernatant was evaporated, and residuum was dissolved in 1 mL of methanol-water (9:1, v/v).

Method IV was performed in the same condition as described above (*Method III*) but included a purification step by SPE.

Analysis of the red caviar sample

Analysis of red caviar sample was performed both on roe fish sample (C0) and on spiked samples at two concentration levels C1 (40.825 µg/g E110; 58.725 µg/g E124) and C2 (81.65 µg/g E110; 117.45 µg/g E124) respectively. The extraction of the dyes was performed according to Method IV followed IP-SPE. The experiments were carried out in triplicates. The obtained extracts were further analysed by HPTLC.

HPTLC analysis

Chromatographic separation was performed on HPTLC Silicagel G60 plates. The samples were applied as 10 µL spots for recovery studies and as 5 µL for caviar samples. All samples were applied in triplicate. Plate development was performed in a normal saturated chamber using as mobile phase a mixture of isopropyl alcohol-ammonium-hydroxide (25%) (2:1, v/v).

After development, the plates were dried and evaluated by scanning at 485 nm and 515 nm for E 110 and E 124, respectively. In order to determine the equation of the calibration curve, spots of 2.5 - 15 µL of 1:5 diluted standard solution were applied on the chromatographic plate. Since limit of detection (LOD) and limit of quantification (LOQ) depend on the quality of the calibration, they were computed based on the regression line and its confidence interval (Statistical Methods in Analytical Chemistry – SMAC soft 0.5).

REFERENCES

1. J.C. Griffiths, *Food technol.*, **2005**, 59, 38-44
2. A. Yadav, A. Kumar, A. Tripathi, M. Das, *Toxicol. Lett.,* **2013**, 217, 197-204
3. Official Journal of the European Union, L 295/1, Commission Regulation (EU) No 1129/2011 of 11 November 2011, amending Annex II to Regulation (EC) No 1333/2008 of the European Parliament and of the Council by establishing a Union list of food additives, available at https://www.fsai.ie/uploadedFiles/Reg1129_2011.pdf
4. Official Journal of the European Union, L 354/16, Regulation (EC) No 1333/2008 of the European Parliament and of the Council of 16 December 2008 on food additives, available at http://eur-lex.europa.eu/legal-content/EN/ALL/?uri=CELEX:32008R1333
5. K. Ntrallou, H. Gika, E.D. Tsochatzis, *Foods*, **2020**, 9(58), 1-27
6. A.W. Sobanska, P. Jakubczyk, J. Pyzowski, E. Brzezinska, *Acta Innovations*, **2018**, 27, 53-60
7. A.H. El-Sheikh, Y.S. Al-Degs, *Dyes Pigm.*, **2013**, 97, 330-339
8. Y.S. Al-Degs, *Food Chem.*, **2009**, 117, 485-490
9. M.H. Sorouraddin, A. Rostami, M.Saadati, *Food Chem.,* **2011**, 127, 308-313
10. S. Bonan, G. Fedrizzi, S. Menotta, E. Caprai, *Dyes Pigm.*, **2013**, 99, 36-40
11. W.A.S. Bento, B.P. Lima, A.P.S. Paim, *Food Chem*., **2015**, 183, 154-160
12. F. Feng, Y. Zhao, W. Yong, L. Sun, G. Jiang, X. Chu, *J. Chromatogr. B*, **2011**, 879, 1813-1818
13. P. Qi, Z. Lin, G. Chen, J. Xiao, Z. Liang, L. Luo, J. Zhou, X. Zhang, *Food Chem.,* **2015**, 181, 101-110
14. D. Casoni, A. Boldan, S.C. Cobzac, *Stud. Univ. Babeş-Bolyai, Chem.,* **2012**, 57(1), 83-92
15. F.I. de Andrade, M.I. Florindo Guedes, I.G. Pinto Vieira, F.N. Pereira Mendes, P.A. Salmito Rodrigues, C.S. Costa Maia, M.M. Marques Ávila, L. de Matos Ribeiro, *Food Chem.*, **2014**, 157, 193-198
16. S.C. Cobzac, D. Casoni. C. Sârbu, *Stud. Univ. Babeş-Bolyai, Chem.,* **2010**, 45(2), 227-235
17. F. Soponar, A.C. Mot, C. Sarbu, *J. Chromatogr. A*, **2008**, 1188, 295-300

18. S.C. Cobzac, D. Casoni, D. Pop, *JPC-J Planar Chromatogr.*, **2012**, 25, 542-547
19. S.C. Cobzac, D. Casoni, A.L. Fazakas, C. Sârbu, *J. Liq. Chromatogr. Relat. Technol.*, **2012**, 35, 1423-1443
20. O. Sha, X. Zhu, Y. Feng, W. Ma, *Food Chem.*, **2015**, 174, 380-386
21. H. Wu, J. Guo, L. Du, H. Tian, C. Hao, Z. Wang, J. Wang, *Food Chem.*, **2013**, 141, 182-186
22. J. Kirschbaum, C. Krause, H. Bruckner, *Eur. Food. Res. Technol*., **2006**, 222, 572-579
23. W.J. Li, X. Zhou, S.S. Tong, Q. Jia, *Talanta*, **2013**, 105, 386–392
24. J.L. Tadeo, C. Sanchez-Brunete, B. Albero, A.I García-Valcárcel, *J. Chromatogr. A*, **2010**, 1217, 2415-2440
25. O.G. Liao, W.H. Li, L.G. Luo, *Anal. Chim. Acta*, **2012**, 716, 128-132
26. T. Zou, P. He, A. Yasen, Z. Li, *Food Chem.*, **2013**, 138, 1742-1748
27. G. Karanikolopoulos, A. Gerakis, K. Papadopoulou, I. Mastrantoni, *Food Chem.*, **2015**, 177, 197-203
28. A. Basu, G.S. Kumar, *J. Hazard. Mater.*, **2014**, 273, 200-206

STUDIA UBB CHEMIA, LXVI, 2, 2021 (p. 277-286)
(RECOMMENDED CITATION)
DOI:10.24193/subbchem.2021.2.24

ECO-FRIENDLY ENZYMATIC SYNTHESIS OF ANISYL PROPIONATE MEDIATED BY LIPASE B FROM *CANDIDA ANTARCTICA*

DIANA MARIA SCROB, MIHAI ANDREI LĂCĂTUȘ[a], ADRIAN IOAN DUDU[a]*

ABSTRACT. In this paper we report a biocatalytic approach for the efficient synthesis of anisyl propionate by direct esterification of anisyl alcohol with propionic acid mediated by commercially available Novozym 435, in presence of molecular sieves which serves for the efficient removal of water formed in the reaction. Process optimization was performed regarding the optimal solvent (2-methyltetrahydrofuran), temperature (60 ˚C), and molecular sieves load (100 mg/mL). Further scaling-ups were performed under optimal conditions increasing the substrates concentration up to 1000 mM with unaltered conversions in anisyl propionate (>95 % after 6 hours reaction time).

Keywords: *lipase, aroma, flavor, biocatalysis, esterification, green solvent*

INTRODUCTION

In recent years the demand for natural products is increasing, therefore the development of biotechnological processes for the production of flavor compounds has been encouraged. Flavor is usually the result of the presence, within complex matrices, of various volatile and nonvolatile components which possess diverse chemical and organoleptic properties. The nonvolatile compounds contribute mainly to the taste, while the volatile ones influence both the taste and aroma [1].

Aroma esters are obtained nowadays by two methods: extraction from natural sources, or by chemical synthesis. Both methods have some disadvantages, for example the extraction from natural sources demands large amounts of starting material to obtain aroma compounds with relatively

[a] *Enzymology and Applied Biocatalysis Research Center, Faculty of Chemistry and Chemical Engineering, Babeș-Bolyai University, Arany János str. 11, RO-400028, Cluj-Napoca, Romania*
** Corresponding author: adrian.dudu@ubbcluj.ro*

low yields and purity. The chemical synthesis of aroma compounds demands the use of toxic reagents and the obtained products, most of the time, demand further purification. These inconveniences can be overcomed by employing a green, biocatalytic approach for aroma esters synthesis, as previously reported [2], [3].

Many enzymatic processes for the preparation of aroma esters were recently developed. For example, the synthesis of banana flavor compounds by esterification reactions mediated by lipase from *Thermomyces lanuginosus* was already reported [4]. Short-chain flavor esters were obtained from natural sources in presence of tailored magnetic biocatalysts containing lipase B from *Candida antarctica* (CaL-B) [5]. Moreover, the Novozym 435 (CaL-B adsorbed on Lewatit VP OC 1600) mediated preparation of benzyl butyrate by the esterification of benzyl alcohol with butyric acid in a solvent-free system (SFS) was also described [6]. Lipase from *Burkholderia ambifaria* immobilized on a mesoporous TiO_2 based support functionalized with phenylaminopropyl trimethoxysilane was used for the synthesis of cinnamyl acetate [7]. Ethyl butyrate and isoamyl acetate, flavor esters found in pineapple and bananas, were prepared in presence of *Candida rugosa* lipase (CrL) covalently immobilized on multiwalled carbon nanotubes (MWCNTs) [8]. Anisyl propionate is a flavor ester used as a flavor or fragrance agent in the food industry or as a perfuming agent in the cosmetics.

Due to its versatility and wide application range, the commercially available immobilized lipase B from *Candida antarctica* was chosen for this study, as it was applied with great success for the enantiospecific production of atenolol acetate [9], in the production of flavor esters [10], [11], and in the enzymatic kinetic resolution of racemic secondary alcohols [12], [13].

2-Methyl-tetrahydrofuran (2-MeTHF), a green solvent derived from renewable resources (from furfural or levulinic acid, for example), is considered a promising alternative solvent in the search for environmentally friendly synthesis strategies. This solvent is characterized by its low miscibility with water, low boiling point and higher stability against peroxide formation, when compared with other cyclic-ethers (tetrahydrofuran, for example). Preliminary toxicological assessments support the use of 2-MeTHF in the pharmaceutical industry [14]. 2-MeTHF has also been successfully used as green solvent in our previous study for biodiesel additives preparation [15].

Based on the above, the main objective of the present work was to prepare anisyl propionate in a reaction system formed of anisyl alcohol, propionic acid, 2-MeTHF as a green and efficient solvent, Novozym 435 as biocatalyst and molecular sieves as an efficient tool to remove the water formed in the system, therefore shifting the reaction equilibrium towards ester formation.

RESULTS AND DISCUSSION

In our first approach the reaction conditions were optimized performing analytical scale biotransformations. The obtained results served as a prerequisite for further experiments in order to maximize the productivity of the procedure.

To shift the equilibrium of the esterification reaction for total conversion of anisyl alcohol into the desired anisyl propionate, the mandatory water removal has been achieved with molecular sieves, as shown in **Scheme 1**.

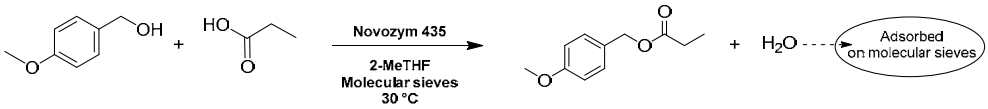

Scheme 1. Synthesis of anisyl propanoate by direct esterification of para-methoxy-benzyl alcohol with propionic acid mediated by Novozym 435 in 2-MeTHF in presence of molecular sieves.

Solvent screening

The esterification reaction of anisyl alcohol with propionic acid mediated by Novozym 435 was tested in five solvents with different polarity.

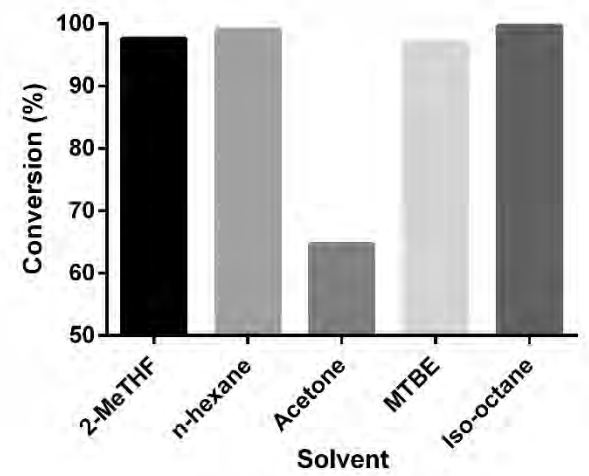

Figure 1. Solvent screening. Reaction conditions: 10 mM anisyl alcohol, 2 equiv. propionic acid, 25 mg Novozym 435, 1 mL solvent, 50 mg molecular sieves, 800 rpm, 30 ˚C, 12 h.

As it can be seen in **Figure 1** high enzymatic activity was found in *n*-hexane, *iso*-octane (over 98%, in both solvents) and in ethers (MTBE and 2-MeTHF, ~ 96%), while much lower conversion (~ 65%) was obtained in

acetone. Since excellent results were obtained also in 2-MeTHF, further experiments were performed in this solvent, also taking into account its classification as a green solvent.

Substrate concentration screening

In order to increase the productivity of the enzymatic esterification, the influence of the substrate (anisyl alcohol) concentration (10-50 mM) upon the reaction conversion was studied, at constant alcohol: propionic acid molar *ratio* (1:2), biocatalyst (25 mg/mL) and molecular sieves load (50 mg/mL).

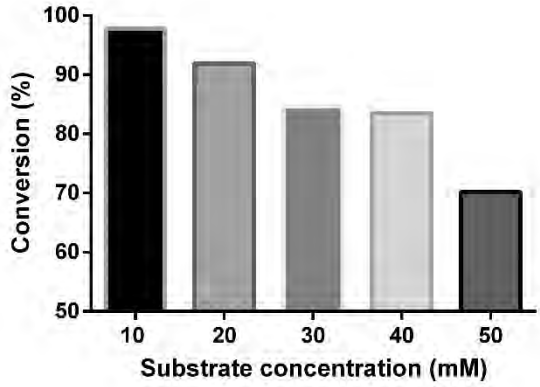

Figure 2. Influence of the anisyl alcohol concentration on the conversion. Reaction conditions: anisyl alcohol at different concentrations (10-50 mM), propionic acid (2 equiv.), 25 mg/mL Novozym 435, 50 mg/mL molecular sieves in 2-MeTHF, 800 rpm, 30 ˚C, 12 h.

As shown in **Figure 2** by increasing the substrate concentration a gradually decrease of conversion was observed from 97.8% (10 mM anisyl alcohol) to 70.2% (50 mM substrate). It was emphasized that the continuous lowering of the conversion could be determined by the inefficient removal of the water from the reaction mass due to the insufficient quantity of molecular sieves (50 mg/mL) in the reaction medium.

Influence of the molecular sieves on the conversion

Accordingly, further the influence of the molecular sieves load upon the efficacy of the enzymatic esterification was investigated at constant anisyl alcohol (50 mM) and propionic acid (100 mM) concentrations at 30 ˚C temperature, as presented in **Figure 3**.

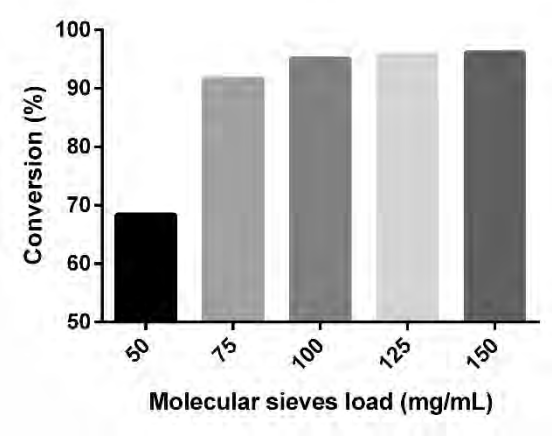

Figure 3. The influence of the molecular sieves load upon the conversion of anisyl alcohol into anisyl propionate. Reaction conditions: 50 mM anisyl alcohol in 2-MeTHF, 2 equiv. of propionic acid, 25 mg/mL Novozym 435, 800 rpm, 30 ˚C, 12 h.

Increasing the molecular sieves load, the conversion of the esterification was considerably improved, from 68.4% (50 mg/mL molecular sieves) up to 95.1% in presence of 100 mg/mL of molecular sieves (**Figure 3**). Higher amounts (125 and 150 mg/mL) of molecular sieves did not improve considerably the reaction conversion. At 150 mg/mL molecular sieves load the reaction conversion was enhanced only with 1%, compared to reactions carried out in presence of 100 mg/mL drying agent. Therefore, further optimization experiments were performed in presence of 100 mg/mL molecular sieves.

Temperature screening

Temperature plays a major role in the kinetics of any reaction. In this context, the influence of temperature upon biocatalyst activity and stability was further studied in experiments which were setup under the previously determined optimum conditions. Samples from the reaction mixtures were taken periodically (2 hours intervals), analyzed and results were plotted as shown in **Figure 4**.

It was demonstrated that Novozym 435 is a stable and active biocatalyst even at 60 ˚C. Analyzing the temperature dependence of the conversion profiles as depicted in **Figure 4**, it can be concluded that at 60 ˚C the previously determined maximal reaction conversion (~96%) was achieved after only 6 hours. Based on this study the optimum temperature was chosen to be 60 ˚C, as it halves the time necessary for the almost complete substrate conversion into the desired product.

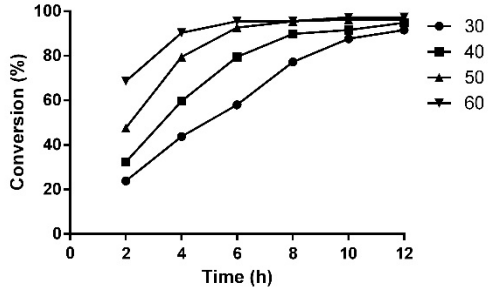

Figure 4. Temperature effect upon the efficacy of the enzymatic esterification of anisyl alcohol with propionic acid. Reaction conditions: 50 mM anisyl alcohol, 2 equiv. propionic acid, 25 mg/mL Novozym 435, 100 mg/mL molecular sieves in 2-MeTHF, 800 rpm.

Process scale-up in optimum conditions

With all these results in hands, which jointly were associated with the optimal conditions for the analytical scale enzymatic synthesis of anisyl propionate, next the improvement of reaction productivity was studied. Maintaining the biocatalyst and molecular sieves load and the reactants molar *ratio*, the substrate concentration was further incrementally increased with 10 units in 60-100 mM substrate concentration domain. Since the performance of the developed reaction system was unaltered even at 100 mM substrate concentration, further reactions were performed at much higher anisyl alcohol content (200, 300, 500 and 1000 mM) and the reaction mixtures were analyzed after 6 hours reaction time (**Figure 5**).

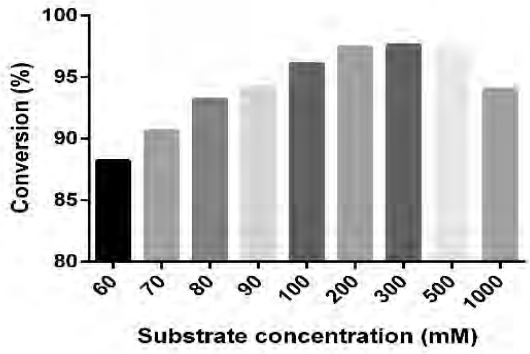

Figure 5. Process scale-up under optimum conditions. Reaction conditions: 60-1000 mM anisyl alcohol, 2 equiv. propionic acid, 25 mg/mL Novozym 435, 100 mg/mL molecular sieves in 2-MeTHF, 800 rpm, 60 ˚C, 6 h.

Ascending the substrate concentration in 10-100 mM range, the conversion of the biocatalytic reaction continuously increased from 88 to 95%, after 6 hours of reaction time. These results can be explained by the dependence of the reaction rate on the reagents concentration, but also demonstrated the absence of the substrate or product inhibition upon enzyme activity. Moreover, it was also concluded that the biocatalyst was used under its maximal capacity. These facts encouraged additional experiments with further increasing the substrate concentration, as illustrated in **Figure 5**. It is important to note that the conversion after 6 hours reaction time was similar (~95%) also for 1000 mM substrate concentration, as compared with those performed at lower concentrations. This result determined us to work-up and isolate the formed ester. The purified ester was obtained with 92% yield and its structure was confirmed by NMR spectroscopy.

CONCLUSIONS

Anisyl propionate was successfully prepared by the enzymatic esterification mediated by Novozym 435 in a green solvent (2-MeTHF) employing molecular sieves as efficient water removal tool. After process optimization, anisyl propionate was obtained with 92% yield starting from anisyl alcohol in 1000 mM concentration. Therefore, the newly developed reaction system can be considered a viable candidate for a potential industrial scale-up.

EXPERIMENTAL SECTION

Materials

Novozym 435 was purchased from Novozyme (Denmark). Molecular sieves (2 mm granule dimension, 5 Å pore dimension) were purchased from Sigma-Aldrich (St. Louis, MO, USA). Anisyl alcohol, propionic acid, 2-Methyltetrahydrofuran (2-MeTHF), *n*-hexane, acetone, methyl *tert*-butyl ether (MTBE), dichloromethane, sodium bicarbonate and sodium sulphate were purchased from Merck (Germany). Anisyl propionate, used as standard, was previously synthesized in the Enzymology and Applied Biocatalysis Research Center, Cluj Napoca. All solvents and reagents were freshly distilled and dried by standard methods before use.

Reactions were incubated under shaking using a Vibramax 110 equipped with a temperature-control module (Heidolph). The enzymatic reactions were monitored using an Agilent HPLC 1206 Infinity series (Santa Clara, CA, USA), equipped with a UV-Vis detector, using a Phenomenex Gemini NX-C18 (150 $\times$ 4.5 mm; 5 µm) chromatographic column.

Methods

Conversion determination

The reaction conversions were determined using reversed phase liquid chromatography. The compounds were separated on a Gemini NX-C18 chromatographic column, with a mix of methanol: water 80:20 (v/v), as mobile phase at 0.5 mL×min^{-1} flow rate, monitoring the absorbance at 208 nm. In order to rigorously determine the conversion of anisyl alcohol into anisyl propionate a relative response factor was determined (R_F=0.9204) by injecting samples of known concentration of alcohol and ester in different molar *ratio*s.

Solvent screening

1.38 mg anisyl alcohol and 1.48 mg (2 equiv.) of propionic acid were mixed in 1 mL organic solvent. 25 mg of Novozym 435 and 50 mg of molecular sieves were added in the reaction medium. The reactions were shaken (800 rpm) at 30 ˚C for 12 h. After 12 h 25 µL samples were taken and evaporated. Samples were reconstituted with 1 mL mobile phase, filtered and injected in order to determine the conversion.

Substrate concentration screening

In 1 mL 2-MeTHF different quantities of anisyl alcohol (1.38, 2.76, 4.14, 5.52 and 6.9 mg), propionic acid (respecting the alcohol: acid molar *ratio* of 1:2), Novozym 435 (25 mg) and molecular sieves (50 mg) were added. Reactions were perfected and sampling was performed as described in the previous section.

Influence of the molecular sieves load upon the conversion

In 1 mL solution of anisyl alcohol (50 mM) and propionic acid (100 mM, 2 equiv.) in 2-MeTHF 25 mg of Novozym 435 and different quantities of molecular sieves (50, 75, 100, 125 and 150 mg) were added. Reactions were perfected and sampling was performed as described in the previous sections.

Temperature screening

In 1 mL solution of anisyl alcohol (50 mM) and propionic acid (100 mM, 2 equiv.) in 2-MeTHF, Novozyme 435 (25 mg) and 100 mg of molecular sieves were added. The reactions were shaken (800 rpm) at 30, 40, 50 and 60 ˚C for 12 hours. Sampling was performed after 2, 4, 6, 8, 10 and 12 hours by taking 25 µL samples and evaporating them. The samples were reconstituted with 1 mL mobile phase, filtered and analyzed by HPLC.

Process scale-up in optimum conditions

In 1 mL solution of anisyl alcohol (60, 70, 80, 90, 100, 200, 300, 500 and 1000 mM) and propionic acid (2 equiv.) in 2-MeTHF, Novozym 435 (25 mg) and 100 mg of molecular sieves were added. The reactions were shaken (800 rpm) at 60 ˚C for 6 h. Samples (25 µL) were taken and evaporated. Samples were reconstituted with 1 mL mobile phase, filtered and analyzed by HPLC.

The reaction performed on 1000 mM alcohol solution was worked up and the structure of purified product (anisyl propionate) was confirmed by NMR spectroscopy. For this, the reaction mixture was filtered in order to remove the enzyme and the molecular sieves. Next, 2-MeTHF was evaporated under reduced pressure, the reaction mass was redissolved in 5 mL dichloromethane and washed with sodium bicarbonate solution (1 M; 2×5 mL) for isolating the unreacted propionic acid. The separated organic layer was extracted and dried over sodium sulphate. Further purification by column chromatography was performed using dichloromethane as eluent.

^{1}H-NMR (400 MHz, $CDCl_3$): 1.17 (3H, *t*), 2.38 (2H, *q*), 3.83 (3H, *s*), 5.07 (2H, *s*), 6.91 (2H, *d*), 7.32 (2H, *d*); ^{13}C-NMR (100 MHz, $CDCl_3$): 9.1, 27.6, 55.3, 66, 113.9, 128.2, 130.1, 159.6, 174.4.

ACKNOWLEDGMENTS

The present work has received financial support through the project: Entrepreneurship for innovation through doctoral and postdoctoral research, POCU/380/6/13/123886 co-financed by the European Social Fund, through the Operation Program for Human Capital 2014-2020.

REFERENCES

1. M.A. Longo; M.A. Sanroman; *Food Technol. Biotechnol.*; **2006**; *44*; 335-353
2. A.G. Almeida Sa; A.C. de Meneses; L.A. Lerin; P.H.H. de Araujo; C. Sayer; D. de Oliveira; *Bioproc. Biosyst. Eng.*; **2018**; *41*; 585-591
3. A.I. Dudu; M.A. Lăcătuș; L.C. Bencze; C. Paizs; M.I. Toșa; *ACS Sustain. Chem. Eng.*; **2021**; *9*; 5461-5469
4. M. Sarno; M. Iuliano; M. Polichetti; P. Ciambelli; *Process Biochem.*; **2017**; *56*; 98-108
5. C. Vasilescu; A. Todea; A. Nan; M. Circu; R. Turcu; I.C. Benea; F. Peter; *Food Chem.*; **2019**; *296*; 1-8

6. A.C. de Meneses; A.G. Almeida Sa; L.A. Lerin; M.L. Corazza; P.H.H. de Araujo; C. Sayer; D. de Oliveira; *Process Biochem.*; **2019**; *78*; 50-57
7. Z. Gao; J. Chu; T. Jiang; T. Xu; B. Wu; B. He; *Process Biochem.*; **2018**; *64*; 152-159
8. S. Asmat; A.H. Anwer; Q. Husain; *Int. J. Biol. Macromol.*; **2019**; *140*; 484-495
9. O. Barbosa; C. Ortiz; R. Torres; R.F. Lafuente; *J. Mol. Catal. B Enzym.*; **2011**; *71*; 124-132
10. J.L.R. Friedrich; F.P. Pena; C. Garcia-Galan; R. Fernandez-Lafuente; M.A.Z. Ayub; R.C. Rodrigues; *J. Chem. Technol. Biotechnol*; **2012**; *88*; 1089-1095
11. M.C.M. de Souza; K.P. dos Santos; R.M. Freire; A.C.H. Barreto; P.B.A. Fechine; L.R.B. Goncalves; *Braz. J. Chem. Eng.*; **2017**; *34*; 681-690
12. H.V. Ferreira; L.C. Rocha; R.P. Severino; A.L.M. Porto; *Molecules*; **2012**; *17*; 8955-8967
13. R.N. Patel; A. Banerjee; V. Nanduri; A. Goswami; F.T. Comezoglu; *J. Am. Oil Chem. Soc.*; **2000**; *77*; 1015-1019
14. V. Pace; P. Hoyos; L. Castoldi; P.D. de Maria; A.R. Alcantara; *ChemSusChem*; **2012**; *5*; 1369-1379
15. M.A. Lacatus; L.C. Bencze; M.I. Toșa; C. Paizs; F.D. Irimie; *ACS Sustain. Chem. Eng.*; **2018**; *6*; 11353-11359

STUDIA UBB CHEMIA, LXVI, 2, 2021 (p. 287-297)
(RECOMMENDED CITATION)
DOI:10.24193/subbchem.2021.2.25

PREPARATION AND CHARACTERIZATION OF ATORVASTATIN-LOADED POLYVINYLPIRROLIDONE-BASED ELECTROSPUN MICROFIBROUS MATS

EMŐKE RÉDAI[a], IZABELLA RÁDULY[a], ZOLTÁN-ISTVÁN SZABÓ[b], ADRIANA CIURBA[a], NICOLETA TODORAN[a], PAULA ANTONOAEA[a]*, ROBERT-ALEXANDRU VLAD[a], PÉTERFI ORSOLYA[a], EMESE SIPOS[b]

ABSTRACT. The aim of this experimental work was the enhancement of water solubility of the lipid lowering drug, atorvastatin, by embedding it in polymer based micro-sized fibers, prepared by electrospinning. Characterization of the fibrous mats included morphological investigations, determination of drug content, disintegration time, small volume dissolution- and DSC studies. The electrospinning process was continuous without droplet formation. The obtained fibers were homogenous, continuous filaments with smooth surfaces. Average fiber diameters were slightly above 1 µm, while disintegration of fiber mats upon contact with water was almost instantaneous (three to ten seconds). Dissolution of the lipid lowering drug was almost complete, when using a solution feed rate of 1 mL/h.

Keywords: *atorvastatin, electrospinning, PVP, microfibrous mats*

INTRODUCTION

The first-line lipid lowering drug, atorvastatin (AT), is a synthetic HMG-CoA reductase inhibitor, which acts mainly by reducing low-density lipoprotein cholesterol levels. It is widely used for the treatment of hypercholesterolemia, effectively reducing morbidity and mortality in patients with atherosclerosis. Benefic effects appear also in patients with normal LDL-cholesterol levels. By

[a] *„George Emil Palade" University of Medicine, Pharmacy, Sciences and Technology of Targu Mures, Faculty of Pharmacy, Pharmaceutical Technology and cosmetology department, Gh. Marinescu street no. 38, 540142 Targu Mures, Romania*
[b] *„George Emil Palade" University of Medicine, Pharmacy, Sciences and Technology of Targu Mures, Faculty of Pharmacy, Pharmaceutical Industry and Management department, Gh. Marinescu street no. 38, 540142 Targu Mures, Romania,*
** Corresponding author: paula.antonoaea@umfst.ro*

inhibiting the cholesterol pathway, atorvastatin also possesses anti-inflammatory effects (1, 2). Although the drug of choice in hyperlipidemia, atorvastatin has a low oral bioavailability (around 12%), which increases its dose (3). According to Biopharmaceutical Drug Classification System (BCS) atorvastatin belongs to class II, possessing low solubility and good permeability (4). In case of BCS class II, solubility is the rate limiting step in oral absorption and solubility enhancing techniques are promising ways to increase bioavailability (5).

One of the greatest challenges in pharmaceutical formulations development is solubility enhancement of poorly water-soluble drugs. Various techniques have been recommended to increase bioavailability, among these are procedures which increase solubility by incorporating the drug in highly hydrophilic polymers (6). Electrospun fiber mats are produced from viscous polymeric solutions, under a high electric field. The benefits of these nano - or microfibrous systems include high surface area-to-volume ratios, high porosity and the possibility of stabilizing the active ingredient in an amorphous state (7) verified by thermal methods (8). Important progresses were also made in the industrial scale-up of the process, hopefully opening the gate to greater acceptance of the method in the pharmaceutical industry also (9).

There are some studies, which address the poor physicochemical properties of AT and other statins, in most of the cases, with the aid of nanotechnology. AT has been incorporated in polyvinyl pyrrolidone K30 based electrospun solid dispersions by Jahangiri et collaborators (10). Chitosan nanoparticles obtained by ionic gelation proved to ensure sustained release of atorvastatin (11). The anti-inflammatory effect of AT containing inclusion complex embedded in a polycaprolactone-based membrane was demonstrated by Schwinte (12). AT coated controlled-release stents (13-15), and also fibers for peripheral nerve injury in rats (16, 17) were also studied. Rosuvastatin fibers with heparin were also embedded in endovascular stents (18-20). Simvastatin fiber mats for bone tissue regeneration (21, 22) including healing of femoral defect (23) were formulated. A poloxamer-based lovastatin nanofibrous formulation was also prepared in order to improve the chemical stability of the drug (24).

Jahangari et al. prepared amorphous dispersions of AT, using PVP K30 (25). The authors prepared methanolic solutions with different ATV:PVP ratios and prepared solid dispersions by the solvent evaporation technique, using a rotavapor. AT was present in an amorphous form in the prepared solid dispersion, which resulted in improved dissolution rate of the active. Moreover, the total cholesterol and LDL cholesterol levels decreased significantly more, when AT was administered in the form of solid dispersions, when compared to the physical mixture.

In a follow-up study, Jahangari et al. (10) presented the preparation and physicochemical evaluation amorphous nano-solid dispersions atorvastatin, either alone or in combination with ezetimibe. In this case, solid dispersions were prepared by electrospraying using PVP K30 as an amorphous carrier. The electrospraying solutions were prepared by dissolving the appropriate amount of the active substance and PVP in methanol:acetone 1:1 (v/v) with drug:polymer concentrations of 10% and 20%. The obtained nano-solid dispersions were characterized by high surface area and contained the active substances in an amorphous state, which lead to higher dissolution rates.

Recently, Iqbal et al. (26) reported the preparation of AT and metformin containing PVP and/or hyaluronic acid-based nanoparticles (either with or without polysorbate 20). Electrospraying was performed on solutions prepared in ethanol:methanol 1:1 (v/v) and the authors achieved around 4% AT drug-load in the prepared formulations. The prepared nanoparticles provided enhanced dissolution rate and higher oral bioavailability for the active substances as compared to the marketed products.

As it can be observed there is a great interest in the preparation of AT containing solid dispersions as it offers an efficient way to increase the solubility, dissolution rate of the active, which in terms can translate into an increase of bioavailability of the lipid-lowering drug. Nano- or microfibrous formulations were yet to be applied for immediate-release AT formulations. In the present study, we aim to describe the incorporation of AT in amorphous form into PVP-based microfibers for solubility and dissolution rate enhancement of the active ingredient. Tracking of physicochemical changes during electrospinning was also aimed as well as characterization of the obtained fibrous mats, including morphological investigations, drug content, disintegration time, dissolution and thermal studies.

RESULTS AND DISCUSSION

In the present study, AT was incorporated into electrospun microfibrous meshes, in order to present a novel, greener platform for the dissolution enhancement of the lipid lowering blockbuster drug. As the lower molecular weight PVP K30 proved to be an excellent choice for preparing AT-containing solid dispersions in previous studies (10, 25-26). Being an inert, pH-stable, biodegradable hydrophilic, amorphous polymer, which displays a complex affinity for both hydrophilic and hydrophobic drugs (27) it represents an excellent choice for the carrier matrix of AT. Moreover, PVP solutions in alcohol-type solvents are easily electrospinnable and the active substances

incorporated in these PVP-based nano- or microfibrous products show increased solubility and enhanced dissolution rate. Thus, in order to increase the solubility of AT, PVP was chosen as a hydrophilic polymer and microfibrous samples could be obtained by electrospinning the prepared viscous solutions. Morphology and diameters of the fibrous samples were determined by a simple optical microscopic approach, calibrated with a standard scale. The obtained fibers were homogenous, continuous filaments with smooth surfaces. The electrospinning process was continuous and droplet formation was not observed. All of the examined samples presented average fiber diameters slightly above 1 µm (being significantly different P <0.0001, by one way Anova test) with relatively narrow individual fiber diameter distributions (Table 1 and Figure 1). The authors are unaware of previously described immediate-release electrospun fibrous formulations of AT, however, the observed fiber diameters are in-line with earlier reported microfibrous formulations of the poorly soluble fenofibrate, prepared by electrospinning ethanolic PVP-based viscous polymeric solutions (28).

Table 1. Summary of the results obtained during the characterization of the microfibrous samples

Batch	***Flow rate (ml/h)***	***Diameters of fibers (µm*** ±SD***)***	***Disintegration time (seconds)***	***Drug content (%w/w*** ±SD***)***	***Dissolved AT after 30 minutes (%w/w*** ±SD***)***
ATV		-	-	-	38.34 ±1.12
I.	0.5	1.381 ± 0.37	5	11.67 ± 0.45	69.29 ±0.28
II.	1	1.335 ± 0.28	4	11.25 ± 0.56	99.21 ±4.02
III.	3	1.059 ± 0.20	3	11.92 ± 0.12	86.31 ±1.21
IV.	4	1.415 ± 0.37	10	12.46 ± 0.70	71.03 ±0.32

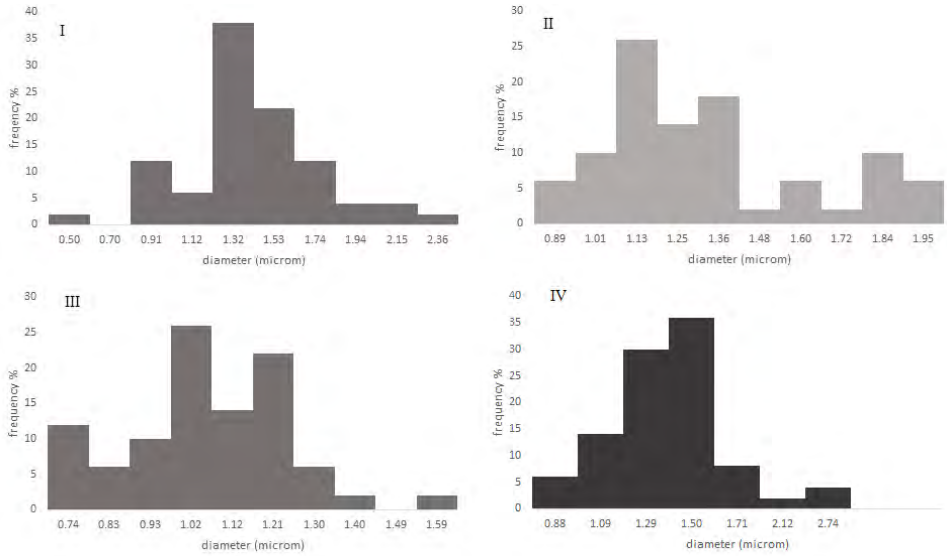

Figure 1. Diameter distribution by image analysis for the different formulations.

A representative image of the obtained fibers is presented in Figure 2.

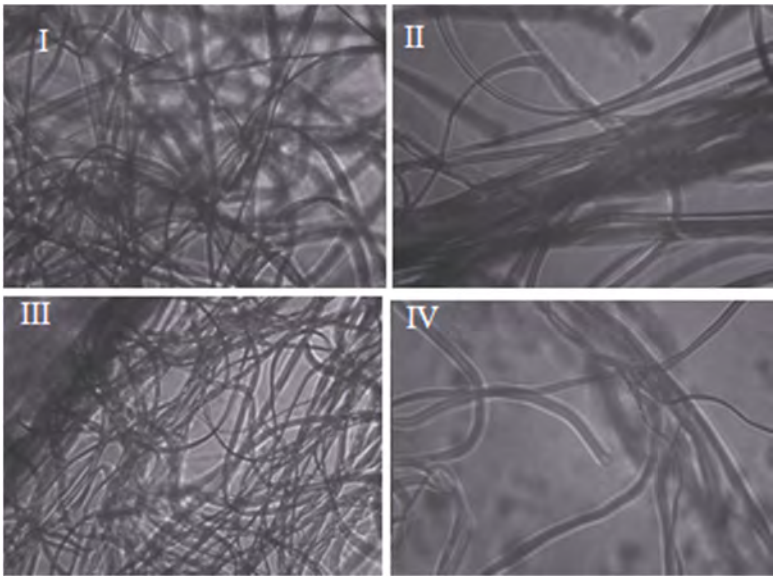

Figure 2. Microscopic images of atorvastatin electospun fibers for batches I-IV (40x)

Using a hydrophilic polymer of lower molecular weight enhances the disintegration of the obtained fiber mats, upon contact with water (29). Moreover, the highly porous structure and high surface area-to-volume ratio can further decrease the disintegration time. Indeed, the obtained fibrous structure disintegrated rapidly in a few seconds, releasing the active ingredient, when in contact with water.

Electrospinning offers an efficient method for incorporation of various small molecules or biomacromolecules in diverse polymeric matrices. Compared to other nanocarrier systems, electrospinning can offer higher drug loading or entrapment efficiency (30). The drug content of the fibers varies between 11.25 and 12.46 % w/w, which is adequate, considering that an average dose of 20 mg AT could be delivered in around 160-180 mg microfibrous mesh.

Incorporation in a solid carrier structure enhanced the dissolution rate compared to pure active substance (Figure 3). An almost complete dissolution was achieved, when a feed rate of 1mL/h was used. A feed rate of 3 mL/h was associated with 86.31% AT dissolved. Lowest feed rate showed the lowest amount of AT liberated after 30 minutes. Dissolution rate and fiber size is influenced by flow rate (31). Lowest fiber size (1.059 µm) was obtained at a feed rate of 3 mL/h and was associated with the rapidest disintegration.

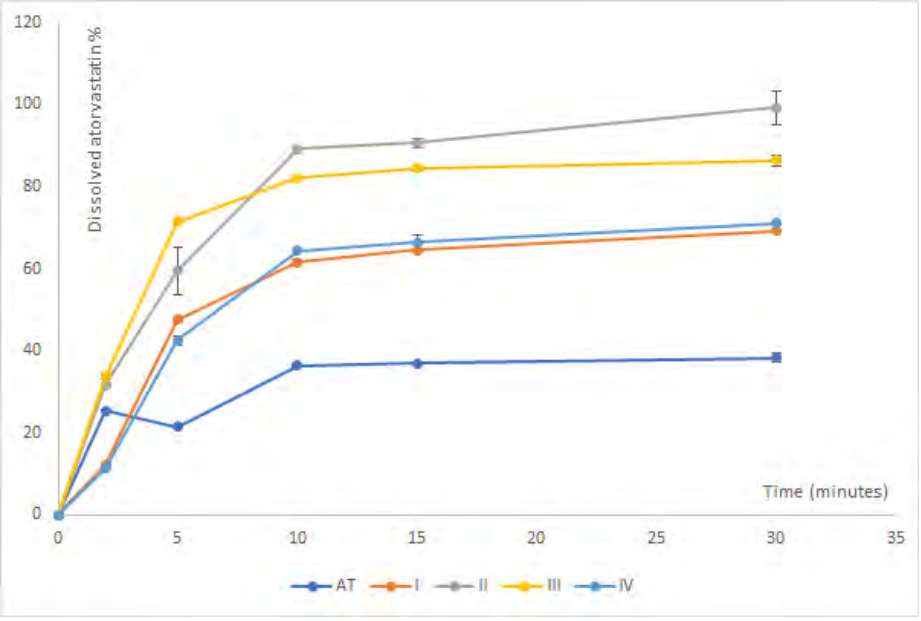

Figure 3. Dissolution curves of the pure drug and samples.

Setting the optimal flow rate for the electrospinning process mainly depends on the volatility of the solvents used and the applied electric field. Higher flow rates should be used in order to compensate for the rapid evaporation of highly volatile solvents and the applied electric field should be high enough to ensure the extraction of the polymer jet from the nozzle tip (30). Generally, using flow rates higher the optimal value, would result in thicker fibers and/or bead formation or sometimes in high residual solvent concentration in the deposited fibers (30). In our case, fiber diameter decreased with increasing the feed rate of the polymeric solution, up until a 3mL/h optimum value was attained. However, a further increase in feed rate resulted in increased fiber diameter, most probably due to thicker jet formation.

The thermogram of pure atorvastatin presents an endothermic heat exchange at 162°C, characteristic of the melting of the crystalline active substance (32). The DSC curve of Plasdone K-29/32 shows an endothermic event below 100°C, characteristic for the dehydration of the polymer. The melting endotherm of AT disappears from the DSC curve of fibrous samples and no enthalpy change is detectable, which could be due to the amorphization of active ingredient. Figure 4 presents the recorded DSC curves. The possibility of inducing the crystalline-to-amorphous transition of the incorporated active substances is often exploited during the immediate release formulations prepared through electrospinning. The formation of an amorphous solid dispersion is favored by electrospinning, due to the rapid solvent evaporation and due to the limited time available for drug crystallization during the process (30).

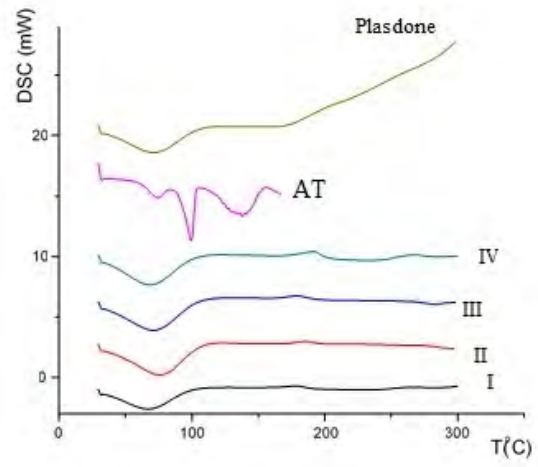

Figure 4. DSC curves of the pure drug and samples.

CONCLUSIONS

AT microfibers were prepared by electrospinning from PVP-based viscous solutions. The obtained fiber mats prepared from the hydrophilic, low molecular weight PVP and presented almost instantaneous disintegration, when in contact with water, rapidly releasing AT. Incorporation of the poorly soluble lipid-lowering blockbuster drug in the polymeric fibers through electrospinning, induces a possible crystalline to amorphous transition of the active, increasing the dissolution rate and solubility of AT.

EXPERIMENTAL SECTION

Materials

AT calcium trihydrate was a kind gift of Morepen Laboratories, New Delhi, India; Polyvinylpyrrolidone K value 29 to 32 (Plasdone K/29-32) was from Gaf Chemicals USP; methanol and ethanol were obtained from Chemical Company, Iasi, Romania; sodium dihydrogen phosphate monohydrate was obtained from Merck, Darmstadt, Germany; potassium dihydrogen phosphate was obtained from Loba Chemie, Austria.

Methods

Preparation of the viscous polymeric solution for electrospinning

The solutions used for electrospinning were prepared by dissolving 0.25 g AT in 3.0 g methanol under stirring using a JKI SMS HS magnetic stirrer (JKI, Shanghai, China). Then, 4.25 g ethanol and 2.5 g Plasdone K-29/32 was added. Stirring continued for another 15 minutes. A homogeneous viscous solution was obtained.

Preparation of atorvastatin fibers by electrospinning

Atorvastatin-loaded fibrous sheets were prepared by electrospinning using an in-house assembled apparatus. The flow rate was set to 0.5, 1, 3 and 4 ml/h (Batch I, II III and IV - using an Ascor AP12 infusion pump) and the voltage 25 kV. The syringe was connected to a size 21 G (0.8 mm external diameter) metallic needle with silicone tube. Fibers were collected on a grounded static sheet covered with aluminum foil after a 10 cm flight.

Morphology investigation by microscopy

Fiber morphology was tracked using a Bresser LCD Micro 5 MP microscope (Bresser, Rhede, Germany) at 40x magnification. Recorder images were examined with ImageJ software (US National Institutes of Health, Bethesda, MD, USA). Finally, the average diameter of nanofibers was calculated using 50 different randomly selected individual filaments.

Differential scanning calorimetry (DSC)

Thermal analysis was performed using a Shimadzu Thermo Analyzer DSC 60 (Shimadzu, Tokyo, Japan) equipment. Samples of 5 mg were accurately measured. Scans were performed at a heating rate of 5°C/min and using a temperature range of 30-300°C in not-hermetically sealed aluminum pans in air atmosphere.

Determination of disintegration time

5 mg of fibrous sheets were introduced in 10 ml distilled water at room temperature, and the disintegration time was measured.

Determination of drug content of atorvastatin microfibers

Drug content was determined using 25 mg fibers (dissolved in 20 ml methyl alcohol and distillated water) with a Dionex Ultimate 3000 system (Dionex, Olten, Switzerland) using a reversed-phase high-performance liquid chromatography method. Chromatographic separation was realized with a Phenomenex Luna C18, 250x4.6 mm column as stationary phase, at a temperature of 40°C. Mobile phase consisted of 1% aqueous acetic acid 1% and acetonitrile. Gradient elution was used, employing a 15 minutes linear gradient from 5 % to 95 % of acetonitrile delivered at a flow rate 1 ml/min. Injection volume was 25 µl. Detection was performed at 244 nm.

Small volume dissolution studies

Small volume dissolution studies were performed with an in-house assembled dissolution setup, which consisted of 11.5 cm long glass tubes immersed in a water bath maintained at 37 ± 1°C, using an Erweka ET 1500I thermostat (Erweka GmbH, Heusenstamm, Germany) (33). Stirring was realized with a 10x2 mm Teflon-coated stirring bar with a magnetic stirrer (Intop AB69, Wenzhou Start Co. Ltd, China) at a speed of 75 rpm. Dissolution media was 10 ml phosphate buffer at pH 6.8. Samples of 1 ml were taken at predefined intervals (2, 5, 10, 15, 30 minutes), filtered through a 0.45 µm filter and assayed with the previously described method. Determinations were performed in triplicate.

ACKNOWLEDGMENTS

Research funded by project 84.2/2017/P.2/EMEOGYSZ.

REFERENCES

1. A.R. Pradeep; M. Kumari; N.S. Rao; S.S. Martande; S.B. Naik; *J. Periodontology*, **2013**, *84*, 871-879
2. J. Li; J.-J. Li; J.-G. He; J.-l. Nan; Y.-l. Guo; C.-M. Xiong; *Cardiovascular Therapeutics,* **2010**, *28*, 8-14
3. M.A. Shaker; H. M. Elbadawy; S. S. Al Thagfan; M.A. Shaker; *Int J Pharm,* **2021**, *592*, 120077
4. S. Kumar; D. Bhargava; A. Thakkar; S. Arora **2013**, *30*, 217-256
5. P. Pandi, R. Bulusu, N. Kommineni, W. Khan, M. Singh, *Int J Pharm*, **2020**, *586*, 119560
6. P. Khadka; J. Ro; H. Kim; I. Kim; J.T. Kim; H. Kim; J.M. Cho; G. Yun; J. Lee, *Asian J Pharm. Sci.*, **2014**, *9*, 304-316
7. I. Sebe; P. Szabó; B. Kállai-Szabó; R. Zelkó; *Int J Pharm*, **2015**, *494*, 516-530
8. P. Antonoaea; N. Todoran; A. Rusu; A. Ciurba; M. Birsan; E. Redai; *Revista de Chimie*, **2018**, *69(12),* 3692-3697
9. P. Vass; E. Szabó; A. Domokos; E. Hirsch; D. Galata; B. Farkas; B. Démuth; S. K. Andersen; T. Vigh; G. Verreck; G. Marosi; Z.K. Nagy; *WIREs Nanomed. Nanobiotechnol.*, **2020**, *12*, e1611.
10. A. Jahangiri; M. Barzegar-Jalali; Y. Javadzadeh; H. Hamishehkar; K. Adibkia; *Artificial Cells; Nanomed. Biotechnol.*; **2017**, *45*, 1138-1145
11. V.J.B; B. Madhusudhan; *Int J Pharm and Bio Sci*, **2015**, *6*, P50-P58
12. P. Schwinte; A. Mariotte; P. Anand; L. Keller; Y. Idoux-Gillet; O. Huck; F. Fioretti; H. Tenenbaum; P. Georgel; W. Wenzel; S. Irusta; N. Benkirane-Jessel; *Nanomedicine,* **2017**; *12*; 2651-2674
13. J. Chu; L. Chen; Z. Mo; G.L. Bowlin; B.A. Minden-Birkenmaier; Y. Morsi; A. Aldalbahi; M. El-Newehy; W. Wang; X. Mo; *Acta Biomat*; **2020**
14. J. Chu; L. Chen; Z. Mo; A. Aldalbahi; M. El-Newehy; W. Wang; X. Mo; 3539225.
15. C.-H. Lee; M.-J. Hsieh; S.-C. Liu; J.-K. Chen; S.-J. Liu; I. C. Hsieh; M.-S. Wen; K.-C. Hung; *Materials Sci. Eng.*: C; **2018**; *88*; 61-69.
16. M.K. Haidar; S.S. Timur; A. Kazanci; O.F. Turkoglu; R.N. Gürsoy; E. Nemutlu; M.F. Sargon; E. Bodur; M. Gök; K. Ulubayram; *Eur J Pharm Biopharm***, 2020**
17. A. Kazanci; F. Turkoglu; N. Gürsoy; E. Nemutlu; F. Sargon; E. Bodur; M. Gök; K. Ulubayram; L. Öner; H. Eroğlu; *Eur J Pharm Biopharm*; **2020**
18. M. Janjic; F. Pappa; V. Karagkiozaki; C. Gitas; K. Ktenidis S. Logothetidis; *Int J of Nanomed*, **2017**, *12*, 6343
19. C.-H. Lee; S.-H. Chang; Y.-H. Lin; S.-J. Liu; C.-J. Wang; M.-Y. Hsu; K.-C. Hung; Y.-H. Yeh; W.-J. Chen; I.-C. Hsieh; *Biomat*; **2014**, *35*, 4417-4427

20. P. Liu; Y. Liu; P. Li; Y. Zhou; Y. Song; Y. Shi; W. Feng; X. Mo; H. Gao; Q. An; *ACS Appl. Mat. Interfaces*, **2018**, *10*; 41012-41018
21. A.I. Rezk; T.I. Hwang; J.Y. Kim; J.Y. Lee; C.H. Park; C.S. Kim; *Mat Lett*, **2019**, *240*, 25-29
22. M. Kouhi; M. Morshed; J. Varshosaz; M.H. Fathi; *Chem Eng J*.; **2013**, *228,* 1057-1065
23. M. Hajializade; M. Moghtadaei; A. Mirzaei; S. Abdollahi; P. Babaheidarian; H. Pazoki-Toroudi; A. Yeganeh; *Mat Sci Eng C,* **2020**, 110861
24. S. Kajdič; Š. Zupančič; R. Roškar; P. Kocbek; *Int J Pharm,* **2020;** *573*; 118809
25. A. Jahangiriab; M. Barzegar-Jalalia; A. Garjanid; Y. Javadzadehc; H. Hamishehkara; A. Afroozianad; K. Adibkiaa; *Pow Technol*, **2015**, *286*; 538-545
26. R. Iqbal; O. Salman Qureshi; A.M. Yousaf; S.A. Raza; H.S. Sarwar; G. Shahnaz; U. Saleem; M.F. Sohai; *Eur J Pharm Sci,* **2021**, *181;* 105817
27. M. Kurakulaa; G.S.N. Koteswara Rao*; J Drug Deliv Sci Technol*, **2020**, *60*; 102046
28. E. Sipos; T. Csatári; A. Kazsoki; A. Gergely; E. Bitay, Z.I. Szabó; R. Zelkó; *Pharmaceutics*, **2020**, *12(7)*, 612
29. Z.K. Nagy; K. Nyúl; I. Wagner; K. Molnár; G. Marosi; *Express polymer letters,* **2010**, *4*, 763-772
30. J. Pelipenko; P. Kocbek; J. Kristl; *Int J Pharm*, **2015**, *484*, 57-74
31. P.R. Vuddanda; A.P. Mathew; S. Velaga; *Reactive Functional Polymers*, **2016**, *99*, 65-72
32. C. Tizaoui; H. Galai; M. Barrio; S. Clevers; N. Couvrat; V. Dupray; G. Coquerel; J.-L. Tamarit; I. B. Rietveld; *Eur J Pharm Sci*, **2020**, *148,* 105334
33. E. Sipos; Z.I. Szabó; E. Rédai; P. Szabó; I. Sebe, R. Zelkó; *J Pharm Biomed Anal,* **2016**, *129*, 224-228

STUDIA UBB CHEMIA, LXVI, 2, 2021 (p. 299-308)
(RECOMMENDED CITATION)
DOI:10.24193/subbchem.2021.2.26

CANNABIDIOL CONTENT EVALUATION IN COMMERCIAL DIETARY SUPPLEMENTS AND STABILITY IN OIL VEHICLE

ROBERT-ALEXANDRU VLAD[a], LÉNÁRD FARCZÁDI[b]*, CAMELIA-MARIA TOMA[b], SILVIA IMRE[c], PAULA ANTONOAEA[a], EMŐKE MARGIT RÉDAI[a], DANIELA-LUCIA MUNTEAN[c], ADRIANA CIURBA[a]

ABSTRACT. Cannabidiol (CBD) is one of the most studied alkaloids found in *Cannabis* species. Also, its occurrence in *Cannabis* plants is higher in most of cases compared with the addictive compound named tetrahydrocannabinol (THC). This study aimed to evaluate CBD concentrations and stability in different commercial products and reconstituted oil. An UHPLC method previously published was applied. Three CBD oils and two powders marketed online together with a reconstituted oil were analyzed. The oils presented concentrations lower than stated on the label. The content of reconstituted CBD oils prepared similarly to the commercial oils decrease linearly with small differences based on the storage conditions. Thus, the CBD oil kept at temperatures of 5±0.3°C tends to decompose slightly slower compared with the oil kept at room temperature. A stabilizer may be needed to slow the decomposition process. Future studies for reconstituted formulation may be needed to establish if the type of oil used is influencing the decomposition process.

Keywords: *CBD-oil, dietary supplements, storage, CBD powders, decomposition*

[a] *George Emil Palade University of Medicine, Pharmacy, Science, and Technology of Targu Mures, Faculty of Pharmacy, Pharmaceutical Technology and Cosmetology Department, 38th Gheorghe Marinescu street, RO-540142, Targu Mures, Romania*

[b] *George Emil Palade University of Medicine, Pharmacy, Science, and Technology of Targu Mures, Center for Advanced Medical and Pharmaceutical Research, 38th Gheorghe Marinescu street, RO-540142, Targu Mures, Romania*

[c] *George Emil Palade University of Medicine, Pharmacy, Science, and Technology of Targu Mures, Faculty of Pharmacy, Analytical Chemistry and Drug Analysis Department, 38th Gheorghe Marinescu street, RO-540142, Targu Mures, Romania*

** Corresponding author: lenard.farczadi@umfst.ro*

INTRODUCTION

Cannabidiol (CBD) whose chemical structure can be found in Figure 1, belongs to the class of cannabinoids [1]. It can be found in numerous pharmaceutical formulations [2-4]. Sadly, many of them are registered as dietary supplements and this can be a huge disadvantage for patients because some studied supplements can contain lower concentrations of active substance than stated on the label [5,6]. Currently, the only pharmaceutical formulation approved worldwide that contains CBD as its active substance CBD is Epidiolex, which contains 10% CBD [7,8]

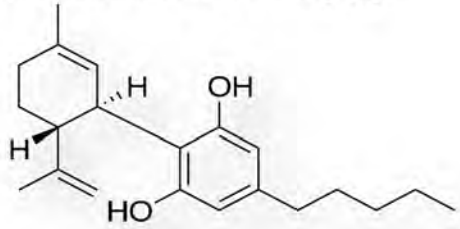

Figure 1. CBD chemical structure

CBD can be found in numerous types of pharmaceutical formulations from therapeutic oils to ointments, creams, gels and, sprays. Its external use can be attributed to the presence of hydroxyl groups which confers CBD an antioxidant property based on which it can be used in cosmetical products as an anti-aging ingredient. The internal use is sustained by a high number of studies many of them demonstrating the antiepileptic effect. Also, studies regarding the use of CBD in Alzheimer disease, cancer, or Parkinson disease were conducted [9].

Usually, the class of dietary supplements consists of vitamins and minerals, so taking into consideration that CBD is a cannabinoid that has proven therapeutic effect it could be stated that it is wrongly attributed to this class and it should only be present in the class of drugs approved by entities such as European Medicines Agency (EMA) or Food and Drug Administration (FDA) [9].

At the moment, numerous dietary supplements are marketed worldwide and many of them can be purchased online without counseling from any healthcare professional. A list of pharmaceutical formulations with CBD registered as supplements that can be purchased online in Romania can be found in Table 1.

Table 1. Pharmaceutical formulations with CBD registered as dietary supplements

Product name	Pharmaceutical form	CBD concentration (%)
CBD oil	Oily solution	5, 10, 15, 25, 30
Body cream	Ointment/cream	0.5
Hand cream	Ointment/cream	0.2
Mouthwash	Solution	0.1
Tablets for animals	Tablets	1.3, 3.2 mg/tablet
Toothpaste	Paste	0.133
Oral Spray	Spray	0.8
Soothing Gel	Gel	0.1

An important issue regarding CBD products is related to their stability and the variable degree of recovery from samples with the natural origin [10], the studies underlying in the same time the importance of non-aqueous liquid vehicles for liquid formulations or extemporaneous preparation.

This study aims to assess the concentration of CBD found in commercial oils and powders together with a stability study of CBD reconstituted oils at different temperatures and under light exposure.

RESULTS AND DISCUSSION

The results obtained show that in the case of the powders, the measured concentrations correspond to the ones mentioned on the label by the manufacturer. The same cannot be said about CBD oils.

In a study conducted by Pacifici et al. [10], it has been stated that the recovery from tea samples of CBD was variable, also mentioning the fact that different parts of the plant tend to have different concentrations of CBD. The same study concluded that the stability in an aqueous solution is very short so an extemporaneous preparation needs to be taken into consideration. In the same research, it has been shown that the CBD is more stable in oily solution compared with an aqueous solution, but a loss of 20% of the initial concentration is recommended to be taken into consideration.

It is well known that solutions represent the most unstable pharmaceutical formulations [11-13], so there is a possibility that initially, during manufacturing, the concentrations were the ones mentioned on the label by the manufacturers but keeping them in certain conditions such as high temperatures, light exposure

and the lack of a stability test might have led to a decrease in terms of concentrations. In the case of CBD oil A (5%), CBD oil B (5%) and, CBD oil C (10%), concentrations lower than 95% of the declared amount were measured (Table 2). In the case of reconstituted oils, it can be noticed that the more time passes the more the CBD concentration tends to decrease (Table 3). A slightly higher decrease can be noticed in the case of the oil kept at room temperature, which indicates the importance of the storage conditions of the oily solution. A maximum absorption at the wavelength of 208 nm (Figure 5) and a retention time of 3.2 minutes corresponding to CBD was observed (Figures 2-4). A shift might occur during the determinations between the signals belonging to the oils and external standards that could be explained by the aging of the column. The shifting process is less than 10% which is deemed acceptable by the in-force European Pharmacopoeia. In figure 3, are represented the peaks corresponding to the external standard (higher signal) and the one belonging to the evaluated CBD oils (lower signal). The concentration of CBD in the blank hemp oil used is negligible – less than 0.4%, which can be correlated with the initially higher concentration of CBD in the reconstituted CBD oil compared to the quantity of CBD powder dissolved, at about 5.38%. An accumulation of the CBD added and dissolved in the solution with the CBD present in the hemp oil caused this final higher concentration. In the Certificate of Analysis, a higher concentration is mentioned in all of the three oils studied compared to the label, which also indicates the existence of the CBD in small quantities in the hemp seed oil.

Table 2. Evaluation of CBD in the samples

Pharmaceutical formulation	Concentration on the label	Concentration at T_0	Absolute Difference (%)	Total relative loss (%)	Concentration at T_2 (%)	Absolute difference (%)	Total relative loss (%)
CBD oil (A)	5.0 %	4.240	-0.760	15.200	3.950	-1.050	21.000
Bio CBD oil (B)	5.0 %	4.580	-0.420	8.400	4.290	-0.710	14.200
CBD oil (C)	10.0 %	8.485	-1.515	30.300	8.449	-1.551	15.150
Powder A	99.8 %	99.093	-0.707	0.7080	97.090	-2.710	2.715
Powder B	99.0 %	97.530	-1.470	1.4840	96.970	-2.030	2.050

In a study conducted by Bonn-Miller et al. 84 oils from 31 companies were evaluated. It has been stated that 69% of the CBD oils were mislabelled. Regrettably, an operation such as dilution, blending and, the rectification of CBD oils is permitted legally [7]. In another study conducted by Fraguas-Sánchez CBD water and alcoholic solution were prepared to determine the t_{95} the results showed that CBD tends to be more stable in alcoholic solution than in water solution (water+0.5% Tween 80), also, the temperature influences the CBD stability, the same study showing that a solution kept at temperatures of 5°C is more stable compared with the solution kept at room temperature (25°C). The authors mentioned above linked the instability by the presence of oxygen, whilst, when the solution is saturated with another gas such as nitrogen the stability of the solution increased [14].

Table 3. Assessment of CBD concentration in the reconstituted oil

Pharmaceutical formulation	T_0 (%)	T_1 (%)	Absolute difference (%)	Total relative loss (%)	T_2 (%)	Absolute difference (%)	Total relative loss (%)
Reconstituted oil kept at (5°C)	5.380	5.170	-0.210	3.903	4.738	-0.642	11.930
Reconstituted oil kept at (25°C)		5.100	-0.280	5.204	4.730	-0.650	12.081

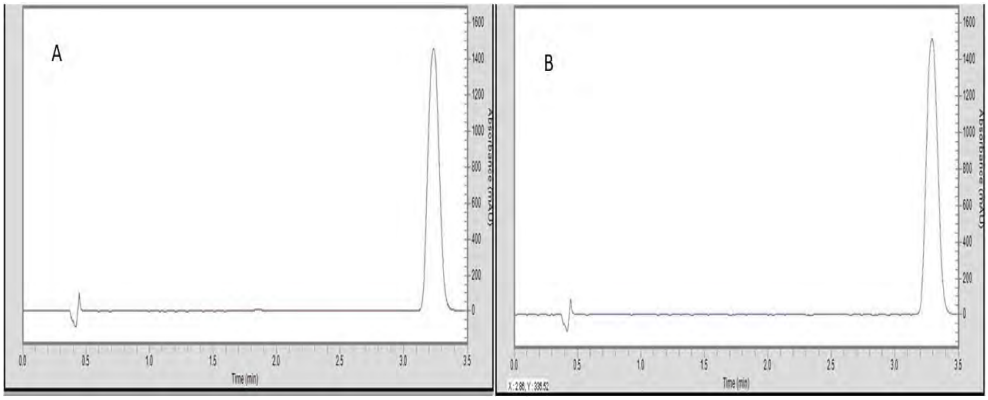

Figure 2. Chromatograms of CBD powders A and B at T_0

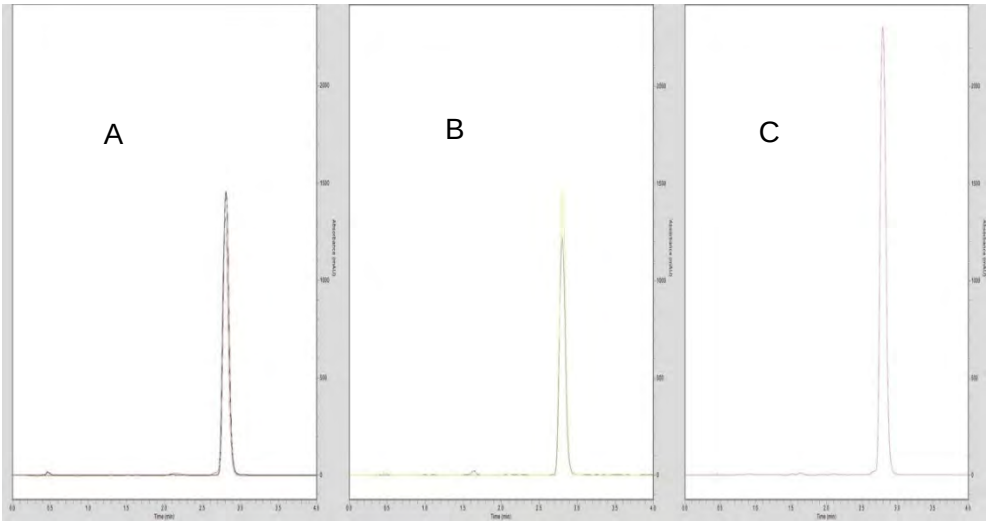

Figure 3. CBD chromatograms of oils A, B, C

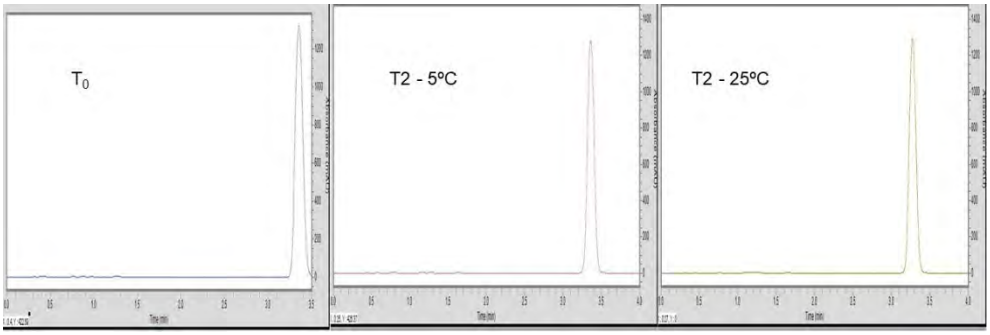

Figure 4. CBD chromatograms of reconstituted oil at T_0 and T_2.

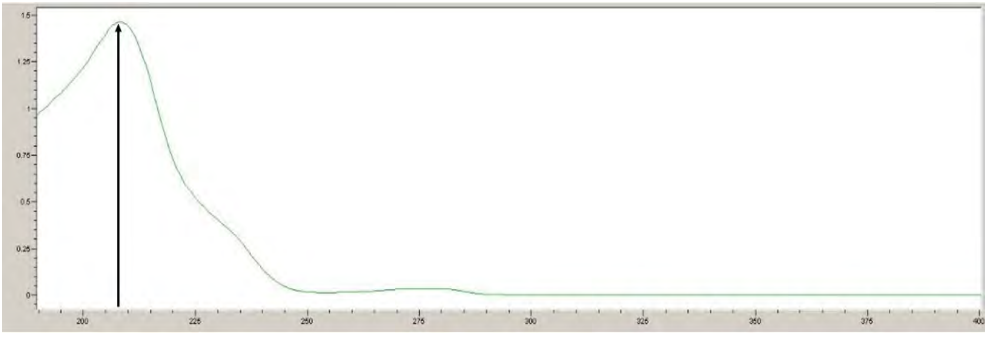

Figure 5. CBD spectra, maximum absorption at 208 nm

Shelf-life evaluation for the reconstituted oils

To determine the shelf life, the reconstituted oils were tested. The time needed for the concentration to decrease to 90% of the initial value was evaluated. After 14 days, concentrations less than 90% were assessed in both of the cases. The main difference consisted in the fact that in the case of the oil kept at room temperature 12 days were needed to reach this value, while in the case of the oil kept at 5°C the decrease in concentration to under 90% was observed after 12 and a half days.

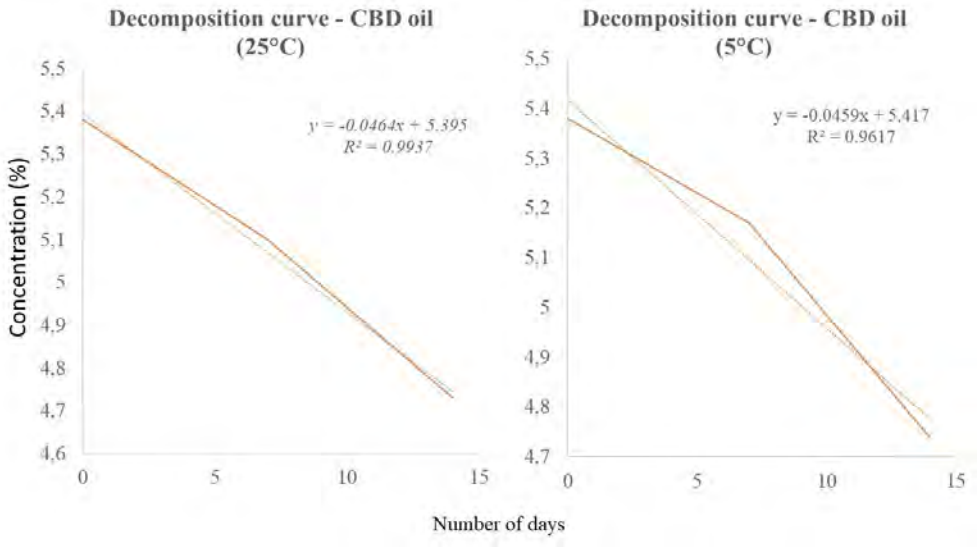

Figure 6. Decomposition curves for reconstituted CBD oil kept at different temperatures

Varying the temperature storage conditions was considered as a result of the lack of stability of CBD in ACN, while kept at room temperature, whilst when the CBD solution in ACN was kept in the refrigerator at 5°C, the stability of the solution was improved. This fact represented the starting point of the present study. It can be observed that in both of the cases the concentration tends to decrease as time passes. Small differences regarding the concentration at T_1 and T_2 were observed in the case of both CBD reconstituted oils kept in different temperature conditions.

CONCLUSIONS

Five dietary supplements found on the market were evaluated, three of them being formulated as an oily solution while two of them were powders. Besides the dietary supplements, a reconstituted CBD oil concentration was assessed. The powders concentration was within the acceptance limit whilst the oily solutions presented concentration under the lower acceptance limit. In the case of the reconstituted oil, it has been observed that as time passes the CBD concentration tends to decrease fact that can be observed in both of the reconstituted oils kept in different storage temperatures. To obtain a concentration close to the one mentioned on the label, the CBD concentration in the hemp oil has to be taken into consideration. Another possibility consists of using other oils that don't contain CBD such as sunflower oil, sesame oil where there is no risk of cumulation of CBD, and obtaining concentrations that are not in accordance with the declared ones. Also, labeling accuracy of CBD sold online might be incorrect, thus including CBD oils as a prescription or over-the-counter drug might be more suitable, due to its therapeutic properties because in the case of drugs available with prescription many analytical tests are conducted, so the concentration of the product coincides with the one written on the label.

EXPERIMENTAL SECTION

a. Reagents and reference substances

During the assessment of CBD concentrations, the following reagents and substances were used: cannabidiol (CBD) 99.5% (Trigal Pharma, Austria), acetonitrile (ACN) (Honeywell, Germany) and, hemp oil (Canah, Romania) ultrapure water obtained using a Millipore Direct Q3 purifier.

b. Chromatographic equipment and method

The chromatographic equipment consisted of a Flexar 10 (Perkin Elmer) UHPLC system with a DAD detector. Due to the aging of the initial column, we needed to replace it, and we chose a column with the same type of stationary phase and the same size but from a different manufacturer. The column used, an InfinityLab Poroshell 120 EC-C18, was manufactured by Agilent and had the following characteristics: dimensions - 3.0 x 100 mm, particle size - 2.7 µm. Other equipment used: magnetic stirrer with a heating source (VWR Hot-Plate Advanced Series) and an ultra-microcentrifuge 5430R (Eppendorf).

To establish the CBD concentration in the studied oils and powders a UHPLC method previously developed and validated was used. [15]

c. Preparing standard and test sample solutions.

The stock solution had a concentration of 1 mg/mL cannabidiol and its preparation was simple, 10 mg of CBD being dissolved in 10ml of ACN. The reference solution had a concentration of 100 µg/mL and was obtained by diluting the stock solution with the same solvent (ACN).

The evaluated samples can be found in Table 4.

Table 4. Analysed samples

Pharmaceutical formulation	Concentration
CBD oil (A)	5.00 %
Bio CBD oil (B)	5.00 %
CBD oil (C)	10.00%
Powder A	99.80 %
Powder B	99 %
CBD oil (reconstituted formulation)	5 % (CBD added)

With the scope of quantification, the CBD from the CBD oils (registered as dietary supplements) was extracted as follows: 200 µL of CBD oil were mixed with ACN in a beaker. The mixture was stirred using a magnetic stirrer at 800 rotations per minute (rpm) for one hour. The resulted solution was transferred and diluted in a 10 mL flask with ACN. The next step consisted of a new dilution of 1:10. From the obtained solution approximately 1.5 mL were centrifuged at 9000 rpm and 20°C for three minutes.

Reconstitution of the oily CBD solution was performed by using CBD – 99.5% and hemp oil, following a concentration of 5% CBD. The reconstitution consisted of the dissolution of the CBD powder (99.5%) in the hemp oil. In order to obtain a homogenous solution, we stirred the reconstituted CBD oil for 1 hour at 1200 rpm. The reconstitution was realized as a result of the variated concentration belonging to the evaluated CBD oil.

It was divided into two equal parts, each to be stored under different conditions, half of it was maintained at room temperature (23°C±2°C) without any exposure to light while the other half was maintained in the refrigerator at temperatures of 5°C±0.3°C. Different conditions of storage were chosen as a result of the instability of the CBD in ACN at room temperature.

Evaluation of the CBD concentration for the oils kept at different temperatures was realized at T_0 – when it was prepared, T_1 – at one week, T_2 – after two weeks.

The hemp oil itself which was used for preparing the reconstituted CBD oils was also tested to establish if it contains any CBD; the reconstituted formulation was prepared as similarly as possible and using the same ingredients as the purchased CBD oils.

ACKNOWLEDGEMENTS

The study was performed with the support of the Center for Advanced Medical and Pharmaceutical Research, George Emil Palade University of Medicine, Pharmacy, Science, and Technology of Targu Mures, Romania.

REFERENCES

1. G.A. Cabral; T.J. Rogers; A.H. Lichtman; *J Neuroimmune Pharmacol*., **2015**, 10(2), 193-203.
2. D. Momekova; E Ivanov; S Konstantinov; F Ublekov; P.D. Petrov; *Polymers*, **2020**, 12(5), 1172.
3. M. Javadi-Paydar; K.M. Creehan; T.M. Kerr; M.A. Taffe; *Pharmacol Biochem Behav.* **2019**, 184, 172741.
4. D.J. Liput; D.C. Hammell; A.L. Stinchcomb; K. Nixon; *Pharmacol Biochem Behav.,* **2013**; 111, 120-127.
5. P.S. Cogan; *Expert Rev Clin Pharmacol.*, **2019**; 12(6), 501-511.
6. K. Sekar; A. Pack; *F1000Res.,* **2019**, 8(F1000 Faculty Rev), 1-8.
7. M.O. Bonn-Miller; M.J.E. Loflin; B.F. Thomas; J.P. Marcu; T. Hyke; R. Vandrey; *JAMA.*, **2017**, 318, 1708–1709.
8. R. Abu-Sawwa; B. Scutt; Y. Park; *J Pediatr Pharmacol Ther.* **2020**, 25(6), 485-499.
9. R.A. Vlad; G. Hancu; A. Ciurba; P. Antonoaea; E.M. Redai; N. Todoran; O. Silași; D.L. Muntean; die Pharmazie, **2020**, 75, 463-469.
10. R. Pacifici; E. Marchei; F. Salvatore; L. Guandalini; F.P. Busardò; S. Pichini; *Clin Chem Lab Med*., **2017**, 55(10), 1555-1563.
11. M.J. Akers; *Int J Pharm Compd.,* **2016**, 20(1), 41-45.
12. N. Unger; U. Holzgrabe; *J Pharm Biomed Anal.,* **2018**, 147, 125-139.
13. M. Jutglar; M. Foradada; F. Caballero; J. Hoogmartens; E. Adam; *J Pharm Biomed Anal.,* **2018**, 159, 60-65.
14. A.I. Fraguas-Sánchez; A. Fernández-Carballido; C. Martin-Sabroso; A.I. Torres-Suárez; *J Chromatogr B Analyt Technol Biomed Life Sci.*, **2020**, 1150, 122188.
15. R.A. Vlad; L. Farczadi; S. Imre; A. Ciurba; N. Todoran; E.M. Redai; P. Antonoaea; D.L. Muntean; *Acta Medica Marisiensis*, **2019**, 65(2): 45-48.

STUDIA UBB CHEMIA, LXVI, 2, 2021 (p. 309-324)
(RECOMMENDED CITATION)
DOI:10.24193/subbchem.2021.2.27

ULTRASONIC EXTRACTION FOR PREPARATION OF PLANT EXTRACTS WITH BIOINSECTICIDAL EFFECTS ON PEST FROM SEED DEPOSITS

GABRIEL MIHAITA DARABAN[a], CARMEN ZAHARIA[a], LACRAMIOARA RUSU[b], ADRIAN CATALIN PUITEL[a], MARINELA BADEANU[c], DANIELA SUTEU[a]*

ABSTRACT. This paper describes the preparation of plant extracts using solid-liquid ultrasonic extraction (sonoextraction), the characterization of prepared extracts and their bioinsecticidal activity. The studied raw vegetal material:*Primula veris*, *Achillea millefolium*, *Origanum vulgare* and *Artemisia absinthium,* was collected from the spontaneous flora of Romania, Moldova region. To assess the efficiency of solid-liquid sonoextraction process, the influence of some operating parameters such as solid/liquid ratio, extraction time, extraction temperature, and extraction efficiency was studied. The qualitative study has in view the interpretation of UV-VIS spectra recorded for the extracts, and the quantitative study consists in the estimation of total polyphenols and flavonoids content of prepared vegetal extracts. The resulted data indicate that the content of polyphenols and flavonoids is dependent of the extraction temperature, extraction time and solid/liquid extraction ratio. The bioinsecticidal activity of *Origanum vulgare* and *Artemisia absinthium* extracts was evaluated on the *Acanthoscelides obtectus* (commonly named as ladybug bean) using two application techniques (i.e. direct and indirect application using a cellulose disk as a porous material impregnated with extract that allows controlled evaporation), being registered a mortality rate of adults in the range of 35-55%. Therefore, the studied extracts proved to be effective in controlling ladybug bean from seed stores.

Keywords: *Acanthoscelides obtectus (ladybug bean), bioinsecticidal activity, chemical characterization, vegetal extract, sono- extraction*

[a] *''Gheorghe Asachi'' Technical University, Iasi, Romania; ''Ion Ionescu de la Brad" University of Life Science, Iasi, Romania; "Cristofor Simionescu" Faculty of Chemical Engineering and Environmental Protection, Iasi, Romania.*

[b] *"Vasile Alecsandri" University of Bacau, Faculty of Engineering, Bacau, Romania*

[c] *"Ion Ionescu de la Brazi" University of Agricultural Sciences and Veterinary Medicine of Iasi, Faculty of Horticulture, Iasi, Romania*

** Corresponding author: danasuteu67@yahoo.com*

INTRODUCTION

In order to protect the food seeds, a series of plant extracts can be successfully used instead of chemical synthesis pesticides.

Assurance of life quality is today one of the key objectives of any economic, agricultural or social activity. The people's life quality concept refers both to the quality of products and services they use, and to the quality of the environment in which they live their lives. An important category of products that directly influence people's health is food and the raw material for food preparation. In this sense, the practice of a new agriculture, of modern and biodynamic type, in accordance with the principles of environmental sustainability, has become a last resort. Moreover, ecological agriculture (organic farming) involves, among other things, the use in agricultural processes of chemical compounds with the role of pesticides, environmentally friendly to ensure optimal crop development, but protecting both the plant and environmental factors (soil, water, air) from the toxic action of these synthetic compounds. In this context, the finding or development of some alternatives to the chemical products existing on the market or intensively used in the agriculture sector is proposed. The attention was directed to certain plants, known to be real laboratories which can offer numerous metabolites extremely useful in cosmetics, foods, pharmaceutical industries, in development of phyto-pharmaceutics and phytosanitary products [1-5]. In the last times, some compounds with biopesticide action, useful in agriculture for combating pests or keeping certain plant seeds, were identified [6-11]. The advantages of such products instead of chemically synthetized pesticides are mainly due to the lack of toxicity to environmental factors and human bodies, the customization of the dose according to the intended purpose and the possibility of use in the form of raw extract as result of the manifestation of the synergistic effect of the compounds present in extract. Comparatively with the interest zone which targets natural additives, phytosanitary products and phytopharmaceutics for human use, the research in the biopesticide area is only just at the beginning. But they are spurred, encouraged and supported by new regulations in agriculture in order to ensure its sustainability.

Our paper aims is to study the preparation of some vegetal extracts using solid-liquid sono-extraction. In this respect, four plants from the spontaneous flora of the region of Moldova (Romania), respectively, the city of Iasi were used: *Achillea millefolium* (Yarrow), *Artemisia absinthium* (Wormwood), *Origanum vulgare* (Oregano) and *Primula veris* (Primrose), their extracts previously prepared by maceration have indicated corresponding efficiency in combating crop or deposit pests. The study of sono-extraction followed the influence of some physical operating parameters on the

extraction process, the influence being appreciated by determination of the extraction yield. Preliminary quantitative analysis followed the determination of the total polyphenols and flavonoids content. Also, the bio-insecticidal effect of the extracts on the pests from the seed deposits, respectively the *ladybug beans* (*Acanthoscelides obtectus*), was followed.

RESULTS AND DISCUSSION

The prepared alcoholic extracts had a brown-greenish colour and a characteristic alcoholic odour which, however, retains some of the initial odours of the plants.

Evaluation of the extraction yield

The calculation of the efficiency of solid-liquid ultrasound-assisted extraction, at different solid/liquid ratios, temperature and time was performed in order to evaluate the extraction performances related to the selected extraction conditions. The results are presented in Table 1. To determine the overall extraction yield, it was necessary to evaporate at the sec a volume of 5 mL of each vegetal extract, at temperature of 60°C, using a thermostatic oven, in order to obtain the dry residue.

In the extraction processes, the temperature is one of the important operating parameters, its value influencing the mass transfer of the solute between the solid phase and the solvent, respectively the quantity of the extracted substance under the selected conditions. Also, the extraction yield depends on the quality of the plant material, because it controls the content of useful compounds, the porosity and the permeability to extraction of the solid material. To these are added the preliminary treatments performed on the plant material, such as drying, crushing, sieving and last but not least the type of solvent selected and the ratio in which it is added onto the solid material (L / S). These influences are observed by studying the results experimentally obtained and systematized in Table 1.

The analysis of the data presented in Table 1 highlights the fact that for each studied plant the extraction yield depends on the temperature and the extraction time, but also on the ratio between the two fractions. Analysing the data by plant type, it results that: for *Artemisia absinthium* the highest percentage of extracted compounds (11.2-11.6%) was obtained at temperature 35 ^{0}C, solid / liquid ratio of 1/20 and an extraction time of 10 and 15 minutes respectively; for *Primula veris*, the highest percentage (9.37%) was achieved at 60 ^{0}C, 15 minutes extraction and a solid / liquid ratio of 1/10, for *Origanum vulgare,* the highest percentage of extracted substances (10-10.88 %) was

obtained at temperature 60 ^{0}C, solid / liquid ratio of 1/10 -1/15 and an extraction time of 30 minutes, and for *Achilleia millefolium,* the best results (9.37%) were obtained in the following conditions: extraction temperature of 60 ^{0}C, solid / liquid ratio of 1/10 and an extraction time of 10 minutes. The conclusion of these data from Table 1 would be that for each plant there are and can be selected distinct conditions that lead to the highest extraction yields, conditions that definitely start from the plant structure, respectively the quantity and type of chemical compounds in their composition. These specific and particular conditions of each plant will be considered for further studies.

Table 1. The extraction yield at different parameters for sono-extraction procedure

Process time (min)	S/L (v/v)	Extraction temperature (^{0}C)	Plant/ extraction yield (%)			
			Origanum vulgare	*Achilleia millefolium*	*Artemisia absinthium*	*Primula veris*
10	1/10	35	3.4	3.4	5.4	2.8
	1/15		6	5.4	8.7	4.8
	1/20		10	8.4	**11.2**	7.2
15	1/10		3.8	4.2	7.4	2.8
	1/15		5.4	6.9	9.3	3
	1/20		9.6	8.4	**11.6**	6.4
30	1/10		5.5	4	7	2.75
	1/15		3.75	7.5	9	4.88
	1/20		10	6	7.5	5
10	1/10	45	5.2	6	8.8	4.2
	1/15		6	6.6	8.4	3.6
	1/20		5.6	6	8.8	4.8
15	1/10		6.8	6	8.8	5
	1/15		6	6	9	5.7
	1/20		5.2	4.4	6.4	4.4
30	1/10		8	6	9	4.5
	1/15		6.75	5.62	7.5	5.25
	1/20		7.5	7	5.5	11
10	1/10	60	6.25	7.5	4.5	5.75
	1/15		3	3.75	2.75	2.75
	1/20		7	4.5	10.5	8
15	1/10		7	**11.25**	5.25	**9.37**
	1/15		6.75	6.37	8.62	5.62
	1/20		7	7	6.5	6
30	1/10		10.25	6	3	3
	1/15		**10.88**	6	3.38	3.75
	1/20		8.5	7.5	7.5	7

Chemical evaluation of the prepared vegetal extract

Vegetal extracts are used in their raw form in pest control, not involving a prior separation on components, their action being based on the synergistic effect of the components. However, for the evaluation of the bioinsecticidal action, it is necessary to determine the chemical composition of the extracts obtained in order to identify the large classes of chemical components. In this sense, it was agreed the quantitative determination of the content of total polyphenols and flavonoids, classes of compounds that contain the most active principles responsible for the bioinsecticidal action.

The chemical analysis of all obtained vegetal extracts, based on the Folin-Ciocalteu reaction [14] to determine the total polyphenols content (TPC) and flavonoids content (TF), led to the results presented in Table 2.

Table 2. The content of total polyphenols and flavonoids in the vegetal extracts

Time (min)	S/L	T (^{0}C)	Plant							
			Artemisia absinthium		*Primula veris*		*Origanum vulgare*		*Achilleia millefolium*	
			C_{TPC} (µg/g)	C_{TF} (mg/g)	C_{TPC} (µg/g)	C_{TF} (mg/g)	C_{TPC} (µg/g)	C_{TF} (mg/g)	C_{TPC} (µg/g)	C_{TF} (mg/g)
10	1/10	35	0.60	13.215	0.4	12.521	1.07	16.688	0.65	17.340
	1/15		0.69	27.522	0.66	24.509	1.01	23.908	0.53	24.250
	1/20		0.51	16.887	0.43	19.987	0.89	18.760	0.48	20.631
15	1/10		0.71	15.303	0.47	12.657	1.14	19.096	0.61	17.353
	1/15		0.63	22.453	0.51	24.314	1.13	24.417	0.53	26.364
	1/20		0.55	18.063	0.63	24.573	1.13	22.560	0.51	22.782
30	1/10		1.1	9.27	1.75	13.43	1.68	19.9	0.93	10.41
	1/15		0.99	6.39	1.44	16.69	1.39	11.89	1.1	14.68
	1/20		1.1	9.27	1.75	13.43	1.68	19.9	0.93	10.41
10	**1/10**	45	0.93	**40.244**	0.78	70.276	1.56	65.432	0.93	42.255
	1/15		0.6	20.807	0.59	48.776	1.18	15.244	0.63	33.053
	1/20		0.55	18.335	0.53	23.503	1.09	24.927	0.48	25.674
15	**1/10**		0.87	**40.516**	0.95	78.234	1.73	29.419	0.84	37.742
	1/15		0.6	25.090	0.72	34.053	1.37	31.400	0.56	46.644
	1/20		0.47	19.392	0.49	23.056	1.03	11.912	0.48	25.123
30	1/10		1.18	10.77	1.65	16.52	1.59	12.27	0.97	12.4
	1/15		1.19	12.52	1.52	14.18	1.47	12.85	1.04	14.81
	1/20		0.99	6.39	1.44	16.69	1.39	11.89	1.1	14.68
10	1/10	60	1	5.64	2.24	22.26	**2.29**	20.09	1.68	17.32
	1/15		0.87	4.7	1.99	18.25	1.97	15.2	1.25	13.82
	1/20		1.18	10.77	1.65	16.52	1.59	12.27	0.97	12.4
15	1/10		0.96	10.84	2.22	29.9	**2.22**	21.64	1.67	21.84
	1/15		**1.39**	10.62	2.01	22.25	2.09	8.5	1.24	11.7
	1/20		1.19	12.52	1.52	14.18	1.47	12.85	1.04	14.81
30	1/10		0.95	6.02	2.5	19.13	**2.25**	24.17	1.32	16.52
	1/15		0.87	4.43	2.28	12.74	**2.29**	18.03	1.11	11.56
	1/20		**1.22**	26.04	1.1	42.56	1.06	36.25	1.24	18.622

The amount of extracted compounds depends, in the case of each plant, on the conditions under which the liquid-solid extraction was carried out, the conditions set out above, because they also significantly influence the overall efficiency of the extraction process. Thus, the data presented in Table 2 show the effect of three most significant operational parameters: (A) S / L ratio; (B) extraction time and (C) extraction temperature, on the quantity of extracted compounds. A preliminary analysis of these data in Table 2 shows that the amount of extracted flavonoids is much higher than the polyphenols, which suggests that the bioinsecticidal activity of the extracts may be probable, determined due to the chemical compounds of this class. These results must be analysed for, taking into account the factors that were selected for monitoring the extraction: temperature, phase contact time and phase ratio.

The effect of solid-solvent ratio on total polyphenols (TPCs) and flavonoids (TFs) content

The influence of the solid / liquid ratio (S / L) (Table 2) was assessed by the values obtained for the content of these compounds present in the plant extract. Comparing the characteristic values of TPC and TF taking into account each plant, it can be concluded that in the case of:

(i) *Artemisia absinthium* regardless of the extraction temperature, the best values were obtained in the case of S / L ratios of 1/10 -1/15, i.e. for TPC values were 1.39 and 1.22 μg GAE / g, respectively for TFCs, obtained values were 40.515 and 42.25 mg QE / g, respectively.

(ii) *Origanum vulgare*, analyzing all the values in the Table 2, it seems that for TPCs, the best values are obtained in the case of the phase ratio S/L of 1/10 (2.29-2.59 μg GAE / g) respectively 1/15 - 2.29 μg GAE / g, and in the case of TFC, the values obtained depend on the phase ratio but also on the temperature these values; the highest value obtained was 65,432 at a ratio S / L of 1/10.

(iii) *Achilleia millefolium* considering the TPC content, the values obtained are close and relatively evenly distributed along the values of the phase ratio and temperature, but the values obtained in the case of the ratio S/L 1/10 of 1.32-1.68 μg GAE / g are detached. Regarding the TFCs content, the phase ratio S/L that ensures the highest values is overall 1/15, corresponding to 46.644 mg QE / g.

(iv) *Primula veris*, the analysis of the TFC content led to the conclusion that overall the S / L ratio of 1/10 ensures the obtaining of the best values for the content of polyphenolic compounds of 2.24-2.5 μg GAE / g. In the case of flavonoids, keep in mind the maximum values of 70,276 mg QE / g and 78,234 mg QE / g obtained in the case of S / L ratios of 1/10.

The effect of extraction time on the content of total polyphenols and flavonoids

The effect of the extraction time can be assessed according to the working temperature (Table 2), different behaviours are identified in this case. Contrary to expectations, the highest values were not recorded at the highest temperature at which the extraction was conducted (60 ^{0}C) but at temperatures up to that value, the reason being that the temperature, although it facilitates better phase contact, can also determine destruction of compounds. If we take into account the fact that at extraction temperature of 45 ^{0}C the highest values for calculated sizes were obtained, then it can be concluded that maximum contents for TPC were obtained at an extraction time of 15 min and S/L ratio of 1/10 for *Primula veris* - 0.95 GAE / g and *Origanum vulgare* – 1.73 g GAE / g) and 10 min in the case of *Artemisia absinthium* and *Achilleia millefolium* -0.93 g GAE /g. The highest total flavonoid content (TFC) was obtained in the case of an extraction time of 15 min for Primula veris - 78.23 mg QE/ g, *Artemisia absinthium* - 40.51 mg QE/ g and *Achilleia millefolium* – 46.64 mg QE/ g and 10 minutes for *Origanum vulgare* – 65.43 mg QE/ g.

The effect of temperature on the content of total polyphenols and flavonoids in plant extracts

Temperature is considered an important factor that significantly influences the solid-liquid extraction by intensifying the denaturing of the cell wall of the plant substrate which allows increasing the cell permeability and releasing the organic compounds from the organic matrix to the extraction solvent [16]. Also, in the scientific literature it is shown that an increase of the temperature contributes to the decrease of the surface tension that allows a better wetting of the vegetal material which facilitates a more complete extraction of the tracked products [16,17]. However, too high a temperature could distort a number of more temperature sensitive compounds. Table 2 also showed the results on the influence of extraction temperature on the content of total polyphenols and flavonoids in plant extracts obtained by extraction. The values obtained confirm that performing the sono-extraction at a temperature of 45 ^{0}C leads to plant extracts much richer in polyphenols and flavonoids than in the case of the extract made at 35 ^{0}C and 60^{0}C respectively.

Physical-chemical characterization of the prepared vegetal extract by UV-VIS spectrometry

The information resulted through the physical-chemical analysis confirm and complete the information resulting from the quantitative analyses.

Physical-chemical characterization was made using UV-Vis spectra for only two extracts, of *Artemisia absinthium* and *Origanum vulgare*, respectively those that showed significant bio-insecticidal activity on ladybug beans (*Acanthoscelides obtectus*), according to previous studies performed with vegetal extracts obtained by other liquid-solid extraction techniques (maceration-based extraction techniques) [18,19].

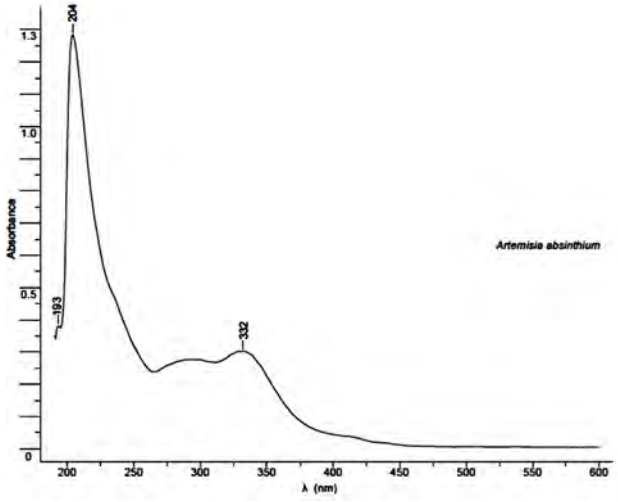

a

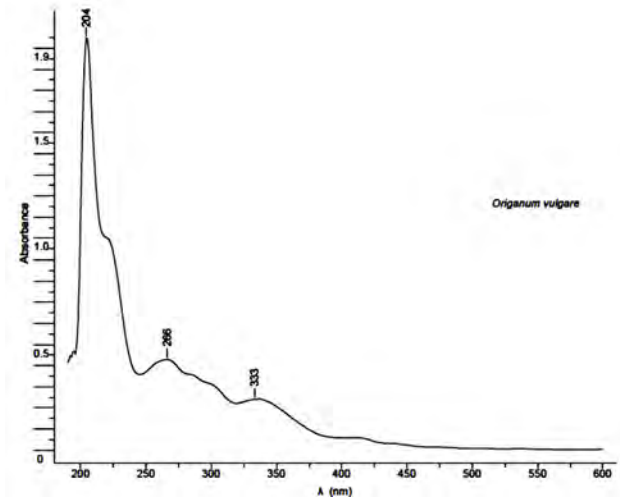

b

Figure 1. UV-Vis spectra of vegetal extracts obtained by solid-liquid sonoextraction: (a) *Artemisia absinthium;* (b) *Origanum vulgare*

UV-Vis spectroscopy has been used as a tool to obtain preliminary information about composition, vis-à-vis a number of classes of compounds (e.g., phenols) that may be present in plant extract. For example, in Figure 1, the UV-Vis spectra characteristic of the plant extracts obtained for the *Artemisia absinthium* and *Origanum vulgare* are presented.

The UV-Vis spectra study of alcoholic extracts can offer a series of pilot information related to the nature of extracted compounds (Table 3).

Table 3. UV-Vis characteristics of the alcoholic vegetal extracts obtained by solid-liquid sono- extraction (UAE)

Plant	λ_{max} (nm) (UAE)	Possible compounds
Artemisia absinthium	193, 204, 332	ursolic acid (210 nm); ferulic acid (214 nm, 325 nm); rosmarinic acid (218 nm, 330 nm) flavanones (320–330 nm); quercetin (256 nm, 354 nm); kaempferol (265 nm); luteolin (265 nm, 330 nm)
Origanum vulgare	204, 266, 333	

The character of the spectra and characteristic wavelengths are consistent with the data presented in our previous publications about the composition of plant extracts obtained by other methods of extraction liquid - solid.

According with the information presented in table 3 it can be underlined that a general characteristic of vegetal extracts is represented by their high amount of total flavonoids (256-265, 330-333 nm) and total polyphenols, which could be correlated with the intensity of the insecticidal effect manifested by these two extracts on ladybug beans (*Acanthoscelides obtectus*). Taking into account the above presented information, it can conclude that an advanced study on these extracts will allow the punctual identification of the chemical compounds from these two classes to which this effect is due.

Bio-insecticidal activity of the prepared vegetal extracts

Using the methodology and study procedure previously applied in our studies on the bioinsecticide action of the vegetal extract types [18,19] it was tested the action of two prepared extracts, i.e. *Origanum vulgare* and *Artemisia absinthium* species, by ultrasound-assisted extraction under 35^0C conditions on ladybug beans (*Acanthoscelides obtectus*). The results obtained are presented in Figure 2.

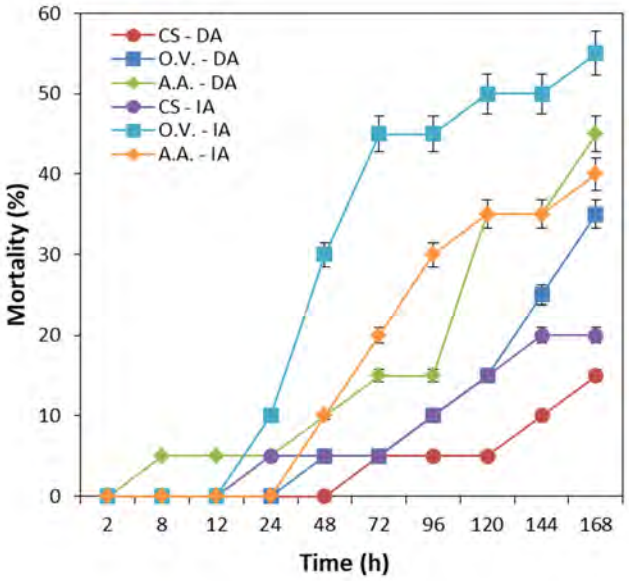

Figure 2. Obtained results about bioinsecticidal activity evaluation in the case of direct and indirect spraying application method (CS - control sample, O.V. – *Origanum vulgare*, A.A. – *Artemisia absinthium*, DA – direct application, IA – indirect application)

Figure 2 shows that the sprayed extracts has a bio-insecticidal effect on the ladybug beans after a certain contact time (24 or 48 hours, respectively) which is accentuated with the increase of contact time and therefore with the intensification of the application of treatments. At the end of the study time, it was observed that the extract of *Artemisia absinthium* shows a slightly stronger effect on ladybug beans compared to *Origanum vulgare*. Also, a better insecticidal action for both extracts is observed in the case of creating a saturated atmosphere in the volatile compounds eliberated from the extract by indirect application than in the case of direct spraying, which from a practical point of view, is much more advantageous and efficient. Correlating these effects of the vegetal extracts with the data presented in Tables 1 and 2, it can be observed that the extract of *Artemisia absinthium* has superior properties to that of *Origanum vulgare*, in terms of extraction yield or flavonoid content.

The performances of the ultrasonic extraction in preparation of efficient extracts in combating the bean gargle were compared with our results obtained by other solid-liquid extraction variants, previously studied. The results are shown in Figures 3 and 4.

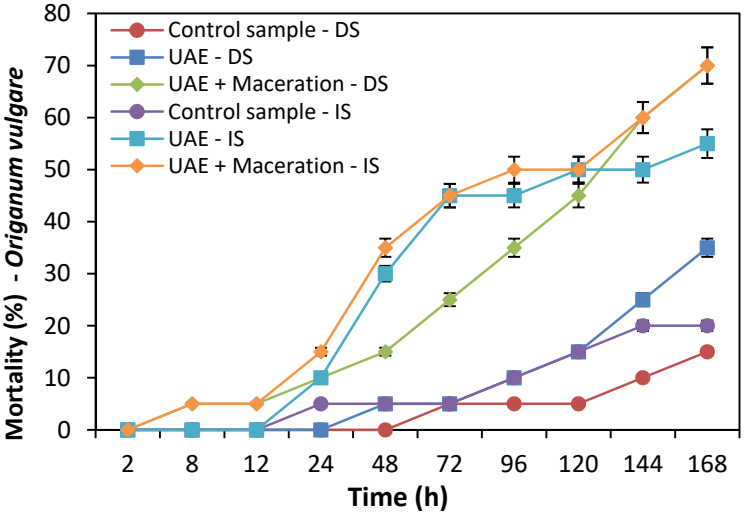

Figure 3. The bio-insecticidal action of *Origanum vulgare* extract obtained by all our used extraction methods by direct (DS) or indirect spraying (IS) technique (Control sample – D = Control sample – Direct Spraying; UAE – DS = UAE - Direct Spraying; UAE + Maceration – DS = UAE + Maceration - Direct Spraying; Control sample – IS = Control sample – Indirect Spraying; UAE – IS = UAE - Indirect Spraying; UAE + Maceration – IS = UAE + Maceration - Indirect Spraying

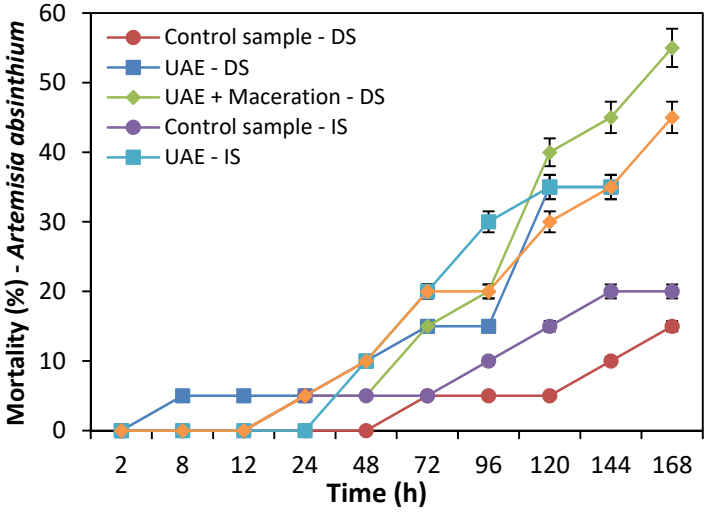

Figure 4. The bio-insecticidal action of *Artemisia absinthium* extract obtained by all our used extraction methods by direct (DS) or indirect spraying (IS) technique (Control sample – DS = Control sample – Direct Spraying; UAE – DS = UAE - Direct Spraying; UAE + Maceration – DS = UAE + Maceration - Direct Spraying; Control sample – IS = Control sample – Indirect Spraying; UAE – IS = UAE - Indirect Spraying; UAE + Maceration – IS = UAE + Maceration - Indirect Spraying)

From figure 3 it is observed that in the case of *Origanum vulgare*, after the sonoextraction, an extract is obtained whose bio-insecticidal action is superior to all other methods used, in the case of indirect spraying (on a cellulosic disk placed inside with ladybug bean) being surpassed only by subsequent maceration. From figure 4, it is observed that in the case of *Artemisia absinthium*, after the sonoextraction, an extract is obtained whose bio-insecticidal action is comparable with the other extraction methods used, the indirect spray technique proving much better performances.

CONCLUSIONS

This work was aimed at preparation of vegetal extracts from a number of characteristic plants of spontaneous flora of Moldova (Romania) (*Primula veris*, *Achilleia millefolium, Origanum vulgare* and *Artemisia absinthium*) by sono-extraction.

For sonoextraction were used flowers, stems and leaves of plants and studied the effects of three physical variables: extraction time, extraction temperature and solid/liquid ratio. The influence of these operating parameters was appreciated by calculating the extraction yields. Vegetal extracts were quantitatively characterized by spectrophotometer-based determination of the total polyphenols and flavonoids content. The results show that the extracts contain appreciable amounts of flavonoids that depend on the time of sonoextraction, extraction temperature and solid/liquid ratio, which can be considered to be responsible for the bioinsecticide action of the extracts. For the evaluation of the bio-insecticidal activity on the ladybug bean (*Acanthoscelides obtectus*), the *Artemisia absinthium* and *Origanum vulgare* extracts were used in experiments. These extracts were selected taking into account the significant in-time increasing bio-insecticidal activity on ladybug beans according to previous studies performed (maceration).

The mortality rate of adults was of 35-55%, thus is reconfirmed their effectiveness in controlling ladybug bean (*Acanthoscelides obtectus*) from seed stores.

EXPERIMENTAL SECTION

Plant material

The plant material used was represented by Yarrow (*Achillea millefolium* - Regn: Plantae; Phylum: Magnoliophyta; Class: Magnoliopsida; Order: Asterales; Family: Asteraceae; Gender: Achillea; Species: millefolium; Binomial name:

Achillea millefolium, L. 1753), Wormwood (*Artemisia absinthium* - Regn: Plantae; Phylum: Tracheophytes; Class: Angiosperms; Order: Asterales; Family: Asteraceae; Gender: Artemisia; Species: A. absinthium; Binomial name; Artemisia absinthium L. [1]), Oregano (*Origanum vulgare* - Regn: Plantae; Division: Tracheophyta; Subdiv.[*] Spermatophytina; Order: Lamiales; Family Lamiaceae; Subfam. Nepetoideae; Gender: Origanum; Binomial name; Origanum vulgare, L. 1753 [1]) and Primrose (*Primula veris* - Regn Plantae; Subregn Viridiplantae; Infraregn[*]; Streptophyta; Division: Tracheophyta; Subdiv.[*] Spermatophytina; Order: Ericales; Family: Primulaceae; Gender: Primula; Binomial name; Primula veris, L. 1753 [1]) collected from Tomesti (Iasi, Romania). The primary processing of the plants involved drying under the indirect influence of the sun, by placing them in a single layer in a well-ventilated space. Subsequently, the dried plants (stems, flowers and leaves) were crushed using a food mill and stored in a sealed, clean and dry laboratory flask until further use.

All necessary reagents or reference standards were of analytical quality (p.a.) (Chemical Company, Romania).

Extraction methodology

For the practical application of the extraction process it was used the same solvent as in our previous studies (in the case of maceration and heat extraction), respectively a solvent having the quality conditions required and accepted by both the food and agriculture industry [12, 13], meaning the ethanol. The concentration of ethanol (Chemical Company, Romania) was 96%, established after the preliminary tests in case of maceration.

The proper weighing of the powder from each plant was done using an analytical balance, RADWAG AC type (230V/400W, 50Hz). The established amount of vegetal powder (1 g) was dispersed separately in adequate volume of ethanol, in order to respect the considered solid-liquid ratio (1/10, 1/15 and 1/20).

Ultrasound-assisted extraction (sonoextraction) was performed in an ultrasonic bath, SONOREX RK type 100 H (produced by Bandeline Electronic GmbH &Co.KG, Berlin, Germany, 35 kHz, 320 W). This set-up allowed the control of extraction time and temperature. The extraction process was carried out at two constant temperatures (35 °C and 45 °C). At each temperature, there were considered two different extraction times (10 and 15 min).

The extraction was practically performed in two manners: (i) with reagents in a static system for the entire period of time required for extraction; (ii) by stirring the phases for the entire period of time required extraction. After the established extraction time, the biphasic systems were separated and the filtrates were collected in a glass laboratory flask and used for the quantitative and qualitative characterization of plants extracts.

Determination of extraction yield

In order to determine the extraction yield (eq.1) a sample of 5 mL of each extract was evaporated to dryness at constant temperature up to 60°C using a thermostatic oven.

$$\eta\,\% = \frac{m_{residue} \cdot V_{extract}}{n_{extract} \cdot m_{solid\ sample}} \cdot 100 \quad (1)$$

where, m_{residue} represents the mass of the residue obtained after evaporation to dryness, (g); V_{extract} - the volume of the extract sample for evaporation to dryness, (mL); n_{extract} - the total volume of extract obtained after the liquid-solid extraction, (mL); $m_{\text{solid sample}}$ - the mass of vegetal powder introduced in liquid-solid extraction process (g).

Physical-chemical characterization of the vegetal extract

For physical-chemical characterization of the vegetal extract it was used the UV-Vis spectrophotometer-based method, with a UV-Vis spectrophotometer Jasco V-550 model in order to register the spectra in the 200-800 nm region of the prepared vegetal extracts.

Quantitative characterization of the vegetal extract

The quantitative characterization of the vegetal extracts consisted of two types of analysis:
(i) Total polyphenolic compounds (TPC) *content* - determined according to Folin-Ciocalteu procedure, using the gallic acid (GAE) as reference standard to register the calibration curve [14]. The absorbance was measurement at 765 nm and the results were expressed in μg GAE/g;
(ii) Total flavonoids (TF) *content* - determined according to spectrophotometer-based method using a solution of $AlCl_3$ 2% in the presence of methanol [14]. The results were expressed in μg QE/g, considering the quercitin (QE)-based reference calibration curve.

Assessment of bio-insecticidal activity of the prepared vegetal extracts

It was worked with the *Origanum vulgare* and *Artemisia absinthium* extracts prepared by sono-extraction at 45^0C. As a pest it was tested on ladybug bean (*Acanthoscelides obsoletus*) which causes bean disease during storage. A number of 20 adults of the ladybug bean species were placed in a 8-liter working enclosure. For pest control, the working protocol includes:

(i) the vegetal extract application using two techniques: directly, consisting in spraying of vegetal extract (in raw form and 100% concentration) on the bean seeds, and indirectly, consisting in spraying vegetal extract on a porous cellulose support to ensure the creation of a saturated atmosphere with extraction compounds in the working enclosure;

(ii) the pest monitoring carried out at well-established intervals (2, 8, 12, 24, 48, 72, 96, 120, 144, 168 h) after the treatment application. The monitoring consisted in the identification of the number of eggs laid, as well as the establishment of the effectiveness of the treatment applied by studying the neuroleptic manifestations of pests (hyperactivity, inconsistency of the hind limbs, unnatural behaviours, etc.) and the identifying of the mortality rate of adults. The method used for monitoring was adapted after Asawalam *et al.* (2006) [15]. The mortality rate of insects was calculated using eq.(2) [15].

$$\%mortality = \frac{N_d}{N_n} \cdot 100 \quad (2)$$

where N_d represents the number of dead insects and N_0 is the number of initial tested insects.

REFERENCES

1. A. Dekebo; Plant Extracts, in *Plant Extracts*; A. Dekebo Ed.; Intech, **2019**, Introductory Chapter, pp.1-10.
2. A. Barbulova, G. Colucci, F. Apone; *Cosmetics,* **2015**, *2*, 82-92.
3. A.S. Ribeiro, M. Estanqueiro, M.B. Oliveira, J.M.S. Lobo; *Cosmetics,* **2015**, *2*, 48-65.
4. D. Suteu, L. Rusu, C. Zaharia, M. Badeanu, G.M. Daraban; *Appl. Sci*., **2020**, *10*, 8913, 21pg.
5. H. Antolak, D.Kregiel; Food Preservatives from Plants, in *Food Additives*, D.N. Karunaratne, G. Pamunuwa, Eds., Intech, Chapter 3, **2017**, 45-85.
6. H.O. Saxena, Y.C. Tripathi, G. Pawar, A. Kakkar, N. Mohammad; Botanicals as Biopesticides: Active chemical constituents and biocidal action, in *Familiarizing with local biodiversity: Notes on Systematics Of Plants And Insects*, P.K. Khatri, P.M. Meshram, (Eds.), Tropical Forest Research Institute (Indian Council of Forestry and Education), PO, RFRC, Mandla Rood Jabalpur-482021, **2014**, Chapter 21, 219-240.
7. S.K. Okwute; Plants as Potential Sources of Pesticidal Agents: A Review, in *Pesticides – Advances*, in *Chemical and Botanical Pesticides*, Soundararajan, R.P. (Ed.), InTech, **2012**, Chapter 9, 207- 232.

8. G.M.W. Lengai, J.W. Muthomi, E.R. Mbega; *Scientific African*, **7**, 2020, e00239.
9. Y. Tembo, A.G. Mkindi, P.A. Mkenda, N. Mpumi, R. Mwanauta, P.C. Stevenson, P. A. Ndakidemi, S.R. Belmain; *Frontiers in Plant Science*, **2018**, *9*, Article 1425, 10pg.
10. B. Singh, A. Kaur; *LWT - Food Sci Technol*, **2018**, *87*, 93-101.
11. J.J. Villaverde, P. Sandin-Espana, B. Sevilla-Moran, C. Lopez-Goti, J.L. Alonso-Prados; *BioResource*, **2016**, *11*(2), 5618-5640.
12. P.O. Lamuka; *Encyclopedia of Food Safety*, **2014**, *4*, 20-26.
13. S. Quijas, P. Balvanera; Biodiversity and Ecosystem Services, in *Encyclopedia of Biodiversity* (Second Edition), Levin S.A. (Ed.), Elsevier Inc. All, **2013**, 341-356.
14. L. Pavun, S. Uskokovic-Markovic, M. Jelikic-Stankov, D. Đikanovic, P. Đurdevic; *Czech J. Food Sci*., **2018**, *36*(3), 233–238.
15. E.F. Asawalam, S.O. Emosairue, A. Hassanali; *Electron. J. Environ. Agric. Food Chem*., **2006**, *5*, 1195-1204.
16. R.E. Ghitescu, I. Volf, C. Carausu, A.M. Bühlmann, I.A. Gilca, V.I. Popa; *Ultrasonics Sonochemistry*, **2015**, *22*, 535–541.
17. S. Boonkird, C. Phisalaphong, M. Phisalaphong; *Ultrason. Sonochem*., **2008**, *15*, 1075–1079.
18. G. Daraban, M. Badeanu, L. Rusu, D. Suteu; *Scientific Papers series of Horticulture (USAMV Iasi, Romania),* **2018**, *61* (1), 269-274.
19. G. Daraban, M. Badeanu, L. Rusu, D. Suteu; *Bull IPI (Iasi, Romania),* **2018**, *64* (68), 33-41.

STUDIA UBB CHEMIA, LXVI, 2, 2021 (p. 325-332)
(RECOMMENDED CITATION)
DOI:10.24193/subbchem.2021.2.28

VINCRISTINE AFFECTS THE REDOX REACTIVITY OF HEMOGLOBIN

VICTORIA CÎRJEU[a], CRISTINA PUȘCAȘ[a], RADU SILAGHI-DUMITRESCU[a]*

ABSTRACT. The anticancer drug vincristine, known to act by inhibiting tubulin function in human cells, is shown to affect autoxidation rates in hemoglobin – either alone or under conditions where nitrite acts as an initiator in a nitrosative stress cascade. This behavior mirrors those observed by us with four other antitubulin agents - irinotecan, docetaxel, paclitaxel and vinorelbine.

Keywords: *vincristine, hemoglobin, autoxidation, nitrite, oxidative stress, nitrosative stress, UV-vis*

INTRODUCTION

Anticancer agents have a wide variety of mechanisms by which they interfere with the growth of tumor cells. The largest group are agents that interact with DNA (by blocking DNA synthesis or by incorporation into DNA). Another important class of anticancer drugs is that of the antitubulin agents, which also affect cell division – but this time by interacting with protein scaffolds rather than with DNA [1–5]. Beyond these mechanisms, or often due precisely to them, chemotherapy can entail debilitating side effects such as bone marrow suppression, gastrointestinal damage, hair loss or nausea [1,2].

Hemoglobin (Hb) is found in large amounts in the blood and is among the first proteins in the human body to come into contact with anticancer drugs, so it is relevant to study the influence of cytotoxic compounds on it to understand the side effects of chemotherapy. Beyond its oxy/deoxy equilibrium in the ferrous state, Hb undergoes a range of redox reactions in blood as well as (or especially) in cases where it escapes the blood vessels

[a] *Babeş-Bolyai University, Faculty of Chemistry and Chemical Engineering, 11 Arany Janos str., RO-400028, Cluj-Napoca, Romania*
** Corresponding author: rsilaghi@chem.ubbcluj.ro*

in cases such as injury (e.g., subarachnoid hemorrhage). These redox reactions include autoxidation to ferric (met) Hb with liberation of superoxide and subsequently hydrogen peroxide, reaction with nitrosative stress agents such as nitrite, or reaction with oxidative stress agents such as peroxides. The chemical products of these reactions, as well as their biomedical relevance, have been explored to some length [6,7,16,17,8–15]. We have recently shown that cisplatin and related platinum complexes, as well as organic anticancer drugs and drug candidates, have the ability to affect the redox reactivity of hemoglobin – in terms of autoxidation rates, reactivity towards peroxides, and reactivity towards nitrite. These effects appear to entail Hb-drug complexes as well as direct redox reactions between the drug and hemoglobin and or small-molecules stress agents [1,2,4,5,16,18–20].

Vincristine (IUPAC (3aR, 3a1R, 4R, 5S, 5aR, 10bR) -methyl 4-acetoxy-3a-ethyl-9 - ((5S, 7S, 9S) -5-ethyl-5-hydroxy-9- (methoxycarbonyl) -2, 4,5,6,7,8,9,10-octahydro-1H-3,7-methane [1] azacycloundecino [5,4-b] indol-9-yl) -6-formyl-5 -hydroxy-8-methoxy-3a, 3a1,4,5,5a, 6,11,12-octahydro-1H-indolizino [8,1-cd] carbazole-5-carboxylate), also known as leurocristine, is a colorless drug from the class of *Vinca* alkaloids used in chemotherapy to treat various types of cancer such as acute lymphocytic leukemia, acute myeloid leukemia, Hodgkin's disease, lung cancer, neuroblastoma and others. Vincristine is given intravenously, typically from preparations at ~ 1mM concentration and in amounts equating to 1 μM concentration in blood, and, like other *Vinca* alkaloids, binds to tubulin and blocks mitosis. X-ray analysis showed that the drug binds equally to α and β-tubulin and causes a curvature at the interface that leads to the spiraling of protofilaments, subsequently reacting with their unstable end and inhibiting protein polymerization, eventually resulting in cell death [21–26]. We have recently explored the reactivity of hemoglobin towards a set of four anti-tubulin agents - irinotecan, docetaxel, paclitaxel and vinorelbine – and found that they affect the Hb autoxidation rates (either alone or in assays where nitrite accelerates autoxidation via a cascade of nitrosative stress reactions) and, for members with more extended aromatic rings (and hence with measurable electronic absorption spectra in the visible domain), they can also serve as direct redox partners acting to reduce high-valent hemoglobin in the presence of peroxide [1].

Reported here is an exploration of Hb reactivity towards vincristine, employing UV-vis spectroscopy and showing similar behavior to that previously observed for other anti-tubulin agents – with two particularities: the effect on Hb autoxidation is very small, while the effect on nitrite-induced autoxidation is remarkably antioxidant.

RESULTS AND DISCUSSION

Figure 1 shows UV-vis spectra collected for oxy hemoglobin before and after incubation with 50 µM vincristine up to 4 hours. There appear to be no discernible differences in the Soret band at ~400 nm. However, closer inspection of the bands at 577 nm (specific to oxy Hb cf. Figure 1) and 630 nm (specific to autoxidized, met Hb, cf. Figure 1) does reveal an (albeit small) influence of vincristine in accelerating autoxidation. Table 1 further shows that the ratio of the oxy to met features (577 vs. 630 nm) in the Hb spectrum increases with vincristine concentration up to 75 µM.

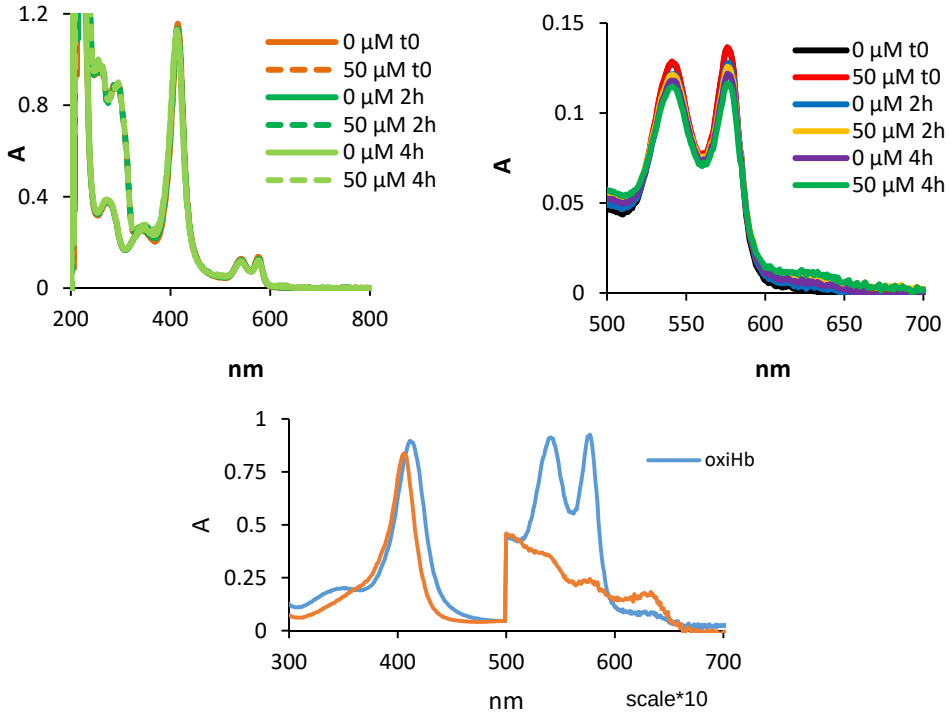

Figure 1. Top row: time dependence of oxy Hb UV-vis spectra with or without vincristine present. Lower row: reference spectra of oxy and met Hb.

Table 1. Met:oxy ratio (calculated as the ratio of absorbance at 630 nm vs. absorbance at 577 nm) from UV-vis spectra collected after 4 hours at 37°C.

vincristine (µM)	0	10	25	50	75	100
met:oxy ratio	0.05	0.07	0.07	0.09	0.12	0.08

The UV-vis spectra of red blood cells (Figure 2) are not affected by vincristine at concentrations of up to 50 µM immediately after mixing. However, after incubation at 37°C for 4 hours, the Soret band in the 50-µM sample is distinctly higher than that of the other two samples (0 and 10 µM vincristine, respectively). In erythrocytes the UV-vis spectrum is due almost exclusively to Hb; however, the intensity of the Soret band is additionally affected by the integrity of the cells: erythrocyte damage from oxidative stress upon Hb autoxidation appears to increase the intensity of the Soret band even when the 500-700 nm region reveals no change in the oxidation state of Hb [16]. We therefore propose that at 4 hours a 50 µM concentration of vincristine (but not a concentration of 10 µM) can induce optically-detectable changes in the state of the red blood cells. It is important to note that such cell lysis cannot be a direct result of Hb autoxidation; rather, autoxidation initially places oxidative stress (via the liberated superoxide) upon the cell. One may expect an initial phase where the cell structure remains intact but the antioxidant reserves (ascorbate, thiols, NADPH and others [27,28]) are consumed. Such a form of stress may then be expected to have manifested itself even in the 10 µM sample; this hypothesis would require subsequent tests on molecular markers of oxidative stress, other than Hb itself.

After incubation of erythrocytes overnight (as also shown in Figure 2), the Soret peak has now clearly shifted to 405 nm (specific to met Hb) from the initial 410 value in fresh (oxy) samples. Similarly to the 4-hour samples, there is a monotonous increase in absorbance from 800 to 200 nm, superimposed over the Hb absorption. This increase is due to diffuse/particulate matter in the sample, most likely protein precipitation; its degree does not appear to be increased proportionally with vincristine concentration.

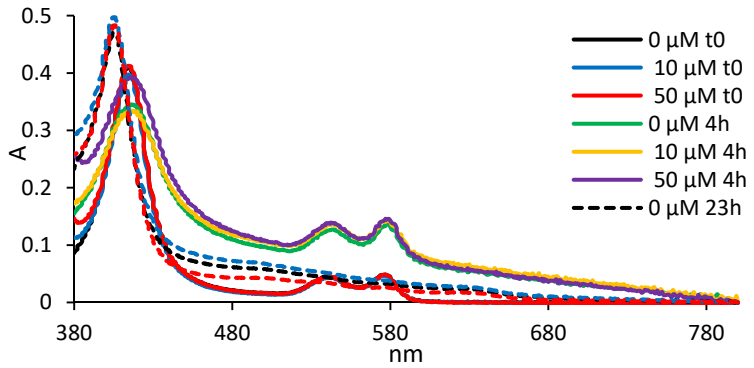

Figure 2. UV-vis spectra of erythrocytes re-suspended in saline phosphate buffer pH 7.4, with or without vincristine at two different concentrations, after incubation at 37°C.

Last but not least, Figure 3 shows the effect of vincristine on the nitrite-induced oxidation of Hb. In this assay, the initial step is reaction of nitrite with oxy Hb to form a caged ferric-peroxynitrate intermediate. However, clear changes in absorbance (e.g., at the oxy bands such as ~540 or ~ 580 nm) are not seen at these low nitrite concentrations until enough side-products (nitrogen oxides, superoxide, and others) accumulate. Hence, the key feature of the reaction time course is the lag time. Any added reactant (e.g., the vincristine) may be expected to affect the reaction either by delaying the change in absorbance (thus protecting the oxy form of Hb – and hence acting as antioxidant), or by shortening the lag time (thus acting as prooxidant). Figure 3 shows that already at a very low concentration, 30 μM, vincristine completely blocks the reaction – thus acting as a very efficient protecting agent against nitrosative stress on Hb.

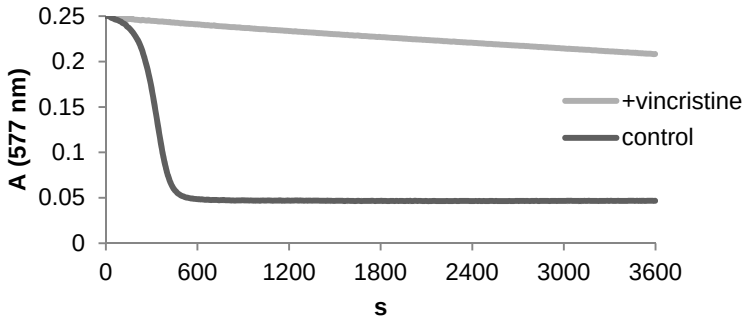

Figure 3. Influence of vincristine on the time evolution of oxy Hb absorbance in the presence of nitrite.

CONCLUSIONS

Vincristine has a very small (concentration-dependent) accelerating effect on Hb autoxidation *in vitro* in the concentration range 10-100 μM. At 50 μM, it also affects the stability of red blood cells. Vincristine also displays a powerful inhibitory effect on the (*in vitro*) nitrite-induced oxidation of Hb. The concentration ranges examined in the present study may be bio-medically relevant, since intravenous injections of vincristine in anticancer treatments are given with ~1000 μM solutions (although one must also note that after dilution in the total blood volume of a patient, even before the drug can exit to various organs in the body, the vincristine concentration would eventually not exceed 1 μM). Further examination at lower concentrations of vincristine

and on other types of cells would be warranted – though in those cases specific molecular markers would have to be measured, other than the very convenient Hb absorbance in UV-vis examined in the present study.

EXPERIMENTAL SECTION

Bovine hemoglobin was purified following the general protocol of Antonini and Brunori as previously described [29], and stored in saline (PBS), pH 7.4. In order to ensure a homogeneous (oxy) composition, the protein was first treated with sodium dithionite and passed through a desalination column. The hemoglobin concentration is given per heme. Vincristine was used as aqueous solutions prepared by mixing solid powder (drug) with saline (0.9% NaCl) without further purification. Electronic absorption were recorded with a Cary 50 instrument (Varian, Inc) in the range of 200-800 nm, in 1 mL quartz cuvettes.

Autoxidation of Hb (10 μM) in the presence of vincristine (at concentrations given in Figures) was monitored in PBS saline, pH 7.4, with the samples incubated at 37°C. Red blood cells were examined under similar conditions, using 30 μL of sample instead of 10 μM pure Hb.

Nitrite-induced autoxidation of was performed using oxyHb (240 μM), nitrite (334 μM) and vincristine (30 μM) in PBS at room temperature.

All results to be analyzed represent the average of at least 3 experiments.

ACKNOWLEDGMENTS

Dr. Eva Fischer-Fodor (IOCN) is thanked for kindly supplying a sample of vincristine. Dr. Alina Matei and drd. Maria Lehene (UBB) are thanked for helpful discussions. Prof. Bogdan Sevastre (USAMV Cluj-Napoca) is thanked for supplying bovine blood.

REFERENCES

1. C. Puscas; A. Mircea; M. Raiu; M. Mic; A.A.A. Attia; R. Silaghi-Dumitrescu; A.A. A. Attia; R. Silaghi-Dumitrescu; *Chem. Res. Toxicol.* **2019**, *32***,** 1402–1411.
2. C. Bischin; V. Taciuc; R. Silaghi-Dumitrescu; in *Metal Elements in Environment, Medicine and Biology* (ed. Radu Silaghi-Dumitrescu G. G.) (Eurobit Publishing House, **2010**). *X***,** 265–270.

3. C. Bischin; Ş. Ţălu; R. Silaghi-Dumitrescu; M. Ţălu; S. Giovanzana; C.A. Lupaşcu; *Ann. Rom. Soc. Cell Biol.* **2012**, *17***,**
4. V. Taciuc; C. Bischin; R. Silaghi-Dumitrescu; in *Metal Elements in Environment, Medicine and Biology Tome IX* (eds. Silaghi-Dumitrescu R. & Garban G.) (Cluj University Press, **2009**). 130–134.
5. C. Bischin; V. Taciuc; R. Silaghi-Dumitrescu; *Studia UBB Chem.* **2010**, *55***,** 313–318.
6. N.B. Vollaard; B.J. Reeder; J.P. Shearman; P. Menu; M.T. Wilson; C.E. Cooper; *Free Radic. Biol .Med.* **2005**, *39***,** 1216–1228.
7. C.E. Cooper; D.J. Schaer; P.W. Buehler; M.T. Wilson; B.J. Reeder; G. Silkstone; D.A. Svistunenko; L. Bulow; A. I. Alayash; *Antioxidants Redox Signal.* **2013**, *18***,** 2264–2273.
8. B.J. Reeder; M.T. Wilson; *Free. Radic. Biol. Med.* **2001**, *30***,** 1311–1318.
9. M.S. Rogers; R.P. Patel; B.J. Reeder; P. Sarti; M.T. Wilson; A.I. Alayash; *Biochem. J.* **1995**, *310***,** 827–833.
10. B.J. Reeder; M.A. Sharpe; A.D. Kay; M. Kerr; K. Moore; M.T. Wilson; *Biochem. Soc. Trans.* **2002**, *30***,** 745–748.
11. B.J. Reeder; M. Grey; R.-L. Silaghi-Dumitrescu; D.A. Svistunenko; L. Bülow; C.E. Cooper; M.T. Wilson; *J. Biol. Chem.* **2008**, *283***,** 30780–30787.
12. B.J. Reeder; D.A. Svistunenko; M.A. Sharpe; M.T. Wilson; *Biochemistry* **2002**, *41*, 367–375.
13. S. Holt; B.J. Reeder; M.T. Wilson; S. Harvey; J.D. Morrow; L.J. Roberts 2nd; K. Moore; L.J. Roberts; K. Moore; L.J. Roberts 2nd; K. Moore; L.J. Roberts; K. Moore; *Lancet* **1999**, *353***,** 1241.
14. B.J. Reeder; D.A. Svistunenko; C.E. Cooper; M.T. Wilson; *Antioxidants Redox Signal.* **2004**, *6***,** 954–966.
15. K.P. Moore; S.G. Holt; R.P. Patel; D.A. Svistunenko; W. Zackert; D. Goodier; B.J. Reeder; M. Clozel; R. Anand; C.E. Cooper; J.D. Morrow; M.T. Wilson; V.M. DarleyUsmar; L.J. Roberts; V. Darley-Usmar; L.J. Roberts 2nd; L.J. Roberts 2nd; V.M. DarleyUsmar; L.J. Roberts; *J. Biol. Chem.* **1998**, *273***,** 31731–31737.
16. M. Lehene; E. Fischer-Fodor; F. Scurtu; N.D. Hădade; E. Gal; A.C. Mot; A. Matei; R. Silaghi-Dumitrescu; *Pharmaceuticals* **2020**, *13*, 107.
17. D. Hathazi; F. Scurtu; C. Bischin; A. Mot; A. Attia; J. Kongsted; R. Silaghi-Dumitrescu; *Molecules* **2018**, *23***,** E350.
18. L.I. Găină; L.N. Mătărângă-Popa; E. Gal; P. Boar; P. Lönnecke; E. Hey-Hawkins; C. Bischin; R. Silaghi-Dumitrescu; I. Lupan; C. Cristea; L. Silaghi-Dumitrescu; *Eur. J. Org. Chem.* **2013**, 5500–5508.
19. L. Gaina; I. Torje; E. Gal; A. Lupan; C. Bischin; R. Silaghi-Dumitrescu; G. Damian; P. Lonnecke; C. Cristea; L. Silaghi-Dumitrescu; *Dye. Pigment.* **2014**, *102*, 315–325.
20. C. Bischin; C. Tusan; A. Bartok; R. Septelean; G. Damian; R. Silaghi-Dumitrescu; *Phosphorus, Sulfur Silicon Relat. Elem.* **2015**, *190***,** 292–299.
21. F. Liu; J. Huang; Z. Liu; *Neuroscience* **2019**, *404***,** 530–540.
22. L. Zhou; L. Ao; Y. Yan; C. Li; W. Li; A. Ye; J. Liu; Y. Hu; W. Fang; Y. Li; *Neurotherapeutics* **2020**, *17***,** 340–355.

23. M.E. Duckett; K.M. Curran; H.J. Leeper; C.E. Ruby; S. Bracha; *Vet. Comp. Oncol.* **2021**, *19***,** 61–68.
24. J.A. Silverman; S.R. Deitcher; *Cancer Chemother. Pharmacol.* **2013**, *71*, 555–564.
25. L.D. Brühwiler; D.L.B. Schwappach; *J. Oncol. Pharm. Pract.* **2020**, *26***,** 51–59.
26. M.L. Madsen; H. Due; N. Ejskjær; P. Jensen; J. Madsen; K. Dybkær; *Cancer Chemother. Pharmacol.* **2019**, *84***,** 471–485.
27. C.E. Cooper; R. Silaghi-Dumitrescu; M. Rukengwa; A.I.I. Alayash; P.W.W. Buehler; *Biochim. Biophys. Acta* **2008**, *1784***,** 1415–1420.
28. B.N. Ames; R. Cathcart; E. Schwiers; P. Hochstein; *Proc. Natl. Acad. Sci. U.S.A.* **1981**, *78***,** 6858–6862.
29. D. Hathazi; A.C. Mot; A. Vaida; F. Scurtu; I. Lupan; E. Fischer-Fodor; G. Damian; D.M. Kurtz Jr.; R. Silaghi-Dumitescu; *Biomacromolecules* **2014**, *15***,** 1920–1927.

STUDIA UBB CHEMIA, LXVI, 2, 2021 (p. 333)
(RECOMMENDED CITATION)

E R A T A

Ms. Anca Becze is the corresponding author for the previously published article: *Evaluation of The Antioxidant Capacity and Total Polyphenols in Different Fruit Teas*, STUDIA UBB CHEMIA, LXI, 3, Tom II, 2016 (p. 505-514).

Ioan Simon, Dorina Simedru, Lucian Dordai, Emil Luca, Vanda Fuss, **Anca Becze***,

**Corresponding author email: anca.naghiu@icia.ro*